UNIVERSIDADE DE LISBOA
FACULDADE DE CIÊNCIAS

Degradação de contaminantes emergentes: um estudo por espectrometria de massa e outras técnicas analíticas

"Documento Definitivo"

Doutoramento em Química
Especialidade de Química Analítica

Rodrigo Arimura Osawa

Tese orientada pela:
Professora Doutora Maria Helena Ferreira da Silva Florêncio

Documento especialmente elaborado para a obtenção do grau de doutor

2019

UNIVERSIDADE DE LISBOA
FACULDADE DE CIÊNCIAS

Degradação de contaminantes emergentes: um estudo por espectrometria de massa e outras técnicas analíticas

Doutoramento em Química

Especialidade de Química Analítica

Rodrigo Arimura Osawa

Tese orientada pela:

Professora Doutora Maria Helena Ferreira da Silva Florêncio

Júri:

Presidente:

- Doutora Amélia Pilar Grases dos Santos Silva Rauter, Professora Catedrática e Presidente do Departamento de Química e Bioquímica da Faculdade de Ciências da Universidade de Lisboa.

Vogais:

- Doutora Maria do Rosário Gonçalves dos Reis Marques Domingues, Professora Associada com Agregação do Departamento de Química da Universidade de Aveiro;
- Doutora Maria do Céu Gonçalves da Costa, Professora Catedrática com Agregação da Escola de Ciências e Tecnologias da Saúde da Universidade Lusófona;
- Doutor Paulo Jorge Amorim Madeira, Gestor do Laboratório de Screening, Separação e Síntese ASCENZA Agro SA, na qualidade de individualidade de reconhecida competência na área científica em que se insere a tese;
- Doutora Maria Helena Ferreira da Silva Florêncio, Professora Catedrática Jubilada da Faculdade de Ciências da Universidade de Lisboa (Orientadora);
- Doutora Ana Isabel Amaral Janeiro Viegas Ferreira, Investigadora Auxiliar da Faculdade de Ciências da Universidade de Lisboa.

Documento especialmente elaborado para a obtenção do grau de doutor

Esta tese teve o financiamento do programa Ciências sem Fronteiras da CAPES-Brasil (BEX 0845/14-0)

2019

Agradecimentos

Muitas pessoas contribuíram diretamente ou indiretamente para a conclusão desta tese e assim gostaria de expressar os meus mais sinceros agradecimentos a todos os envolvidos.

Primeiramente, gostaria de agradecer a Professora Maria Helena Florêncio pela orientação com seus conselhos, críticas construtivas e ideias para o andamento da tese. Pois foram essenciais em momentos de incerteza e insegurança durante a realização deste trabalho e assim contribuiu para o meu crescimento como futuro doutor.

À Professora Maria da Conceição de Oliveira pela disponibilização do laboratório, amizade e discussões na área de espectrometria de massa, que se demostraram fundamentais para a concretização do doutoramento.

À Professora Olinda Monteiro pelo suporte dos laboratórios, conversas e total disponibilidade na colaboração na área da fotocatálise durante as atividades da tese.

À Professora Ana Paula Carvalho, pela colaboração com as coletas de efluentes.

Gostaria de agradecer a todos os alunos e ex-alunos do grupo de Espectrometria de Massa Ambiental e Biológica e do Laboratório de FTICR e Espectrometria de Massa Estrutural de Lisboa, dos quais fiz parte durante os anos do doutoramento. Em especial ao Professor Carlos Cordeiro pelas conversas casuais e esclarecimentos de dúvidas sobre a espectrometria de massa.

Aos meus amigos e colegas da universidade Ana Marques, Nuno, Samir, Alessandra, Ana Dias e Beatriz pelos almoços, companheirismo e momentos de descontração.

À minha família pelo apoio incondicional e incentivos em todos os momentos do doutoramento, mesmo estando do outro lado do Atlântico, meu eterno agradecimento.

À Eliane pela paciência, compreensão e companheirismo em todos os momentos.

E por último e não menos importante, à Coordenação de Aperfeiçoamento de Pessoal de Nível Superior pela bolsa de doutoramento.

Resumo

Contaminantes emergentes são químicos que incluem compostos farmacêuticos, produtos de higiene pessoal e pesticidas encontrados em diversas matrizes ambientais como água potável, água superficial, efluentes e solo. Estes poluentes podem apresentar riscos para a saúde humana e o meio ambiente já que alguns foram reconhecidos por apresentarem ecotoxicidade aquática, interferência endócrina, genotoxicidade e desenvolvimento de resistência em microrganismos, porém, ainda não há uma legislação ambiental sobre as concentrações seguras permitidas em águas. Um grupo de contaminantes emergentes resultantes do amplo consumo pela sociedade moderna são os fármacos. A principal fonte desta classe de poluentes no ambiente provém de efluentes domésticos e estudos concluíram que muitos destes contaminantes não são completamente degradados em estações de tratamento de águas residuais (ETARs), logo, torna-se essencial desenvolver novas técnicas de remoção. Adicionalmente, há a preocupação da formação dos produtos de transformação (TPs), que são produtos gerados por processos bióticos a abióticos que podem apresentar ainda maior persistência e toxicidade em comparação com o contaminante de origem.

No capítulo 2 foi desenvolvido um método para a quantificação de nove contaminantes emergentes, sendo eles seis fármacos antidepressivos: amitriptilina (AMI), bupropiona, citalopram (CIT), duloxetina (DUL), trazodona (TRA) e venlafaxina (VEN) e três fármacos citostáticos: ciclofosfamida (CP), ifosfamida (IF) e metotrexato (MET). O trabalho consistiu em validar a extração em fase sólida em cromatografia líquida acoplada a espectrometria de massa do tipo triplo quadrupolo (HPLC-TQMS) para em seguida aplica-las em amostras reais. O método de extração apresentou valores de recuperação acima dos 80,2 % e limites de quantificação entre 2 e 4 ng L^{-1}. Em seguida, os contaminantes foram quantificados em efluentes em concentrações entre 16 ng L^{-1} a 954 ng L^{-1}, levando a concluir que não há uma completa remoção destes poluentes nos sistemas convencionais de tratamento.

Nos capítulos 3 e 4 foram estudadas as formações de TPs do CIT e do DUL, respetivamente, por simulações controladas de processos que podem ocorrer no meio aquático e em ETARs: hidrólise, fotodegradação (sob irradiação UV-vis) e cloração.

As análises por cromatografia líquida de ultra performance acoplada à espectrometria de massa do tipo quadrupolo-tempo de voo (UHPLC-QTOF-MS) revelaram dezassete TPs do CIT e onze TPs do DUL com diversos caminhos de degradações e diferentes níveis de toxicidade obtidos por métodos computacionais (*in silico*) tendo posteriormente, alguns destes TPs sido identificados em efluentes. Este facto demonstra que estes TPs podem ter sido formados durante o tratamento de efluentes.

No capítulo 5 foi avaliada a eficiência de remoção do AMI, TRA e VEN na fotocatálise usando nanofios de titanato dopados com 1% de cobalto (Co-TNW), sob radiação UV−Vis, tendo sido demonstrada atividade fotocatalítica para o AMI e o VEN. Vinte TPs foram elucidados por UHPLC-QTOF-MS, sendo oito do AMI, sete do TRA e 5 do VEN com diferentes perfis de tempo durante a fotocatálise e a fotólise. Adicionalmente, a toxicidade *in silico* resultou em alguns TPs com potencial tóxico maior que os fármacos de origem. Para complementar, foi examinado a atividade fotocatalítica do catalisador sob radiação visível na degradação do AMI e foi observado um aumento na taxa de degradação com o Co-TNW com diferentes TPs formados.

No capítulo 6, nanofios de titanato modificados com ruténio (Ru-TNW) foram utilizados na degradação do CP e IF em efluentes do tratamento secundário sob radiação UV−Vis e foi observado um aumento da taxa de degradação usando este catalisador. Foi constatado também que diferentes TPs foram formados usando água destilada e efluente como matriz. No total dez TPs foram identificados por UHPLC-QTOF-MS.

No capítulo 7, as taxas de degradação do TRA foram avaliadas em fotólise e fotocatálise com os diferentes catalisadores: nanofios de titanato (TNW), nanofios de titanato dopados com ferro (Fe-TNW), Co-TNW e Ru-TNW sob radiação de luz visível. Foi demonstrado que os catalisadores podem formar diferentes TPs com distintos perfis de formação e degradação pelo facto de se usar uma fonte de radiação diferente do utilizado pelo estudo no capítulo 5. O Fe-TNW foi o que apresentou maior taxa de degradação tendo como base a área superficial do catalisador e, no total, treze TPs foram identificados, sendo dez deles inéditos. Na sua maioria, os TPs apresentaram toxicidade para os organismos aquáticos, além de não serem biodegradáveis por predições de métodos computacionais.

Palavras chave: poluentes, espectrometria de massa de alta resolução, fotocatálise, produtos de transformação, vias de degradação, toxicidade *in silico*.

Abstract

Emerging contaminants are chemicals that include pharmaceutical compounds, personal care products and pesticides found in environmental matrices such as drinking water, surface water, effluent and soil. These pollutants may present risks to human health and aquatic organisms as some have been identified for their ecotoxicity, endocrine interference, genotoxicity and development of resistance in microorganisms, however, there is no environmental legislation regarding the safe concentrations in water. A group of emerging contaminants widely consumed by modern society are the drugs. The main source of this class of pollutants in the environment is originated from domestic effluents and studies have concluded that many of these contaminants are not completely degraded in wastewater treatment plants (WWTPs), therefore, it becomes essential to develop new removal techniques. In addition, the formation of transformation products (TPs), which are products generated by biotic or abiotic processes are a matter of concern since they may present greater persistence and toxicity compared to the contaminant of origin.

In Chapter 2 a method was developed for the quantification of nine emerging contaminants, being six antidepressant drugs: amitriptyline (AMI), bupropion, citalopram (CIT), duloxetine (DUL), trazodone (TRA) and venlafaxine (VEN) and three cytostatic drugs: cyclophosphamide (CP), ifosfamide (IF) and methotrexate (MET). The work consisted in validating the method of the solid-phase extraction by liquid chromatography coupled to a triple quadrupole (HPLC-TQMS) and then applying it to real samples. The extraction method presented recovery values above 80.2% and limits of quantification between 2 and 4 ng L^{-1}. Then, the contaminants were quantified in effluents at concentrations ranging from 16 ng L^{-1} to 954 ng L^{-1}, showing that there is no complete removal of these pollutants in conventional treatment systems.

In Chapters 3 and 4, the TP of CIT and DUL were studied by, respectively, controlled simulations of processes that may occur in the aquatic environment, ETAR: hydrolysis, photo-degradation (under UV-vis irradiation) and chlorination. Ultra-high-performance liquid chromatography coupled to a time-of-flight quadrupole mass spectrometry (UHPLC-QTOF-MS) revealed seventeen CIT TPs and eleven for DUL TPs with diversified pathways of degradation and different levels of toxicity were

obtained by computational methods (*in silico*) being finally, some of these TPs identified in effluents. This demonstrates that these TPs may have been formed during the treatment of effluents.

In Chapter 5, the efficiency of removal of AMI, TRA and VEN on photocatalysis was evaluated using modified cobalt-titanate nanowires (Co-TNW), under UV-Vis radiation, in which the catalyst showed photocatalytic activity for AMI and VEN. Twenty TPs were elucidated by UHPLC-QTOF-MS, eight from AMI, seven from TRA and 5 from VEN with different time profiles during photocatalysis and photolysis. In addition, *in silico* toxicity resulted in some TPs with toxic potential higher than the parent drugs. Furthermore, the photocatalytic activity of the catalyst under visible radiation in the AMI degradation was examined and an increase of the degradation rate using Co-TNW with different TPs was observed.

In Chapter 6, ruthenium-modified titanate nanowires (Ru-TNW) was used in the degradation of CP and IF in effluents from the secondary treatment under UV-Vis radiation and, an increase in the degradation rate was shown using this catalyst. It was also found that different TPs were formed using distilled water and effluent as matrix. In total ten TPs were identified by UHPLC-QTOF-MS.

In chapter 7, TRA degradation rates were evaluated in photolysis and photocatalysis with different catalysts: titanate nanowires (TNW), titanate nanowires doped with iron (Fe-TNW), Co-TNW and Ru-TNW under visible light. It has been demonstrated that the catalysts may form different TPs with different profiles of formation and degradation by the use of a source of radiation different from that used in the study of chapter 5. Fe-TNW was the one that presented the highest rate of degradation based on the area surface of the catalyst and, in total, thirteen TPs were identified. To the best of our knowledge, ten of them have never been published in the literature. Most TPs presented toxicity to aquatic organisms and were not biodegradable by predictions of computational methods.

Keywords: pollutants, high resolution mass spectrometry, photocatalysis, transformation products, degradation pathways, in silico toxicity.

Índice

Símbolos e abreviaturas

°C	temperatura em graus celsius
µg	micrograma
µm	micrómetro
•OH	radical hidroxilo
ACN	acetonitrilo
AMI	amitriptilina
AMI-d_3	amitriptilina-d_3
B	setor magnético
BC	banda de condução
BUP	bupropiona
BV	banda de valência
CdS	sulfureto de cadmio
CID	dissociação induzida por colisão (*collision induced dissociation*)
CIT	citalopram
Co-TNW	nanofios de titanato dopados com cobalto
CP	ciclofosfamida
CRM	modelo de carga residual (*charged residue mode*)
DA	domínio de aplicabilidade
Da	dalton
DC	corrente continua
DT_{50}	tempo de meia vida em solo
DUL	duloxetina

e^-	eletrão
E/ESA	setor eletrostático
ECOSAR	*Ecological Structure Activity Relationships*
ESI	ionização por eletrospray
ETAR	estação de tratamento de águas residuais
eV	*electrão volt*
FDA	*Food and Drug Administration*
Fe_2O_3	óxido de ferro (III)
Fe-TNW	nanofios de titanato dopados com ferro
FT-ICR	ressonância ciclotrónica de ião com transformada de Fourier (*fourier-transform ion-cyclotron-resonance*)
FWHM	largura total do pico a metade de sua altura máxima (*full width of the peak at half of its maximum height*)
g	grama
h	constante de Planck
h^+	*electron hole*
H_2O_2	peroxido de hidrogénio
HCl	ácido clorídrico
HLB	balanço hidrofílico-lipofílico (*hydrophilic-lipophilic balance*)
HPLC	Cromatografia líquida de alta eficiência (*high performance liquid chromatography*)
hv	luz (*light*)
ICH	Conferência Internacional de Harmonização (*International Conference for Harmonization*)
IEM	modelo de evaporação iónica (*ion evaporation model*)
IF	ifosfamida

IT	*ion trap*
IUPAC	União Internacional de Química Pura e Aplicada (*International Union of Pure and Applied Chemistry*)
K	constante de Boltzmann
K_d	coeficiente de distribuição sólido-água
K_{ow}	coeficiente de partição octanol-água
$K_{reação}$	constante da taxa de reação
kV	kilovolt
L	litro
L.D	limite de deteção
L.Q	limite de quantificação
LC-MS	cromatografia líquida acoplada à espectrometria de massa
M	massa de um único ião
m	metro
M.E	efeito matriz
m/z	razão massa-carga
MALDI	ionização/dessorção a laser assistida por matriz (*matrix assisted laser desorption/ionization*)
MET	metotrexato
min	minuto
mL	mililitro
mmu	mnidades de milimassa
MRM	monitorização de reações múltiplas (*multiple reaction monitoring*)
ms	milisegundo
MS/MS	espectrometria de massa *tandem*

MS^n	espectrometria de massa sequencial
N	número de cargas média da gotícula
ng	nanograma
nm	nanometro
O_3	ozono
oa	aceleração ortogonal
pH	potencial hidrogeniónico
pK_a	logaritmo negativo da constante de dissociação de ácido
ppm	partes por milhão
PTFE	politetrafluoroetileno
q	carga da gotícula
Q	quadrupolo
Q1	primeiro quadrupolo
Q2	segundo quadrupolo
Q3	terceiro quadrupolo
QSARs	Relações quantitativas estrutura-atividade (q*uantitative structure activity relationships*)
QTOF-MS	espectrometria de massa do tipo quadrupolo-tempo de voo (*quadrupole time-of-flight mass spectrometer*)
r	raio da gotícula
R	gotícula de maior raio
R	constante de gás ideal
r^2	coeficiente de correlação
Re	recuperação

REACH	Registo, Avaliação, Autorização e Restrição de Substâncias Químicas (*European legislation on chemicals, Registration, Evaluation, Authorization and Restriction of Chemicals*)
RF	radiofrequência
RSD	desvio padrão relativo
Ru-TNW	nanofios de titanato dopados com ruténio
s	segundo
S/N	relação sinal/ruído
SIM	monitorização de ião selecionado (*selected ion monitoring*)
SPE	extração em fase sólida (*solid phase extraction*)
T	temperatura
T.E.S.T	*Toxicity Estimation Software Tool*
Th	Thomson
TiO_2	dióxido de titânio
TNW	nanofios de titanato
TOF	tempo de voo (*time-of-flight*)
TP	produtos de transformação (*transformation products*)
TQMS	espectrómetro de massa do tipo triplo quadrupolo (*triple quadrupole mass spectrometer*)
Tr	tempo de retenção
TRA	Trazodona
u	unidade de massa atómica unificada
UHPLC	cromatografia líquida de ultra performance (u*ltra-high performance liquid chromatography*)
UNODC	Escritório das Nações Unidas sobre Drogas e Crime (*United Nations Office on Drugs and Crime*)

US EPA	Agência de Proteção Ambiental dos Estados Unidos (*United States Environmental Protection Agency)*
UV	radiação ultravioleta
UV−Vis	ultravioleta−visível
V	volt
VEN	venlafaxina
WO3	trióxido de tungstênio
ZnO	óxido de zinco
ZnS	sulfureto de zinco
γ	tensão superficial
ΔG	variação da energia de ativação
ΔM	variação da largura do pico a uma determinada altura
Δt	variação do tempo necessário para a fissão
$\varepsilon 0$	permissividade elétrica
σ	densidade da carga superficial
Φ_0	potencial aplicado
$L1$	distância de voo antes do *reflectron*
$L2$	distância de voo do *reflectron*
U	voltagem da corrente continua
V	amplitude da voltagem da radiofrequência
d	comprimento total de voo no *reflectron*
ez	carga total do ião
r_0	raio do quadrupolo
ω	frequência angular

Capítulo 1

Introdução geral

1.1. Contaminantes emergentes: visão geral

Atualmente, águas superficiais e efluentes são monitorizadas em função da legislação ambiental relativa a contaminantes inorgânicos e orgânicos provenientes de atividades industriais, urbanas e agrícolas. Porém, dado que nas últimas décadas estudos em matrizes ambientais identificaram novos contaminantes de origem antropogénicas vindo principalmente de efluentes domésticos, estes compostos foram denominados contaminantes emergentes.

Os primeiros estudos detectaram o ácido clofíbrico, metabolito de fármacos reguladores lipídicos, em águas subterrâneas nos Estados Unidos na faixa de 0,8 – 2 μg L^{-1} [1]. Hignite e Azarnoff (1977) identificaram aspirina, cafeína e nicotina em efluentes domésticos [2].

Por definição, os contaminantes emergentes são compostos químicos que não são monitorizados, mas que podem ser encontrados no ambiente e podem apresentar toxicidade relativamente ao ecossistema aquático e à saúde humana. Os compostos emergentes podem ser de origem sintética ou natural e são encontrados em produtos consumidos por uma vasta gama da população e acabam em ecossistemas naturais (**Tabela 1.1**) [3,4].

Tabela 1.1. Classes de contaminantes emergentes.

Grupo	Exemplos
Compostos farmacêuticos	
Antibióticos	Trimetoprim, eritromicina, amoxicilina
Analgésicos	Cetoprofeno, ibuprofeno, naproxeno, diclofenaco, ácido acetilsalicílico
Antidepressivos	Citalopram, duloxetina, amitriptilina, fluoxetina, bupropion
Anticancerígenos	Metotrexato, ifosfamida
Antidiabéticos	Clorofibrato, genfibrozila, bezafibrato
Antivirais	Aciclovir, penciclovir
Produtos de higiene pessoal	
Cosméticos	Parebenos, microplásticos
Protetores solares	Benzofenona, 4-metil benzilideno cânfora, metoxicinamato de etilhexilo

Fragrâncias	Ftalatos, almíscar macrocíclico
Antissépticos	Triclosan, clorofeno
Interferentes endócrinos	
Retardantes de chama	Éteres difenílicos polibromados, tetrabromobisfenol A
Hormonas e esteroides	Estradiol, etinilestradiol, estrona
Surfactantes	Etoxilatos de alquilfenol, 4-octilfenol
Nanomateriais	Dióxido de titânio, nanotubos de carbono, óxido de zinco
Drogas ilícitas	Cocaína, morfina, metanfetamina, metadona, codeína
Produtos de transformação	TPs de drogas ilícitas, de fármacos

Com o avanço de técnicas analíticas como as cromatografias líquida e em fase gasosa acopladas à espectrometria de massa, compostos que antes não eram possíveis de serem identificados em matrizes ambientais, agora podem sê-lo em concentrações na ordem de ng L^{-1}. Instituições e grupos de investigação têm estudado não só a deteção destes compostos no meio ambiente como o seu potencial tóxico, as formas de remoção e degradação e as possíveis reações físico-químicas que podem ocorrer no meio, formando os denominados produtos de transformação [5,6].

Um grupo de contaminantes emergentes que tem sido estudado nos últimos anos pelo seu elevado consumo e possíveis efeitos ecotoxicológicos e de saúde pública são os compostos farmacêuticos.

1.2. Contaminantes emergentes: fármacos

Estudos vários encontraram fármacos em diversas matrizes ambientais como águas superficiais, efluentes domésticos [7,8], águas subterrâneas [9,10], solos [11] e água para consumo humano [12,13].

Pesquisas concluíram que esses compostos podem causar efeitos adversos como toxicidade aquática, genotoxicidade, interferência endócrina e desenvolvimento

de resistência em microrganismos [14,15,16], o que tem levantado a questão sobre os possíveis impactos na saúde humana.

Atualmente não há legislações ambientais para estes contaminantes, uma vez que se desconhecem as concentrações seguras nas águas, mas alguns órgãos ambientais estão monitorizando os fármacos com o objetivo de determinar os efeitos no ambiente. A Agência de Proteção Ambiental dos Estados Unidos (US EPA, *United States Environmental Protection Agency*), por meio do programa de monitorização de contaminantes não regulamentados em água potável (UCM), monitorizou 7 hormonas utilizadas para fins farmacêuticos: estradiol, etinilestradiol, estrona, estriol, testosterona, androstenediona e equilina [17]. Na União Europeia, a Diretiva-Quadro da Água [18] monitoriza três compostos farmacêuticos em ambientes aquáticos: estradiol, etinilestradiol e diclofenaco.

A principal fonte de fármacos para o meio ambiente são estações de tratamento de esgoto. Estudos encontraram numerosas classes de drogas em efluentes [19,20]. E muitos destes fármacos podem formar produtos de degradação / transformação (TP, *transformation products*), que podem apresentar uma maior toxicidade aquática em comparação com o composto original [21,22].

1.2.1.Fontes e rotas de exposição dos fármacos

Os fármacos chegam ao meio ambiente por diferentes fontes (**Figura 1.1**) e podem ser divididos em dois grupos: substâncias para uso humano e para uso veterinário.

Os medicamentos podem ser administrados por duas grandes vias: enteral como via oral e sublingual e parenteral como via subcutânea e intravenosa. Uma vez administrado, o fármaco é absorvido e distribuído no organismo onde irá atuar. Após atingir os efeitos farmacológicos, o composto é metabolizado pelo fígado ou rins por meio de mecanismos enzimáticos complexos, para inativar compostos endógenos ativos e eliminar compostos xenobióticos [23,24].

Após as biotransformações enzimáticas, o composto é eliminado do organismo, a principal via de excreção é a renal em que o fármaco é convertido em compostos mais polares e hidrofílicos [24].

Em seguida os compostos são detetados em estações de tratamento de esgoto, quer na forma de metabolitos quer na forma inalterada. Muitos metabolitos são persistentes e contaminam as águas superficiais [25,26]. Outra forma, embora não recomendada, é o descarte direto nas instalações sanitárias do medicamento não utilizado ou fora do prazo de validade. Uma outra fonte de fármacos para o meio ambiente é o lodo produzido nos tratamentos de esgoto (biossólidos) que pode ser usado para a agricultura [27,28].

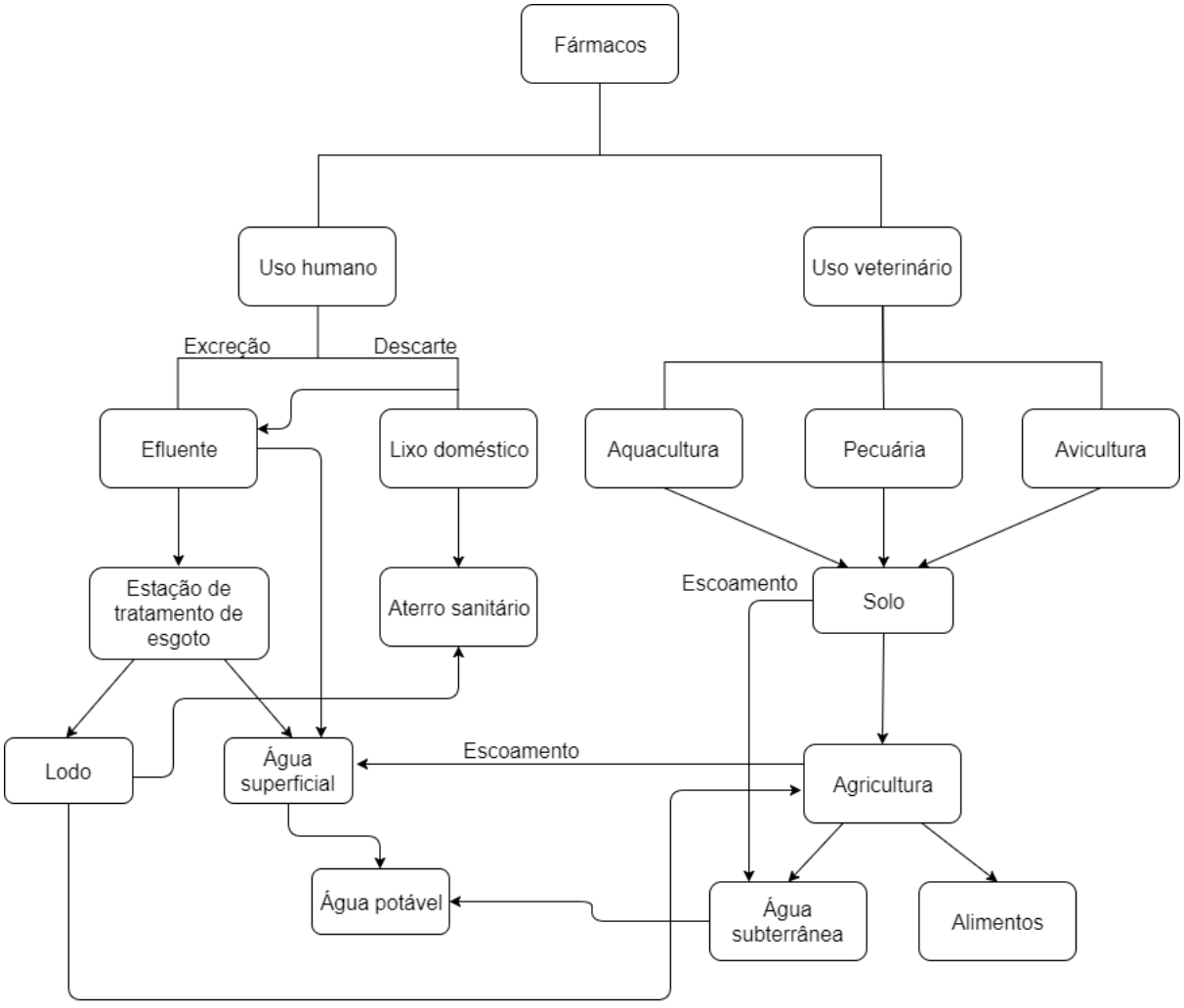

Figura 1.1. Fontes e rotas de exposição dos fármacos no ambiente.

Fármacos de uso veterinário como antibióticos e anti-inflamatórios chegam ao meio ambiente através dos resíduos gerados pelas atividades pecuária, aquicultura e avicultura. Uma vez no solo, os fármacos e metabolitos podem ser escoados para as águas subterrâneas e superficiais como resultado da ocorrência de precipitação,

contaminando o ecossistema aquático e podendo contaminar os alimentos pelo uso do solo para as atividades agrícolas e assim afetar a saúde humana [29,30,31].

A principal fonte de fármacos no meio ambiente são os efluentes das estações de tratamento de esgoto devido ao facto dos fármacos não serem completamente removidos pelos sistemas de tratamento convencionais.

1.2.2. Persistência

Muitos fármacos não são removidos nas estações de tratamento de esgoto devido às suas propriedades físico-químicas e, assim, chegam a ser detetados em água para o consumo, de que resulta um risco para a saúde humana. Características como os coeficientes de partição octanol-água (K_{ow}), de distribuição sólido-água (K_d) e constante de dissociação de ácido (pK_a) têm influência na biodisponibilidade e persistência dos compostos [19,20,25,26]. Outro fator a ser considerado são as transformações abióticas que podem ocorrer no meio ambiente como a fotodegradação e a hidrólise [21,22].

Existem ainda os compostos denominados de pseudo-persistentes, ou seja, que apresentam degradabilidade, porém, devido ao seu uso constante e em larga escala, esses fármacos acabam comportando-se como persistentes.

Loffler et al. (2005) classificou dez compostos farmacêuticos de acordo com a persistência no sistema água-sedimento baseado no tempo necessário para um declínio de 50% na concentração do composto em processo de dissipação (DT_{50}). Diazepam, carbamazepina, CBZ-diol (metabolito da carbamazepina) e ácido clofíbrico apresentaram alta persistência com DT_{50}>119 dias, enquanto que oxazepam, iopromida e ivermectina resultaram em moderada persistência com DT_{50}>15 dias e parecetamol, ibuprofeno e 2-hidroxi-ibuprofeno apresentaram baixa persistência no meio com DT_{50}<7 dias [32].

Noutro estudo foram analisados oito fármacos de acordo com a persistência em ensaios de fotodegradação em que os fármacos propranolol, indometacina, e ifenprodil foram facilmente fotodegradados enquanto que carbamazepina, ibuprofeno, ácido mefenâmico, acetaminofeno e atenolol apresentaram relativa persistência com a luz solar [33].

Bueno et al. (2012) estudou a persistência dos contaminantes em estações de tratamento de efluentes e concluiu que a maioria dos fármacos analisados das classes dos antibióticos e antidepressivos apresentavam taxas baixas de remoção, <50% na maior parte dos casos [34].

Tanto os fármacos de fácil degradação como os persistentes são detetados nas descargas de efluentes das estações de tratamento, podendo contaminar as águas superficiais e os organismos aquáticos. A tabela abaixo (**Tabela 1.2**) mostra a eficiência de remoção de alguns fármacos em estações de tratamento convencionais.

Tabela 1.2. Eficiência de remoção de dez fármacos de diferentes classes em estações de tratamento de efluentes.

Fármaco	**Influente ($ng\ L^{-1}$)**	**Efluente ($ng\ L^{-1}$)**	**Remoção (%)**	**Fonte**
Atenolol	1220	594	51	[20]
	2224	274	88	[35]
Carbamazepina	460	510	-11	[36]
	90	91	-1	[37]
Ciprofloxacina	410	65	84	[35]
	600	22	96	[38]
Citalopram	83	73	12	[35]
	133	280	-111	[20]
Diclofenaco	288	309	-7	[35]
	436	376	14	[39]
Fluoxetina	31	16	48	[40]
	23	28	-22	[39]
Genfibrozila	1009	184	82	[35]
	5120	1018	80	[39]
Ibuprofeno	2488	114	95	[37]
	8600	510	94	[38]
Valsartan	100	90	10	[39]
	1511	99	93	[35]
Venlafaxina	290	280	3	[35]
	415	480	-16	[20]

1.2.3. Toxicidade

Os estudos atuais sobre a toxicidade dos contaminantes emergentes, estão, na sua maioria, limitados aos efeitos biológicos e fisiológicos de organismos aquáticos não alvos e, para além disso, as possíveis implicações com a toxicidade humana são complexas e em grande parte desconhecidas [14,15,16,41].

A toxicidade dos fármacos pode depender de fatores como o tipo de organismo exposto, a concentração do contaminante e o tempo de exposição. Por exemplo, um estudo sobre o ecotoxicidade da fluoxetina mostrou que em concentrações de 0,3 μg L^{-1} com sete dias de tempo de exposição, peixes da espécie *Aphanius díspar* foram afetados em relação à velocidade de locomoção [42] porém, outro estudo, relatou que eram necessárias concentrações mínimas de 350 μg L^{-1} com o tempo de exposição de oito dias, para ocorrerem mudanças comportamentais nos peixes da espécie *Betta splendens* [43].

No meio aquático os contaminantes sofrem inúmeras reações sinérgicas e complexas com a biota e abiota pelo que, estudos de toxicidade isolados, com concentrações encontradas no ambiente, na ordem de ng L^{-1}, não parecem ser realístas. Pesquisas várias mostraram que existe o efeito sinérgico de dois ou mais contaminantes em organismos aquáticos, Cleuvers (2003) mostrou que a carbamazepina, combinada com o acido clofíbrico resultou no aumento da toxicidade em *Daphnia magna* quando comparado com a toxicidade dos compostos isoladamente e na mesma concentração [44]. Schnell et al. (2009) estudou os efeitos sinérgicos de diferentes classes de fármacos (anti-inflamatórios, antidepressivos e reguladores lipídicos) e fragâncias (almíscares nitro e policíclicos) em experiências para avaliar a citotoxicidade e concluiu que esses compostos apresentaram maior toxicidade quando combinados [45]. Outro estudo avaliou a toxicidade do fármaco e surfactante docusato de sódio com dois compostos antissépticos, triclosan e 2,4,6-triclorofeno e observou que, nas misturas binárias, os efeitos foram antagónicos na alga *P. subcapitata*, ou seja, apresentavam toxicidade menor que o valor obtido quando da soma dos compostos separados. Porém, nas misturas ternárias, ocorreu o efeito sinérgico nos organismos analisados [46].

Grande parte dos estudos encontrados na literatura não consideram a ecotoxicidade dos metabolitos ou produtos de transformação, no entanto, é de notar

que esses compostos podem apresentar maior toxicidade que o composto de origem. Trovó et al. (2009) estudou a transformação fotoquímica do sulfametoxazol e concluiu que os produtos formados apresentaram maior toxicidade para o organismo teste (*Daphnia magna*) [47]. Isidori et al. (2005) concluiu que os produtos de transformação do naproxeno exibiram maiores toxicidades agudas e crónicas em algas, rotíferos e microcrustáceos [48]. Outro estudo sugeriu que o metabolito do metoprolol, O-desmethylmetoprolol, apresentava maior toxicidade aguda para as bactérias bioluminescentes *Vibrio fischeri* quando comparado com o metoprolol [49].

1.2.4.Degradação e produtos de transformação

No ambiente, os contaminantes podem sofrer inúmeras transformações por processos bióticos, como a biotransformação e abióticos como a fotodegradação e a hidrólise formando os produtos de transformação.

Processos de biodegradação podem ocorrer por meio dos microrganismos como bactérias, fungos, protozoários e microalgas encontrados em estações de tratamento de efluentes ou no meio ambiente [50]. Nas estações de tratamento, existem dois processos de degradação biológica: o aeróbico, como sistemas de lodos ativados e o anaeróbico, como reatores de digestão do lodo. Estes processos podem reduzir as concentrações dos compostos até à sua completa mineralização em carbono inorgânico, oxigénio, azoto ou hidrogénio. De notar, no entanto, que as atividades biológicas dependem de fatores ambientais como temperatura, oxigénio dissolvido, pH, salinidade, nutrientes e disponibilidade de substrato [51,52]. Enzimas exercem um papel importante para a biodegradação, pois atuam como catalisador, reduzindo a energia de ativação. Porém, a atividade biológica pode gerar produtos de transformação. Como exemplo, um estudo sobre as transformações do fármaco etoposide, sugeriu que alguns TPs foram formados por processos biológicos num ensaio com efluente artificial [53].

No que respeita à degradação fotoquímica no ambiente aquático ela pode ocorrer de duas maneiras, diretamente por absorção da radiação solar ou indiretamente pelos organismos fotossintetizantes [53]. Os contaminantes, em ambos os processos, são transformados em compostos com maior biodegradabilidade e

hidrossolubilidade. Fatores como temperatura, pH, profundidade da água, presença de nuvens, altitude, latitude e hora do dia afetam a eficiência dos mecanismos de degradação e transformação [54,55].

Processos de fotodegradação podem formar TPs, como exemplo, pode citar-se Salgado et al. (2013) que identificou fotoprodutos do diclofenaco, atenolol e cetoprofeno numa experiência com radiação ultravioleta (UV) [56]. Ferrer et al. (2004) detetou quatro TPs do triclosan em efluentes com radiação com luz solar natural [57].

Porém, pouco se sabe sobre a toxicidade dos TPs, já que a maior parte deles não possuem padrões comerciais disponíveis. Portanto, há estudos que têm utilizado métodos computacionais para estimar o potencial tóxico destes poluentes e estes métodos apresentam vantagens como o custo e tempo reduzidos em comparação com testes *in vivo* e *in vitro* [58,59]. Os modelos *in silico* são basicamente dos seguintes tipos: banco de dados dos compostos químicos em relação á sua toxicidade e propriedade; modos para geração de descritores moleculares; ferramentas para simulação em sistemas biológicos e da dinâmica molecular; modelos de predição de toxicidade; sistemas de modelos pré construídos em servidores da web e ferramentas de visualização [60].

Nos modelos de predição de toxicidade existem diversos métodos matemáticos com vantagens e limitações. Os modelos de relações de atividade de estrutura quantitativa (QSARs, *quantitative structure activity relationships*) e read-across são amplamente aplicados na Legislação Europeia Sobre Produtos Químicos, Registo, Avaliação, Autorização e Restrição de Substâncias Químicas (REACH, *European legislation on chemicals, Registration, Evaluation, Authorization and Restriction of Chemicals*) [61,62]. Modelos QSARs são baseados em técnicas de regressão entre os descritores químicos da substância com a sua atividade biológica. Existem disponíveis diversas ferramentas. Por exemplo QSARs disponíveis como: ECOSAR (*Ecological Structure Activity Relationships*, US EPA); T.E.S.T (*Toxicity Estimation Software Tool*, US EPA) e a VEGA, que consiste em uma plataforma onde existem diversos modelos e parâmetros para a predição de toxicidade.

Para garantir a confiabilidade dos resultados é necessário considerar o domínio de aplicabilidade (DA), que define a limitação do método na predição dos valores de toxicidade. Caso a predição resulte em um valor fora do DA, esta predição não pode ser considerada como resultado confiável. Neste contexto, os métodos *in silico* constituem uma ferramenta importante para a predição da toxicidade visto que podem

calcular diversos parâmetros como ecotoxicidade, mutagenicidade e biodegradabilidade. Mas para além de avaliar a toxicidade, é essencial desenvolver novas tecnologias de degradação dos contaminantes.

1.3. Tecnologias de remoção

Existem inúmeros estudos sobre tecnologias de tratamento para a remoção dos contaminantes em efluentes, como o uso de processos oxidativos avançados que consistem na total oxidação dos compostos orgânicos em dióxido de carbono, água e minerais. Os agentes oxidantes mais utilizados são o ozono (O_3), radiação UV e peroxido de hidrogénio (H_2O_2) que podem ser usados em modo combinado juntamente com o dióxido de titânio (TiO_2) e processos Fenton. Como exemplo, Perez-Moya et al. (2010) [63] removeram totalmente a sulfametazina em menos de 2 min. via processo foto-Fenton. Um estudo envolvendo tratamento por UV/H_2O_2 teve alta eficiência na remoção dos fármacos diclofenaco, atrazine e sulfametoxazol enquanto que a carbamazepina apresentou resistência ao tratamento [64].

Uma das tecnologias que tem obtido destaque nas últimas décadas é a fotocatálise. O principal mecanismo de degradação consiste na ativação do material semicondutor pela absorção da radiação a um determinado comprimento de onda. Existem diversos semicondutores como CdS, Fe_2O_3, ZnO, WO_3, ZnS, porém o mais utilizado é o TiO_2. Grupos de investigação têm utilizado a fotocatálise como uma forma de remoção de contaminantes. pode citar-se como exemplo a sua utilização, para remoção de contaminação por efluente de refinarias de petróleo, poluentes em solos contaminados e efluente de indústrias farmacêuticas [65,66,67] Detalhes sobre o processo da fotocatálise encontra-se abaixo.

1.3.1.Fotocatálise

Existem dois tipos de fotocatálise: homogénea e heterogénea. A primeira fundamenta-se na dissolução do catalisador na solução formando uma única fase, os catalisadores mais empregados são o O_3 e o H_2O_2. Na fotocatálise heterogénea, a

solução e o catalisador estão presentes em diferentes fases, sendo geralmente utlizados semicondutores inorgânicos neste processo [68,69].

O processo da fotocatálise consiste na ativação do fotocatalisador pela absorção da radiação em que a energia é igual ou maior que a energia do fotocatalisador. Este processo excita o electrão da banda de valência (BV) para a banda de condução (BC), esta transição gera uma lacuna na BV (h^+) com potenciais positivos, na faixa de +2,0 a +3,5 V que são capazes de produzir radicais •OH a partir de moléculas de água adsorvidas na superfície do catalisador, os quais podem oxidar os poluentes orgânicos (**Figura. 1.2**) [68,69].

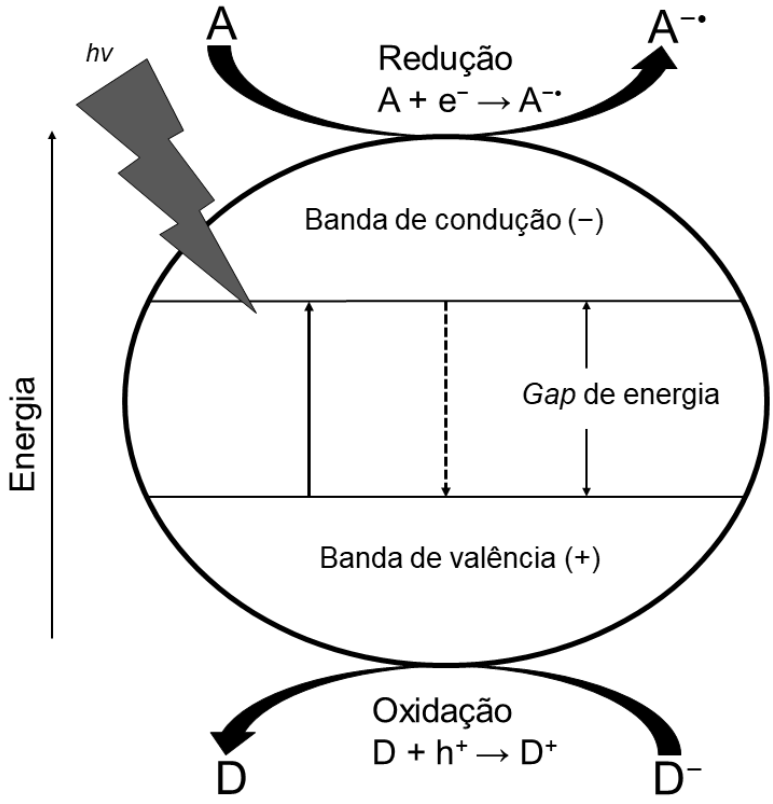

Figura 1.2. Representação do processo de fotocatálise.

Os materiais semicondutores apresentam limitações que podem ser superadas por meio de modificações nos materiais, diversos métodos têm sido desenvolvidos para o efeito como dopagem, compósitos e sensibilização de corantes. A dopagem baseia-se na adição de impurezas, que podem ser de origem catiónica (V, Co, Ru, Cr, Fe, entre outros) ou aniónica (N, S, F, C, entre outros). Cada tipo de elemento modifica a estrutura cristalina do fotocatalisador, no qual pode aumentar a absorção da banda

do espectro de luz por meio da criação de novos níveis de energia entre o BV e o BC com o objetivo de reduzir o *band gap* [68]. Estudos mostraram um aumento nos processos de fotodegradação utilizando catalisadores dopados com metais em comparação com os não dopados [70,71,72]. O compósito também tem como objetivo aumentar a capacidade absorção do fotocatalisador, consistindo o método em acoplar um semicondutor com um *band gap* alto com um outro semicondutor de *band gap* pequeno. Como consequência, os electrões podem ser injetados do semicondutor de *band gap* pequeno para o de *band gap* alto. O mecanismo de sensibilização de corantes baseia-se no mesmo princípio do método de compósitos. O semicondutor é modificado na sua superfície por meio da sensibilizado por um corante. Este método é frequentemente aplicado em células solares [73].

1.4. Espectrometria de massa: visão geral

Espectrometria de massa é umas das técnicas mais versáteis, eficientes e sensíveis para a identificação de compostos desconhecidos e elucidação de estruturas moleculares em diversas áreas da química como química analítica, farmacêutica, forense, ambiental e inorgânica e ainda bioquímica.

Os princípios da técnica da espectrometria de massa remontam a 1897 e a J. J. Thomson da Universidade de Cambridge com a descoberta do electrão e a sua razão massa/carga, na tentativa de explicar o comportamento de partículas carregadas num campo magnético e eletroestático. Em 1912, Thomson desenvolveu o primeiro espectrómetro de massa denominado espectrógrafo de parábola para determinar a razão massa/carga de íões por meio de campos magnéticos [74]. Posteriormente os trabalhos de A. J. Dempster (1918) e F. W. Aston (1919) foram importantes para aprimorar a técnica com os princípios da focagem de direção e de velocidade dos íões, respectivamente [75,76].

Atualmente, o espectrómetro de massa possui, de um modo geral, cinco componentes principais e a **Figura 1.3** mostra o diagrama do funcionamento de um espectrómetro de massa. O sistema de entrada tem como função introduzir a amostra no sistema por meio da pressão atmosférica ou vácuo para a fonte de ionização. Na fonte de ionização, as moléculas na fase gasosa são ionizadas e transferidas para o

analisador de massa, onde são separadas de acordo com a razão massa/carga. O detector, por sua vez, tem como finalidade identificar os íões produzidos convertendo-os em sinais elétricos para, em seguida, transferir esses sinais para um computador, onde é possível controlar o equipamento.

Todo o espectrómetro de massa está ligado a um sistema de vácuo, denominado alto vácuo (baixa pressão), que tem como objetivo minimizar as possíveis colisões dos iões com moléculas gasosas. As colisões dos iões poderiam gerar reações não esperadas dando por exemplo origem a outras espécies e assim interferir nas análises. Em situações especificas, a pressão na fonte de ionização ou em outro componente do sistema pode ser aumentada intencionalmente para estudar precisamente as reações dos íões com moléculas em fase gasosa, como por exemplo na técnica de dissociação induzida por colisão, usada nos analisadores de massa para elucidar a estrutura do analito por meio da análise das suas fragmentações [77,78].

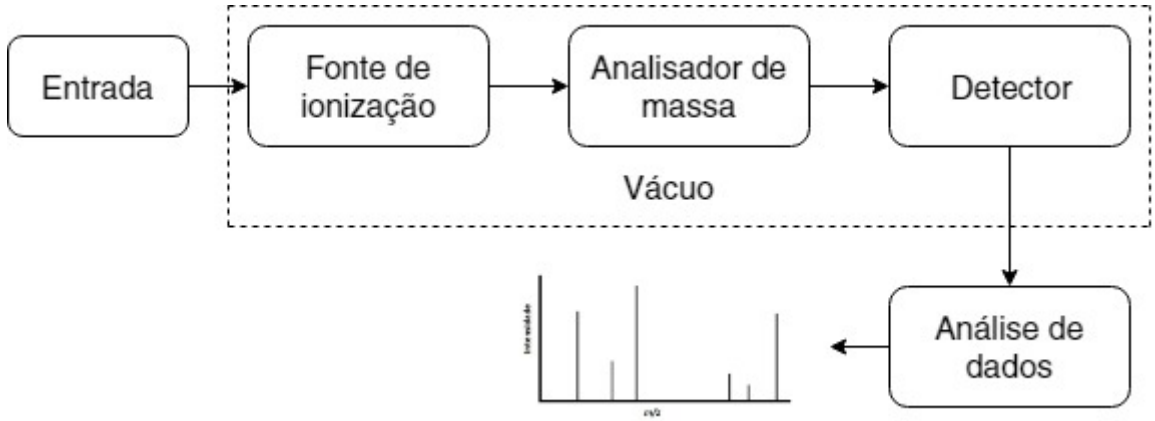

Figura 1.3. Diagrama de um espectrómetro de massa.

Os sistemas de entrada podem variar de acordo com a matriz da amostra e o tipo de analitos a ser analisados. As principais técnicas de ionização operam com as moléculas em fase gasosa, portanto, os sistemas de entrada transferem os analitos já em fase gasosa para a fonte de ionização. Amostras gasosas ou com alta pressão de vapor podem ser injetadas diretamente no sistema. Amostras líquidas e sólidas normalmente necessitam de aquecimento com o objetivo de aumentar a pressão de vapor para a análise [77,78,79]. Os principais sistemas de entrada para amostras ambientais são a cromatografia em fase gasosa e a cromatografia em fase líquida. Neste estudo foi utilizada a cromatografia em fase líquida em que a amostra foi

previamente separada pela coluna cromatográfica para em seguida ocorrer a ionização dos analitos.

Existem diversas técnicas de ionização em espectrometria de massa tais como a ionização eletrónica, ionização química e ionização de campo que são indicadas para compostos termicamente estáveis e voláteis. Porém, grande parte dos compostos apresentam baixa pressão de vapor ou são termicamente instáveis e, para estes analitos, a ionização ocorre diretamente da fase condensada para a fase gasosa.

Para a ionização de amostras sólidas, líquidas ou gasosas podem citar-se como exemplo o caso em que o analito é um sólido e está adsorvido em uma matriz solida ou num fluido viscoso, podendo a ionização ocorrer por meio da irradiação por partículas enérgicas ou fotões na superfície da matriz, para dessorver os íões. Técnicas de ionização/dessorção a laser assistida por matriz (MALDI, *matrix assisted laser desorption/ionization*), dessorção de plasma dessorção de campo utilizam esse processo. Se a amostra está na fase líquida, a amostra pode por exemplo ser nebulizada à pressão atmosférica na fonte para ser analisada no espectrómetro de massa, método este empregado nas fontes de eletrospray e também, de certo modo, na fotoionização à pressão atmosférica. Ou se a amostra está na fase gasosa pode recorrer-se por exemplo à ionização química, em que é utilizado um gás reagente para ionização [77,78,79].

Neste trabalho foram utilizados um espectrómetro de massa do tipo triplo quadrupolo (TQMS) e um espectrómetro de massa do tipo quadrupolo-tempo de voo (QTOF-MS), ambos com a fonte de ionização por eletrospray (ESI, *electrospray ionization*). Os princípios de funcionamento estão descritos na secção abaixo.

1.5. Ionização por eletrospray

A ionização por eletrospray é a principal técnica empregada para a cromatografia líquida acoplada à espectrometria de massa (LC-MS). Esta técnica de ionização é abrangente para macromoléculas não voláteis (proteínas e polímeros de ácido nucleicos), pequenas moléculas polares (contaminantes ambientais), complexos de metais iónicos e soluções inorgânicas.

A primeira fonte de ionização por eletrospray foi desenvolvido por Fenn et al. (1989) que identificou íões carregados a partir da análise de proteínas, ou seja, no princípio a técnica de ionização era indicada para macromoléculas [80]. Posteriormente, a ionização por eletrospray foi aperfeiçoada para pequenas moléculas polares.

O processo de ionização por eletrospray do analito em solução para a fase gasosa ocorre basicamente em três etapas (**Figura 1.4**):

–Produção de gotículas carregadas no capilar de alta tensão;

–Evaporação do solvente proveniente da gotícula carregada;

–Injeção do íão em fase gasosa no sistema.

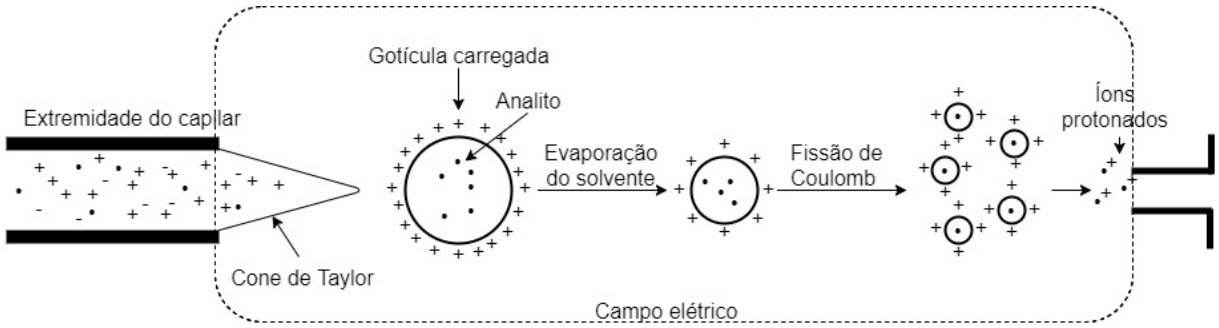

Figura 1.4. Mecanismo geral de ionização por eletrospray.

Para a produção de gotículas carregadas, a amostra é passada através de um capilar (normalmente 1−20 μL min^{-1}) à pressão atmosférica. É aplicada alta voltagem (2,5 – 6,0 kV) na extremidade do capilar, cuja função é criar um campo elétrico na ordem de 10^6 V m^{-1} para dispersar a amostra sob a forma de aerossol, altamente carregada, com a mesma polaridade da tensão gerada no capilar, isto é, em modo positivo o aerossol formado é carregado positivamente (tipicamente por protões) a partir da oxidação dos aniões e em modo negativo o aerossol é carregado negativamente (íões negativos como OH^-) a partir da redução dos catiões. O gás nebulizador (por exemplo, o azoto), é injetado no sistema para limitar a dispersão do spray e aumentar a taxa de fluxo da amostra [79,81].

Ao aplicar um potencial elétrico na extremidade do capilar, o líquido adquire um formato elipsoidal, que é o resultado do equilíbrio de duas forças que atuam na superfície do líquido: a tensão superficial, que atrai o líquido para a extremidade do capilar e a atração eletrostática de Coulomb, que atua no contra eletrodo. Ao desestabilizar o equilibro, mediante determinada tensão elétrica, o formato elíptico da

gotícula é alterado para um formato de cone, denominado cone de Taylor. A tensão aplicada na superfície do líquido é denominada tensão do cone de Taylor. A partir da formação do cone a amostra é pulverizada em direção ao contra eletrodo [79].

A segunda etapa no processo de ionização envolve a evaporação do solvente nas gotículas carregada até próximo ao limite teórico de Rayleigh. Com a evaporação do solvente, a densidade das cargas na superfície da gotícula aumenta até ao ponto em que a atração eletrostática exceda a tensão superficial e consequentemente ocorre a formação de gotículas menores [79]. Acreditava-se que este processo de formação de microgotículas era formado pela desintegração da gotícula inicial a partir da explosão de Coulomb ou fissão de Coulomb. Porém, Gomez e Tang (1994) demonstraram que a gotícula não se desintegra, mas forma-se um jato alongado em série com as microgotículas (**Figura 1.5**), este processo foi denominado fissão de jato [82]. As microgotículas não possuem um formato esférico perfeito e apresentam uma densidade de carga maior na região da curvatura na superfície das microgotículas. Cole (2000) concluiu que as microgotículas formadas possuem cerca de 1-2% de massa e 10–18% de carga em comparação com a gotícula primária [83].

Na última etapa, ocorre a formação de íões em fase gasosa originados das microgotículas. Existem dois modelos propostos para explicar este processo: modelo de carga residual (CRM, *charged residue model*) e modelo de evaporação iónica (IEM, *ion evaporation model*).

O modelo de carga residual, incialmente proposto por Dole et al. (1968), considera a completa dessolvatação das gotículas geradas pelo eletrospray por meio das perdas das moléculas do solvente [84]. O resultado é a formação de uma gotícula que tem somente um íão do analito. Este processo não está limitado pela massa do analito e sim pela eficiência da evaporação do solvente e pela capacidade de gerar gotículas menores. Winger et al. (1993) demonstrou que macromoléculas de proteínas seguem o CRM [85]. A equação abaixo relata a carga máxima que a gotícula pode acumular antes de desestabilizar o equilibro entre a atração eletrostática de Coulomb e a tensão superficial, ou seja, a equação descreve a condição para a formação do cone de Taylor (**Equação 1.1**).

$$q = 8\pi * r\sqrt{\varepsilon_0 \gamma * r} \;\leftrightarrow\; \sigma = 2\sqrt{\frac{\varepsilon_0 \gamma}{r}} \qquad \textbf{(Equação 1.1)}$$

O q representa a carga da gotícula no limite de instabilidade de Rayleigh, r é o raio da gotícula, ε_0 significa a permissividade elétrica no meio, γ é a tensão superficial e σ é a densidade da carga superficial.

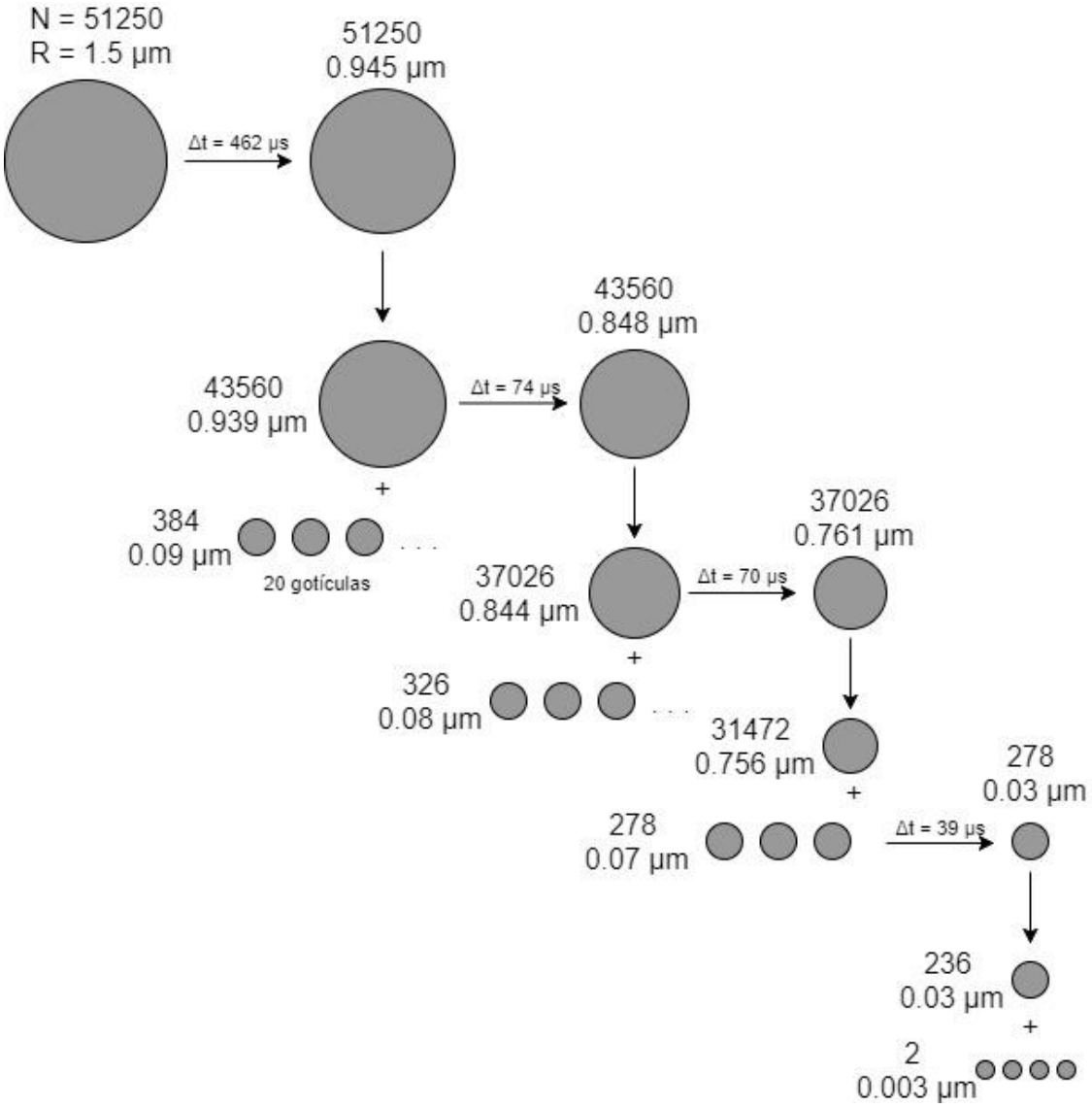

Figura 1.5. Gotículas de metanol produzida pela fissão de jacto. A gotícula de maior raio (R) representa a gotícula inicial formada na extremidade do capilar. N retrata o número de cargas média da gotícula, Δt corresponde ao tempo necessário para a fissão. Adaptado de [82].

O modelo de evaporação iônica, relatado por Iribarne e Thomson em 1976, descreve a expulsão dos íões solvatados diretamente da superfície da gotícula causado por um campo elétrico [86]. Três características são necessárias para o IEM. Primeiro, o íão é evaporado somente quando a gotícula possuir um diâmetro menor que 20 nm. O segundo fator é sobre as características químicas do íão que influenciam

diretamente a cinética da reação, isto é, para o ião ser expelido é necessário ocorrer uma diferença de entalpia livre de reação (**Figura 1.6**). Por último, a gotícula altamente carregada não atinge a carga máxima teórica permitida pelo limite de Rayleigh [83,86]. A equação abaixo mostra a taxa constante para a emissão de íões carregados da superfície da gotícula (**Equação 1.2**).

$$K_{reação} = \frac{KT}{h} * e^{-\frac{\Delta G}{RT}} \qquad \textbf{(Equação 1.2)}$$

A constante da taxa de reação é representada pelo $K_{reação}$, K é a constante de Boltzmann, T é a temperatura, ΔG caracteriza a energia de ativação para a reação, h corresponde à constante de Planck e R é a constante de gás ideal.

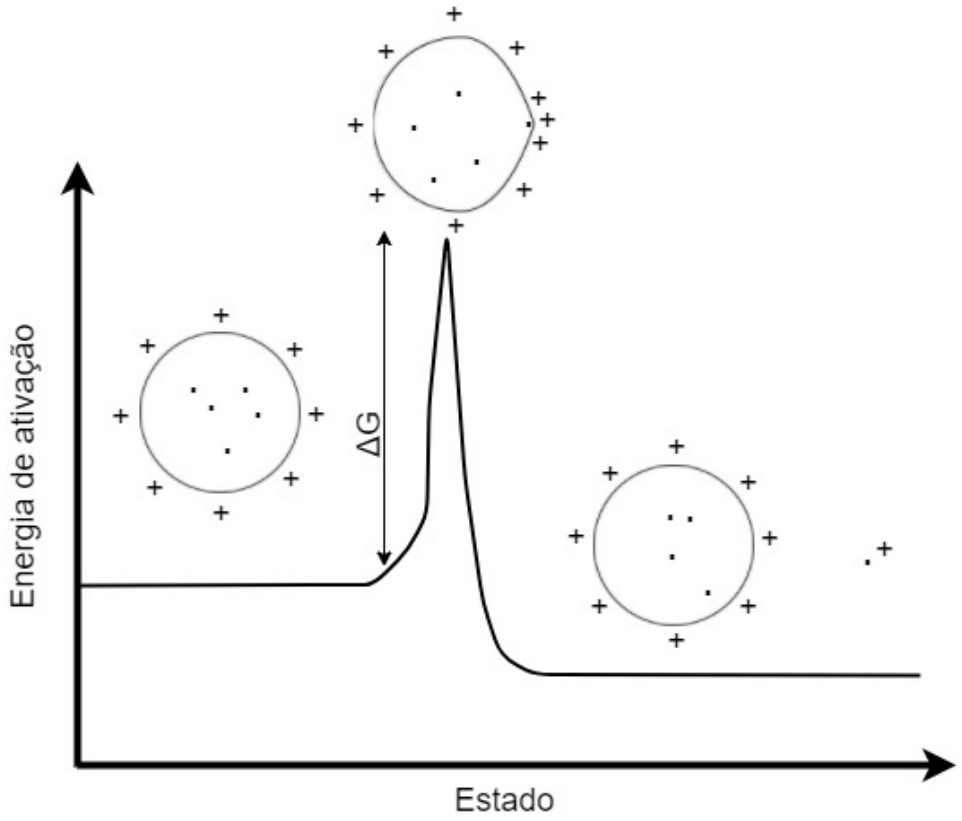

Figura 1.6. Energia de ativação para o processo do IEM.

Atualmente, o CRM é explicado para íões moleculares acima de 1000 Da, que são gerados por dessolvatação passiva. O IEM é amplamente aceite para íões menores, expulsos da gotícula por um campo elétrico [87].

Após o processo de eletrospray, os íões gerados são fragmentados na célula de colisão para obter as informações estruturais dos analitos através de um analisador de massa.

1.6. Analisadores de massa

Cada analisador de massa possui diferentes características de separação, conforme a tabela abaixo (**Tabela 1.3**), que têm vantagens e limitações. Para a seleção do analisador de massa, devem considerar-se propriedades como intervalo de massa, tempo de análise, transmissão, precisão de massa e resolução [79]:

- Intervalo de massa é o intervalo de *m/z* a que o analisador de massa opera. É expresso em Th (Thomson) ou u (unidade de massa aómica unificada);
- Tempo de análise ou velocidade de varrimento, expresso em unidade de massa por segundo (u s^{-1}) ou em unidade de massa por milissegundo (u ms^{-1}), é a taxa de varrimento em um intervalo de massa específico;
- Transmissão é a razão entre o número de íões que são detectados e os íões produzidos na fonte de ionização. A eficiência é limitada pelas perdas ao longo do processo;
- Precisão de massa é a diferença entre o *m/z* teórico e o *m/z* observado, é normalmente expresso em partes por milhão (ppm) ou em unidades de milimassa (mmu);
- Poder de resolução é a capacidade do analisador em distinguir dois íões com *m/z* próximos. A IUPAC recomenda dois métodos para avaliar o poder de resolução [88]: método da definição de 10% do vale, em que dois iões da mesma intensidade com massas M e ΔM, respectivamente, separados por um vale cujo ponto mais baixo representa 10% da altura dos picos (**Figura 1.7A**); no método da definição da largura dos picos correspondentes aos iões, o poder de resolução é definido por M/ΔM, onde M se refere- à massa de um único ião e ΔM é a largura do pico a uma determinada altura que é uma fração da sua altura máxima (**Figura 1.7B**). É recomendado o uso de três frações: 50, 5 ou 0.5%. A fração frequentemente utilizada é a de 50%, denominado-se largura total do pico

a metade de sua altura máxima (FWHM, *full width of the peak at half its maximum height*).

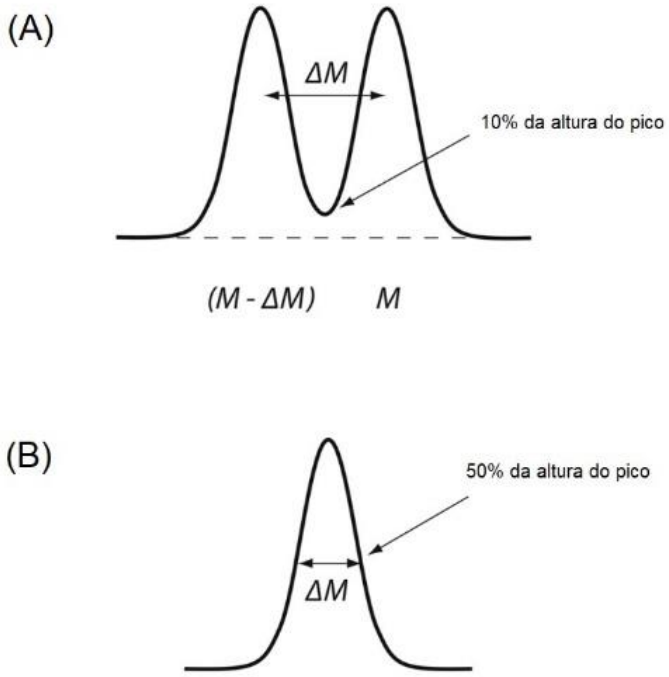

Figura 1.7. Métodos para avaliar o poder de resolução. (A) representa o método da definição de 10% do vale e (B) a largura total do pico na metade da sua altura máxima. Adaptado de [89].

Tabela 1.3. Analisadores de massa e os princípios de separação [79].

Analisador de massa	**Símbolo**	**Princípio de separação**
Setor elétrico	E ou ESA	Energia cinética
Setor magnético	B	*Momentum*
Quadrupolo	Q	Estabilidade da trajetória (*m/z)*
Íon trap	IT	Frequência de ressonância (*m/z)*
Tempo de voo	TOF	Velocidade do tempo de voo
Orbitrap	orbitrap	Frequência de ressonância (*m/z*)
Ressonância ciclotrónica de ião com transformada de Fourier	FT-ICR	Frequência de ressonância (*m/z*)

Este trabalho utilizou dois tipos de analisadores tandem (MS/MS), mais propriamente MS/MS no espaço, ou seja, dois analisadores de massa em série: TQMS e QTOF-MS. Os fundamentos destes analisadores de massa estão descritos abaixo.

1.6.1. Analisador de massa do tipo quadrupolo

O analisador de massa quadrupolar consiste em quatro hastes cilíndricas ou hiperbólicas configuradas em uma formação quadrada com pares opostos (**Figura 1.8**). O princípio foi inicialmente elaborado por Paul e Steinwegen em 1953 [90]. Um par de hastes opera com potencial positivo, enquanto o outro, opera a um potencial negativo, alternando o potencial entre si ao longo da trajetória dos iões. Este tipo de analisador possui como vantagens o tamanho, o ser compacto e de baixo peso, rápida taxa de varrimento, baixo custo, alta eficiência de transmissão e uma gama de massa até *m/z* 4000 [79].

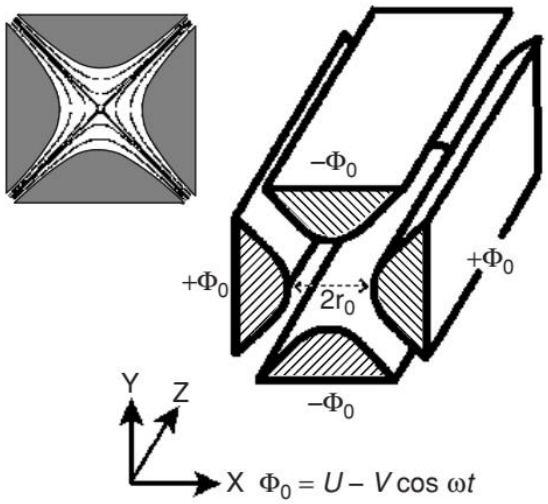

Figura 1.8. Quadruplo com barras hiperbólicas e a potência aplicada [78].

O princípio baseia-se na separação dos iões de acordo com a razão *m/z.* O valor *m/z* é definido pela aplicação de uma corrente contínua (DC) combinada com radiofrequência (RF) nas barras. O campo elétrico produzido tem a função de filtrar os valores *m/z* selecionados por meio da alteração da trajetória dos iões. Segue abaixo a equações do potencial elétrico do quadrupolo (**Equação 1.3**):

$$\Phi_0 = +(U - Vcos\omega t);\ -\Phi_0 = -(U - Vcos\omega t) \qquad \textbf{(Equação 1.3)}$$

Onde Φ_0 representa o potencial aplicado no par de barras; ω, a frequência angular (em radiano por segundo); U, a voltagem da DC e V, a amplitude da voltagem da RF.

As trajetórias dos iões entre as barras são influenciadas pelo campo elétrico. Os iões que não estão em ressonância com o campo aplicado terão as suas trajetórias instáveis e serão eliminados do sistema ao atingir as barras do quadrupolo [73,85]. As equações abaixo mostram dois fatores importantes para a definição de trajetória estável do ião (**Equação 1.7**):

$$a_x = a_u = -a_y = \frac{8zU}{(m/z)r_0^2\omega^2}\ ; q_x = q_u = -q_y = \frac{4zV}{(m/z)r_0^2\omega^2} \qquad \textbf{(Equação 1.4)}$$

Onde, a_x e q_x são os fatores no eixo *x*, a_y e q_y, fatores no eixo *y*, r_0 (raio do quadrupolo) e ω (frequência angular). Apresentam valores fixos e os parâmetros U (voltagem da DC) e V (amplitude da voltagem RF) são variáveis. A combinação desses dois fatores produz uma trajetória estável para o ião, a **Figura 1.9** mostra as regiões estáveis para o eixo x e y.

O quadrupolo pode ser utilizado em modo de varrimento de massa, porém esse método é indicado para análise qualitativa pelo fato de possuir baixa sensibilidade ou em modo de monitorização de ião selecionado (*SIM, selected ion monitoring*), onde o ião com *m/z* específico é detectado enquanto os outros iões de diferentes *m/z* são filtrados [79,91,92].

O analisador do tipo TQMS apresenta maior seletividade e sensibilidade em comparação com o quadrupolo único e consiste em três quadrupolos em série, sendo que o primeiro (Q1) e o terceiro (Q3) são considerados espectrómetros de massa, enquanto que o segundo (Q2) tem a função de atuar como célula de colisão, azoto ou árgon são os mais utilizados como gás de colisão (**Figura 1.10**).

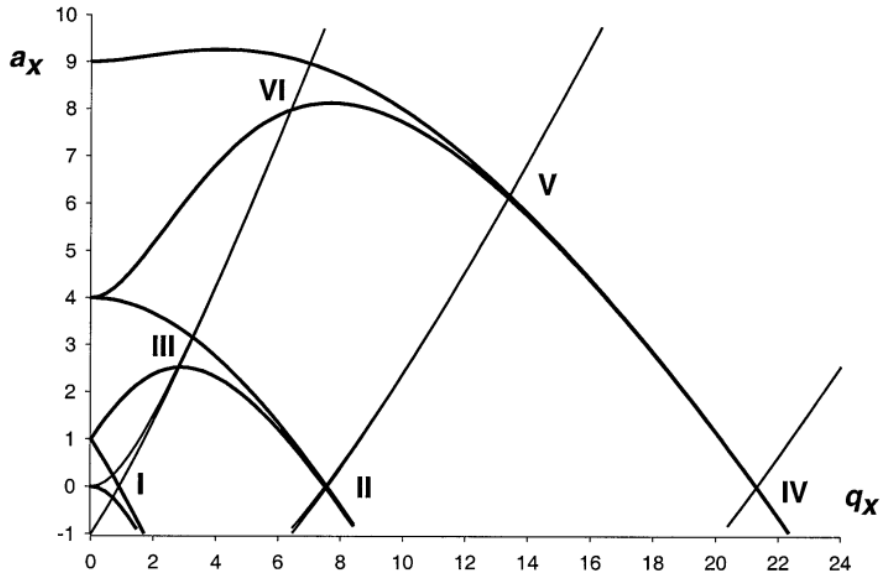

Figura 1.9. Diagrama geral de estabilidade 2d para o movimento do ião. Os números indicam diferentes regiões com estabilidade simultânea do eixo x e y [85].

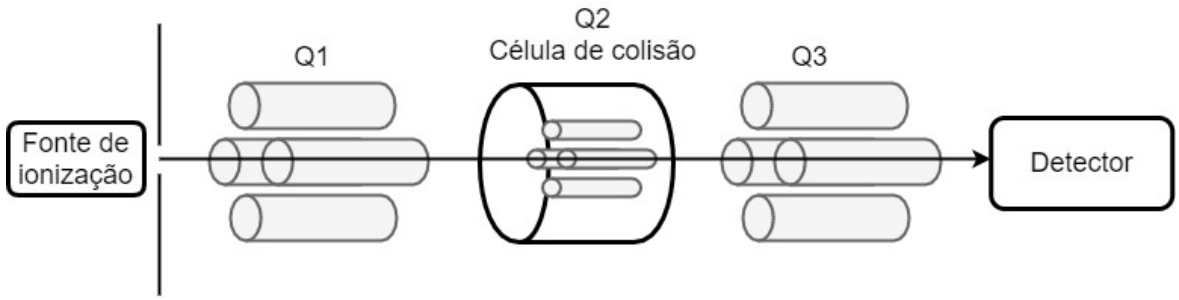

Figura 1.10. Diagrama do triplo quadrupolo (TQMS).

O principal modo de varrimento é a monitorização de reação múltipla (MRM) para a análise quantitativa, onde o Q1 seleciona o ião precursor de interesse e outros iões gerados de diferentes *m/z* são excluídos no primeiro quadrupolo. Na célula de colisão, onde ocorre a dissociação induzida por colisão (CID - *collision induced dissociation*) os iões produto gerados são transferidos para o Q3, onde somente os iões produto selecionados serão detectados [78,79].

No sistema triplo quadrupolo existem vários modos de análise (**Figura 1.11**). O modo de varrimento do ião produto consiste em selecionar o ião precursor no Q1 para em seguida colidir com o gás inerte e gerar iões fragmento para serem detectados, este modo tem como função obter informação estrutural sobre o ião precursor [78,79].

O modo de varrimento do ião precursor consiste em selecionar o ião produto específico no Q3 enquanto o Q1 realiza o varrimento de massa, este modo pode ser utilizado para detectar iões fragmento comuns numa classe de compostos. No modo varrimento de perda neutra, tanto Q1 quanto Q3 realizam o varrimento de massa porém, com um deslocamento de massa constante entre os dois. A função deste modo é semelhante ao modo de varrimento do ião precursor, ou seja, é útil para a identificação dos compostos pela análise da perda de um fragmento neutro [78,79].

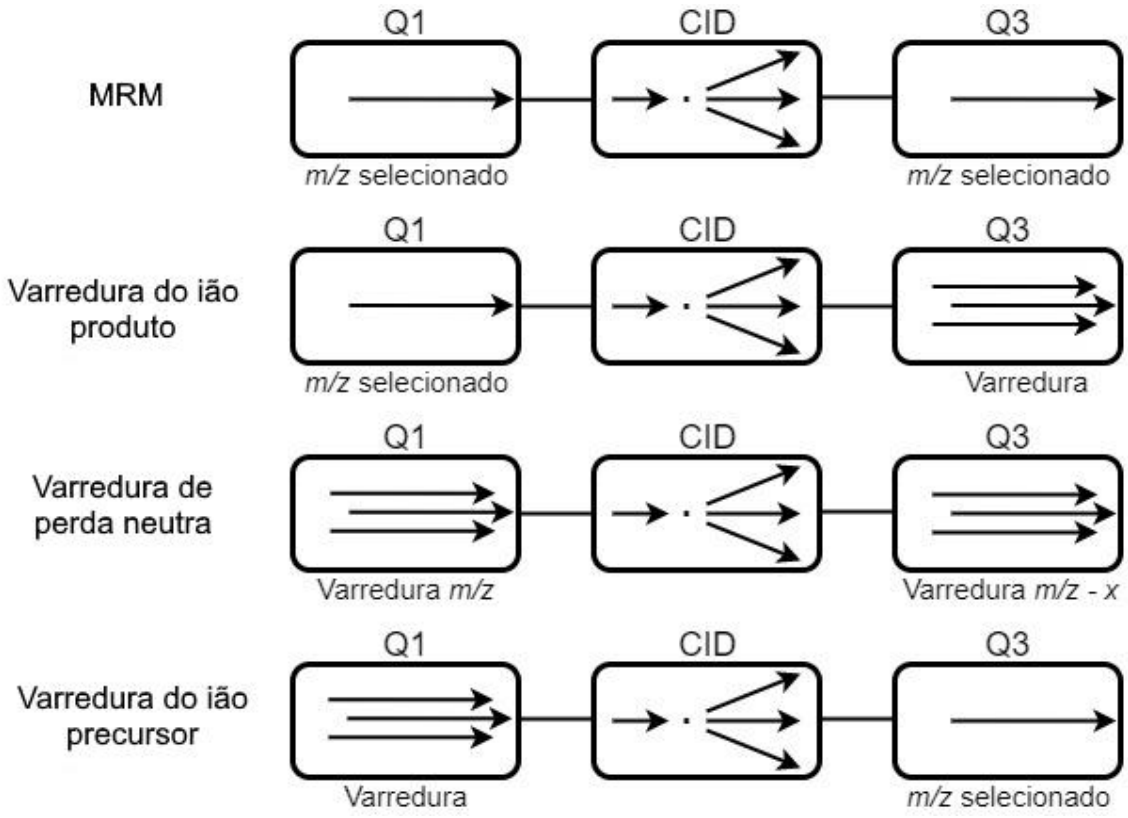

Figura 1.11. Diferentes modos de varrimento para o TQMS.

1.6.2. Analisador de massa do tipo tempo de voo

O primeiro analisador de massa do tipo tempo de voo foi construído por W. E. Stephens em 1946 [93]. O princípio básico de separação ocorre pelo tempo de voo dos iões, após serem acelerados em alta velocidade por um campo elétrico num tubo (*drift tube)*, em que iões de menores massas moleculares chegam antes ao detector em comparação com iões de maiores massas moleculares. Este processo,

idealmente, exige uma fonte de ionização pulsada. A **Figura 1.12** abaixo mostra um esquema de um TOF linear.

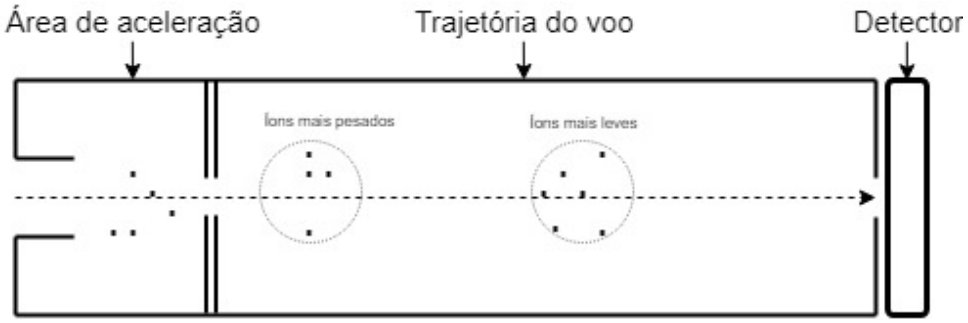

Figura 1.12. Representação de um TOF linear.

A velocidade estimada do íão é calculada pela equação (**Equação 1.5**):

$$v = \sqrt{\frac{2ezU}{m}} \qquad \textbf{(Equação 1.5)}$$

Onde ez é a carga total do íão com massa m e U é o potencial aplicado no processo, ou seja, a velocidade alcançada pelo íão é inversamente proporcional à raiz quadrada da massa.

O íão percorre o tubo a uma velocidade constante até ser detectado. O tempo necessário para o íão atingir o detector é calculado pela relação entre a distância s e a velocidade v (**Equação 1.6**):

$$t = \frac{s}{v} \qquad \textbf{(Equação 1.6)}$$

Logo, o tempo t é proporcional à raiz quadrada de $\frac{m}{z}$ (**Equação 1.7**):

$$t = \frac{s}{\sqrt{2eU}}\sqrt{\frac{m}{z}} \qquad \textbf{(Equação 1.7)}$$

Teoricamente, quanto maior o percurso e o tempo de voo dos iões, maior é o poder de resolução porém, com o aumento do *drift tube* ocorre a perda dos iões após a colisão com moléculas de gás ou por dispersão angular do feixe de iões, diminuindo o desempenho do analisador. Uma das maneiras de melhorar a resolução é o uso de um refletor *(reflectron)*.

O *reflectron* foi desenvolvido por Mamyrin em 1994 e é composto por uma série de lentes eletroestáticas localizadas ao final da trajetória de vôo que tem como função refletir os iões por meio de um campo eletrostático [94]. O refletor corrige o tempo de vôo dos iões, com valores *m/z* iguais, causadas pelas diferenças na energia cinética de dispersão. A **Figura 1.13** mostra um esquema genérico de um *reflectron*.

O tempo total de vôo com o *reflectron* é calculado pela equação (**Equação 1.8**):

$$t^2 = \frac{m}{z}\frac{(L1+L2+4d)^2}{2ez} \qquad \textbf{(Equação 1.8)}$$

Onde $L1$ e $L2$ são as distâncias de vôo antes e depois do *reflectron*, respectivamente e d é o comprimento total de vôo no *reflectron*.

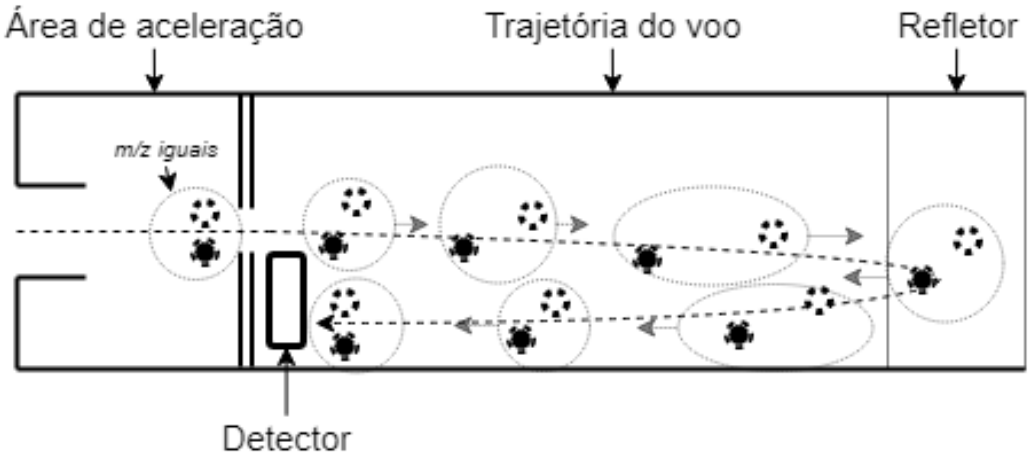

Figura 1.13. TOF linear com *reflectron*, onde é possível identificar duas moléculas com valores *m/z* iguais, mas com energias cinéticas iniciais diferentes.

O uso do *reflectron* pode aumentar em dez ou mais vezes o poder de resolução de massa deste equipamento em comparação com um TOF linear, porém possui a desvantagem de diminuir ligeiramente a sensibilidade devido à perda de íiões e à dispersão do feixe de iões, principalmente com iõess de maiores massas moleculares.

Outro modo de aumentar a resolução é o uso do sistema de aceleração ortogonal (*oa*, *orthogonal acelleration*), que tem como função extrair os pulsos de iões de um feixe de iões contínuo por meio de uma aceleração pulsada ortogonal. Como exemplo, a fonte de ionização por eletrospray, que produz um feixe contínuo de iões, pode ser acoplada a um oa-TOF [78,83].

A amostra é ionizada no sistema por um feixe de iões contínuo os quais são enviados na direção da região do campo livre, seguindo a orientação original. Porém, ao aplicar uma voltagem na placa, os iões alteram a orientação original e movem-se em direção ortogonal para serem detectados no analisador de massa. Após ocorrer a alteração na direção, os iões são acelerados por um potencial e ocorre a separação por *m/z*.

O oa-TOF pode ser empregado em sistemas lineares ou com *reflectrons* e possui vantagens em comparação com o TOF linear como: maior sensibilidade, maior poder de resolução, alta taxa de espectros por segundo, maior precisão de massa e *design* compacto [78,79,95].

1.6.3. Analisadores de massa híbridos

Analisadores híbridos são sistemas que possuem dois ou mais espectrómetros de massa que atuam de modo combinado com o objetivo de obter as vantagens de cada analisador de massa num único instrumento. A **Figura 1.14** mostra o princípio de funcionamento de um sistema híbrido QTOF-MS, que consiste em dois quadrupolos em série, sendo que o segundo tem a função de célula de colisão seguido do TOF com aceleração ortogonal e *reflectron*. Em alguns analisadores híbridos o segundo quadrupolo é substituído por um hexapolo [96], mas o princípio básico permanece o mesmo.

No caso do QTOF-MS, em modo MS, os quadrupolos operam somente em radiofrequência, ou seja, têm somente a função de transmissão em que todos os iões são acelerados para o TOF. O espectro apresenta alta resolução e alta precisão de massa, mas a transmissão dos quadrupolos limita a faixa de massas analisada.

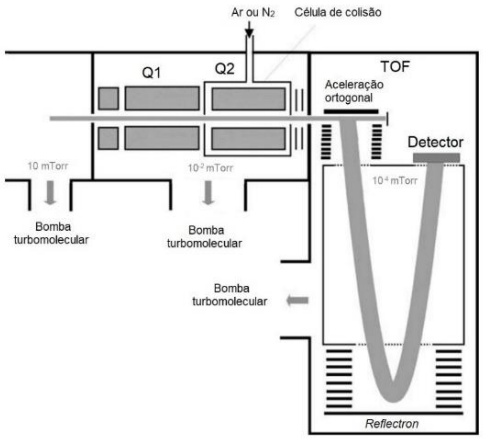

Figura 1.14. Esquema de um espectrómetro híbrido QTOF-MS. Adaptado de [78].

Em modo MS/MS, o Q1 tem a finalidade de selecionar os iões precursores de interesse. Então, os iões são acelerados por uma diferença de potencial entre 20 a 200 eV para o Q2, onde ocorre o CID por meio das moléculas neutras de gás (árgon ou azoto). Os fragmentos gerados e os iões precursores restantes são acelerados ortogonalmente para serem refletidos no *reflectron* e finalmente serem detectados [79,89]. A **Figura 1.15** resume possíveis combinações dos analisadores de massa.

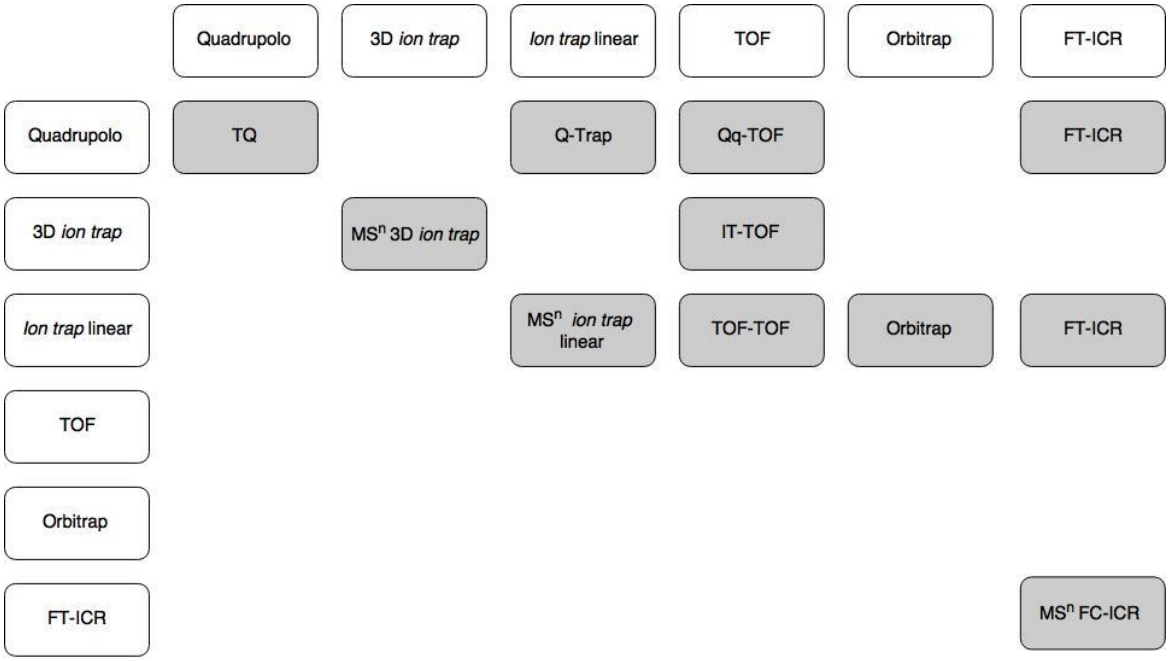

Figura 1.15. Esquema das combinações dos analisadores de massa. Adaptado de [89].

1.7. Objetivos da tese

A tese teve como objetivo inicial quantificar os fármacos em efluentes para avaliar a persistência destes contaminantes. O desenvolvimento e a validação do método foram realizados por extrações em fase sólida (SPE) e HPLC-TQMS. A partir deste resultado preliminar, foram empregados diferentes processos de degradação destes poluentes como a cloração, fotólise e fotocatálise sob irradiação UV−Vis e Vis utilizando nanomateriais dopados com metais. Em seguida, os perfis cinéticos foram avaliados e as rotas de degradações juntamente com as estruturas dos TPs foram propostas por meio das análises dos padrões de fragmentações obtidos por UHPLC-QTOF-MS. Por fim, as toxicidades por modelos computacionais (*in silico*) foram empregadas para identificar os potenciais tóxicos dos TPs.

1.8. Referências

1. Garrison, A.W., Pope, J.D., Allen, F.R. 1975. GC/MS analysis of organic compounds in domestic wastewaters. Em: *Identification and Analysis of Organic Pollutants in Water*. Ann Arbor Science Publishers, Michigan. 517–556.

2. Hignite, C., Azarnoff, D.L. 1977. Drugs and drug metabolites as environmental contaminants: Chlorophenoxyisobutyrate and salicyclic acid in sewage water effluent. *Life Sci*. 20, 337–341.

3. Sanderson, H., Brain, R.A., Johnson, D.J., Wilson, C.J., Solomon, K.R., 2004. Toxicity classification and evaluation of four pharmaceuticals classes: antibiotics, antineoplastics, cardiovascular, and sex hormones. *Toxicology* 203, 27–40. doi:10.1016/j.tox.2004.05.015

4. Stuart, M., Lapworth, D., Crane, E., Hart, A., 2012. Review of risk from potential emerging contaminants in UK groundwater. *Sci. Total Environ*. 416, 1-21. doi: 10.1016/j.scitotenv.2011.11.072

5. Postigo, C., Richardson, S.D., 2014. Transformation of pharmaceuticals during oxidation / disinfection processes in drinking water treatment. *J. Hazard. Mater*. 279, 461–475. doi:10.1016/j.jhazmat.2014.07.029

6. Salma, A., Thoröe-boveleth, S., Schmidt, T.C., Tuerk, J., 2016. Dependence of transformation product formation on pH during photolytic and photocatalytic degradation of ciprofloxacin. *J. Hazard. Mater*. 313, 49–59. doi:10.1016/j.jhazmat.2016.03.010

7. Wang, P., Yuan, T., Hu, J., Tan, Y., 2011. Determination of cephalosporin antibiotics in water samples by optimised solid phase extraction and high performance liquid

chromatography with ultraviolet detector. *Int J Environ Anal Chem*. 91(13), 37–41. doi:10.1080/03067311003778649

8. Negreira, N., López, M., Alda, D., Barceló, D., 2014. Cytostatic drugs and metabolites in municipal and hospital wastewaters in Spain: Filtration, occurrence and environmental risk. Sci. *Total Environ.* 498, 68–77. doi:10.1016/j.scitotenv.2014.07.101

9. Vulliet, E., Wiest, L., Baudot, R., 2008. Multi-residue analysis of steroids at sub-ng/L levels in surface and ground-waters using liquid chromatography coupled to tandem mass spectrometry. *J. Chromatogr. A* 1210, 84–91. doi:10.1016/j.chroma.2008.09.034

10. Sorensen, J.P.R., Lapworth, D.J., Nkhuwa, D.C.W., Stuart, M.E., Gooddy, D.C., Bell, R.A., Chirwa, M., Kabika, J., Liemisa, M., Chibesa, M., Pedley, S., 2014. Emerging contaminants in urban groundwater sources in Africa. *Water Res*. 72, 51–63. doi:10.1016/j.watres.2014.08.002

11. Aznar, R., Sánchez-brunete, C., Albero, B., Rodríguez, J.A., Tadeo, J.L., 2013. Occurrence and analysis of selected pharmaceutical compounds in soil from Spanish agricultural fields. *Environ Sci Pollut Res Int*. 21(6), 4772-4782. doi:10.1007/s11356-013-2438-7

12. Caban, M., Lis, E., Kumirska, J., Stepnowski, P., 2015. Determination of pharmaceutical residues in drinking water in Poland using a new SPE-GC-MS (SIM) method based on Speedisk extraction disks and DIMETRIS derivatization. *Sci. Total Environ*. 538, 402–411. doi:10.1016/j.scitotenv.2015.08.076

13. Simazaki, D., Kubota, R., Suzuki, T., Akiba, M., 2015. Occurrence of selected pharmaceuticals at drinking water purification plants in Japan and implications for human health. *Water Res*. 76, 187–200. doi:10.1016/j.watres.2015.02.059

14. Kasprzyk-Hordern, B., Dinsdale, R.M., Guwy, A.J., 2008. The occurrence of pharmaceuticals, personal care products, endocrine disruptors and illicit drugs in surface water in South Wales, UK. *Water Res*. 42, 3498–518. doi:10.1016/j.watres.2008.04.026

15. Pino-Otín, M.R., Muñiz, S., Val, J., Navarro, E., 2017. Effects of 18 pharmaceuticals on the physiological diversity of edaphic microorganisms. *Sci. Total Environ*. 595, 441–450. doi:10.1016/j.scitotenv.2017.04.002

16. Rainieri, S., Barranco, A., Primec, M., Langerholc, T., 2017. Occurrence and toxicity of musks and UV filters in the marine environment. *Food Chem. Toxicol*. 104, 57–68. doi:10.1016/j.fct.2016.11.012

17. U.S. EPA. Third Unregulated Contaminant Monitoring Rule. 2012. Federal Register 77, Issue 85.

18. Directive 2013/39/EU. 2013. Directive 2013/39/EU of the European Parliament and of the Council of 12 August 2013 amending Directives 2000/60/EC and 2008/ 105/EC as regards priority substances in the field of water policy. *Off. J. Eur.Union* 226, 1-17.

19. Evgenidou, E.N., Konstantinou, I.K., Lambropoulou, D.A., 2015. Occurrence and removal of transformation products of PPCPs and illicit drugs in wastewaters : A review. *Sci. Total Environ*. 505, 905–926. doi:10.1016/j.scitotenv.2014.10.021

20. Subedi, B., Kannan, K., 2015. Occurrence and fate of select psychoactive pharmaceuticals and antihypertensives in two wastewater treatment plants in New York. *Sci. Total Environ*. 514, 273–280. doi:10.1016/j.scitotenv.2015.01.098

21. Escher, B.I., Fenner, K., 2011. Recent Advances in Environmental Risk Assessment of Transformation Products. *Environ. Sci. Technol*. 45, 3835–3847. doi:10.1021/es1030799

22. Trautwein, C., Kümmerer, K., 2012. Degradation of the tricyclic antipsychotic drug chlorpromazine under environmental conditions, identification of its main aquatic biotic and abiotic transformation products by LC–MS^n and their effects on environmental bacteria. *J. Chromatogr. B* 889–890, 24–38. doi:10.1016/j.jchromb.2012.01.022

23. Halling-Dørensen, B.J., Nors, S.N., Lanzky, P.F., Ingerslev, F., Liitzhofl, H.H.C., Jorgenson, S.E. 1998. Occurrence, Fate and Effects of Pharmaceutical Substances in the Environment- A Review. *Chemosphere*. 36(2), 357-393. doi:10.1016/S0045-6535(97)00354-8

24. Bauer, L. A. 2008. *Applied Clinical Pharmacokinetics*, 3ª edição, McGraw-Hill. New York. doi:10.1036/0071476288

25. Verlicchi, P., Al Aukidy, M., Zambello, E., 2012. Occurrence of pharmaceutical compounds in urban wastewater: removal, mass load and environmental risk after a secondary treatment--a review. *Sci. Total Environ*. 429, 123–55. doi:10.1016/j.scitotenv.2012.04.028

26. Gurke, R., Rößler, M., Marx, C., Diamond, S., Schubert, S., Oertel, R., Fauler, J., 2015. Occurrence and removal of frequently prescribed pharmaceuticals and corresponding metabolites in wastewater of a sewage treatment plant. *Sci. Total Environ*. 532, 762–770. doi:10.1016/j.scitotenv.2015.06.067

27. Petrovic, M., 2009. Fate and distribution of pharmaceuticals in wastewater and sewage sludge of the conventional activated sludge (CAS) and advanced membrane bioreactor (MBR) treatment. *Water Res*. 43, 831–841. doi:10.1016/j.watres.2008.11.043

28. Ben, M.E., Tarchitzky, J., Chen, Y., Shenker, M., Chefetz, B., 2017. Composted biosolids and treated wastewater as sources of pharmaceuticals and personal care products for plant uptake: A case study with carbamazepine. *Environ. Pollut*. 232, 164-172. doi:10.1016/j.envpol.2017.09.029

29. Schwake-anduschus, C., Rubner-institut, M., Heyser, W., 2007. Incorporation of veterinary antibiotics into crops from manured soil. *Landbauforschung Völkenrode* 1 (57), 25-32

30. Xian-gang, H.U., Yi, L., Qi-xing, Z., Lin, X.U., 2008. Determination of thirteen antibiotics residues in manure by solid phase extraction and high performance liquid chromatography. *Chinese J. Anal. Chem.* 36, 1162–1166. doi:10.1016/S1872-2040(08)60063-8

31. Hu, X., Zhou, Q., Luo, Y., 2010. Occurrence and source analysis of typical veterinary antibiotics in manure, soil, vegetables and groundwater from organic vegetable bases, northern China. *Environ. Pollut*. 158, 2992–2998. doi:10.1016/j.envpol.2010.05.023

32. Löffler, D., Römbke, J., Meller, M., Ternes, T.A. 2005. Environmental Fate of Pharmaceuticals in Water/Sediment Systems. *Environ. Sci. Technol*. 39, 5209-5218. doi:10.1021/es0484146

33. Yamamoto, H., Nakamura, Y., Moriguchi, S., Nakamura, Y., Honda, Y., Tamura, I., Hirata, Y., Hayashi, A., Sekizawa, J. 2009. Persistence and partitioning of eight selected pharmaceuticals in the aquatic environment : laboratory photolysis, biodegradation, and sorption experiments. Water Res. 43(2), 351–361. doi:10.1016/j.watres.2008.10.039

34. Bueno, M.J.M., Gomez, M.J., Herrera, S., Hernando, M.D., Agüera, A., Fernández-alba, A.R., 2012. Occurrence and persistence of organic emerging contaminants and priority pollutants in five sewage treatment plants of Spain: Two years pilot survey monitoring. *Environ. Pollut*. 164, 267–273. doi:10.1016/j.envpol.2012.01.038

35. Collado, N., Rodriguez-mozaz, S., Gros, M., Rubirola, A., Barceló, D., Comas, J., Rodriguez-roda, I., Buttiglieri, G., 2014. Pharmaceuticals occurrence in a WWTP with significant industrial contribution and its input into the river system. *Environ. Pollut*. 185, 202–212. doi:10.1016/j.envpol.2013.10.040

36. Golovko, O., Kumar, V., Fedorova, G., Randak, T., Grabic, R., 2014. Chemosphere Seasonal changes in antibiotics, antidepressants/ psychiatric drugs, antihistamines and lipid regulators in a wastewater treatment plant. *Chemosphere* 111, 418–426. doi:10.1016/j.chemosphere.2014.03.132

37. Baalbaki, Z., Sultana, T., Metcalfe, C., Yargeau, V., 2017. Estimating removals of contaminants of emerging concern from wastewater treatment plants: The critical role of wastewater hydrodynamics. *Chemosphere* 178, 439–448. doi:10.1016/j.chemosphere.2017.03.070

38. Guerra, P., Kim, M., Shah, A., Alaee, M., Smyth, S.A., 2014. Science of the Total Environment Occurrence and fate of antibiotic, analgesic/anti-in fl ammatory, and antifungal compounds in five wastewater treatment processes. *Sci. Total Environ*. 473–474, 235–243. doi:10.1016/j.scitotenv.2013.12.008

39. Gros, M., Rodríguez-mozaz, S., Barceló, D., 2012. Fast and comprehensive multi-residue analysis of a broad range of human and veterinary pharmaceuticals and some of their metabolites in surface and treated waters by ultra-high-performance liquid chromatography coupled to quadrupole-linear ion trap tandem mass spectrometry. J*. Chromatogr. A* 1248, 104–121. doi:10.1016/j.chroma.2012.05.084

40. Baker, D.R., Kasprzyk-hordern, B., 2013. Spatial and temporal occurrence of pharmaceuticals and illicit drugs in the aqueous environment and during wastewater treatment: New developments. *Sci. Total Environ*. 454–455, 442–456. doi:10.1016/j.scitotenv.2013.03.043

41. Fent, K., Weston, A., Caminada, D. 2006. Ecotoxicology of human pharmaceuticals. *Aquat. Toxicol*. 76(2), 122–59. doi: 10.1016/j.aquatox.2005.09.009

42. Barry, M.J., 2013. Effects of fluoxetine on the swimming and behavioural responses of the Arabian killifish. *Ecotoxicology* 22(2), 425–432. doi:10.1007/s10646-012-1036-7

43. Kohlert, J.G., Mangan, B.P., Kodra, C., Drako, L., Long, E., Simpson, H., 2012. Decreased aggressive and locomotor behaviors in Betta splendens after exposure to fluoxetine. *Psychol. Rep*. 110(1), 51–62. doi:10.2466/02.13.PR0.110.1.51-62

44. M, Cleuvers. 2003. Aquatic ecotoxicity of pharmaceuticals including the assessment of combination effects, *Toxicol. Lett*. 142(3), 185–194. doi: 10.1016/S0378-4274(03)00068-7

45. Schnell, S., Bols, N.C., Barata, C., Porte, C., 2009. Single and combined toxicity of pharmaceuticals and personal care products (PPCPs) on the rainbow trout liver cell line RTL-W1. *Aquat. Toxicol*. 93(4), 244–252. doi:10.1016/j.aquatox.2009.05.007

46. Rosal, R., Rodea-palomares, I., Boltes, K., Fernández-piñas, F., Leganés, F., Petre, A., 2010. Ecotoxicological assessment of surfactants in the aquatic environment: Combined toxicity of docusate sodium with chlorinated pollutants. *Chemosphere* 81, 288–293. doi:10.1016/j.chemosphere.2010.05.050

47. Trovó, A.G., Nogueira, R.F.P., Agüera, A., Sirtori, C., Fernández-alba, A.R., 2009. Photodegradation of sulfamethoxazole in various aqueous media: Persistence, toxicity and photoproducts assessment. *Chemosphere* 77, 1292–1298. doi:10.1016/j.chemosphere.2009.09.065

48. Isidori, M., Lavorgna, M., Nardelli, A., Parrella, A., Previtera, L., Rubino, M., 2005. Ecotoxicity of naproxen and its phototransformation products. *Sci. Total Environ.* 348, 93–101. doi:10.1016/j.scitotenv.2004.12.068

49. Rubirola, A., Llorca, M., Rodriguez-mozaz, S., Casas, N., 2014. Characterization of metoprolol biodegradation and its transformation products generated in activated sludge batch experiments and in full scale WWTPs. *Water Res*. 63, 21–32. doi:10.1016/j.watres.2014.05.031

50. Ferrando-Climent, L., Collado, N., Buttiglieri, G., Gros, M., Rodriguez-Roda, I., Rodriguez-Mozaz, S., Barcelo, D., 2012. Comprehensive study of ibuprofen and its metabolites in activated sludge batch experiments and aquatic environment. *Sci. Total Environ*. 438, 404–413. doi: 10.1016/j.scitotenv.2012.08.073

51. Christensen, E.R., Li, A. 2014. *Physical and chemical processes in the aquatic environment*. 1ª edição, Wiley & Sons, Inc. Hoboken. 255–259

52. Ghattas, A., Fischer, F., Wick, A., Ternes, T.A., 2017. Anaerobic biodegradation of (emerging) organic contaminants in the aquatic environment. *Water Res*. 116, 268–295. doi:10.1016/j.watres.2017.02.001

53. Koumaki, E., Mamais, D., Noutsopoulos, C., Nika, M., Bletsou, A.A., Thomaidis, N.S., Eftaxias, A., Stratogianni, G., 2015. Degradation of emerging contaminants from water under natural sunlight: The effect of season, pH, humic acids and nitrate and identification of photodegradation by-products. *Chemosphere* 138, 675–681. doi:10.1016/j.chemosphere.2015.07.033

54. Heberer, T., 2002. Occurrence, fate, and removal of pharmaceutical residues in the aquatic environment: a review of recent research data. *Toxicol. Lett*. 131, 5–17. doi: 10.1016/S0378-4274(02)00041-3

55. Remucal, C.K., 2014. The role of indirect photochemical degradation in the environmental fate of pesticides: a review. *Environ. Sci. Process*. *Impacts* 16 (4), 628–653. doi: 10.1039/C3EM00549F

56. Salgado, R., Pereira, V.J., Carvalho, G., Soeiro, R., Gaffney, V., Almeida, C., Cardoso, V.V., Ferreira, E., Benoliel, M.J., Ternes, T.A., Oehmen, A., Reis, M.A.M., Noronha, J.P.,

2013. Photodegradation kinetics and transformation products of ketoprofen, diclofenac and atenolol in pure water and treated wastewater. *J. Hazard. Mater*. 244–245, 516–527. doi:10.1016/j.jhazmat.2012.10.039

57. Ferrer, I., Mezcua, M., Thurman, Jose, M.J., Thurman, E.M., Agüera, A., Hernando, M.D., Fernández-Alba, A.R., 2004. Liquid chromatography/time-of-flight mass spectrometric analyses for the elucidation of the photodegradation products of triclosan in wastewater samples. *Rapid Commun. Mass Spectrom*. 18(3), 443–450. doi:10.1002/rcm.1351

58. Gutowski, L., Olsson, O., Leder, C., Kümmerer, K., 2015. A comparative assessment of the transformation products of S-metolachlor and its commercial product Mercantor Gold® and their fate in the aquatic environment by employing a combination of experimental and *in silico* methods. *Sci. Total Environ*. 506–507, 369–379. doi:10.1016/j.scitotenv.2014.11.025

59. Melnikov, F., Kostal, J., Voutchkova-Kostal, A., Zimmerman, J.B., Anastas, P.T., 2016. Assessment of predictive models for estimating the acute aquatic toxicity of organic chemicals. *Green Chem*. 18, 4432–4445. doi:10.1039/c6gc00720a

60. Raies, A.B., Bajic, V.B., 2016. *In silico* toxicology: computational methods for the prediction of chemical toxicity. *WIREs Comput. Mo.l Sci*. 6, 147–172. doi:10.1002/wcms.1240

61. Bakhtyari, N.G., Raitano, G., Benfenati, E., Martin, T., Young, D., 2013. Comparison of in silico models for prediction of mutagenicity. *J. Environ. Sci. Heal. - Part C Environ. Carcinog. Ecotoxicol. Rev*. 31, 45–66. doi:10.1080/10590501.2013.763576

62. Golbamaki, A., Cassano, A., Lombardo, A., Moggio, Y., Colafranceschi, M., Benfenati, E., 2014. Comparison of in silico models for prediction of *Daphnia magna* acute toxicity. *SAR QSAR Environ. Res*. 25, 673–694. doi:10.1080/1062936X.2014.923041

63. Pérez-Moya, M., Graells, M., Castells, G., Amigó, J., Ortega, E., Buhigas, G., Pérez, L.M., Mansilla, H.D. 2010. Characterization of the degradation performance of the sulfamethazine antibiotic by photo-Fenton process. *Water Res*. 44, 2533–2540. doi:10.1016/j.watres.2010.01.032

64. Lekkerkerker-teunissen, K., Benotti, M.J., Snyder, S.A., Dijk, H.C. Van, 2012. Transformation of atrazine, carbamazepine, diclofenac and sulfamethoxazole by low and medium pressure UV and UV/H_2O_2 treatment. *Sep. Purif. Technol*. 96, 33–43. doi:10.1016/j.seppur.2012.04.018

65. Ani, I.J., Akpan, U.G., Olutoye, M.A., Hameed, B.H., 2018. Photocatalytic degradation of pollutants in petroleum refinery wastewater by TiO_2- and ZnO-based photocatalysts: Recent development. *J. Clean. Prod*. 205, 930–954. doi:10.1016/j.jclepro.2018.08.189

66. Deng, F., Zhong, F., Lin, D., Zhao, L., Liu, Y., Huang, J., Luo, X., Luo, S., Dionysiou, D.D., 2017. One-step hydrothermal fabrication of visible-light-responsive $AgInS_2$/$SnIn_4S_8$ heterojunction for highly-efficient photocatalytic treatment of organic pollutants and real pharmaceutical industry wastewater. *Appl. Catal. B Environ*. 219, 163–172. doi:10.1016/j.apcatb.2017.07.051

67. Wang, A. nan, Teng, Y., Hu, X. feng, Wu, L. hua, Huang, Y. juan, Luo, Y. ming, Christie, P., 2016. Diphenylarsinic acid contaminated soil remediation by titanium dioxide (P25)

photocatalysis: Degradation pathway, optimization of operating parameters and effects of soil properties. *Sci. Total Environ*. 541, 348–355. doi:10.1016/j.scitotenv.2015.09.023

68. Ameta, R., Ameta, S.C., 2017. *Photocatalysis: Principles and applications*. CRC Press. Taylor & Francis Group. New York.

69. Kischm H. 2015. Semiconductor photocatalysis principles and applications. Wiley-VCH. Weinheim.

70. Barrocas, B.T., Oliveira, M.C., Nogueira, H.I.S., Fateixa, S., Monteiro, O.C., 2019. ruthenium-modified titanate nanowires for the photocatalytic oxidative removal of organic pollutants from water. *ACS Appl. Nano Mater*. acsanm.8b02215. doi:10.1021/acsanm.8b02215

71. Belver, C., Bedia, J., Rodriguez, J.J., 2017. Zr-doped TiO_2 supported on delaminated clay materials for solar photocatalytic treatment of emerging pollutants. *J. Hazard. Mater*. 322, 233–242. doi:10.1016/j.jhazmat.2016.02.028

72. Li, C., Chen, G., Sun, J., Rao, J., Han, Z., Hu, Y., Xing, W., Zhang, C., 2016. Doping effect of phosphate in Bi_2WO_6 and universal improved photocatalytic activity for removing various pollutants in water. *Appl. Catal. B Environ*. 188, 39–47. doi:10.1016/j.apcatb.2016.01.054

73. Mahmoud, S.A., Fouad, O.A., 2015. Synthesis and application of zinc/tin oxide nanostructures in photocatalysis and dye sensitized solar cells. *Sol. Energy Mater. Sol. Cells* 136, 38–43. doi:10.1016/j.solmat.2014.12.035

74. Thomson, J.J. 1913. *Rays of positive electricity and their application to chemical analysis*. 2ª edição, Longmans Green. London.

75. Dempster, A.J. 1918. A new Method of Positive Ray Analysis. *Phys. Rev.* **11**, 316–325. doi:10.1080/14786441208636004

76. Aston, F.W. 1919. A positive ray spectrograph. *Philos. Mag.* **38**, 707–714. doi:10.1080/14786441208636004

77. Van Bramer, S.E. 1997. *An Introduction to Mass Spectrometry*. Widener University. Chester, PA.

78. Gross, J.H. 2011. *Mass Spectrometry: A Textbook*. 2ª edição, Springer. Heldenberg. doi:10.1007/978-3-642-10711-5

79. Hoffmann, E., Stroobant, V. 2012. *Mass spectrometry: principles and applications*. 3ª edição, John Wiley & Sons. Chichester.

80. Fenn, J. B., Mann, M., Meng, C. K., Wong, S. F., Whitehouse, C. M. 1989. Electrospray ionization for mass spectrometry of large biomolecules. *Science* 246, 64–71

81. Ho, C.S., Lam, C.W.K., Chan, M.H.M., Cheung, R.C.K., Law, L.K., Lit, L.C.W., Ng, K.F., Suen, M.W.M., Tai, H.L., 2003. Electrospray Ionisation Mass Spectrometry: Principles and Clinical Applications. *Clin. Biochem. Rev*. 24, 3–12.

82. Gomez, A. and Tang, K. 1994. Charge and fission of droplets in electrostatic sprays. *Phys. Fluids* 6, 404. doi:10.1063/1.868037

83. Cole, R.B. 2000. Some tenets pertaining to electrospray ionization mass spectrometry. *J. Mass Spectrom*. 35, 763–772.

84. Dole, M., Mack, L.L., Hines, R.L., Mobley, R.C., Ferguson, L.D., Alice, M.B. 1968. Molecular beams of macroions. *J. Chem. Phys*. 49, 2240–2249.

85. Winger B.A., Light-Wahl K.J., Ogorzalek Loo R.R., Udseth H.R., Smith R.D. 1993. Observations and implications of high mass-to-charge ratio ions from electrospray ionization mass spectrometry. *J. Am. Soc. Mass. Spectrom*. 4, 536–545.

86. Iribarne, J., Thompson, B. 1976. On the evaporation of small ions from charged droplets. *J. Chem. Phys*. 64, 2287–2294.

87. Wilm, M. 2011. Principles of electrospray ionization. Mol. Cell. Proteomics 10(7). doi:10.1074/mcp.R111.009407

88. McNaught, A.D., Wilkinson, A. 1997. *IUPAC compendium of chemical terminology*. 2ª edição, Blackwell Scientific Publications. Oxford.

89. Hart-Smith, G. Blanksby, S.J. 2011. Mass Analysis. Em: *Mass Spectrometry in Polymer Chemistry*. Wiley Weinheim. doi: 10.1002/9783527641826.ch1

90. Paul, W. Steinwedel, H.S. 1953. Notizen: Ein neues Massenspektrometer ohne Magnetfeld (Notes: A new mass spectrometer without magnetic field). *Z. Naturforsch*. 8(7), 448–450.

91. Douglas, D.J. 2009. Linear quadrupoles in mass spectrometry. *Mass Spectrom. Rev.* 28, 937–960. doi:10.1002/mas.20249

92. Konenkov, N.V., Sudakov, M., Douglas, D.J. 2002. Matrix methods for the calculation of stability diagrams in quadrupole mass spectrometry. *J. Am. Soc. Mass Spectrom*. 13(6), 597–613. doi:10.1016/S1044-0305(02)00365-3

93. Stephens, W.E. 1946. A pulsed mass spectrometer with time dispersion. *Phys. Rev.* 69, 691. doi:10.1103/PhysRev.69.674.2

94. Mamyrin, B.A. 1994. Laser assisted reflectron time-of-flight mass spectrometry. *Int. J. Mass Spectrom. Ion Proc*. 131, 1–19. doi: 10.1016/0168-1176(93)03891-O

95. Chen, Y.H., Gonin, M., Fuhrer, K., Dodonov, A., Su, C.S., Wollnik, H. 1999. Orthogonal electron impact source for a time-of-flight mass spectrometer with high mass resolving power. *Int. J. Mass Spectrom.* 185–187, 221–226. doi:10.1016/S1387-3806(98)14152-0

96. Morris, H.R., Paxton, T., Dell, A. Langhorne, J., Berg, M., Bordoli, R.S., Hoyes, J., Bateman, R.H. 1996. High sensitivity collisionally-activated decomposition tandem mass spectrometry on a novel quadrupole/orthogonal-acceleration time-of-flight mass spectrometer. *Rapid Commun. Mass Spectrom*. 10, 889–896. doi: 10.1002/(SICI)1097-0231(19960610)10:8<889::AID-RCM615>3.0.CO;2-F

Capítulo 2

Validação do método analítico por SPE e HPLC-TQMS

2.1. Introdução

A espectrometria de massa tandem (MS/MS) acoplada a técnicas de separação, como cromatografia líquida de alta performance (HPLC) e cromatografia em fase gasosa, tem sido notável nos últimos anos para a detecção de contaminantes em matrizes ambientais. Neste contexto, a validação do método analítico é necessária para garantir resultados confiáveis.

A validação de um novo método analítico consiste em estabelecer parâmetros e requisitos mínimos para um procedimento analítico específico por meio de estudos para garantir a confiabilidade, consistência e precisão dos dados.

Os parâmetros para a validação de um novo método podem sofrer alterações entre organizações nacionais e internacionais. A União Internacional de Química Pura e Aplicada (IUPAC, *International Union of Pure and Applied Chemistry*) possui um documento técnico para validação de métodos analíticos [1]. A *US Food and Drug Administration* (FDA) elaborou dois documentos para validação de métodos [2], um para validação de métodos analíticos e outro para validação de métodos bioanalíticos. Existem guias para validação de métodos em amostras específicas, conforme proposto pelo Escritório das Nações Unidas contra Drogas e Crime (UNODOC, *United Nations Office on Drugs and Crime*) para drogas biológicas e materiais apreendidos [3].

Os parâmetros utilizados para a validação do método foram: seletividade, linearidade, sensibilidade, precisão, limite de detecção e quantificação e robustez.

- A seletividade é a capacidade de detectar o analito de interesse em uma amostra com componentes que podem interferir no resultado, como impurezas e produtos de degradação. A seletividade garante que o pico do analito seja exclusivamente do composto.
- Linearidade é a capacidade do método para obter resultados linearmente proporcionais às concentrações de analito.
- Sensibilidade é a capacidade do método para diferenciar duas concentrações.
- A precisão é o acordo entre a concentração real de analito e a estimativa pela análise.

- O limite de detecção é a menor concentração de analito que pode ser detectada, mas não quantificada, enquanto o limite de quantificação representa a menor concentração de analito que pode ser quantificada.

Este trabalho tem como objetivo otimizar os parâmetros de preparação de amostra e validar o método analítico por HPLC-TQMS para a análise de antidepressivos e anticancerígenos em matrizes ambientais.

2.2. Validação do método analítico

2.2.1. Químicos e reagentes

Os padrões cloridrato de duloxetina (DUL), cloridrato de bupropiona (BUP), cloridrato de venlafaxina (VEN) e bromidrato de citalopram (CIT) foram adquiridos da TCI Chemicals (Zwijndrecht, Bélgica). O cloridrato de amitriptilina (AMI), cloridrato de trazodona (TRA) e metotrexato (MET) e o padrão interno cloridrato de amitriptilina-d_3 (AMI- d_3) foram obtidos da Sigma-Aldrich Co (St. Louis, EUA) e a ifosfamida (IF) e monohidrato de ciclofosfamida (CP) foram adquiridos da Fluka (Buchs, Suíça). A água ultrapura foi preparada com o sistema Ultrapure Milli-Q (Barnstead International, Dubuque, EUA), o acetonitrila de grau LC-MS (ACN) foi adquirido da Sigma-Aldrich (Bedford, EUA) e o ácido clorídrico (HCl) foi adquirido da Fluka Chemical (Suíça).

Todos os fármacos possuem grau de pureza acima de 98%. As soluções foram preparadas em concentrações de 1000 mg L^{-1} de cada composto em metanol e armazenadas a uma temperatura de 60 °C.

2.2.2. Instrumentação

A separação foi realizada numa coluna recheada de octadecilsilano (C18-Sunfire 5 µm × 3 mm × 150 mm, Waters) num HPLC (Alliance, Waters 2695). A quantificação foi realizada num TQMS (Micromass Quattro Micro API, Waters) equipado com uma fonte de ionização por eletrospray.

As condições ideais para a separação cromatográfica foram realizadas a uma temperatura de 35 °C, consistindo a fase móvel em água ultrapura com 0.1% de ácido acético (A) e acetonitrila (B): 0 min, 1% de B; 8 min, 100% B; 8−10 min, 100% B; 15 min, 1% B. O fluxo foi de 0,3 mL min^{-1} e o volume de injeção das amostras foi de 10 µL. O amostrador automático foi mantido a 4 °C.

O espectrómetro de massa operou em modo de ionização positiva (ESI+) com voltagem capilar de 3 kV, temperatura da fonte de 120 °C, temperatura de dessolvatação de 350 °C, fluxo de gás de cone de 50 L h^{-1} e fluxo de gás de dessolvatação 750 L h^{-1}. Foi utilizado o modo de monitorização de reações múltiplas (MRM). As análises de dados foram realizadas usando o software Waters MassLynx v4.1.

2.2.3.Preparação de amostras

Amostras de água superficial (250 mL) foram coletadas em garrafas âmbar e armazenadas em caixas térmicas até à chegada ao laboratório. As garrafas foram previamente descontaminadas.

Dois filtros de membrana foram comparados na etapa de filtração da amostra: membrana de politetrafluoroetileno (PTFE) e de nylon, para identificar se existe a retenção dos compostos de interesse. A água potável foi utilizada sem ajuste do pH e os filtros de membrana tinham um tamanho de poro de 0,45 µm e a concentração foi de 1 mg L^{-1} de cada composto na mistura.

Após a escolha da membrana com o melhor resultado, a amostra foi ajustada para pH 3 (2% de ácido acético) ou 7 (hidróxido de amônio a 5%). As amostras foram extraídas em cartuchos de extração em fase sólida em um fluxo de 5−8 mL min^{-1} (Oasis HLB 200mg, 6 mL, Waters) previamente condicionadas com 5 mL de metanol e 5 mL de água ultrapura.

Posteriormente o cartucho foi lavado com uma solução de 5 mL de água com metanol a 5%. Os cartuchos foram secos com fluxo de azoto e foram eluídos com 5 mL de metanol e 2 mL de acetona/metanol (1:1). O resíduo seco foi reconstituído com 0,1 mL de água/metanol (4:1) e armazenado a −80 °C para posterior análise.

2.2.4. Validação do método

As águas superficiais foram coletadas para determinar a validação do método por meio do método de adição de padrão. As amostras foram previamente analisadas para verificar a ausência dos fármacos analisados.

Para a validação, os seguintes parâmetros foram analisados: precisão, exatidão, linearidade, seletividade, limites de deteção e quantificação. Os parâmetros foram baseados seguindo o guia da *International Conference for Harmonization* (ICH) [4].

A precisão foi calculada pela repetitividade por meio da adição de concentrações conhecidas dos fármacos em triplicados com as mesmas condições operacionais em um curto período de tempo. A exatidão foi obtida por ensaios de recuperação em que foram adicionadas concentrações de 40 e 400 ng L^{-1} em triplicado para avaliar o método de extração em fase sólida. A linearidade foi calculada pela curva de calibração externa com concentrações de 0,001 a 0,1 mg L^{-1}.

A seletividade foi obtida usando o espectrômetro de massa na identificação dos iões precursores e produtos dos contaminantes com duas transições (MRM) para cada composto, otimizando os parâmetros de energia de colisão e a voltagem do cone.

Os limites de deteção (L.D) e quantificação (L.Q) foram calculados pela adição de padrão em amostras de água superficiais. O L.D foi definido pela razão sinal/ruído igual a 3 e o L.Q foi calculado pela razão sinal/ruído igual a 10. Foi escolhida uma transição MRM com maior sensibilidade para cada composto para ambos os parâmetros.

Foi calculado o efeito matriz pela adição dos padrões após a etapa de SPE em concentrações de 40 e 400 ng L^{-1} nas amostras de água superficial e o método do padrão interno foi utilizado para monitorizar a supressão ou aumento do sinal do ião.

2.3. Resultados e discussão

2.3.1. Análise em HPLC-TQMS

Duas transições MRM foram monitorizadas para cada composto com propósito de aumentar a seletividade da análise. As energias de colisões e a voltagem do cone foram otimizadas (**Tabela 2.1**). **A Figura 2.1** mostra os cromatogramas dos 10 fármacos em modo MRM numa mistura de padrões.

Tabela 2.1. Condições para a quantificação dos compostos farmacêuticos.

Composto	**Tr**	**Íon precursor**	**Precursor →Produto *m/z* (Quantificação)**	**Precursor →Produto *m/z* (Confirmação)**	**Cone (V)**	**CE (eV)**
CIT	6,0	$[M+H]^+$	325>108,8	325>262	25	20
VEN	5,5	$[M+H]^+$	278,1>57,7	278,1>260,1	25	15
AMI	6,3	$[M+H]^+$	278,1>90,8	278,1>233	35	20
BUP	5,4	$[M+H]^+$	240>184	240>166	25	15
TRA	5,8	$[M+H]^+$	372>176,1	372>147,9	30	25
DUL	6,2	$[M+H]^+$	298>153,9	298>43,7	15	15
MET	5,6	$[M+H]^+$	454,9>308	454,9>175	30	15
IF	7,1	$[M+H]^+$	260,9>153,9	260,9>91,8	40	20
CP	7,2	$[M+H]^+$	261>139,9	261>119,8	35	20-25
AMI-d_3	6,2	$[M+H]^+$	281>117	281>233	30	20

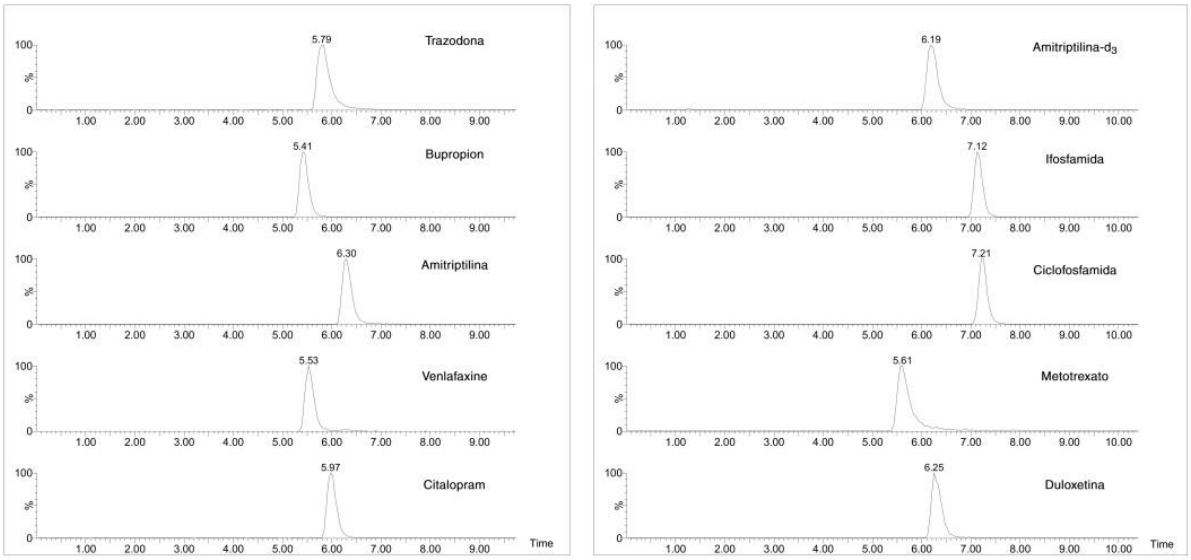

Figura 2.1. Cromatogramas em modo MRM.

Após a otimização do método cromatográfico, foram testados diferentes solventes na amostra: água ultrapura, metanol e proporções de água:metanol de 20:80 e 80:20. O racio de água:metanol (80:20) foi o que apresentou melhor resultado, conforme mostra a **Figura 2.2**. As amostras com metanol apresentaram picos duplos no composto MET (**Figura 2.3**) e esses resultados podem ser explicados por meio da perda dos analitos no volume morto da coluna, além de terem a intensidade de sinal inferior ao solvente 80/20.

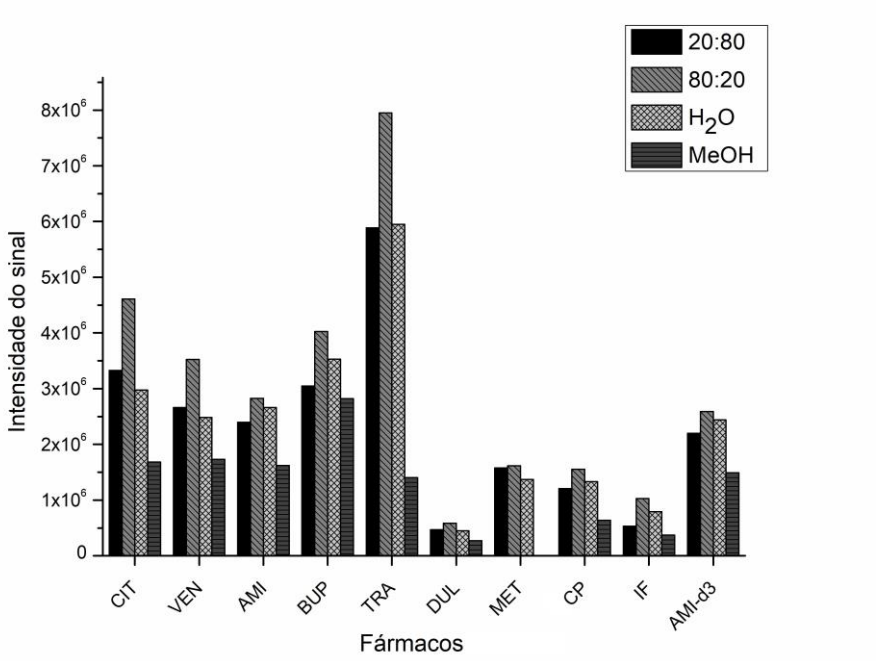

Figura 2.2. Intensidade do sinal de cada composto para diferentes solventes.

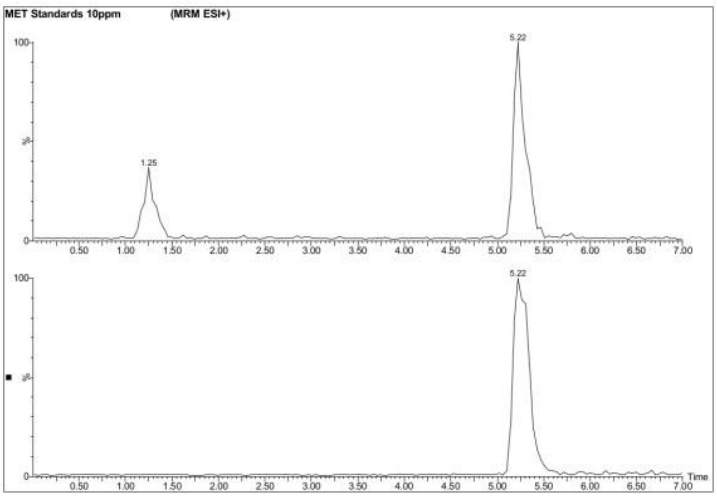

Figura 2.3. Cromatogramas com analítos na concentração de 10 mg L^{-1}. (A) e (B) são cromatogramas do MET com 100% metanol e 100% água, respetivamente.

2.3.2.Preparação da amostra - filtração

A etapa de filtração é essencial para remover a matéria orgânica em suspensão em análises de contaminantes ambientais porém, pode haver adsorção de contaminantes orgânicos no material filtrante, de notar que existem poucos estudos da influência no processo de filtração. Kiehm e Dressman [5] investigaram a recuperação do fármaco prednisolona em diversos filtros de membrana e concluíram que as membranas de nylon e nylon/poliamida, ambas com 0,45 µm de diâmetro de poro, apresentaram baixas recuperações quando os primeiros 2 mL da amostra filtrada foram analisados. Ng e Cao [6] utilizaram filtros de membrana de polietersulfona com diâmetro de poro de 0,2 µm e verificaram que compostos hormonais (estrona, estradiol, 17α-etinil estradiol e testosterona) apresentaram retenção de até 96% da concentração inicial. Este trabalho comparou membranas filtrantes com 0,45 µm de diâmetro de poro de dois materiais: nylon e PTFE para verificar a adsorção. Os resultados mostraram que para a maioria dos compostos as membranas são equivalentes porém, para o composto DUL e AMI houve grande diferença nas recuperações (**Figura 2.4**).

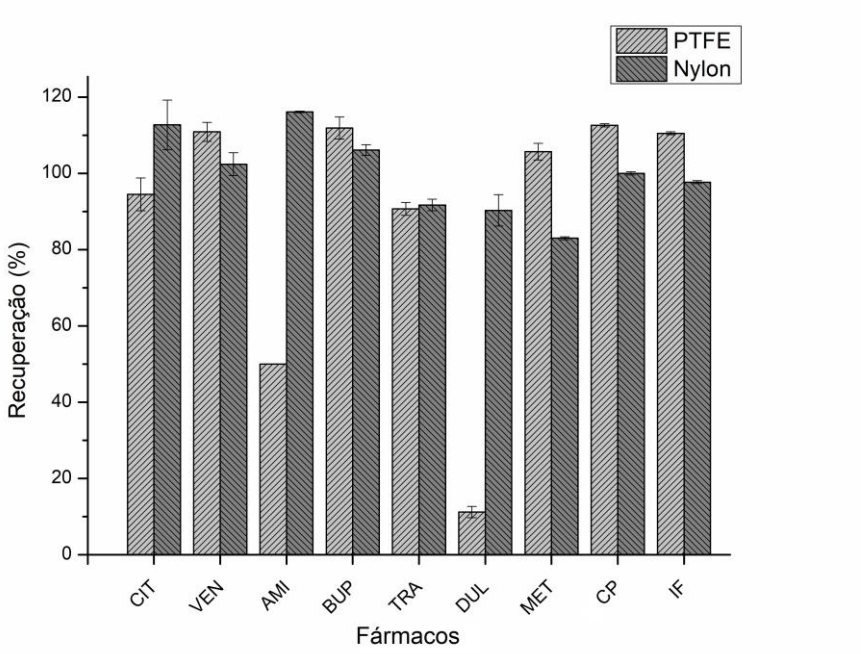

Figura 2.4. Recuperações dos fármacos em filtros de membrana de nylon e de PTFE.

2.3.3.Preparação da amostra - extração em fase sólida

Os ensaios da validação da extração em fase sólida foram realizados em água superficial previamente analisada para confirmar a ausência dos compostos de interesse. O pH das amostras foi ajustado para pH 3 e pH 7, por meio da diluição de ácido acético ou hidróxido de amônio, para determinar a influência do pH nas recuperações da SPE. Em análises multiresíduos é comum acidificar a amostra para uma melhor recuperação na extração com o objetivo de abranger diferentes grupos de contaminantes [7,8]. A escolha do adsorvente Oasis HLB (*hydrophilic-lipophilic balance*) foi pelo facto de ser indicado para compostos ácidos, neutros e básicos.

Conforme observado na **Figura 2.5** a extração com pH 3 obteve resultados mais satisfatórios, BUP, VEN, MET, CP e IF apresentaram resultados próximos na extração em ambos os pH, porém AMI, DUL e TRA resultaram em baixa recuperação em pH neutro. Schultz e Furlong concluíram que acidificando a amostra antes da técnica de SPE (Oasis HLB), resultou em uma melhoria na recuperação dos fármacos antidepressivos [9]. Sheng et al. ao quantificar antidepressivos em matrizes ambientais observou recuperações em cartuchos Oasis HLB entre 81,2% to 118% com amostras de pH 3 [10]. Os fármacos anticâncerígenos (MET, CP e IF)

apresentaram pouca variação nas extrações. Por meio deste resultado, conclui-se que a acidificação da amostra é necessária. A **Figura 2.6** resume o processo da extração em fase sólida.

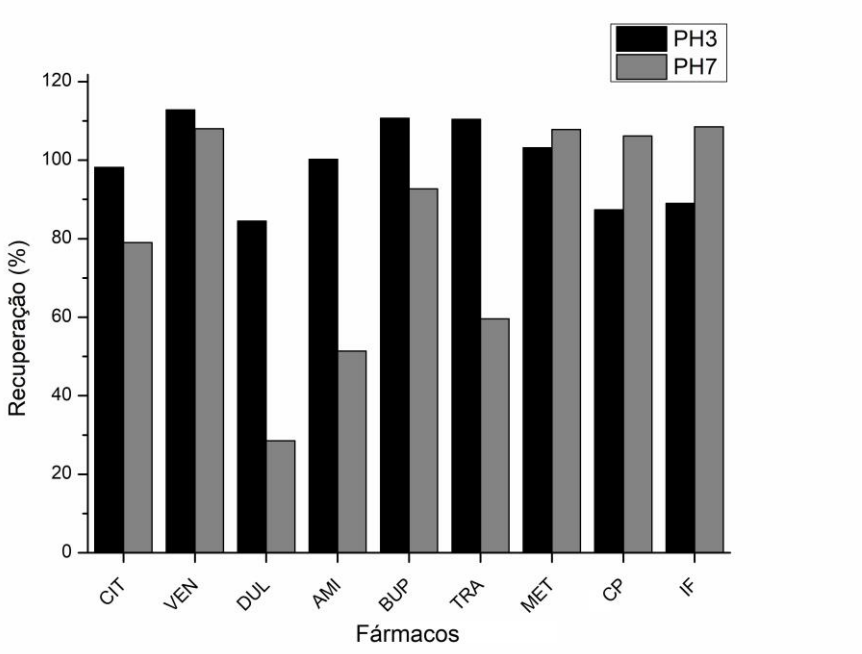

Figura 2.5. Recuperações nas extrações em fase sólida com diferentes condições de pH.

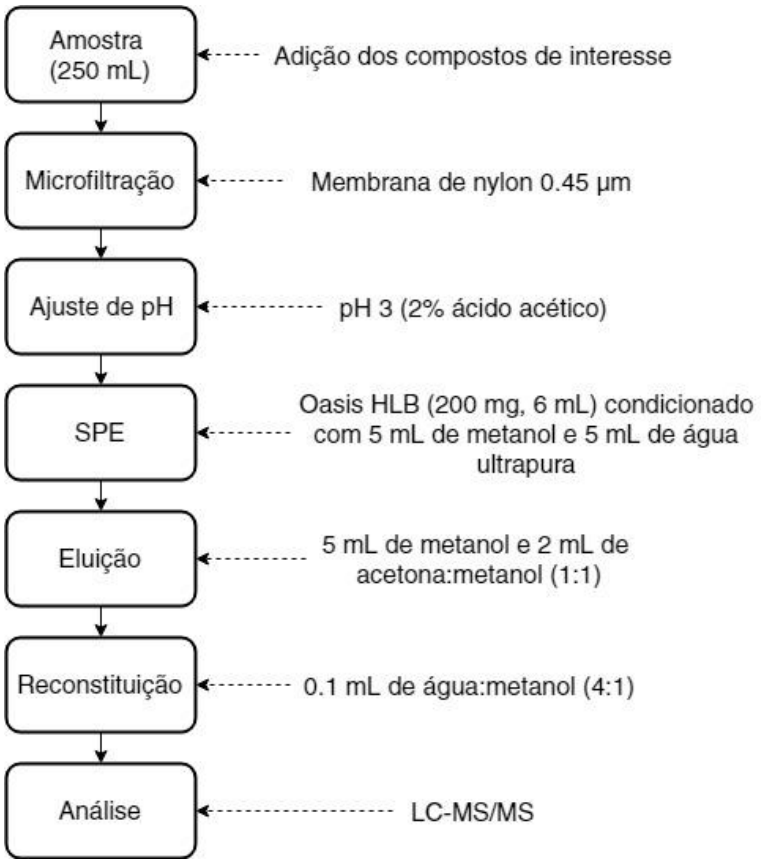

Figura 2.6. Esquema da extração em fase sólida.

2.3.4. Validação do método

O método apresentou baixos limites de deteção e quantificação dos compostos (**Tabela 2.2**). Para cada composto foi aplicado o método da regressão linear para a reta de calibração. Os coeficientes de recuperação (r^2) para todos os fármacos foram acima de 0,99 na faixa de concentração de 0,001 a 0,1 ng L^{-1}. As recuperações em água superficial foram entre 80,2 % e 116,5% para ambas as concentrações (40 e 400 ng L^{-1}) e os desvios padrão relativos (RSD, *relative standard deviation*) foram inferiores a 20% (**Tabela 2.3**).

Tabela 2.2. Limites de detecção e quantificação, linearidade e coeficiente de correlação.

Composto	L.D (ng L^{-1})	L.Q (ng L^{-1})	Linearidade (ng L^{-1})	r^2
CIT	1,2	4	1-100	0,9974
VEN	0,6	2	0,5-100	0,9954
AMI	1,2	4	1-100	0,9980
BUP	1,2	4	1-100	0,9962
TRA	0,6	2	0,5-100	0,9976
DUL	1,2	4	1-100	0,9952
MET	1,2	4	1-100	0,9930
CP	0,6	2	0,5-100	0,9952
IF	1,2	4	1-100	0,9927

Na ionização por eletrospray, o efeito matriz pode ocorrer devido à presença de componentes da matriz co-extraídos. Esse efeito foi largamente estudado em diversas matrizes [11,12,13]. O efeito matriz pode resultar na supressão do ião ou no aumento do sinal pelo que, estudar o efeito da matriz é relevante pela complexidade das matrizes ambientais. O efeito matriz foi calculado pela equação (**Equação 2.1**):

$$M.E(\%) = \frac{S_b}{S_a} * 100 \qquad \textbf{(Equação 2.1)}$$

Onde S_b é a área do pico do analito na amostra com o padrão adicionado após a extração e S_a é a área do pico do analito em solvente puro. Os resultados sem efeito de matriz são representados com valores de 100% e valores > 100% ou < 100% correspondendo a aumento ou supressão do sinal, respectivamente. Para corrigir os

desvios causados pelo efeito matriz podem utilizar-se o método da adição do padrão interno, que consiste em adicionar concentrações conhecidas de um composto deuterado do analito de interesse com o objetivo de monitorizar as variações do sinal do analito analisado. Golovko et al. [14] quantificou antidepressivos em efluentes de estações de tratamento e o método do padrão interno foi empregado para correção dos efeitos de supressão ou aprimoramento dos iões. Ferrando-Climent et al. [15] analisou fármacos anticancerígenos em efluentes hospitalares e para diminuir o efeito matriz, foram adicionados padrões internos às amostras.

Neste estudo foi utilizado como padrão interno AMI-d_3. O ideal seria utilizar um padrão interno para cada composto, mas a análise tornava-se dispendiosa. Foram utilizadas duas concentrações para a análise do efeito matriz (40 e 400 ng L^{-1}). Conforme a Tabela 4, ocorreu supressão do sinal do ião para a maioria dos compostos analisados. O método apresentou resultados satisfatórios para a análise ambiental, com variação de 75,5 a 104,8 % de efeito matriz e RSD menor que 15%.

Tabela 2.3. Recuperações (Re) e efeito matriz (M.E) em concentrações de 40 and 400 ng L^{-1}.

Composto	Re (RSD %) n=3 (40 ng L^{-1})	Re (RSD %) n=3 (400 ng L^{-1})	M.E (RSD %) n=3 (40 ng L^{-1})	M.E (RSD %) n=3 (400 ng L^{-1})
CIT	115,0 (6,0)	98,2 (11,2)	93,9 (8,2)	84,0 (11,6)
VEN	101,4 (15,7)	112,8 (1,3)	80,2 (7,3)	97,3 (4,7)
AMI	87,3 (3,3)	84,5 (3,9)	89,6 (4,8)	97,7 (8,3)
BUP	116,5 (1,2)	100,2 (15,9)	74,7 (9,3)	61,4 (5,9)
TRA	92,6 (0,9)	110,7 (6,5)	85,8 (11,4)	68,3 (3,8)
DUL	96,4 (2,0)	110,4 (0,8)	104,8 (11,6)	91,7 (8,0)
MET	80,2 (4,4)	103,2 (1,3)	96,2 (11,8)	84,8 (9,1)
CP	114,7 (7,4)	87,4 (7,5)	76,5 (3,8)	72,8 (0,6)
IF	100,4 (3,5)	89,0 (11,8)	75,5 (5,8)	81,7 (0,2)

2.3.5. Aplicação do método em matriz ambiental

Amostras do efluente da WWTP de Lisboa e água para consumo humano foram coletadas com o objetivo de aplicar o método desenvolvido para nove fármacos utilizando SPE e HPLC-TQMS. Foram quantificados sete fármacos no efluente, a

maior concentração foi da CP (954 ng L^{-1}), seguido da IF (947 ng L^{-1}), podendo as elevadas concentrações das drogas citostáticas ser explicadas pela presença de efluentes de diversos hospitais de Lisboa. As concentrações encontradas para os outros fármacos foram: CIT, 236,5 ng L^{-1}; VEN, 304,3 ng L^{-1}; TRA, 16,1 ng L^{-1}; DUL, 368,3 ng L^{-1} e AMI, 192,4 ng L^{-1}.

2.4. Conclusão

O método para HPLC-TQMS apresentou baixos limites de detecção (entre 0,6 e 1,2 ng L^{-1}) e quantificação (entre 2 e 4 ng L^{-1}) e o método utilizando SPE resultou em bons valores de recuperação, entre 80,2 % e 116,5% e os valores de RSD foram inferiores a 20%, o que não compromete a análise. O efeito matriz na análise de efluentes era esperado pelo facto de a amostra apresentar complexidade e efetivamente para a maioria dos compostos ocorreu a supressão dos iões. A seleção do material da membrada de filtração é essencial não só para a remoção da matéria orgânica, mas para os analitos de interesse, já que podem ficar retidos na membrana, afetando a análise.

A análise em matriz real, efluente de ETAR, quantificou sete fármacos, com concentrações entre 16,1 ng L^{-1} para o composto DUL e 954 ng L^{-1} referente ao CP. O resultado demonstrou que o tratamento empregado na WWTP de Lisboa não removem totalmente os contaminantes estudados e provavelmente outros contaminantes emergentes podem estar presentes no efluente. Logo, incluir estes contaminantes na legislação ambiental poderia ser relevante.

2.5. Referências

1. Thompson, M., Ellison, S.L.R., Wood, R., 2002. Harmonized guidelines for single-laboratory validation of methods of analysis. *Pure Appl. Chem*. 74(5), 835–855.

2. FDA - Food and Drug Administration., 1998. Validation of analytical procedures: methodology. Final guidance. U.S. Department of Health and Human Services Food and Drug Administration. VICH GL2 (validation methodology).

3. UNODOC - United Nations Office on Drugs and Crime., 2009. Guidance for the validation of analytical methodology and calibration of equipment used for testing of illicit drugs in seized materials and biological specimens. Laboratory and scientific section. United Nations. New York.

4. ICH., 2005. Q2(R1) validation of analytical procedures: text and methodology. Genova.

5. Kiehm, K., Dressman, J.B., 2008. Evaluation of drug adsorption to membrane filters under biowaiver test conditions. *Dissolut. Technol*. 15(4), 13–17.

6. Ng, C.K., Cao, B., 2015. What exactly are you filtering out?. *Environ. Sci. Technol*. 49, 5259−5260

7. Nurmi, J., Pellinen, J., 2011. Multiresidue method for the analysis of emerging contaminants in wastewater by ultra performance liquid chromatography – time-of-flight mass spectrometry. *J. Chromatogr. A* 1218, 6712–6719. doi:10.1016/j.chroma.2011.07.071

8. Petrie, B., Youdan, J., Barben, R., Kasprzyk-Hordern, B., 2016. Multi-residue analysis of 90 emerging contaminants in liquid and solid environmental matrices by ultra-high-performance liquid chromatography tandem mass spectrometry. *J. Chromatogr. A*. 1431, 64–78. doi:/10.1016/j.chroma.2015.12.036

9. Schultz, M.M., Furlong, E.T., 2008. Trace analysis of antidepressant pharmaceuticals and their select degradates in aquatic matrixes by LC/ESI/MS/MS. *Anal. Chem*. 80, 1756–1762. doi:10.1021/ac702154e

10. Sheng, L.-H., Chen, H.-R., Huo, Y.-B., Wang, J., Zhang, Y., Yang, M., Zhang, H.-X., 2014. Simultaneous determination of 24 antidepressant drugs and their metabolites in wastewater by ultra-high performance liquid chromatography–tandem mass spectrometry. *Molecules* 19, 1212–1222. doi:10.3390/molecules19011212

11. Zrostlíková, J., Hajšlová, J., Poustka, J., Begany, P., 2002. Alternative calibration approaches to compensate the effect of co-extracted matrix components in liquid chromatography– electrospray ionisation tandem mass spectrometry analysis of pesticide residues in plant materials. *J. Chromatogr. A*. 973 13–26. doi:10.1016/S0021-9673(02)01196-2

12. Chu, S., Metcalfe, C.D., 2007. Analysis of paroxetine, fluoxetine and norfluoxetine in fish tissues using pressurized liquid extraction, mixed mode solid phase extraction cleanup and liquid chromatography–tandem mass spectrometry. *J. Chromatogr. A*. 1163, 112–118. doi:10.1016/j.chroma.2007.06.014

13. Caban, M., Migowska, N., Stepnowski, P., Kwiatkowski, M., Kumirska, J., 2012. Matrix effects and recovery calculations in analyses of pharmaceuticals based on the determination of -blockers and -agonists in environmental samples. *J. Chromatogr. A*. 1258, 117–127. doi:10.1016/j.chroma.2012.08.029

14. Golovko, O., Kumar, V., Fedorova, G., Randak, T., Grabic, R., 2014. Seasonal changes in antibiotics, antidepressants/psychiatric drugs, antihistamines and lipid regulators in a wastewater treatment plant. *Chemosphere* 111, 418–428. doi:10.1016/j.chemosphere.2014.03.132

15. Ferrando-Climent, L., Rodriguez-Mozaz, S., Barceló, D., 2014. Incidence of anticancer drugs in an aquatic urban system: From hospital effluents through urban wastewater to natural environment. *Environ. Pollut*. 193, 216–223. doi:10.1016/j.envpol.2014.07.002

Capítulo 3

Produtos de transformação do citalopram por processos de degradação analisadas por UHPLC-QTOF-MS

3.1. Introdução

Citalopram (CIT) pertence ao grupo dos fármacos antidepressivos da classe dos inibidores selectivos da recaptação da serotonina. Após o consumo, este fármaco pode alcançar diversas matrizes ambientais como águas superficiais, efluentes e águas subterrâneas visto que os tratamentos de efluentes convencionais não o eliminam completamente [1,2,3]. Porém, existem poucos estudos sobre a formação dos TPs do CIT por processos físicos e químicos [4,5].

A toxicidade dos TPs é um fator importante a ser considerado, pois podem apresentar características físicas e químicas diferentes do composto original [4], podendo ser mais tóxicos e mais persistentes, mas há poucos dados sobre a ecotoxicidade dos TPs de compostos farmacêuticos. Uma maneira de obviar a esta questão seria utilizar métodos computacionais (*in silico*) para estimar a toxicidade [6,7]. Existem várias metodologias para a previsão de toxicidade e cada método apresenta vantagens e limitações, tais como: alertas estruturais, modelos farmacocinéticos e modelos farmacodinâmicos, relação quantitativa estrutura-atividade.

O objetivo deste trabalho foi identificar a formação de TPs do CIT por meio de simulações controladas de processos que podem ocorrer no meio aquático e nas estações de tratamento de águas residuais: hidrólise; fotodegradação (sob irradiação UV−Vis) e cloração por cromatografia líquida de ultra performance acoplada a espectrometria de massa do tipo quadrupolo-tempo de voo (UHPLC-QTOF-MS) e, posteriormente, analisar amostras em efluentes e prever as toxicidades dos compostos por avaliação de toxicidade computacional.

Este capítulo é uma representação integral do artigo:

Osawa, R.A., Carvalho, A.P., Monteiro, O.C., Oliveira, M.C.,Florêncio, M.H., 2019. Transformation products of citalopram: Identification, wastewater analysis and *in silico* toxicological assessment. *Chemosphere* 217, 858–868. doi:10.1016/j.chemosphere.2018.11.027.

Chemosphere 217 (2019) 858–868

Contents lists available at ScienceDirect

Chemosphere

journal homepage: www.elsevier.com/locate/chemosphere

Transformation products of citalopram: Identification, wastewater analysis and *in silico* toxicological assessment

Rodrigo A. Osawa [a, b, *], Ana P. Carvalho [a], Olinda C. Monteiro [a], M. Conceição Oliveira [c], M. Helena Florêncio [a]

[a] Centro de Química e Bioquímica, Faculdade de Ciências, Universidade de Lisboa, 1749-016, Lisboa, Portugal
[b] CAPES Foundation, Ministry of Education of Brazil, 70040-020, Brasília-DF, Brazil
[c] Centro de Química Estrutural, Instituto Superior Técnico, Universidade de Lisboa, 1049-001, Lisboa, Portugal

HIGHLIGHTS

- Elucidated seventeen transformation products of citalopram by UHPLC-QTOF.
- Hydrolysis, photodegradation and chlorination experiments under laboratory conditions.
- Time profile of TPs formation were monitored.
- *In silico* toxicity assessment resulted in TPs with mutagenic potentials.
- Citalopram and two TPs were detected in wastewater samples.

GRAPHICAL ABSTRACT

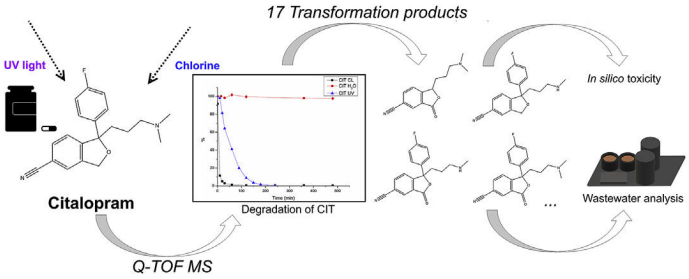

ARTICLE INFO

Article history:
Received 11 September 2018
Received in revised form
24 October 2018
Accepted 2 November 2018
Available online 5 November 2018

Handling Editor: A. Gies

Keywords:
Transformation products
Time-of-flight mass spectrometry
Citalopram
In silico toxicity prediction
Wastewater

ABSTRACT

The objective of this study was to identify transformation products (TPs) of citalopram (CIT), an antidepressant drug, in laboratory experiments. Moreover, toxicity predictions and analyzes in wastewater samples were performed. For the formation of TPs, raw water was used for the processes of hydrolysis; photodegradation under ultraviolet (UV) irradiation and chlorination. The toxicities were predicted by computational toxicity assessment. The TPs were identified by liquid chromatography quadrupole time-of-flight mass spectrometry (LC-QTOF/MS) in broadband collision induced dissociation (bbCID) acquisition mode and product ion scan mode (MS/MS). The probable structures of the TPs under study were established based on accurate mass, fragmentations observed in the MS spectra and prediction tools software. The experiments resulted in seventeen possible identified TPs and their stability and formation was monitored over time in the experiments. Two of these TPs were identified in wastewater samples It was also observed that most of TPs formed were either less toxic then CIT or had a similar toxicity.

1. Introduction

Pharmaceuticals have been found in the last decades in the environment such as in surface water, wastewater, drinking water, groundwater and sea water and the question about their toxic potential for aquatic life and human health has raised. These compounds can cause adverse effects leading to aquatic toxicity,

* Corresponding author. DQB/FCUL, Campo Grande Ed. C8, 1749-016, Lisbon, Portugal.
E-mail address: raosawa@fc.ul.pt (R.A. Osawa).

https://doi.org/10.1016/j.chemosphere.2018.11.027
0045-6535/

genotoxicity, endocrine interference and development of resistance in microorganisms (Kasprzyk-Hordern et al., 2008; Rainieri et al., 2017; Pino-Otín et al., 2017). However, most of the studies developed so far were focused on the parent compound of the contaminants and the transformation products (TPs) were not considered. TPs, by definition are products generated by biotic and abiotic processes from the original compound (Stuart et al., 2012; Yuan et al., 2013; Giebułtowicz and Nałęcz-Jawecki, 2014; Golovko et al., 2014). Some reports concluded that selected TPs presented greater persistence in the environment than their parent compounds (Escher and Fenner, 2011; Hübner et al., 2015) or presented a higher toxicity to aquatic organisms (Trautwein and Kümmerer. 2012; Li et al., 2016).

The contaminant, once in the environment, can degrade in different pathways that is, at the biological level (biodegradation) or by physical and chemical processes such as hydrolysis, photodegradation or chlorination. These processes may occur in wastewater treatment plant (WWTP). It is important to know the mechanisms of degradation that can occur to understand their fate in the environment and aquatic biota. Some studies have elucidated the formation of TPs under controlled experimental conditions (Negreira et al., 2015; Salma et al., 2016; Wilde et al., 2016; Trawiński and Skibi. 2017).

Citalopram (CIT), a selective serotonin reuptake inhibitor (SSRI) antidepressant, has a high consumption in the world for the treatment of depression. There are numerous studies that have detected the drug in effluents and surface waters usually in the order of ng L^{-1} but there are few studies of the fate and TPs in the environment or in the wastewater treatment plant and, consequently, little is known about their removal mechanisms (Collado et al., 2014; Silva et al., 2014; Sheng et al., 2014). This pharmaceutical compound had an elimination rate about 33% in the WWTP under aerobic process (Schlüsener et al., 2015) whereas other investigations showed a removal of approximately 18% (Golovko et al., 2014). These studies argue for the stability of CIT in WWTP. There are, however, few data about its TPs, and they may present different physical and chemical characteristics from the parent compound (Horsing et al., 2012; Beretsou et al., 2016).

Another aspect to be considered is the toxicity. Studies have shown that CIT has low toxicity compared to other SSRIs but, it was the least tested compound with regard to toxicological effects (Christensen et al., 2007). TPs may be more toxic and more persistent than the parent compound but there are few data on the ecotoxicity of TPs from pharmaceutical compounds. As such, it is common to use predictive tools to estimate the ecotoxic range (Fatta-Kassinos et al., 2011; Negreira et al., 2015). There are several methodologies for predicting toxicity such as: structural alerts and rule-based models, chemical category, pharmacokinetic models and pharmacodynamic models, quantitative structure–activity relationships. Each method presents advantages and limitations. *In silico* toxicology is a way to complement toxicity *in vitro* or *in vivo*.

The great challenge is to identify the TPs, since most of them are unknown and, therefore, do not have reference standards for confirmation. High resolution mass spectrometry with analyzers such as Q-Orbitrap, FT-ICR or Quadrupole time-of-flight (QTOF) coupled with liquid chromatography (LC) system such as ultra-high-performance liquid chromatography (UHPLC), are important tools for elucidating the structures of the compounds through the analysis of fragment ions in the mass spectrum and accurate mass (Castro et al., 2016; Matsushita et al., 2016).

The objectives in this study were to elucidate the formation of CIT TPs, to identify the TPs in real matrices and to perform the *in silico* toxicity analysis. For the formation of the TPs, simulations of processes that may occur in the aquatic environment and in the WWTP: hydrolysis; photodegradation under ultraviolet (UV) irradiation, chlorination, were carried out in raw water. All analyzes were performed by mass spectrometry using the LC-QTOF/MS.

2. Materials and methods

2.1. Reagents and materials

Standard CIT hydrobromide (purity > 98%) was purchased from TCI Chemicals (Zwijndrecht, Belgium). Ultrapure water was prepared with the Milli-Q ultrapure system (Barnstead International, Dubuque, USA). Sodium hypochlorite solution (10%) was obtained from Labkem (Barcelona, Spain), and water, methanol, formic acid and acetonitrile LC-MS grade Optima purchased from Fisher Scientific (Hampton, USA). L (+) Ascorbic acid was obtained from Merck (Darmstadt, Germany). Nylon membrane filter (0.45 μm) was purchased from Teknokroma (Barcelona, Spain). For solid phase extraction (SPE), the cartridge sorbent materials HLB (OASIS, 500 mg, 6 cc) were obtained from Waters (Milford, USA). Standard stock solution was prepared in 1000 mg L^{-1} in water stored at −80 °C.

2.2. Instrumentation

Samples were analyzed by liquid chromatography-high resolution tandem mass spectrometry using an Ultimate 3000 RSLCnano system (Thermo Fischer Scientific, Idstein, Germany) interfaced with a QTOF Impact II mass spectrometer equipped with an electrospray source (Bruker Daltonics, Bremen, German). Chromatography separation was carried out on a Kinetex 1.7 μm C18 100 Å, LC column 150 × 2.1 mm (Phenomenex, California, USA), at flow rate of 150 μL min^{-1}. Mobile phase consisted of 0.1% of acid formic in ulturapure water v/v (A) and acetonitrile (B). The elution conditions were as follows: 5% B for 1.5 min; 5–75% B for 11.5 min; 75–100% B for 5 min; 100% B for 3 min; 100 to 5% 2 min and finally 5% B for 7 min. The column and the sampler were maintained at 35 °C and 10 °C, respectively.

The mass spectrometer was operated in the ESI positive mode in the high-resolution mode. The optimized parameters were as follows: ion spray voltage, 2.5 kV; end plate offset, −500 V, nebulizer gas (N_2), 2.8 bars; dry gas (N_2), 8 L min^{-1}; dry heater, 200 °C. Internal calibration was performed on the high-precision calibration mode (HPC) with a solution of sodium formate 10 mM introduced to the ion source *via* a 10 μL loop at the beginning of each analysis using a six-port valve. Acquisition was performed in full scan mode in the *m/z* 50–1000 range, and in broadband collision-induced dissociation (bbCID) mode with an acquisition rate of 3 Hz. In this acquisition mode the mass spectrometer worked in rapid and continuous cycles between low collision energy (TOF-MS) and high collision energy (bbCID) resulting in precursor ion and fragmentation patterns in a single analysis. The product ion scan mode (MS/MS) was used to confirm the fragment ions.

2.3. Identification of TPs

2.3.1. TPs experiments

Raw water was collected from Serra da Estrela (Portugal). The sample was pre-filtered through a 0.45 μm nylon membrane. The experiment was performed under laboratory conditions in attempt to simulate the processes occurring in the aquatic environment: hydrolysis and photodegradation as well as processes that can occur in wastewater treatment plant such as chlorination.

The sample was spiked with CIT in the concentration of 0.5 mg L^{-1}, being the high concentration of the compound to elucidate the formation of TPs. The concentration of the TPs found

in the environment is in the order of ng L^{-1} (Collado et al., 2014; Silva et al., 2014; Sheng et al., 2014) and the pH was monitored (5–6) but not modified to simulate the real environmental conditions.

The processes of hydrolysis, chlorination and photodegradation were carried out at room temperature (20 °C) and in the dark room. Hydrolysis consisted in studying the stability of CIT in water.

In the chlorination experiment, sodium hypochlorite solution was diluted in 20 mL of sample to have a concentration of 5 mg L^{-1} free chlorine, the reaction was quenched with ascorbic acid at concentration of 600 mg L^{-1} to stop the reaction of TPs formation.

Photodegradation experiments were conducted using an Ace Glass photoreactor with 100 mL of sample cooled by water circulation. The UV irradiation source was a 450 W medium-pressure mercury-vapor lamp (Hanovia, UK) with irradiance around 0.37 W cm^{-2}. The lamp's spectral energy distribution and details of the photoreactor was previously published (Pinto da Costa et al., 2015). All experiments were performed with magnetic stirring bars.

The experiments consisted of 0.1 mL withdrawn aliquots in certain time periods (hydrolysis at 0–8 h; chlorination at 0–4 h and photodegradation at 0–4 h) and were stored for further analysis at −80 °C. The samples were injected directly into the LC-QTOF/MS. A schematic pathway of the methodology can be found in Supplementary Information (Fig. S1).

2.3.2. Data analysis

The LC-MS acquisition data were processed using DataAnalysis 4.1 (Bruker) to extract the mass spectral features from blank and samples raw data. From the comparison between control blanks and sample sets it was possible to identify TPs precursor ions by accurate *m/z* values. Identification of proposed TPs was based on accurate mass estimated with mass error less than 5 ppm, isotopic patterns observed on MS spectra, as well as on the MS/MS fragmentation patterns, and on the accurate mass values of the fragment ions.

The probable structures of TPs were established taking into account two prediction tools software's, based on biotransformation rules: EAWAG-BBD: Pathway Prediction System (Gao et al., 2010 and MetabolitePredict (Bruker Daltonics, Bremen, Germany). However, in this work the TPs were identified by abiotic processes because there are abiotic degradation mechanisms that can occur in biodegradation processes (Ueno et al., 2007) for which reason the above-mentioned software can be applied.

2.4. Toxicity assessment

To study the possible toxicological effects of the molecules, *in silico* methods were used to predict their toxicity. These methods were: Toxicity Estimation Software Tool (TEST, version 4.2) (Martin, 2016) from US Environmental Protection Agency; and VEGA (version 1.1.4), a platform that has several models of prediction. These tools are freely available to users. The simplified molecular-input line-entry system (SMILES) is a specification that describes the molecular structure of one compound in the form of a line notation. The SMILES for each compound was generated in order to calculate the toxicity prediction in both softwares (TEST and VEGA).

The methodology of TEST is based on Quantitative Structure Activity Relationships (QSARs), which are mathematical models that predict toxicity from the physical characteristics of the structure of a molecule. The consensus method from TEST was applied in the TPs that used the average of the predictions of toxicity from other QSAR methodologies. Three toxicity endpoints were selected: 96-h F. minnow LC_{50}; 48-h *D. magna* LC_{50}; 48-h *T. pyriformis* IGC_{50}. The F. minnow and *D. magna* toxicity are calculated by the lethal concentration required to cause the death of 50% of the organism (LC_{50}). *T. Pyriformis* is a prediction method that indicates the concentration required to inhibit 50% growth (IGC_{50}). As for the VEGA platform it has different methods to predict mutagenicity and carcinogenicity based in QSAR. The mutagenicity prediction was based in AMES test that studies the mutagenic potential of the compound in bacteria, and where positive results indicate that the compound is mutagenic and may have carcinogenic potential.

To estimate mutagenicity, the QSAR analysis was performed in at least three models, to verify the false positives according to the European Chemicals Agency recommendation. VEGA platform was used by the following methods: CAESAR, SarPy, ISS and KNN. The consensus method was used in which each model presents a weight and the prediction result is the sum of these weights for each model. To predict carcinogenicity three models were used by VEGA platform: CAESAR; ISS and IRFMN/ANTARES.

2.5. Sample preparation for wastewater analysis

Effluent and influent were collected (250 mL) from WWTP of Lisbon (Portugal) in amber bottles and stored in thermal boxes until arrival in the laboratory. Sample preparation details can be found in Supplementary Information (Text S1 and Table S1).

3. Results and discussion

3.1. Time profile of CIT and TPs

The degradation experiments using chlorination showed almost complete removal of CIT in 1 h (removal of 98%). Fig. 1a–b shows the time profiles of CIT and TPs formed by chlorination. The details of the experiment conditions are in section 2.3.1. The result obtained is according to the literature, Hörsing et al. (2012) reported the removal of about 95% of CIT in water using chlorine dioxide. Another study showed 90% removal of CIT in biological treated wastewater with chlorination (Hey et al., 2012). In chlorination time profile (Fig. 1a–b), most TPs reach maximum intensity after 1 h of reaction and decay over time, with exception of TP-355A that showed stability over time. The two most abundant TPs in the mass spectrum were TP-311 and TP-325. For comparison purposes, if the signals intensity of the chromatograms of the TPs is in the same order of magnitude of the signals intensity of CIT ($C_0 = 0.5$ mg L^{-1}), the relative concentration (C_R) can be obtained. The maximum concentrations of TP-311 and TP-325 were 0.28 mg L^{-1} (t = 60 min) and 0.025 mg L^{-1} (t = 60 min), respectively.

The photodegradation experiments completely removed CIT in 4 h (Fig. 1c). In the literature, other study showed a complete removal of CIT after 30 min with UV light (Hörsing et al., 2012). The TPs formed by UV irradiation presented different profiles. Nevertheless, all TPs decayed after reaching the maximum intensity of formation (Fig. 1c–e). This enables to conclude that it is necessary to pay attention to the exposure time of wastewater treatment to UV light. The TPs with the highest signal intensities of the chromatograms were: TP-323 ($C_R = 0.2$ mg L^{-1} at t = 30 min), TP-337 ($C_R = 0.077$ mg L^{-1} at t = 60 min) and TP-339A ($C_R = 0.068$ mg L^{-1} at t = 10 min). Interestingly, some TPs may be related, for example the TP-341A2 decays while TP-339B increases or TP-339A decomposes while TP-245 is produced.

In hydrolysis experiments, four TPs were identified: TP-311, TP-323, TP-339A and TP-341A2. These TPs showed stability until the end of the experiment, in other words, they were not degraded over time. However, as seen in Fig. 1f, the intensities were much lower than those found in chlorination: TP-311, TP-339A (Fig. 1a) and photodegradation: TP-311, TP-323, TP-339A and TP-341A2 (Fig. 1c–e). For example, TP-311 had $C_R = 0.0004$ mg L^{-1} at

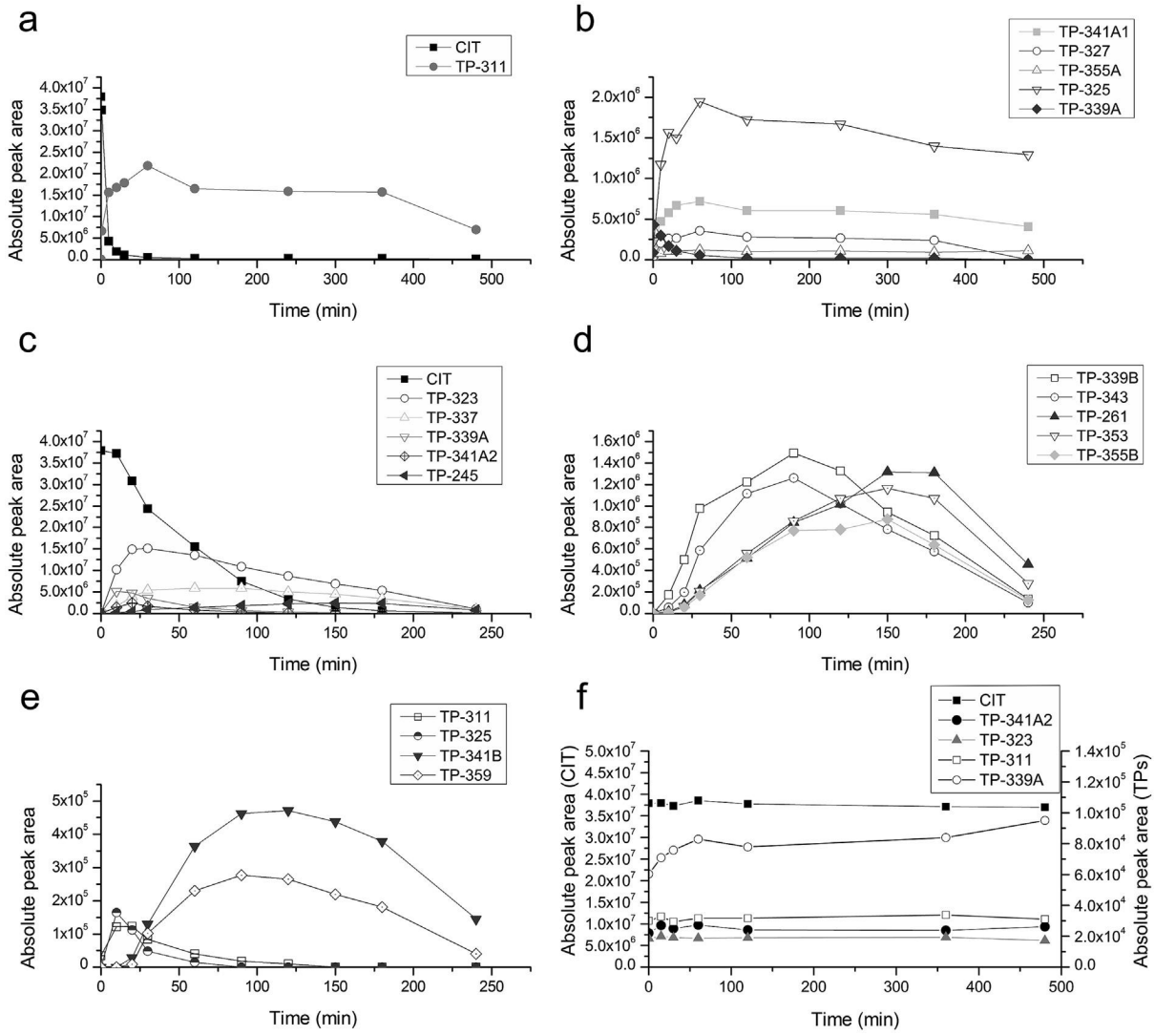

Fig. 1. Time profile of CIT and TPs: (a–b) chlorination process, (c–e) photodegradation process and (f) hydrolysis.

t = 480 min.

A pathway for the formation of TPs was proposed for each process: chlorination (Fig. S2), photodegradation (Fig. S3) and hydrolysis (Fig. S4). Reactions of oxidation, hydroxylation, *N*-Demethylation, *N*-Oxidation, *N*-Hydrolysis and dehalogenation were observed. However, chlorinated TPs were not identified in the chlorination process.

To elucidate the identification methodology used, the rationale for the structures proposed is detailed below for each TP. It should be noted that they were ordered according to their degree of similarity to CIT.

3.2. Behaviour of CIT under electrospray ionization conditions

Fig. 2 Exhibits the high-resolution MS/MS spectrum of the protonated molecule of CIT (*m/z* 325.1718) together with the proposed structures for the main fragment ions. The MS/MS spectrum (Fig. 2) displayed fragmentation patterns associated with three major losses: water (H_2O) giving rise to the fragment ion at *m/z* 307 ($C_{20}H_{20}FN_2^+$), dimethylamine ($(CH_3)_2NH$) leading to the fragment ion at *m/z* 280 ($C_{18}H_{15}FNO^+$) and fluorobenzene (C_6H_5F) leading to the fragment ion at *m/z* 166 ($C_{12}H_8N^+$), along with the losses of H_2O and $(CH_3)_2NH$ from the precursor ion. The loss of H_2O could only have occurred from the furan ring after an extensive rearrangement involving two hydrogens, whereas the loss of $(CH_3)_2NH$ was a simple fragmentation occurring in the tertiary amine group of the compound. The fragmentation of ($C_{16}H_9FN^+$) at *m/z* 234, from *m/z* 262 ($C_{18}H_{13}FN^+$), showed the loss of ethyl group (C_2H_4), possibly from the aliphatic chain.

3.3. Identification of TPs

For a better understanding, the identification process for each TP is presented below.

3.3.1. TP-311 (*m/z* 311.1554; $C_{19}H_{20}FN_2O^+$)

This product was probably formed by the transformation of the tertiary amine group, into a secondary amine. This hypothesis is supported by the presence in its MS/MS spectrum of the fragment ion *m/z* 262 ($C_{18}H_{13}FN^+$), which results from the elimination of a CH_3NH_2 molecule from *m/z* 293 ($C_{19}H_{18}FN_2^+$). Other neutral losses occurring in the MS/MS spectrum were similar to the ones of CIT. This TP is a human metabolite named desmethylcitalopram (CAS 62498-67-3), and its fragmentation pattern showed similarities

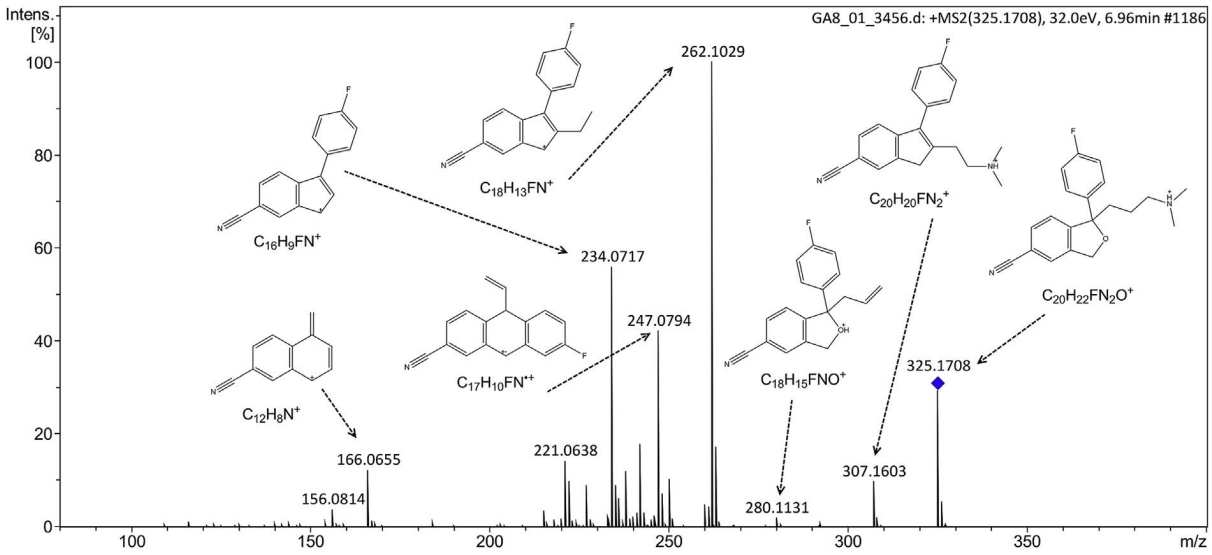

Fig. 2. Tandem mass spectrum of CIT and proposed structures for the main fragment ions.

(Fig. S5) with that presented by Beretsou et al. (2016).

3.3.2. TP-339A (m/z 339.1503; $C_{20}H_{20}FN_2O_2^+$)

The MS/MS spectrum of TP-339A displays neutral losses similar to those observed for CIT (Fig. S6). The analysis of the MS/MS spectrum further shows a fragment ion at *m/z* 248 ($C_{17}H_{11}FN^+$) that may be attributed to cleavage of CO. This latter fragmentation led us to conclude that TP-339A may have resulted from an oxidation reaction in the CIT molecule, that possibly occurred in the furan ring. Horsing et al. (2012) and Beretsou et al. (2016) identified the same fragments for this TP, a TP that is an CIT human metabolite intermediate, named 3-oxo citalopram (CAS 372941-54-3).

3.3.3. TP-325 (m/z 325.1348; $C_{19}H_{18}FN_2O_2^+$)

The TP-325 appears to have been formed by an oxidation process, probably adding an oxygen atom at the furan ring. The MS/MS spectrum is in agreement with this assumption since it displays a fragment ion at *m/z* 248 ($C_{17}H_{11}FN^+$) that corresponds to the neutral loss of CO from *m/z* 276 ($C_{18}H_{11}FNO^+$) indicating the loss of a carbonyl group in the molecule (Fig. S7). The fragment ion at *m/z* 294 ($C_{18}H_{13}FNO_2^+$) formed by the loss of a NH_2CH_3 group suggests that a secondary amine has been formed. Furthermore, the DBE value calculated for this TP (Table 1) was higher than that of CIT, which may indicate the presence of the carbonyl group.

3.3.4. TP-341A1 and TP-341A2 (m/z 341.1660; $C_{20}H_{22}FN_2O_2^+$)

TP-341A1 and TP-341A2 have the same elemental composition but their tandem mass spectra showed different fragmentation patterns. The MS/MS spectrum of TP-341A1 exhibits the fragment ion *m/z* 280 ($C_{18}H_{15}FNO^+$) attributed to loss of $(CH_3)_2NHO$, which suggests the formation of an *N*-oxide (TP-341A1). This TP could also have been formed by hydroxylation at the methyl group. To note that the MS/MS fragmentation pattern of this TP (Fig. S8) shows similarities with literature data (Horsing et al., 2012) claiming that this TP is a citalopram *N*-oxide, a known metabolite (CAS 63284-72-0). The MS/MS spectrum of TP-341A2 showed two peaks, 1 at *m/z* 323 ($C_{20}H_{20}FN_2O^+$) and other at *m/z* 305 ($C_{20}H_{18}FN_2^+$) resulting from loss of one and two H_2O molecules respectively (Fig. S9). This could indicate a structure bearing one hydroxyl group in the aliphatic chain arguing for the occurrence of an hydroxylation reaction. The hydroxyl group could, in theory, be bound to methyl, but the fragment (methylamino)methanol (C_2H_7NO) was not detected.

3.3.5. TP-327 (m/z 327.1488; $C_{19}H_{20}FN_2O_2^+$)

TP-327 MS/MS mass spectrum indicated the presence of an OH group, suggesting a structure where OH was possibly attached to the methyl group by a hydroxylation process. The fragment ion at *m/z* 262 ($C_{18}H_{13}FN^+$) was the most abundant ion in the mass spectrum (Fig. S10) and argues for the loss of both H_2O and CH_2NH_2OH. The latter loss supports the assumption that in the TP structure the hydroxyl group was attached to the methyl group of the secondary amine.

3.3.6. TP-355A (m/z 355.1452; $C_{20}H_{20}FN_2O_3^+$)

The TP-355A MS/MS spectrum suggests a TP structure bearing a carbonyl group, probably in the furan ring. The detection of a neutral loss of CO at *m/z* 248 ($C_{17}H_{11}FN^+$) from *m/z* 276 along with the fragmentation of $(CH_3)_2NHO$ at *m/z* 294 ($C_{18}H_{13}FNO_2^+$) from the protonated parent ion, support this proposal (Fig. S11). The latter fragmentation, corroborated by the fact that only the loss of one H_2O molecule from the parent ion was observed (in other words, there was no formation of alcohol in the molecule, that is, there was no hydroxylation process) argues for a TP with an *N*-oxide structure.

3.3.7. TP-343 (m/z 343.1816; $C_{20}H_{24}FN_2O_2^+$)

The MS/MS spectrum of TP-343 exhibited fragmentation reactions corresponding to CIT behavior (Fig. S12). Neutral loss of CHNO from *m/z* 280 giving rise to the fragment ion *m/z* 237 ($C_{17}H_{14}F^+$), the most abundant ion in the mass spectrum, argues for a TP structure bearing an amide group, which may have been formed by nitrile hydrolysis of CIT.

3.3.8. TP-359 (m/z 359.1765; $C_{20}H_{24}FN_2O_3^+$)

The fragmentation patterns in the MS/MS spectrum of TP-359 (Fig. S13), exhibited similarities to TP-343 with respect to the neutral losses observed namely, the neutral loss of CHNO from *m/z* 280 ($C_{18}H_{15}FNO^+$) giving rise to fragment ion *m/z* 237 ($C_{17}H_{14}F^+$). This enabled us to conclude that TP-359 bared an amide group. The difference consisted in two neutral losses of H_2O instead of one, as for TP-343. This suggests the presence of an alcohol group, through

Table 1
Identification of TPs of CIT. CL: chlorination, UV: photodegradation and H_2O: hydrolysis.

TP code	t_R (min.)	Theoretical mass $[M+H]^+$	Elemental formula $[M+H]^+$	Mass error (ppm)	DBE	Proposed structure	Process
CIT	6.96	325.1711	$C_{20}H_{22}FN_2O^+$	−0.9	10.5	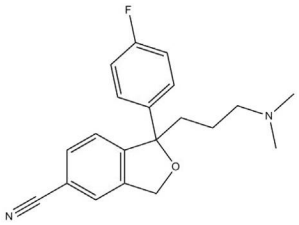	
		307.1605	$C_{20}H_{20}FN_2^+$	−0.6	11.5		
		280.1132	$C_{18}H_{15}FNO^+$	−0.3	11.5		
		262.1027	$C_{18}H_{13}FN^+$	0.8	12.5		
		247.0792	$C_{17}H_{10}FN^+$	0.8	13		
		234.0714	$C_{16}H_9FN^+$	1.3	12.5		
		166.0651	$C_{12}H_8N^+$	2.4	9.5		
TP-245	2.90	245.1285	$C_{14}H_{17}N_2O_2^+$	−0.8	7.5	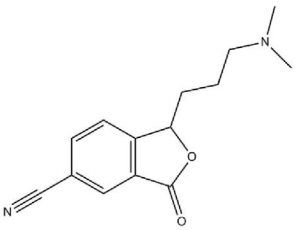	UV
		227.1179	$C_{14}H_{15}N_2O^+$	−2.6	8.5		
		200.0706	$C_{12}H_{10}NO_2^+$	1.0	8.5		
		182.0600	$C_{12}H_8NO^+$	0	9.5		
		158.0237	$C_9H_4NO_2^+$	−1.9	8.5		
		154.0651	$C_{11}H_8N^+$	−1.9	8.5		
TP-261	2.65	261.1234	$C_{14}H_{17}N_2O_3^+$	3.4	7.5	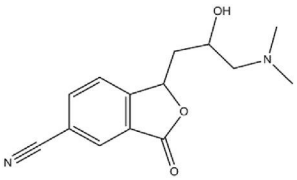	UV
		243.1128	$C_{14}H_{15}N_2O_2^+$	−1.2	8.5		
		216.0655	$C_{12}H_{10}NO_3^+$	0	8.5		
		198.0550	$C_{12}H_8NO_2^+$	−4.0	9.5		
		180.0444	$C_{12}H_6NO^+$	−3.3	10.5		
		174.0180	$C_9H_4NO_3^+$	3.4	8.5		
		170.0600	$C_{11}H_8NO^+$	−2.9	8.5		
TP-311	6.90	311.1554	$C_{19}H_{20}FN_2O^+$	1.3	10.5	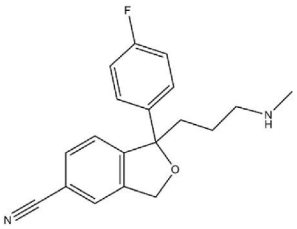	UV. CL, H_2O
		293.1449	$C_{19}H_{18}FN_2^+$	−3.0	11.5		
		262.1027	$C_{18}H_{13}FN^+$	−4.6	12.5		
		247.0765	$C_{14}H_{12}FO_3^+$	4.0	8.5		
		234.0714	$C_{16}H_9FN^+$	−3.4	12.5		
		166.0651	$C_{12}H_8N^+$	−3.6	9.5		
TP-323	5.10	323.1754	$C_{20}H_{23}N_2O_2^+$	−1.2	10.5	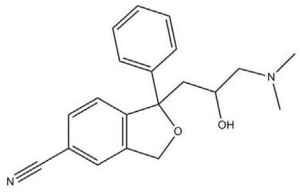	UV, H_2O
		305.1648	$C_{20}H_{21}N_2O^+$	−2.0	11.5		
		278.1176	$C_{18}H_{16}NO_2^+$	−1.4	12.5		
		260.1070	$C_{18}H_{14}NO^+$	−2.7	12.5		
		242.0964	$C_{18}H_{12}N^+$	2.0	13.5		
		232.0757	$C_{16}H_{10}NO^+$	−3.4	12.5		
		204.0808	$C_{15}H_{10}N^+$	−4.9	11.5		
		166.0651	$C_{12}H_8N^+$	−4.8	9.5		
TP-325	6.59	325.1348	$C_{19}H_{18}FN_2O_2^+$	0.3	11.5	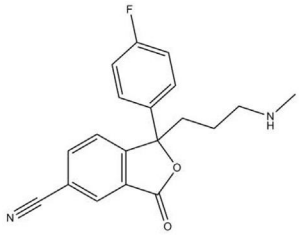	CL, UV
		307.1241	$C_{19}H_{16}FN_2O^+$	0.6	12.5		
		294.0925	$C_{18}H_{13}FNO_2^+$	0.3	12.5		
		276.0819	$C_{18}H_{11}FNO^+$	−0.4	13.5		
		258.0714	$C_{18}H_9FN^+$	−1.2	14.5		
		248.0870	$C_{17}H_{11}FN^+$	0	12.5		
		172.0393	$C_{10}H_6NO_2^+$	−1.7	8.5		
TP-327	5.60	327.1488	$C_{19}H_{20}FN_2O_2^+$	4.6	10.5	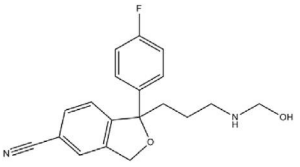	CL
		291.1295	$C_{19}H_{16}FN_2^+$	0	12.5		
		262.1027	$C_{18}H_{13}FN^+$	−0.4	12.5		
		260.0870	$C_{18}H_{11}FN^+$	−0.4	13.5		
		240.0819	$C_{15}H_{11}FNO^+$	1.6	10.5		
		234.0714	$C_{16}H_9FN^+$	0	12.5		
		166.0651	$C_{12}H_8N^+$	0.6	9.5		

(*continued on next page*)

Table 1 (*continued*)

TP code	t_R (min.)	Theoretical mass $[M+H]^+$	Elemental formula $[M+H]^+$	Mass error (ppm)	DBE	Proposed structure	Process
TP-337	4.9	337.1547	$C_{20}H_{21}N_2O_3^+$	−2.4	11.5	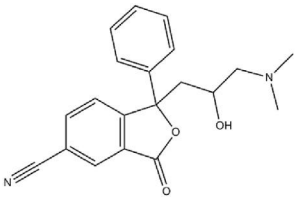	UV
		319.1441	$C_{20}H_{19}N_2O_2^+$	−1.6	12.5		
		292.0968	$C_{18}H_{14}NO_3^+$	−2.0	12.5		
		274.0863	$C_{18}H_{12}NO_2^+$	−1.8	13.5		
		256.0757	$C_{18}H_{10}NO^+$	−2.7	14.5		
		246.0913	$C_{17}H_{12}NO^+$	−2.4	12.5		
		172.0393	$C_{10}H_6NO_2^+$	−4.1	8.5		
TP-339A	6.69	339.1503	$C_{20}H_{20}FN_2O_2^+$	−1.7	11.5	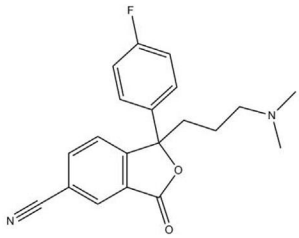	UV, CL, H_2O
		321.1398	$C_{20}H_{18}FN_2O^+$	−0.9	12.5		
		294.0925	$C_{18}H_{13}FNO_2^+$	1.0	12.5		
		276.0819	$C_{18}H_{11}FNO^+$	−2.5	13.5		
		258.0714	$C_{18}H_9FN^+$	−3.1	14.5		
		248.0870	$C_{17}H_{11}FN^+$	−0.8	12.5		
		228.0808	$C_{17}H_{10}N^+$	−4.0	13.5		
TP-339B	4.27	339.1703	$C_{20}H_{23}N_2O_3^+$	−3.5	10.5	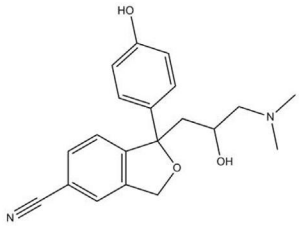	UV
		321.1598	$C_{20}H_{21}N_2O_2^+$	1.2	11.5		
		276.1019	$C_{18}H_{14}NO_2^+$	−0.4	12.5		
		258.0913	$C_{18}H_{12}NO^+$	−2.7	13.5		
		240.0808	$C_{18}H_{10}N^+$	−4.2	14.5		
		230.0964	$C_{17}H_{12}N^+$	−3.0	12.5		
		166.0651	$C_{12}H_8N^+$	−0.6	9.5		
TP-341A1	7.29	341.1660	$C_{20}H_{22}FN_2O_2^+$	−1.7	10.5	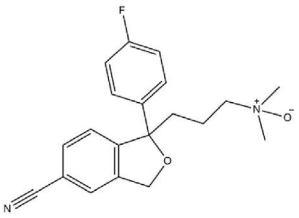	CL
		280.1132	$C_{18}H_{15}FNO^+$	0.3	11.5		
		262.1027	$C_{18}H_{13}FN^+$	0	12.5		
		247.0792	$C_{17}H_{10}FN^+$	−2.8	13		
		234.0714	$C_{16}H_9FN^+$	0.4	12.5		
		166.0651	$C_{12}H_8N^+$	−0.6	9.5		
TP-341A2	6.27	341.1660	$C_{20}H_{22}FN_2O_2^+$	−3.8	10.5	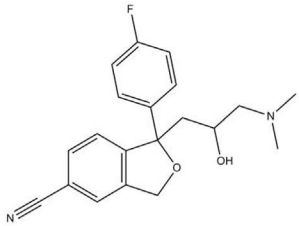	UV, H_2O
		323.1554	$C_{20}H_{20}FN_2O^+$	−0.9	11.5		
		305.1449	$C_{20}H_{18}FN_2^+$	−1.3	12.5		
		278.0976	$C_{18}H_{13}FNO^+$	−2.1	12.5		
		260.0870	$C_{18}H_{11}FN^+$	−3.5	13.5		
		240.0808	$C_{18}H_{10}N^+$	−2.9	14.5		
		234.0714	$C_{16}H_9FN^+$	0.4	12.5		
		166.0651	$C_{12}H_8N^+$	−4.2	9.5		
TP-341B	2.48	341.1860	$C_{20}H_{25}N_2O_3^+$	0.3	9.5	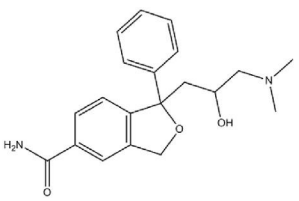	UV
		323.1754	$C_{20}H_{23}N_2O_2^+$	0.9	10.5		
		279.1016	$C_{18}H_{15}O_3^+$	1.0	11.5		
		278.1187	$C_{18}H_{16}NO_2^+$	−0.2	11.5		
		261.0921	$C_{18}H_{13}O_2^+$	−4.9	12.5		
		250.0863	$C_{16}H_{12}NO_2^+$	−2.4	11.5		
		235.1117	$C_{17}H_{15}O^+$	−1.8	10.5		
		217.1023	$C_{17}H_{13}^+$	−1.4	11.5		
		184.0757	$C_{12}H_{10}NO^+$	−4.3	8.5		
TP-343	5.16	343.1816	$C_{20}H_{24}FN_2O_2^+$	−2.9	9.5	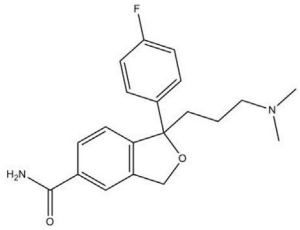	UV
		325.1711	$C_{20}H_{22}FN_2O^+$	−2.1	10.5		
		298.1238	$C_{18}H_{17}FNO_2^+$	−1.0	10.5		
		280.1132	$C_{18}H_{15}FNO^+$	−1.8	20.5		
		263.0867	$C_{18}H_{12}FO^+$	−4.6	12.5		
		252.0819	$C_{16}H_{11}FNO^+$	−2.0	11.5		
		237.1074	$C_{17}H_{14}F^+$	−4.6	10.5		
		217.1012	$C_{17}H_{13}^+$	−1.8	11.5		

Table 1 (*continued*)

TP code	t_R (min.)	Theoretical mass $[M+H]^+$	Elemental formula $[M+H]^+$	Mass error (ppm)	DBE	Proposed structure	Process
TP-353	4.03	353.1496	$C_{20}H_{21}N_2O_4^+$	−1.7	11.5	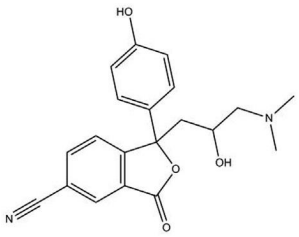	UV
		290.0812	$C_{18}H_{12}NO_3^+$	−0.7	13.5		
		272.0706	$C_{18}H_{10}NO_2^+$	−1.1	14.5		
		262.0863	$C_{17}H_{12}NO_2^+$	−1.4	12.5		
		244.0757	$C_{17}H_{10}NO^+$	−1.2	13.5		
		216.0808	$C_{16}H_{10}N^+$	−4.6	12.5		
		172.0393	$C_{10}H_6NO_2^+$	−4.0	8.5		
TP-355A	6.93	355.1452	$C_{20}H_{20}FN_2O_3^+$	0.8	11.5	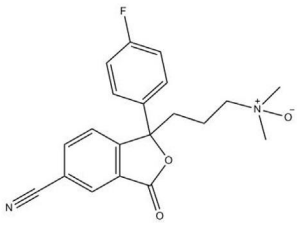	CL
		337.1347	$C_{20}H_{18}FN_2O_2^+$	2.0	12.5		
		294.0925	$C_{18}H_{13}FNO_2^+$	−0.7	12.5		
		276.0819	$C_{18}H_{11}FNO^+$	1.4	13.5		
		258.0714	$C_{18}H_9FN^+$	1.2	14.5		
		252.0455	$C_{15}H_7FNO_2^+$	−1.2	12.5		
		248.0870	$C_{17}H_{11}FN^+$	1.6	12.5		
TP-355B	3.10	355.1652	$C_{20}H_{23}N_2O_4^+$	−3.7	10.5	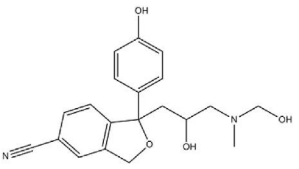	UV
		337.1547	$C_{20}H_{21}N_2O_3^+$	−2.3	11.5		
		319.1441	$C_{20}H_{19}N_2O_2^+$	0	12.5		
		292.0968	$C_{18}H_{14}NO_3^+$	−1.7	12.5		
		276.1019	$C_{18}H_{14}NO_2^+$	0.4	12.5		
		258.0913	$C_{18}H_{12}NO^+$	−0.8	13.5		
		230.0964	$C_{17}H_{12}N^+$	−4.0	12.5		
		209.1073	$C_{14}H_{13}N_2^+$	−1.9	9.5		
		182.0600	$C_{12}H_8NO^+$	2.7	9.5		
		166.0651	$C_{12}H_8N^+$	−4.2	9.5		
TP-359	3.43	359.1765	$C_{20}H_{24}FN_2O_3^+$	0.5	9.5	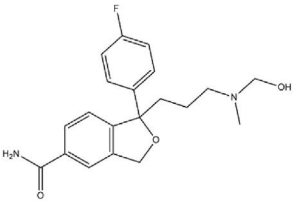	UV
		341.1660	$C_{20}H_{22}FN_2O_2^+$	0.9	10.5		
		323.1554	$C_{20}H_{20}FN_2O^+$	−2.5	11.5		
		296.1081	$C_{18}H_{15}FNO_2^+$	1.3	11.5		
		280.1132	$C_{18}H_{15}FNO^+$	−1.1	11.5		
		252.0819	$C_{16}H_{11}FNO^+$	4.4	11.5		
		237.1074	$C_{17}H_{14}F^+$	−2.1	10.5		
		184.0768	$C_9H_{11}FNO_2^+$	−2.2	4.5		

hydroxylation of the methyl group. Hydroxylation on the TP β-carbon could be possible, however, after the two H_2O molecules eliminations, loss of C_2H_5N was detected at *m/z* 280. This fragment ion loses one C_2H_5N moiety, meaning that in *m/z* 341 the loss of alcohol attached to methyl has occurred. Another fragment ion from *m/z* 341 is *m/z* 296, formed by the loss of C_2H_7NO, which reinforces the idea that hydroxylation occurred in the methyl group.

3.3.9. TP-323 (*m/z* 323.1759; $C_{20}H_{23}N_2O_2^+$)

The TP-323 should have been formed by fluorine dehalogenation and hydroxylation at the β-carbon of the aliphatic chain (α-carbon might result in a less stable compound). This assumption is based on the analysis of its MS/MS fragmentation patterns showing that the neutral losses were similar to the ones of CIT, with one exception (Fig. S14). The latter is the loss of one more H_2O molecule, that is, from fragment ion *m/z* 260 ($C_{18}H_{14}NO^+$) to *m/z* 242 ($C_{18}H_{12}N^+$). This observation may corroborate the formation of an alcohol by hydroxylation at the β-carbon. The absence of a neutral loss of C_2H_7NO from *m/z* 260 also argues for this proposal since a dimethylamine oxide or (methylamino)methanol could not have been possible.

3.3.10. TP-339B (*m/z* 339.1703; $C_{20}H_{23}N_2O_3^+$)

The analysis of TP-339B MS/MS spectrum (Fig. S15) showed fragmentation patterns compatible with hydroxylation reactions responsible for its formation. Indeed, the elimination of $2H_2O$ molecules, one from *m/z* 339 to *m/z* 321 ($C_{20}H_{21}N_2O_2^+$) and the other from *m/z* 276 ($C_{18}H_{14}NO_2^+$) to *m/z* 258 ($C_{18}H_{12}NO^+$) argue for the elimination of one H_2O from the furan group whereas the other H_2O elimination appears to be related to hydroxylation on the aliphatic β-carbon. Interestingly, a neutral loss of CO from *m/z* 258 to *m/z* 230 ($C_{17}H_{12}N^+$) may indicate a structure bearing a phenol group. The neutral loss of C_2H_7NO was not detected then, dimethylamine oxide or (methylamino)methanol should not have been responsible for TP 339-B formation.

3.3.11. TP-337 (*m/z* 337.1547; $C_{20}H_{21}N_2O_3^+$)

The MS/MS spectrum of this TP exhibits fragmentation patterns similar to the ones of TP-323 (Fig. S16). Therefore, for the formation of this TP, hydroxylation on β-carbon (on α-carbon, the compound would be less stable) and dehalogenation of fluorine could be considered. The loss of CO, however, was also identified, suggesting that oxidation should have occurred, probably in the furan ring by the fragmentation of *m/z* 274 ($C_{18}H_{12}NO_2^+$) to *m/z* 246 ($C_{17}H_{12}NO^+$).

3.3.12. TP-353 (*m/z* 353.1496; $C_{20}H_{21}N_2O_4^+$)

The behavior of this TP under MS/MS conditions presented similarities to TP-337 (Fig. S17). Indeed, neutral losses of H_2O, CO and $(CH_3)_2NH$ molecules were also detected, in other words, *m/z* 353 to *m/z* 290 ($C_{18}H_{12}NO_3^+$) presented losses of H_2O and $(CH_3)_2NH$, *m/z* 290 to *m/z* 244 ($C_{17}H_{10}NO^+$), neutral losses of H_2O and CO, argue for a TP structure encompassing hydroxylation at β-carbon

and oxidation of the furan ring. Nevertheless, the elimination of one CO molecule from *m/z* 244 ($C_{17}H_{10}NO^+$) to *m/z* 216 ($C_{16}H_{10}N^+$) was detected in the MS/MS spectrum, which may suggest a TP structure bearing a phenol group that may have been formed by dehalogenation of fluorine.

3.3.13. TP-355B (m/z 355.1652; $C_{20}H_{23}N_2O_4^+$)

TP-355B MS/MS spectrum showed the neutral loss of three H_2O molecules (Fig. S18), being the loss of one H_2O molecule from the furan ring leading to *m/z* 337 ($C_{20}H_{21}N_2O_3^+$). The other two, *m/z* 337 to *m/z* 319 ($C_{20}H_{19}N_2O_2^+$) and *m/z* 276 ($C_{18}H_{14}NO_2^+$) to *m/z* 258 ($C_{18}H_{12}NO^+$) suggested a TP structure bearing two alcohol groups formed by hydroxylation reactions, one at the β-carbon, corroborated by *m/z* 258 ($C_{18}H_{12}NO^+$) and the other at the methyl group from the tertiary amine. The fragment ion at *m/z* 276 ($C_{18}H_{14}NO_2^+$) formed by the loss of C_2H_7NO from *m/z* 337 ($C_{20}H_{21}N_2O_3^+$), corroborated a (methylamino)methanol TP structure. Dehalogenation of fluorine was detected with the formation of phenol at *m/z* 182 ($C_{12}H_8NO^+$) by the neutral losses of one H_2O, C_2H_7NO and phenol C_6H_5OH molecules from the protonated TP-355B at *m/z* 355.

3.3.14. TP-341B (m/z 341.1860; $C_{20}H_{25}N_2O_3^+$)

The analysis of the MS/MS spectrum of this TP showed two neutral losses of H_2O (Fig. S19), one from *m/z* 341 to *m/z* 323 and the other from *m/z* 235 to *m/z* 217. These may indicate the loss of oxygen in the furan ring and the loss of one alcohol, probably formed by hydroxylation at the β-carbon of the aliphatic chain (on α-carbon a hemiaminal group might form but would result in a less stable compound), respectively. The formation of the amide group is supported by the elimination of NHCO from *m/z* 278 ($C_{18}H_{16}NO_2^+$), indicated by fragment ion $C_{17}H_{15}O^+$ (*m/z* 235), the most intense peak in the spectrum. The loss of NH_3 was also identified at *m/z* 279 ($C_{18}H_{15}O_3^+$) from protonated parent ion ($C_{20}H_{25}N_2O_3^+$) with neutral loss of $(CH_3)_2NH$, which may occur with the amide group. This is in agreement with Tu (2004) that detected the loss of NH_3 in MS/MS spectrum in protonated benzamides.

3.3.15. TP-245 (m/z 245.1285; $C_{14}H_{17}N_2O_2^+$)

Based on the analysis of the MSMS spectrum the TP was formed by the loss of fluorobenzene and an oxidation reaction on the furan ring. The loss of CO, which means the oxidation of furan ring, was identified by a fragmentation reaction where *m/z* 182 ($C_{12}H_8NO^+$) leads to *m/z* 154 ($C_{11}H_8N^+$), by the loss of CO. Other neutral losses correspond to similar losses found in the MS/MS spectrum of CIT (Fig. S20), namely (H_2O and $(CH_3)_2NH$).

3.3.16. TP-261 (m/z 261.1285; $C_{14}H_{17}N_2O_3^+$)

Analysis of the fragmentation in the MS/MS spectrum (Fig. S21) of this TP showed a fragment ion at *m/z* 180 ($C_{12}H_6NO^+$) that resulted from the loss of H_2O from *m/z* 198 ($C_{12}H_8NO_2^+$) which also did fragment to give *m/z* 170 ($C_{11}H_8NO^+$) by CO loss. Based on these observations and on the fact that the elemental formula of TP-261, when compared to CIT, suggested the loss of a fluorobenzene ring we propose a TP structure formed by hydroxylation of β-carbon (α-carbon might form an unstable compound) and a furan ring oxidation (fragment ion at *m/z* 170 ($C_{11}H_8NO^+$)).

3.4. Summary of fragmentation patterns

The analysis of the tandem mass spectra of the TPs enabled to attribute structures to these compounds. Table 1 summarizes the results that enabled the identification of the seventeen TPs and includes their retention times, processes of formation, proposed structures, numbers of double bond equivalent (DBE), elemental formula and their respective fragmentation ions. Mass error was below 5 ppm for the prediction. Chromatograms of the TPs are shown in Fig. S22.

3.5. In silico toxicity assessment

Details of prediction toxicity were described in section 2.4 and Table S2. For endpoint F. Minnow 96-h LC_{50}, most of TPs presented low toxicity compared to CIT, with the exception of TP-353, TP-325 and TP-339A, the first TP was formed only by UV light and both were degraded until the end of the experiment, TP-353 in 240 min about 76%. was removed. The TP-339A was identified in the three experiments: hydrolysis, chlorination and photodegradation. In hydrolysis TP-339A was stable, however, showed a low signal intensity compared to CIT. In the hydrolysis experiments, the TP was stable, but showed very low signal intensity in comparison to CIT. For comparison purposes, if the TP-339A signal has the same intensity as the CIT signal, the maximum concentration found for TP formed by hydrolysis was 0.0012 mg L^{-1}. In chlorination and photodegradation, the TP-339A formed and degraded after 240 min of UV irradiation and 480 min with chlorine.

With respect to the parameter *D. magna* 48-h LC_{50} all TPs had low toxicity compared to CIT and for *T. Pyriformis* 48-h IGC_{50}, two TPs had a higher toxicity than CIT: TP-325 and TP-339A. The characteristics of TP-325 and TP-339A were discussed above.

For comparison criteria, Christensen et al. (2007) determined the toxicity of CIT in *algae* and *daphnia* and the results of 48 h EC_{50} were 1.6 and 20 mg L^{-1}, respectively. Studies about the effects of CIT on adhesion to the substrate in species of marine snails showed induced foot detachment from the substrate and the lowest-observed-effect concentration (LOEC) for CIT was 405 μg L^{-1} (Fong and Molnar. 2013).

The mutagenic prediction of QSAR identified 2 TPS with positive result for AMES test: TP-339B and TP-355B (Table S3), both were detected in the photodegradation experiment and, after 240 min on contact with UV light, approximately 90% of TP-339B and 86% of TP-355B were removed.

For the prediction of carcinogenicity, three *in silico* models were used. The TP-341A1 presented positive results for the three models and this TP was detected only in chlorination process which removed only 44% of its concentration. 10 TPs and CIT showed positive results in at least two models for *in silico* carcinogenicity.

It is difficult to evaluate the toxicity of these TPs, since most of them do not have standards and although the *in vitro* method would be ideal, it would be difficult to evaluate which TPs present greater toxicity, whereas in these experiments several TPs were formed at the same time.

4. Wastewater samples

Finally, real samples from wastewater were analyzed to identify the TPs. The tertiary treatment used in the WWTP is by chlorination, unfortunately the UV treatment is unavailable.

CIT and only two TPs were detected and confirmed by retention time, precursor ion and fragmentation patterns: TP-311, TP-341A1 (Chromatograms are shown in Fig. S23). In laboratory experiments, TP-311 was identified in all experiments and was completely degraded in photodegradation and chlorination and TP-341A1 was only identified in chlorination. Also, these TPs are human metabolites. The WWTP has a chlorination system, which may explain the non-detection of most TPs formed by UV light. The concentration of CIT was 137 ng L^{-1} in effluent, and the relative concentrations of the TPs were 14 ng L^{-1} for TP-311 and 12 ng L^{-1} for TP-341A1, if the signals intensity of the TPs has the same proportion of the signal intensity of the CIT. In the influent, only CIT was detected, and quantified at 227 ng L^{-1}, which leads to believe that the TPs may be

formed by the processes of the WWTP. However, it would be necessary to analyze more samples to confirm this assumption. In the literature, some studies argue for this assumption, since it detected the metabolite of CIT, desmethylcitalopram (TP-311) in higher concentrations in the effluent from sewage treatment plants compared to the raw influent (Subedi and Kannan, 2015).

5. Conclusions

The experiments performed encompassed degradation of CIT, identification of the TPs formed using LC-QTOF/MS, toxicity assessment of these TPs and analysis of effluent samples. Degradation of CIT at three different laboratory conditions: hydrolysis, chlorination and photodegradation process, resulted in seventeen possible identified TPs, seven of them having never been reported in the literature. The products had different behavior with respect to time profile. All TPs from photodegradation processes were formed and completely or partially degraded in 240 min. TP-339A (3-oxo citalopram, $C_{20}H_{19}FN_2O_2$) TP-311 (desmethylcitalopram, $C_{19}H_{19}FN_2O$) and TP-341A1 (citalopram *N*-oxide, $C_{20}H_{21}FN_2O_2$), human metabolites, were detected in these experiments, and showed that the compounds can be formed under abiotic conditions. CIT was degraded almost entirely in chlorination and by UV light.

Toxicity predictions by *in silico* methods showed most TPs were less toxic or had toxicity equal to CIT. For mutagenicity predictions, TP-339B and TP-355B presented mutagenicity and for carcinogenicity ten TPs presented positive results in at least two models.

Analysis in real matrices (wastewater samples) showed that only TP-311 and TP-341A1 were detected, however, it is not possible to identify whether these compounds are metabolites or transformation products, presumably because in sewage treatment plant and in the environment complex interactions can occur.

In conclusion LC-QTOF/MS proved to be a useful tool for elucidating TPs.

Acknowledgments

The authors are grateful to Águas de Portugal for providing samples. This work was supported by Brazilian Federal Agency Coordenação de Aperfeiçoamento de Pessoal de Nível Superior (CAPES) for PhD grants (99999.000845/2014-00) and Fundação para a Ciência e a Tecnologia (FCT) Portugal (Projects UID/MULTI/00612/2013, PEst-OE/QUI/UI0612/2013 and LISBOA-01-0145-FEDER-022125).

Appendix A. Supplementary data

Supplementary data to this article can be found online at https://doi.org/10.1016/j.chemosphere.2018.11.027.

References

Beretsou, V.G., Psoma, A.K., Gago-Ferrero, P., Aalizadeh, R., Fenner, K., Thomaidis, N.S., 2016. Identification of biotransformation products of citalopram formed in activated sludge. Water Res. 103, 205–214. https://doi.org/10.1016/j.watres.2016.07.029.

Castro, G., Casado, J., Rodríguez, I., Ramil, M., Ferradás, A., Cela, R., 2016. Time-of-flight mass spectrometry assessment of fluconazole and climbazole UV and UV/H2O2 degradability: kinetics study and transformation products elucidation. Water Res. 88, 681–690. https://doi.org/10.1016/j.watres.2015.10.053.

Christensen, A.M., Faaborg-Andersen, S., Ingerslev, F., Baun, A., 2007. Mixture and single-substance toxicity of selective serotonin reuptake inhibitors toward algae and crustaceans. Environ. Toxicol. Chem. 26, 85–91. https://doi.org/10.1897/06-219r.1.

Collado, N., Rodriguez-Mozaz, S., Gros, M., Rubirola, A., Barceló, D., Comas, J., Rodriguez-Roda, I., Buttiglieri, G., 2014. Pharmaceuticals occurrence in a WWTP with significant industrial contribution and its input into the river system. Environ. Pollut. 185, 202–212. https://doi.org/10.1016/j.envpol.2013.10.040.

Escher, B.I., Fenner, K., 2011. Recent advances in environmental risk assessment of transformation products. Environ. Sci. Technol. 45, 3835–3847. https://doi.org/10.1021/es1030799.

Fatta-Kassinos, D., Vasquez, M.I., Kümmerer, K., 2011. Transformation products of pharmaceuticals in surface waters and wastewater formed during photolysis and advanced oxidation processes - degradation, elucidation of byproducts and assessment of their biological potency. Chemosphere 85, 693–709. https://doi.org/10.1016/j.chemosphere.2011.06.082.

Fong, P.P., Molnar, N., 2013. Antidepressants cause foot detachment from substrate in five species of marine snail. Mar. Environ. Res. 84, 24–30. https://doi.org/10.1016/j.marenvres.2012.11.004.

Gao, J., Ellis, L.B.M., Wackett, L.P., 2010. The university of minnesota biocatalysis/biodegradation database. Improv. Public Access 38, 488–491. https://doi.org/10.1093/nar/gkp771.

Giebułtowicz, J., Nałęcz-Jawecki, G., 2014. Occurrence of antidepressant residues in the sewage-impacted Vistula and Utrata rivers and in tap water in Warsaw (Poland). Ecotoxicol. Environ. Saf. 104, 103–109. https://doi.org/10.1016/j.ecoenv.2014.02.020.

Golovko, O., Kumar, V., Fedorova, G., Randak, T., Grabic, R., 2014. Seasonal changes in antibiotics, antidepressants/psychiatric drugs, antihistamines and lipid regulators in a wastewater treatment plant. Chemosphere 111, 418–426. https://doi.org/10.1016/j.chemosphere.2014.03.132.

Hey, G., Grabic, R., Ledin, A., la Cour Jansen, J., Andersen, H.R., 2012. Oxidation of pharmaceuticals by chlorine dioxide in biologically treated wastewater. Chem. Eng. J 185–186, 236–242. https://doi.org/10.1016/j.cej.2012.01.093.

Hörsing, M., Kosjek, T., Andersen, H.R., Heath, E., Ledin, A., 2012. Fate of citalopram during water treatment with O_3, ClO_2, UV and fenton oxidation. Chemosphere 89, 129–135. https://doi.org/10.1016/j.chemosphere.2012.05.024.

Hübner, U., von Gunten, U., Jekel, M., 2015. Evaluation of the persistence of transformation products from ozonation of trace organic compounds - a critical review. Water Res. 68, 150–170. https://doi.org/10.1016/j.watres.2014.09.051.

Kasprzyk-Hordern, B., Dinsdale, R.M., Guwy, A.J., 2008. The occurrence of pharmaceuticals, personal care products, endocrine disruptors and illicit drugs in surface water in South Wales, UK. Water Res. 42, 3498–3518. https://doi.org/10.1016/j.watres.2008.04.026.

Li, J., Ma, L., Xu, L., 2016. Transformation of benzophenone-type UV filters by chlorine: kinetics, products identification and toxicity assessments. J. Hazard. Mater. 311, 263–272. https://doi.org/10.1016/j.jhazmat.2016.02.059.

Martin, T., 2016. Toxicity Estimation Software Tool (TEST) Version 4.2. U.S. Environmental Protection Agency, Washington, DC. Avaliable from. https://www.epa.gov/chemical-research/toxicity-estimation-software-tool-test. (Accessed 28 July 2017).

Matsushita, T., Hashizuka, M., Kuriyama, T., Matsui, Y., Shirasaki, N., 2016. Use of orbitrap-MS/MS and QSAR analyses to estimate mutagenic transformation products of iopamidol generated during ozonation and chlorination. Chemosphere 148, 233–240. https://doi.org/10.1016/j.chemosphere.2016.01.037.

Negreira, N., Regueiro, J., López de Alda, M., Barceló, D., 2015. Transformation of tamoxifen and its major metabolites during water chlorination: identification and *in silico* toxicity assessment of their disinfection byproducts. Water Res. 85, 199–207. https://doi.org/10.1016/j.watres.2015.08.036.

Pino-Otín, M.R., Muñiz, S., Val, J., Navarro, E., 2017. Effects of 18 pharmaceuticals on the physiological diversity of edaphic microorganisms. Sci. Total Environ. 595, 441–450. https://doi.org/10.1016/j.scitotenv.2017.04.002.

Pinto da Costa, J., Girão, A.V., Monteiro, O.C., Trindade, T., Costa, M.C., 2015. Biotechnologically obtained nanocomposites: a practical application for photodegradation of Safranin-T under UV-Vis and solar light. J. Environ. Sci. Heal. A. 50, 996–1010. https://doi.org/10.1080/10934529.2015.1038155.

Rainieri, S., Barranco, A., Primec, M., Langerholc, T., 2017. Occurrence and toxicity of musks and UV filters in the marine environment. Food Chem. Toxicol. 104, 57–68. https://doi.org/10.1016/j.fct.2016.11.012.

Salma, A., Thoröe-Boveleth, S., Schmidt, T.C., Tuerk, J., 2016. Dependence of transformation product formation on pH during photolytic and photocatalytic degradation of ciprofloxacin. J. Hazard. Mater. 313, 49–59. https://doi.org/10.1016/j.jhazmat.2016.03.010.

Schlüsener, M.P., Hardenbicker, P., Nilson, E., Schulz, M., Viergutz, C., Ternes, T.A., 2015. Occurrence of venlafaxine, other antidepressants and selected metabolites in the Rhine catchment in the face of climate change. Environ. Pollut. 196, 247–256. https://doi.org/10.1016/j.envpol.2014.09.019.

Sheng, L.-H., Chen, H.-R., Huo, Y.-B., Wang, J., Zhang, Y., Yang, M., Zhang, H.-X., 2014. Simultaneous determination of 24 antidepressant drugs and their metabolites in wastewater by ultra-high performance liquid chromatography–tandem mass spectrometry. Molecules 19, 1212–1222. https://doi.org/10.3390/molecules19011212.

Silva, L.J.G., Pereira, A.M.P.T., Meisel, L.M., Lino, C.M., Pena, A., 2014. A one-year follow-up analysis of antidepressants in Portuguese wastewaters: occurrence and fate, seasonal influence, and risk assessment. Sci. Total Environ. 490, 279–287. https://doi.org/10.1016/j.scitotenv.2014.04.131.

Stuart, M., Lapworth, D., Crane, E., Hart, A., 2012. Review of risk from potential emerging contaminants in UK groundwater. Sci. Total Environ. 416, 1–21. https://doi.org/10.1016/j.scitotenv.2011.11.072.

Subedi, B., Kannan, K., 2015. Occurrence and fate of select psychoactive pharmaceuticals and antihypertensives in two wastewater treatment plants in New York. Sci. Total Environ. 514, 273–280. https://doi.org/10.1016/j.scitotenv.2015.01.098.

Trawiński, J., Skibi, R., 2017. Photolytic and photocatalytic degradation of tandospirone: determination of kinetics, identi fi cation of transformation products and in silico estimation of toxicity. Sci. Total Environ. 591, 775–798. https://doi.org/10.1016/j.scitotenv.2017.03.050.

Trautwein, C., Kümmerer, K., 2012. Degradation of the tricyclic antipsychotic drug chlorpromazine under environmental conditions, identification of its main aquatic biotic and abiotic transformation products by LC – MS^n and their effects on environmental bacteria. J. Chromatogr. B 889–890, 24–38. https://doi.org/10.1016/j.jchromb.2012.01.022.

Ueno, D., Darling, C., Alaee, M., Campbell, L., Pacepavicius, G., Teixeira, C., Muir, D., 2007. Detection of hydroxylated polychlorinated biphenyls (OH-PCBs) in the abiotic environment: surface water and precipitation from Ontario, Canada. Environ. Sci. Technol. 41, 1841–1848. https://doi.org/10.1021/es061539l.

VEGA version 1.1.4. Istituto di Ricerche Farmacologiche Mario Negri Milano Available from: http://www.vega-qsar.eu. (Accessed July 28, 2017).

Wilde, M.L., Menz, J., Trautwein, C., Leder, C., Kümmerer, K., 2016. Environmental fate and effect assessment of thioridazine and its transformation products formed by photodegradation. Environ. Pollut. 213, 658–670. https://doi.org/10.1016/j.envpol.2016.03.018.

Yuan, S., Jiang, X., Xia, X., Zhang, H., Zheng, S., 2013. Detection, occurrence and fate of 22 psychiatric pharmaceuticals in psychiatric hospital and municipal wastewater treatment plants in Beijing, China. Chemosphere 90, 2520–2525. https://doi.org/10.1016/j.chemosphere.2012.10.089.

Appendix A. Supplementary data

Transformation products of citalopram: Identification, wastewater analysis and *in silico* toxicological assessment

S1. Sample preparation and validation

The effluent samples were previously filtered by nylon membrane (0.45 µm) and the pH was adjusted to 3 (2% acetic acid) for solid phase extraction (Oasis HLB 200mg, 6 mL, Waters). The cartridges were preconditioned with 5 mL of methanol and 5 mL of ultrapure water and washed with 5 mL of ultrapure water containing 5% of methanol. The cartridges were dried with nitrogen flow, eluted with 5 mL of methanol and 2 mL of acetone/methanol (1:1). The dried residue was reconstituted with 0.1 mL of water/methanol (4:1) and stored at -4 °C for further analysis.

The method showed low limits of detection and quantification (Table S1) through the signal-to-noise ratio (S/N), for L.D, S/N = 3 and for L.Q, S/N = 10. The correlation coefficient (r^2) for CIT was above 0.99 at the concentration range of 0.0005 to 0.05 mg L^{-1}. Recoveries were between 98.2% and 115.0% for both concentrations (40 and 400 ng L^{-1}) and the relative standard deviations were less than 20% (Table S1).

In electrospray ionization, a matrix effect may occur due to the presence of co-extracted matrix components. The matrix effect may result in ion suppression or enhancement in environmental contaminant analyzes, therefore, studying the matrix effect is relevant because of the complexity of the environmental matrices. The matrix effect was calculated by equation (Equation S1):

$$M.E(\%) = \frac{S_b}{S_a} * 100 \qquad \text{(Equation S1)}$$

Where, S_b is the analyte peak area of the effluent sample with the standard added after the extraction and S_a is the analyte peak area in effluent sample. Results with no matrix effect are represented with values of 100% and values >100% or <100% represent enhancement or suppression of the signal, respectively.

Table S1. Recoveries, matrix effect (M.E), limits of detection (L.D) and quantification (L.Q) and correlation coefficient (r^2) of CIT.

Compound	Re (RSD %) n=3 (40 ng L^{-1})	Re (RSD %) n=3 (400 ng L^{-1})	M.E (RSD %) n=3 (400 ng L^{-1})	L.D (ng L^{-1})	L.Q (ng L^{-1})	r^2
CIT	115.0 (6.0)	98.2 (11.2)	80.8 (6.6)	2.4	8	0.997

Table S2. Ecotoxicity prediction of CIT and its TPs by TEST (all results are expressed in mg L^{-1}).

Compound	F. Minnow 96-h LC_{50}	*D. magna* 48-h LC_{50}	*T. Pyriformis 4*8-h IGC_{50}
CIT	1.20	0.36	7.99
TP-245	4.20	0.83	30.79
TP-261	5.62	5.85	97.50
TP-311	1.25	1	9.51
TP-323	4.73	2.08	19.12
TP-325	0.57	1.13	6.51
TP-327	1.30	2.81	17.66
TP-337	2.29	2.06	24.17
TP-339A	0.59	0.72	5.54
TP-339B	3.32	1.33	17.66
TP-341A1	[a]	[a]	[a]
TP-341A2	3.18	1.58	22.06
TP-341B	17.78	25.38	22.63
TP-343	4.56	3.14	8.33
TP-353	0.93	2.19	9.47
TP-355A	[a]	[a]	[a]
TP-355B	5.50	2.93	34.05
TP-359	7.53	6.68	12.43

[a] No prediction could be made

Table S3. Mutagenicity and carcinogenicity prediction of CIT and its TP by VEGA plataform. (positive results is indicated by + and negative by -).

Compound	Mutagenicity	Carcinogenicity		
	Consensus method	CAESAR	ISS	IRFMN/ Antares
CIT	-	+	+	-
TP-245	-	-	-	-
TP-261	-	+	-	-
TP-311	-	-	+	-
TP-323	-	+	-	-
TP-325	-	-	+	+
TP-327	-	-	+	-
TP-337	-	+	-	+
TP-339A	-	-	+	+
TP-339B	+	+	-	-
TP-341A1	-	+	+	+
TP-341A2	-	+	+	-
TP-341B	-	+	-	+
TP-343	-	-	+	+
TP-353	-	-	-	+
TP-355A	-	-	+	+
TP-355B	+	+	+	-
TP-359	-	-	+	+

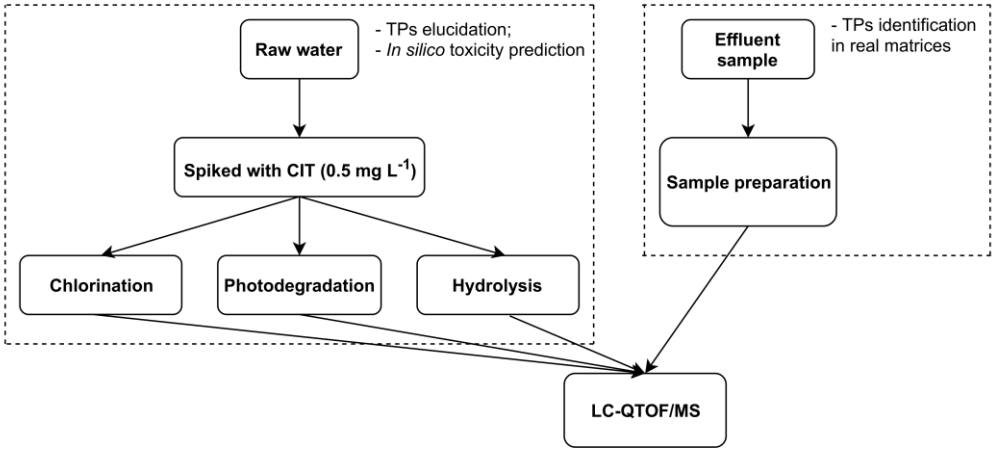

Fig. S1. A schematic pathway of the methodology.

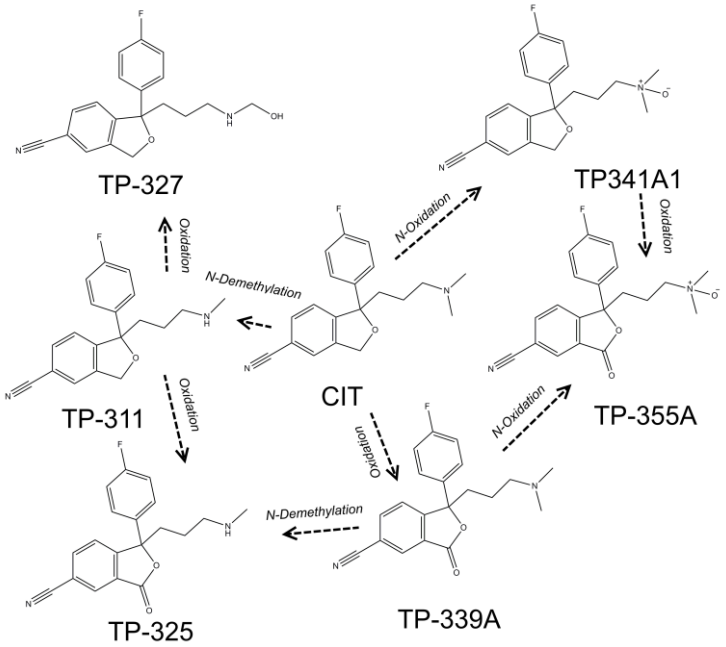

Fig. S2. Pathway proposed for TPs formed by chlorination.

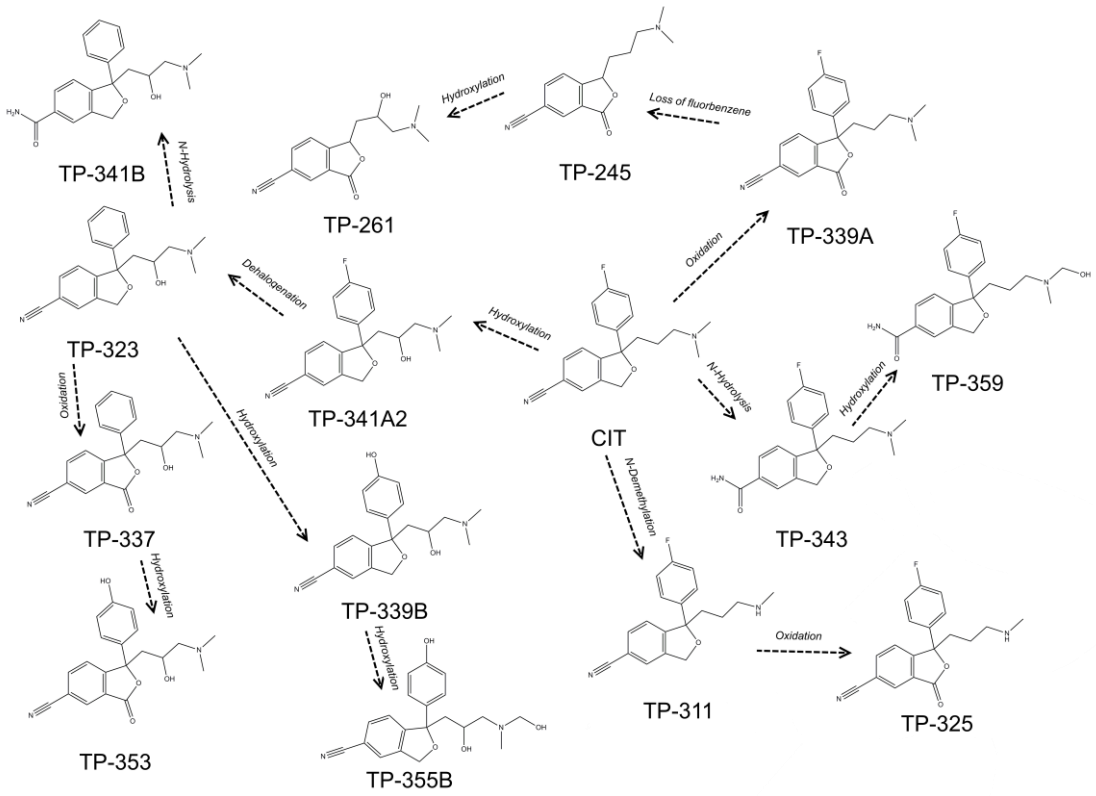

Fig. S3. Pathway proposed for TPs formed by photodegradation.

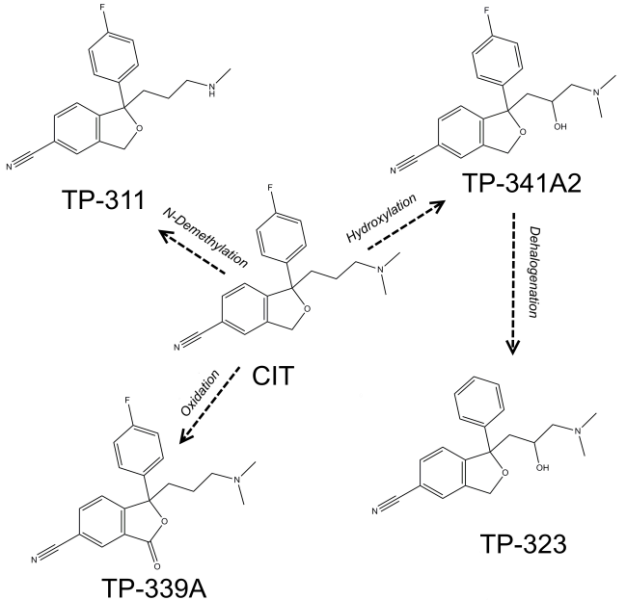

Fig. S4. Pathway proposed for TPs formed by hydrolysis.

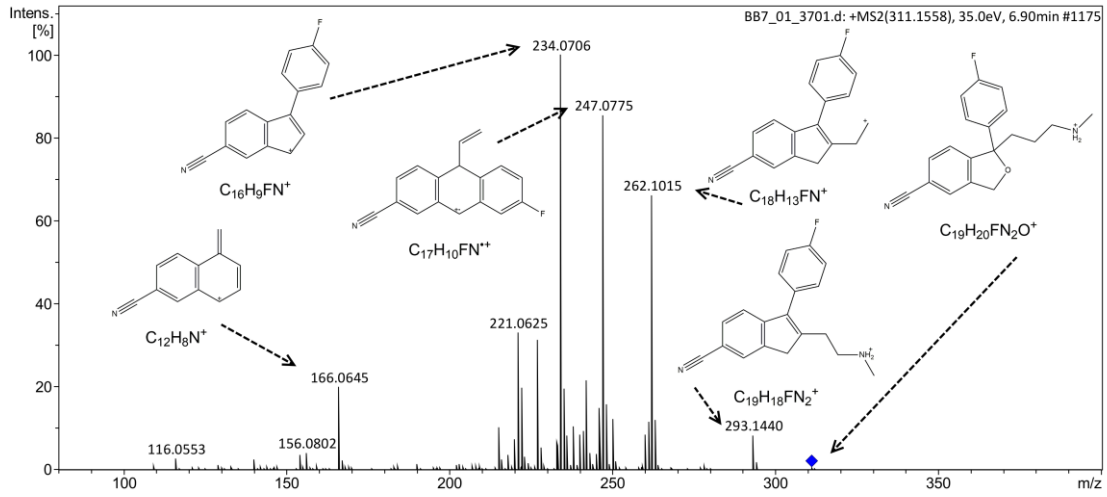

Fig. S5. MS/MS spectrum and proposed structures for TP-311.

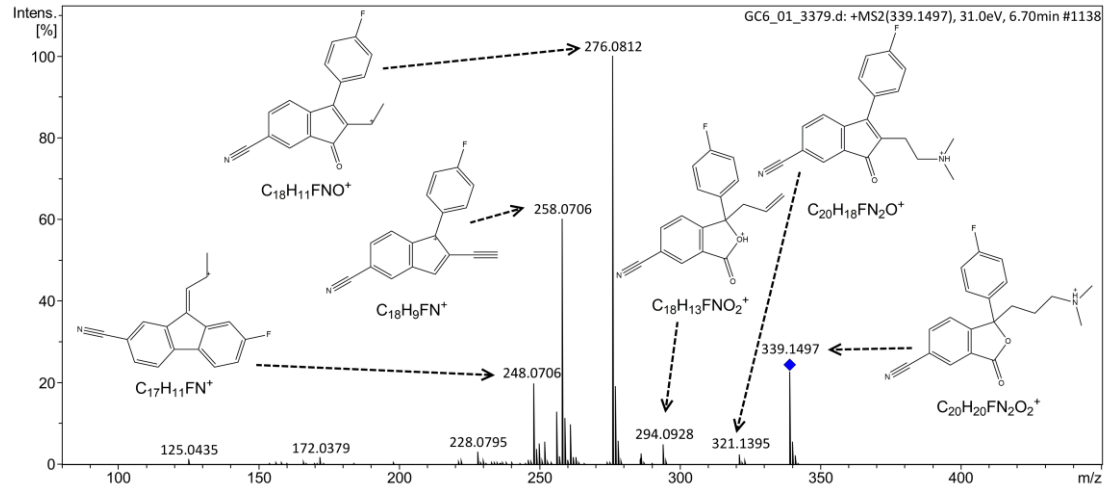

Fig. S6. MS/MS spectrum and proposed structures for TP-339A.

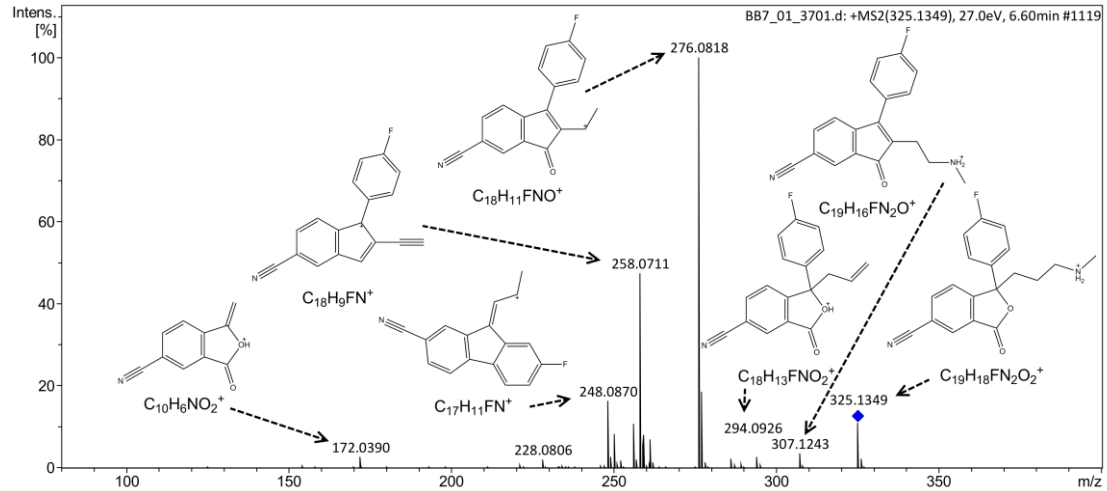

Fig. S7. MS/MS spectrum and proposed structures for TP-325.

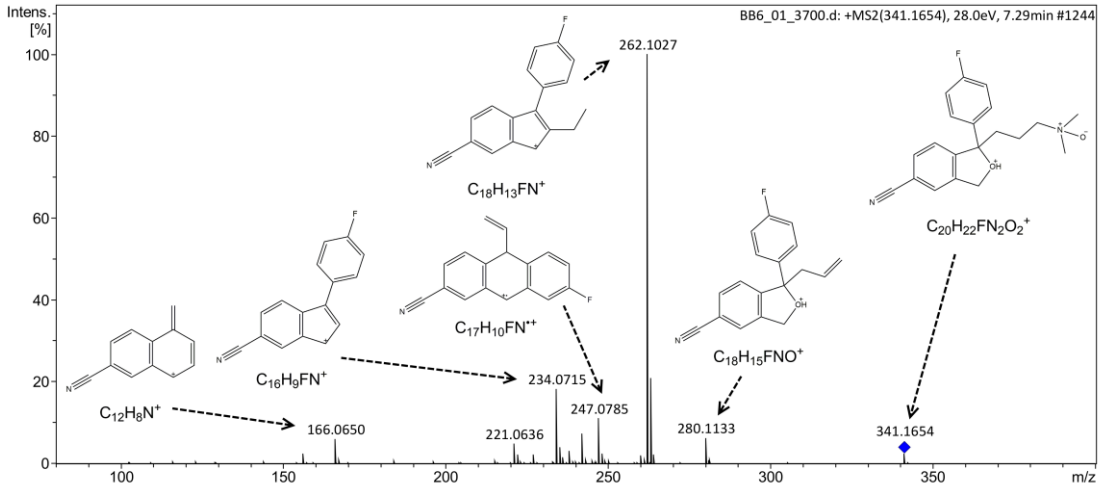

Fig. S8. MS/MS spectrum and proposed structures for TP-341A1.

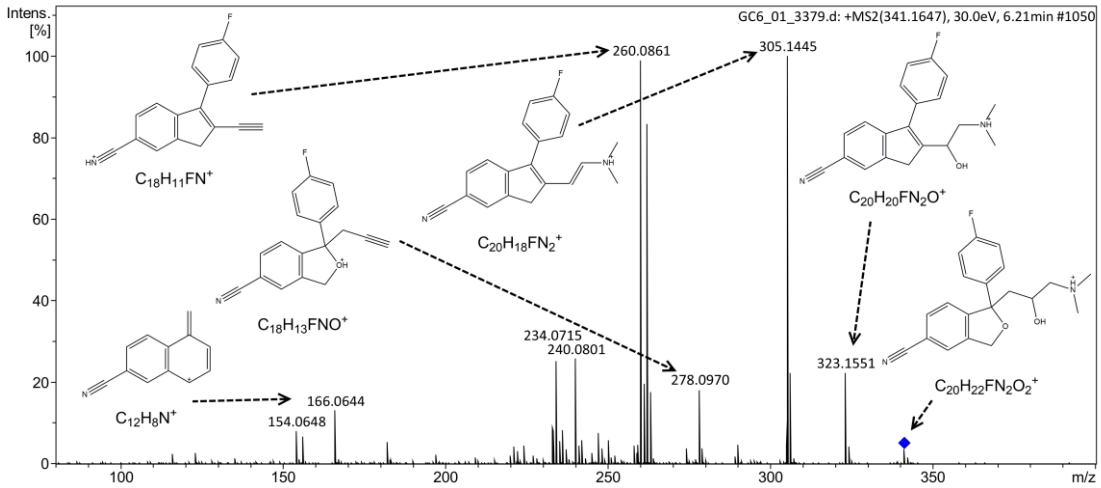

Fig. S9. MS/MS spectrum and proposed structures for TP-341A2.

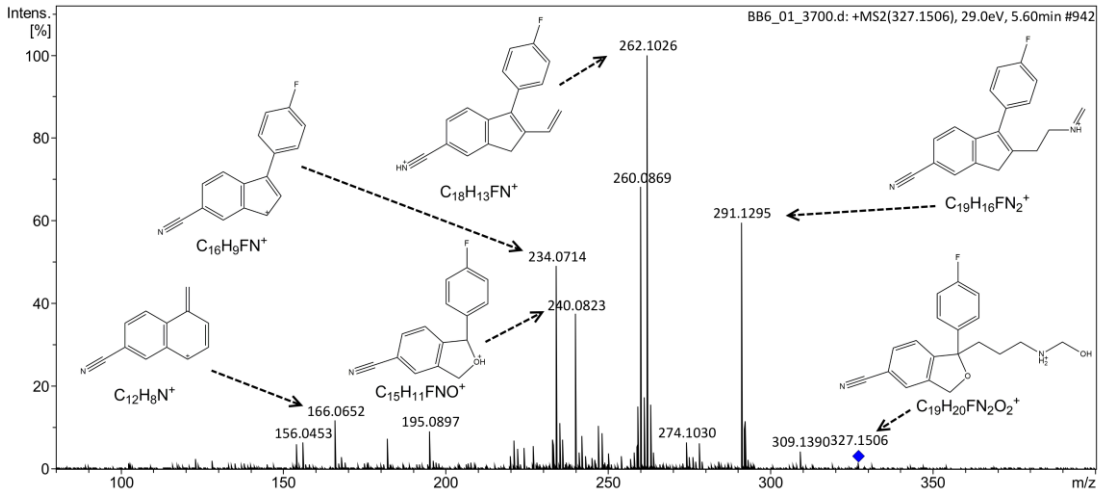

Fig. S10. MS/MS spectrum and proposed structures for TP-327.

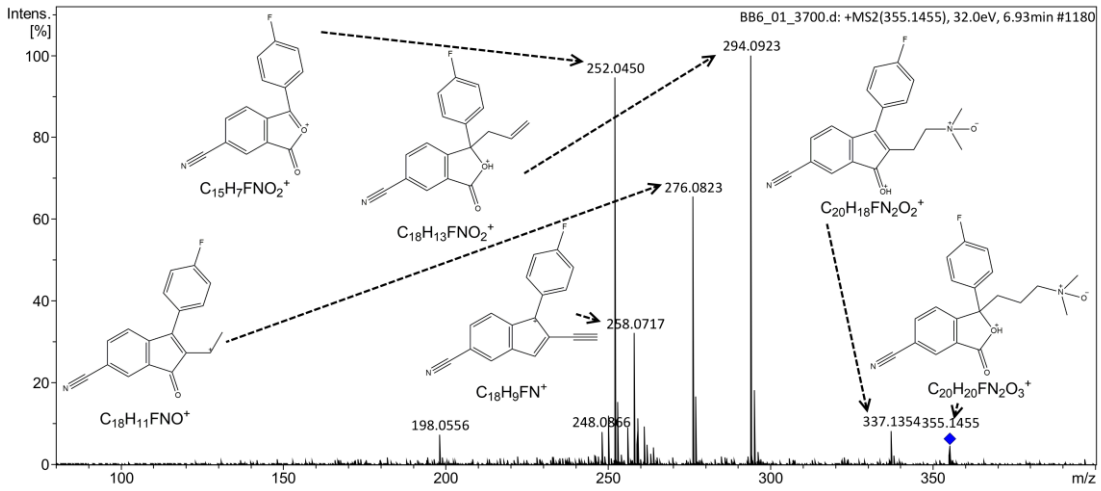

Fig. S11. MS/MS spectrum and proposed structures for TP-355A.

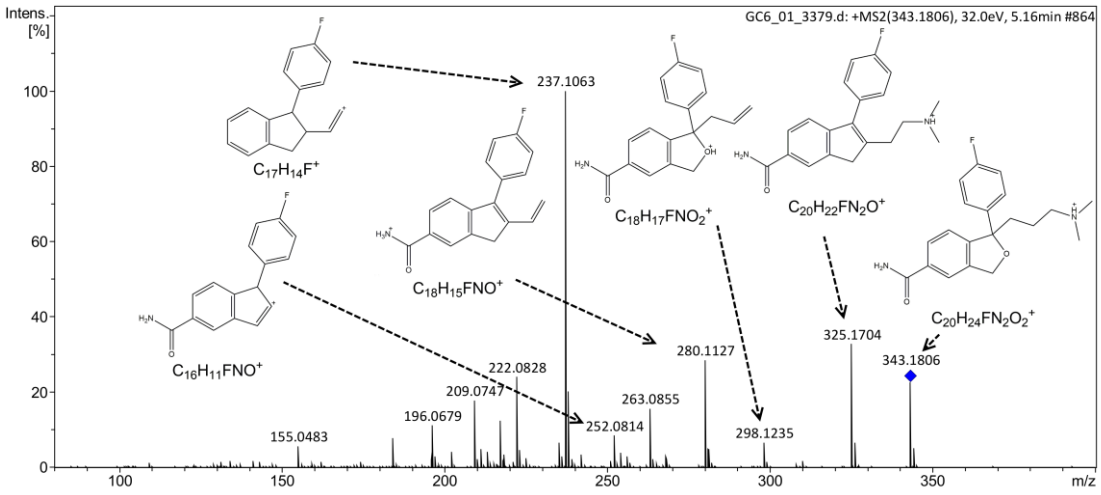

Fig. S12. MS/MS spectrum and proposed structures for TP-343.

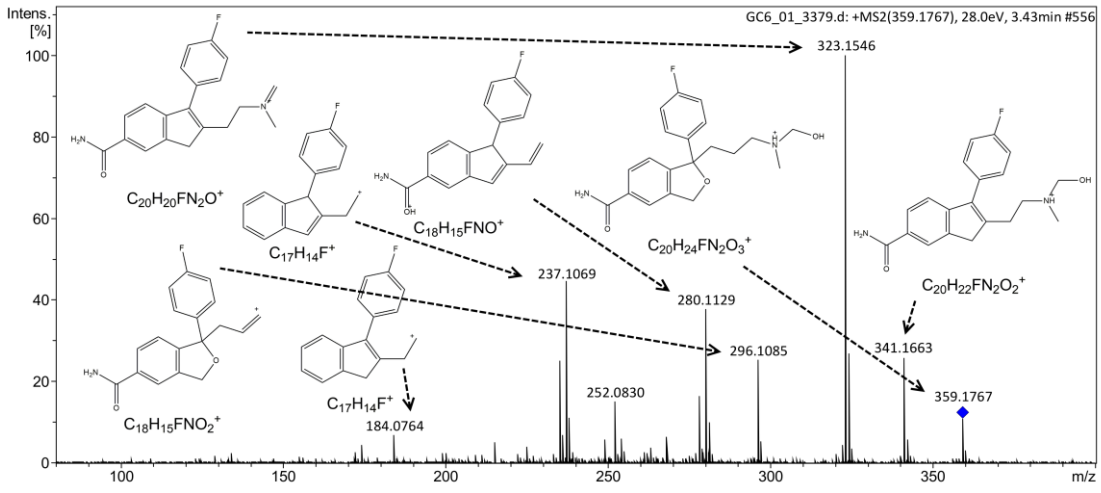

Fig. S13. MS/MS spectrum and proposed structures for TP-359.

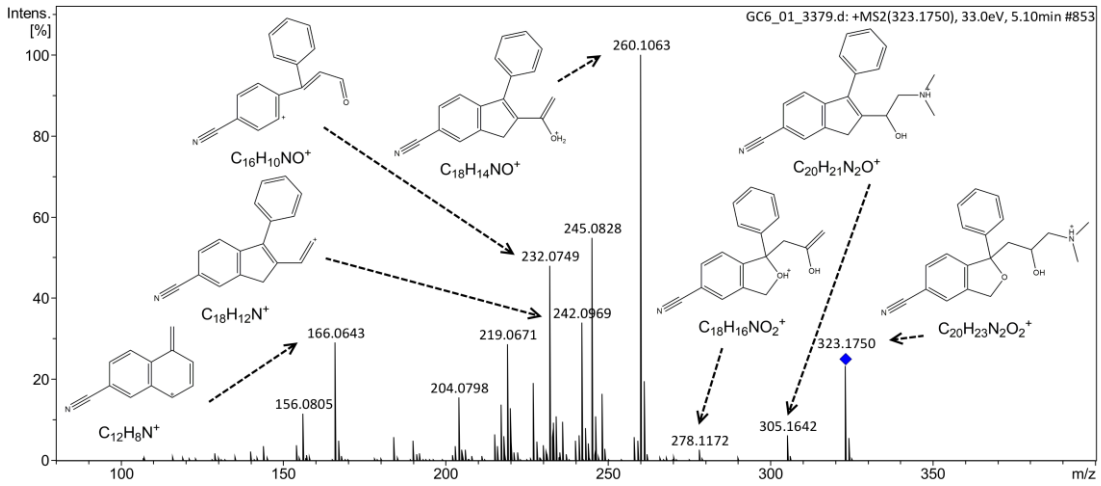

Fig. S14. MS/MS spectrum and proposed structures for TP-323.

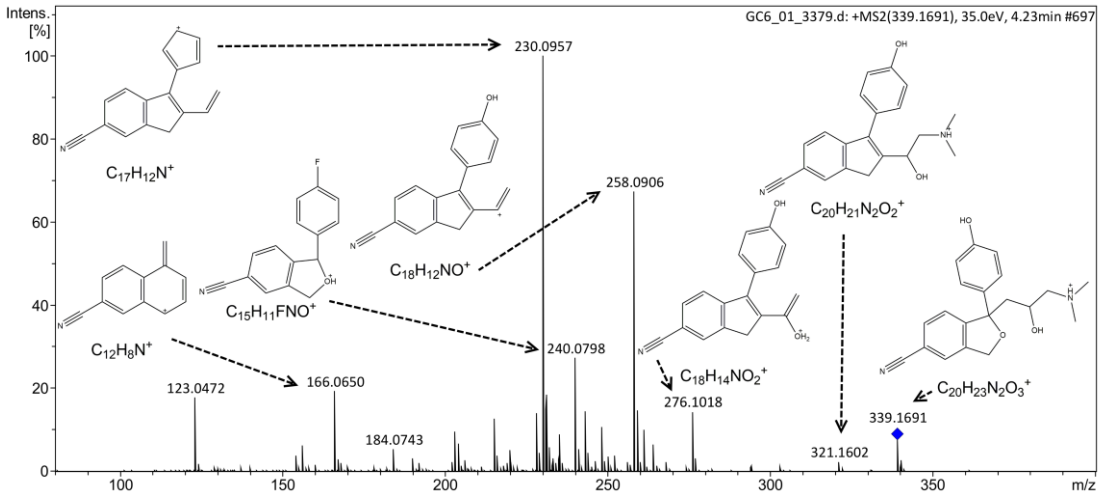

Fig. S15. MS/MS spectrum and proposed structures for TP-339B.

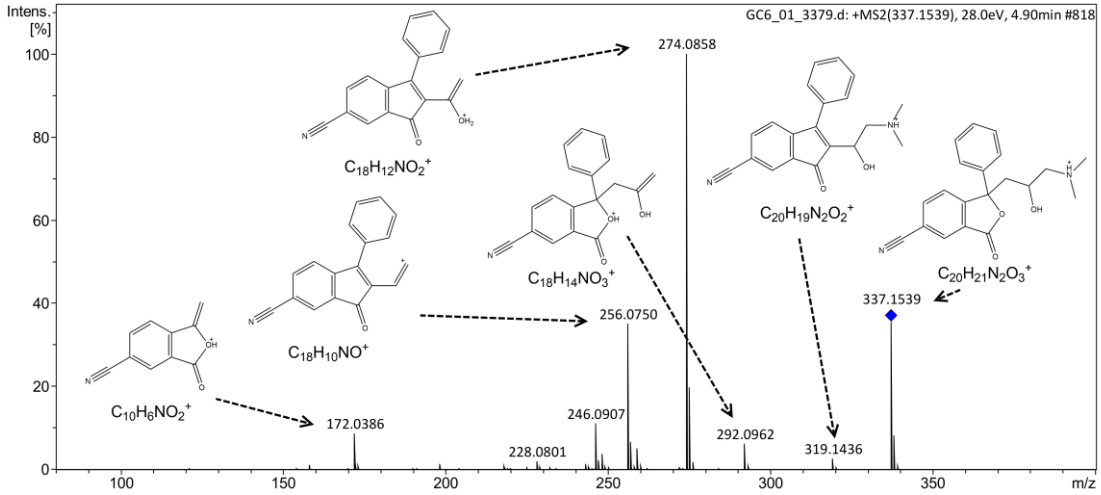

Fig. S16. MS/MS spectrum and proposed structures for TP-337.

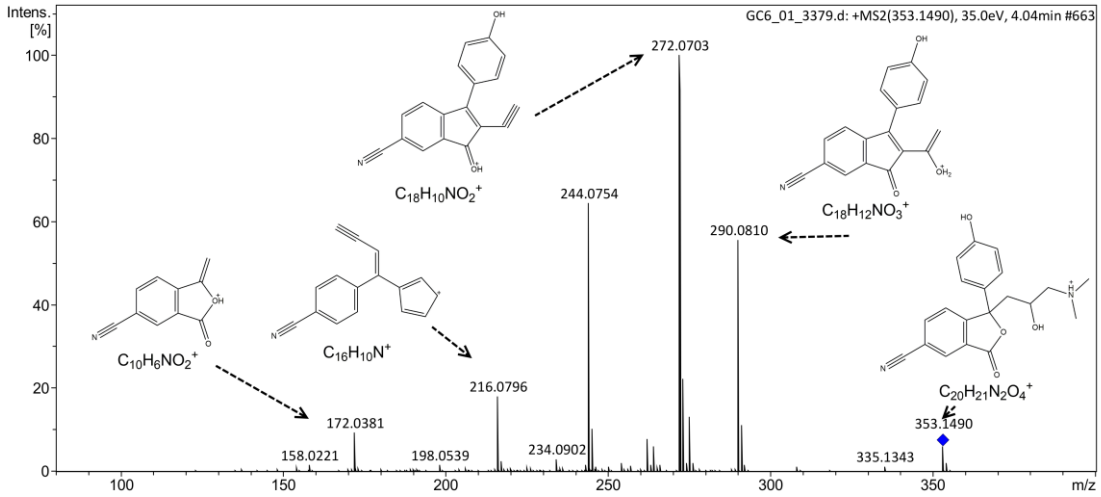

Fig. S17. MS/MS spectrum and proposed structures for TP-353.

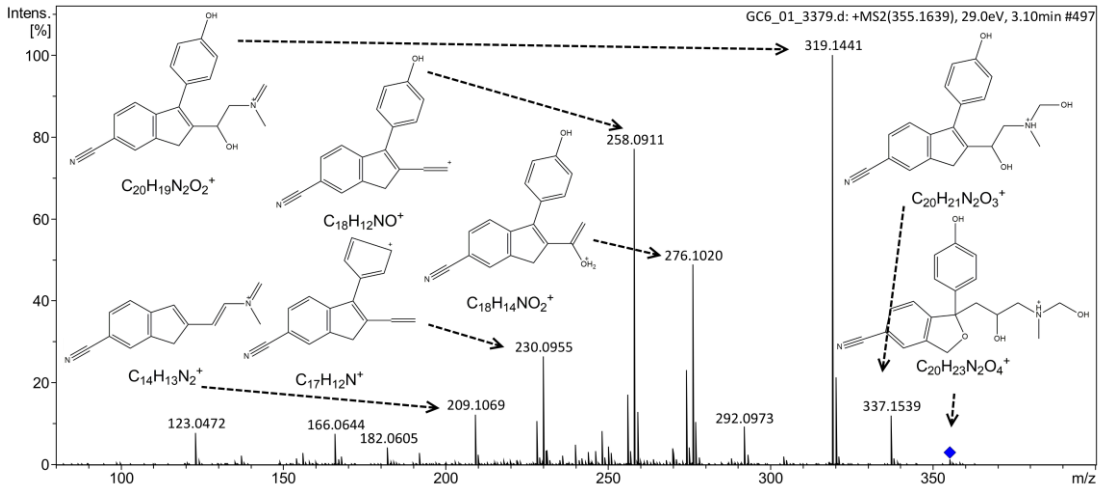

Fig. S18. MS/MS spectrum and proposed structures for TP-355B.

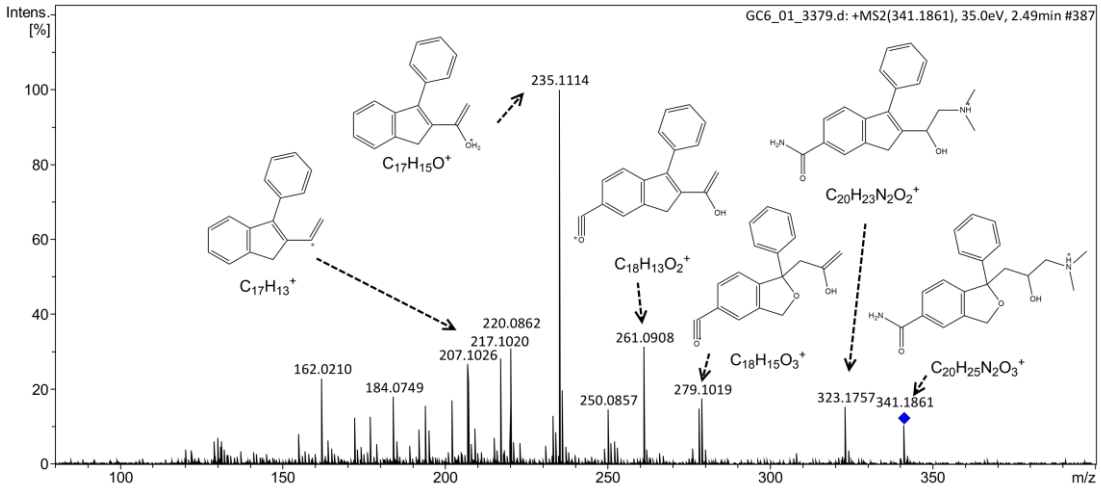

Fig. S19. MS/MS spectrum and proposed structures for TP-341B.

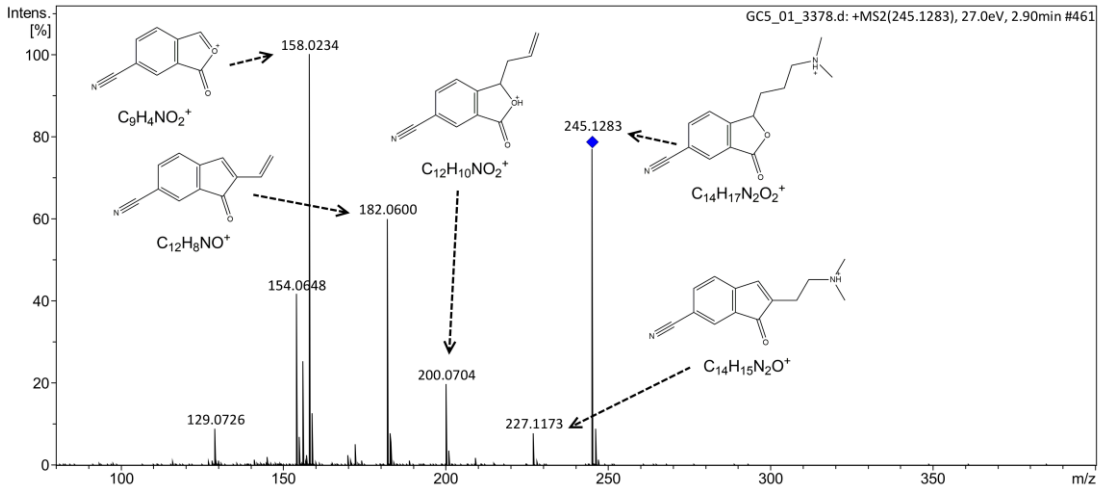

Fig. S20. MS/MS spectrum and proposed structures for TP-245.

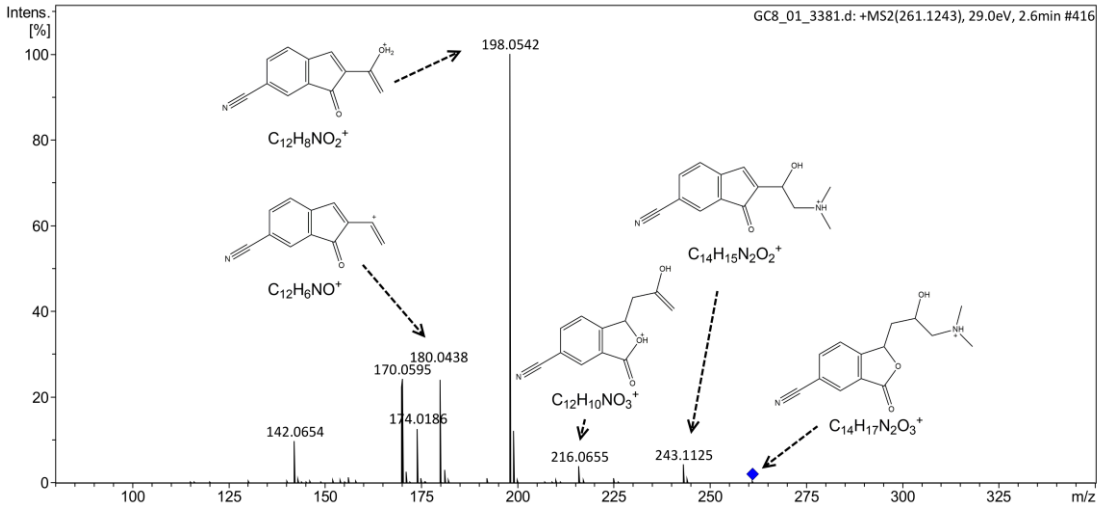

Fig. S21. MS/MS spectrum and proposed structures for TP-261.

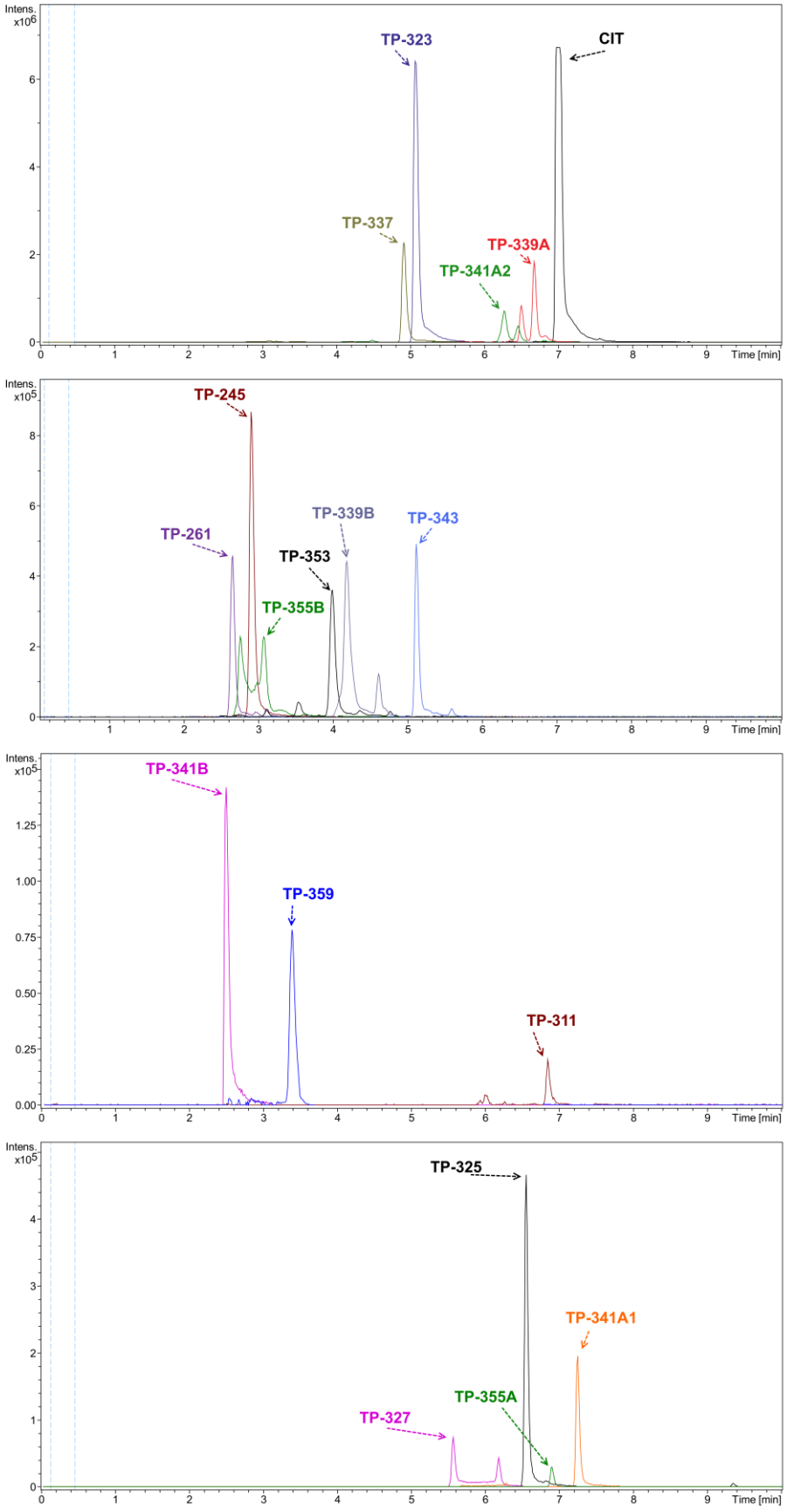

Fig. S22. Chromatograms of CIT and TPs.

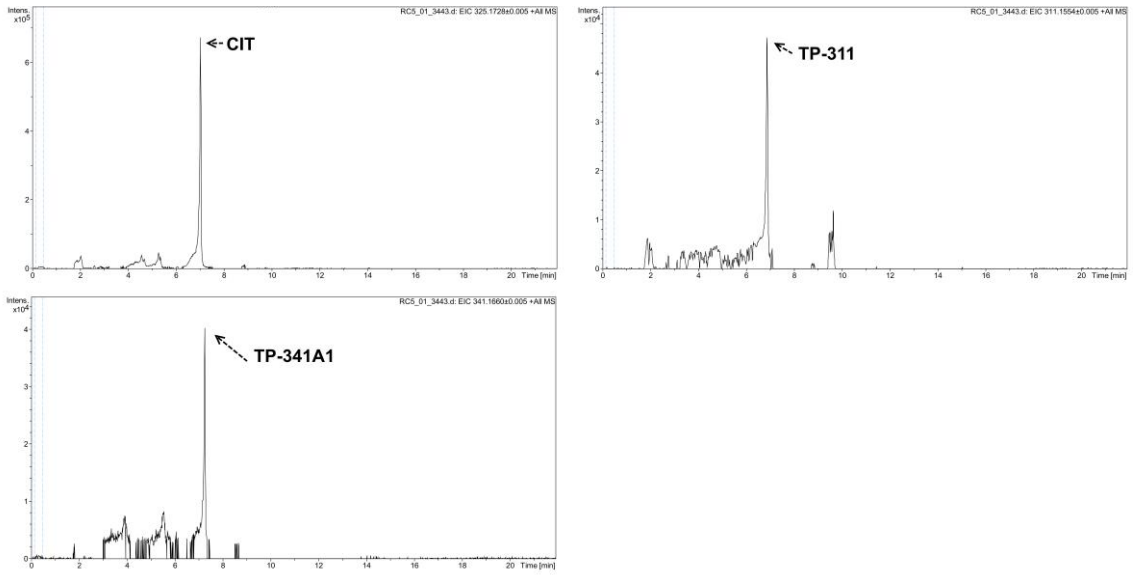

Fig. S23. Chromatograms of CIT and TPs from STP effluent.

3.2. Conclusões

Foram propostos dezassete TPs do CIT por meio das análises dos padrões de fragmentação nos espectros MS/MS adquiridos pela espectrometria de massa de alta resolução, sete deles nunca foram reportados. Estes TPs foram formados em três condições experimentais: hidrólise, fotólise e cloração com o objetivo de simular processos físicos que ocorrem no meio ambiente e em estações de tratamento de efluentes. Foi constatado que três deles: TP-339A (3-oxo citalopram, $C_{20}H_{19F}N_2O_2$) TP-311 (desmetilcitalopram, $C_{19}H_{19}FN_2O$) e TP-341A1 (citalopram-N-oxido, $C_{20}H_{21}FN_2O_2$) são metabolitos humanos, em outras palavras, estes produtos também podem ser formados por processos abióticos. Foram observados processos de hidroxilação, oxidação e demetilação da molécula parente na geração dos TPs. Foi notado que os quatro TPs identificados no processo de hidrólise e o CIT permaneceram estáveis ao longo do experimento (480 min) enquanto que ao fim de 240 min durante a fotólise, o CIT e quatorze TPs foram parcialmente ou completamente eliminados do sistema. Na literatura, o CIT foi degrado após 30 min sob radiação UV [5]. Durante a cloração, embora o CIT foi rapidamente degradado com aproximadamente 98% de remoção após 1 h, os TPs de maneira geral permaneceram estáveis. Estudos indicaram uma remoção de 95% do CIT com dióxido de cloro e 90% durante a cloração em efluente biológico [5,8].

As predições *in silico* dos TPs na ecotoxicidade com os parâmetros: 96-h F. minnow LC_{50}; 48-h *D. magna* LC_{50}; 48-h *T. pyriformis* IGC_{50} mostraram uma toxicidade menor que o CIT, embora para a maiorias dos TPs, os valores preditos foram abaixo de 10 mg L^{-1}. Nas predições de mutagenicidade, somente dois TPs apresentaram potencial mutagénico: TP-339B eTP-355B. Entretanto, para a carcinogenicidade, ao menos dez TPs mostraram resultados positivos em pelo menos dois modelos.

Amostras de efluentes foram preparadas e extraídas por SPE, em que o método foi devidamente validado, para a quantificação do CIT e deteção dos TPs previamente identificados. O CIT foi quantificado na concentração de 137 ng L^{-1} no efluente e 227 ng L^{-1} no influente e os TP-311 e TP-341A1 foram detetados. Estes TPs podem ser metabolitos do CIT ou podem ter sido formados durante o tratamento terciário, que é por processos de radiação UV e cloração. Os resultados mostraram que o UHPLC-

QTOF-MS é uma ferramenta ideal para a elucidação das estruturas químicas de compostos desconhecidos.

3.3. Referências

1. Collado, N., Rodriguez-Mozaz, S., Gros, M., Rubirola, A., Barcelo, D., Comas, J., Rodriguez-Roda, I., Buttiglieri, G., 2014. Pharmaceuticals occurrence in a WWTP with significant industrial contribution and its input into the river system. *Environ. Pollut*. 185, 202–212. doi:10.1016/j.envpol.2013.10.040

2. Sheng, L.-H., Chen, H.-R., Huo, Y.-B., Wang, J., Zhang, Y., Yang, M., Zhang, H.-X., 2014. Simultaneous determination of 24 antidepressant drugs and their metabolites in wastewater by ultra-high performance liquid chromatography–tandem mass spectrometry. *Molecules* 19, 1212–1222. doi:10.3390/molecules19011212

3. Silva, L.J.G., Pereira, A.M.P.T., Meisel, L.M., Lino, C.M., Pena, A., 2014. A one-year follow-up analysis of antidepressants in Portuguese wastewaters: occurrence and fate, seasonal influence, and risk assessment. *Sci. Total Environ*. 490, 279–287. doi:10.1016/j.scitotenv.2014.04.131

4. Beretsou, V.G., Psoma, A.K., Gago-Ferrero, P., Aalizadeh, R., Fenner, K., Thomaidis, N.S., 2016. Identification of biotransformation products of citalopram formed in activated sludge. *Water Res*. 103, 205–214. doi:10.1016/j.watres.2016.07.029

5. Horsing, M., Kosjek, T., Andersen, H.R., Heath, E., Ledin, A., 2012. Fate of citalopram during water treatment with O_3, ClO_2, UV and fenton oxidation. *Chemosphere* 89, 129–135. doi:10.1016/j.chemosphere.2012.05.024

6. Fatta-Kassinos, D., Vasquez, M.I., Kümmerer, K., 2011. Transformation products of pharmaceuticals in surface waters and wastewater formed during photolysis and advanced oxidation processes - degradation, elucidation of byproducts and assessment of their biological potency. *Chemosphere* 85, 693–709. doi:10.1016/j.chemosphere.2011.06.082

7. Negreira, N., Regueiro, J., Lopez de Alda, M., Barcel o, D., 2015. Transformation of tamoxifen and its major metabolites during water chlorination: identification and *in silico* toxicity assessment of their disinfection byproducts. *Water Res*. 85, 199–207. doi:10.1016/j.watres.2015.08.036

8. Hey, G., Grabic, R., Ledin, A., la Cour Jansen, J., Andersen, H.R., 2012. Oxidation of pharmaceuticals by chlorine dioxide in biologically treated wastewater. *Chem. Eng. J* 185–186, 236–242. doi:10.1016/j.cej.2012.01.093

Capítulo 4

Produtos de transformação da duloxetina por processos de degradação analisadas por UHPLC-QTOF-MS

4.1. Introdução

Duloxetina (DUL) é um fármaco antidepressivo da classe dos inibidores seletivos da recaptação de serotonina e noradrenalina e assim como o CIT, também é encontrado em matrizes ambientais como águas superficiais e efluentes [1,2]. Na literatura, somente um estudo elucidou TPs do DUL por meio da fotodegradação [3].

Este trabalho teve como objetivo elucidar os TPs originados da degradação do fármaco antidepressivo DUL pelos processos de hidrólise, fotólise por radiação UV−Vis e cloração por meio da técnica de espectrometria de massa de alta resolução. Adicionalmente, amostras da ETAR foram analisadas e a toxicidade *in silico* calculadas. Este capítulo é uma representação integral do artigo:

Osawa, R.A., Carvalho, A.P., Monteiro, O.C., Oliveira, M.C.,Florêncio, M.H., 2019. Degradation of duloxetine: Identification of transformation products by UHPLC-ESI(+)-HRMS/MS, *in silico* toxicity and wastewater analysis. *J. Environ. Sci*. 82, 113–123. doi:10.1016/j.jes.2019.02.025.

JOURNAL OF ENVIRONMENTAL SCIENCES 82 (2019) 113–123

Available online at www.sciencedirect.com

ScienceDirect

www.elsevier.com/locate/jes

JES JOURNAL OF ENVIRONMENTAL SCIENCES

www.jesc.ac.cn

Degradation of duloxetine: Identification of transformation products by UHPLC-ESI(+)-HRMS/MS, *in silico* toxicity and wastewater analysis

Rodrigo A. Osawa[1,2,*], *Ana P. Carvalho*[1], *Olinda C. Monteiro*[1], *M. Conceição Oliveira*[3], *M. Helena Florêncio*[1,2]

1. *Centro de Química e Bioquímica, Faculdade de Ciências, Universidade de Lisboa, Campo Grande, 1749-016 Lisbon, Portugal*
2. *Laboratório de FTICR e Espectrometria de Massa Estrutural, Faculdade de Ciências, Universidade de Lisboa, Campo Grande, 1749-016 Lisbon, Portugal*
3. *Centro de Química Estrutural, Instituto Superior Técnico, Universidade de Lisboa, 1049-001 Lisbon, Portugal*

ARTICLE INFO

Article history:
Received 5 December 2018
Revised 22 February 2019
Accepted 25 February 2019
Available online xxxx

Keywords:
High resolution mass spectrometry
Duloxetine
Degradation processes
Transformation products
Wastewater analysis
In silico toxicity

ABSTRACT

Duloxetine (DUL), an antidepressant drug, has been detected in surface water and wastewater effluents, however, there is little information on the formation of its transformation products (TPs). In this work, hydrolysis, photodegradation (UV irradiation) and chlorination experiments were performed on spiked distillated water, under controlled experimental conditions to simulate abiotic processes that can occur in the environment and wastewater treatment plants (WWTPs). Eleven TPs, nine from reaction with UV light and two from chlorine contact, were formed and detected by ultra-high performance liquid chromatography coupled to quadrupole time-of-flight mass spectrometry, and nine of them had their chemical structures elucidated upon analyses of their fragmentation patterns in MS/MS spectra. The formation and degradation of the TPs were observed. The parent compound was completely degraded after 30 min in photodegradation and after 24 hr in chlorination. Almost all TPs were completely degraded in the experiments. The ecotoxicity and mutagenicity of the TPs were predicted based on several *in silico* models and it was found that a few of these products presented more ecotoxicity than DUL itself and six TPs showed positive mutagenicity. Finally, wastewater samples were analyzed and DUL and one TP, possibly formed by chlorination process, were detected in the effluent, which showed that WWTP not only did not remove DUL, but also formed a TP.

Introduction

Pharmaceutical compounds have been found in drinking water, groundwater, surface waters and treated wastewater since many of these compounds cannot be completely removed by conventional treatment systems (Writer et al., 2013; Subedi and Kannan, 2015). There is concern about the effects of these compounds on the environment and human health and several studies have already been carried out on the ecotoxicity and environmental risks of drugs, studies that can be found in the literature (Taylor and Senac, 2014; Acuña et al., 2015; Silva et al., 2015). Nevertheless, a pharmaceutical compound in the environment may undergo complex interactions with biotic and abiotic factors, forming

* *Corresponding author. E-mail:* raosawa@fc.ul.pt. (Rodrigo A. Osawa).

https://doi.org/10.1016/j.jes.2019.02.025
1001-0742 © 2019 The Research Center for Eco-Environmental Sciences, Chinese Academy of Sciences. Published by Elsevier B.V.

transformation products (TPs) which may have different physical and chemical proprieties from the original compound, changing their ecotoxicity or persistence in the environment (El Najjar et al., 2013; Carpinteiro et al., 2017; Yin et al., 2017).

Another concern is that there are no regulatory laws for safe concentrations of drugs in waters. Currently, in the European Union, the Water Framework Directive (Directive 2013/39/EU, 2013) monitors some pharmaceutical compounds in the aquatic environments and in the United States, the Unregulated Contaminant Monitoring Regulation monitored several drugs in drinking water (US EPA, 2017a).

Duloxetine (DUL) is a selective serotonin-norepinephrine reuptake inhibitor (SNRI) antidepressant drug, mostly used to treat major depression, generalized anxiety disorders, fibromyalgia, and stress urinary incontinence. DUL had sales in the order of $5 billion in the United States under the brand name Cymbalta and was the seventh bestselling prescription drug in 2013 (Cymbalta Sales Data. https://www.drugs.com/stats/cymbalta Accessed September 17, 2018). In Portugal, DUL was the ninth most prescribed antidepressant in 2015, resulting in a defined daily dose (60 mg) of more than 7.4 million (DGS, 2016).

Only few publications reported DUL in wastewater or surface waters. One work has reported the presence of the compound in effluent of wastewater treatment plant (WWTP) and surface water located downstream of the WWTP in the order of ng/L (Schultz and Furlong, 2008). Fick et al. (2011) performed a study that detected DUL in the effluent from 1 to 14 ng/L with an average removal efficiency of 29% in WWTP. Then it is to be expected that this drug is found in the environmental matrices.

There are a few studies on the degradation of DUL, but most are focused on its stability for pharmaceutical use and none of them focuses on the formation of products in the environment and in the wastewater treatment plant (Sinha et al., 2009; Chhalotiya et al., 2010; Kumar et al., 2012; Datar and Waghmare, 2014; Chadha et al., 2016). However, to the best of our knowledge, to date only one study has been published on the TPs formed by DUL, this paper showed that seven TPs were formed from DUL by gamma radiolysis in humic acid solutions to simulate real environmental conditions (Santoke et al., 2012). There is little information about the behavior of the compound with chlorine, and that would be relevant since chlorination may be present in the disinfection step in WWTP. Elucidating TPs in degradation processes such as photodegradation and chlorination is an important step to understand their pathways and potential risks to the aquatic environment.

An essential tool to identify TPs is high resolution mass spectrometry (HRMS). High resolution mass spectrometers, such as orbitrap, time-of-flight (TOF) or fourier-transform ion cyclotron resonance (FTICR), which provide high resolution and high mass measurement accuracy to elucidate the chemical structure by elemental compositions, fragmentation patterns and isotopic distributions could be used (Bletsou et al., 2015; Beretsou et al., 2016).

Another essential point to consider is the toxicity of the TPs in environment and human health. Most of these compounds, however, do not have analytical reference standards to evaluate the toxicity *in vitro* or *in vivo*. In addition, these methods are often expensive and time-consuming. As an alternative, *in silico* methods, based on computational models to simulate and estimate the toxicity can be useful for toxicity prediction (Wilde et al., 2016; Trawiński and Skibiński, 2017). There are several methods for predicting *in silico* toxicity in which each presents advantages and limitations such as quantitative structure–activity relationships (QSAR) model, which uses molecular descriptors of chemical to predict toxicity. A significant tool to give reliability in the results of the QSAR model is the applicability domain (AD), which means the limitations of the model and predictions outside the AD may not be considered as a result (Worth et al., 2004).

The objective of this work was to elucidate the TPs that may occur in environment and WWTP through abiotic processes: hydrolysis, chlorination and photodegradation, under controlled experimental conditions by ultra-high-performance liquid chromatography (UHPLC) coupled to quadrupole time-of-flight mass spectrometer (QTOF/MS). The formation/degradation of TPs was also analyzed by their respective time profile. After elucidating the TPs, toxicity was predicted by *in silico* tools, to estimate mutagenicity and ecotoxicity and in addition, method validation was carried out to accurately measure the concentration of DUL and finally, the TPs were investigated in wastewater samples.

1. Materials and methods

1.1. Standards and reagents

Duloxetine hydrochloride of high purity grade (>98%) was purchased from TCI Chemicals (Zwijndrecht, Belgium). Methanol, acetonitrile, formic acid and water, LC–MS grade were supplied from Fisher Scientific (Hampton, USA). Sodium hypochlorite 10% (W/V) solution was supplied by Panreac (Barcelona, Spain) and sodium hydroxide (NaOH) 0.1 mol/L was obtained from Honeywell (Seelze, Germany). L(+) Ascorbic acid was purchased from Merck (Darmstadt, Germany). Milli-Q ultrapure system from Millipore (Barnstead International, Dubuque, USA) was used to obtain ultrapure water. Nylon membrane filter (0.45 μm) was purchased from Teknokroma (Barcelona, Spain). Stock solutions of 1000 mg/L duloxetine hydrochloride were prepared and stored at −80°C in ultrapure water.

1.2. Degradation experiments

In chlorination, hydrolysis and photodegradation experiments, distillated water was spiked with 4 mg/L of the pharmaceutical compound. The high concentration was used to facilitate the identification of the products. The pH of samples was adjusted to 7.5 with 0.1 mol/L NaOH and was not buffered to avoid influences on the formation of TPs with buffering agents. The reason for pH 7.5 is that it is a close value to be found in effluents and surface waters. Samples were carried out at room temperature and in the dark room. For the identification of the TPs, the spiked samples were compared to blanks (distillated water).

In the chlorination experiments, sodium hypochlorite (5 mg/L free chlorine) solution was added to 20 mL of sample and when removing the aliquot, a quenching agent (ascorbic acid at concentration of 600 mg/L) was added to neutralize chlorine.

In photodegradation, a photoreactor with 100 mL of sample cooled by water circulation was used. The lamp was a 450 W medium-pressure mercury-vapor lamp (Hanovia, UK) with irradiance around 0.37 W/cm and with the total irradiated energy being 40%–48% in the ultraviolet range and 40%–43% in the visible region. The details of the photoreactor have been published elsewhere (Pinto da Costa et al., 2015).

The hydrolysis experiment was performed to evaluate the stability of DUL in distillated water. In all experiments the solutions were stirred with a magnetic bar. Aliquots of 0.1 mL volume were withdrawn in ambers glass vials with inserts in certain times: hydrolysis at 0 hr, 1 hr, 3 hr, 6 hr, 1 day, 2 days, 4 days; chlorination at 0 min, 1 min, 15 min, 30 min, 1 hr, 2 hr, 3 hr, 4 hr, 1 day and photodegradation at 0 min, 5 min, 10 min, 15 min, 30 min, 45 min 1 hr, 1.5 hr, 2 hr and were stored for further analyses at −80°C. Samples were directly injected in UHPLC-QTOF/MS.

1.3. Toxicity assessment by *in silico* tools

The toxicity assessments of the identified TPs of DUL were performed using *in silico* tools: Ecological Structure Activity Relationships (ECOSAR, 2.0, Washington DC, USA), Toxicity Estimation Software Tool (T.E.S.T, version 4.2.1 Washington DC, USA), VEGA KNN/read-across and VEGA SARpy/IRFMN (VEGA Platform, version 1.1.4, Milan, Italy http://www.vega-qsar.eu). These tools are based on QSARs and SA methods freely available to users and uses SMILES in the canonical form of chemical structure for predictions. QSARs are mathematical models which estimate the toxicities based on the difference of the physiochemical characteristics of chemicals and their biological activities. In ECOSAR, the methodology is built on a linear mathematical relationship between logK_{ow}, estimated if no experimental value is available, and log of toxicity values. If the toxicity result of the chemical compound has different classes, we will consider the value of higher toxicity, in other words, of lower concentration. In ECOSAR, 96-hr fish LC_{50}, 48-hr *D. magna* LC_{50} and 96-hr green algae EC_{50} endpoints were predicted. The tool does not provide a value for AD in prediction toxicity. However, the software shows the logK_{ow} cut-off for each class, which means that it is the point at which a compound is no longer soluble. Therefore, if the logK_{ow} of the compound is higher than logK_{ow} cut-off, then no effects at saturation are expected (US EPA, 2017b).

T.E.S.T was used for the prediction of mutagenicity by the AMES test endpoint, in which positive results indicated a mutagenic potential and ecotoxicity by 96-hr F. minnow LC_{50}, 48-hr *D. magna* LC_{50} and *T. pyriformis* IGC_{50} endpoints. The consensus method was used based on average of toxicity prediction QSAR methods, were: Hierarchical clustering, FDA, nearest neighbor, single model and group contribution. Details of molecular descriptors and QSARs methods are documented in User's Guide for T.E.S.T. (US EPA, 2016). The consensus method consists of the AD for each QSAR method to use in the prediction and if it results in only one QSAR method, the consensus method will be outside the AD.

VEGA SARpy/IRFMN performs the prediction of the structural alerts for mutagen present in the compound and the AD of predictions is based on the Applicability Domain Index (ADI), which can result in values from 0 to 1. The ADI is established by other models in which the majority is calculated by similar compounds found in the training set and test set of the model. Values between 1 and 0.9, the predicted compound is inside the AD, values between 0.9 and 0.65, the compound could be out the AD and values below 0.65, the compound is out of the AD of the model. VEGA KNN/read-across uses the same AD, based on the ADI. In this work, a prediction greater than 0.65 was considered within the AD and models in which most of the results are outside the AD will not be shown.

1.4. Wastewater sampling and sample preparation

Raw wastewater (influent) and effluent samples were collected from WWTP of Lisbon in amber bottles and stored in thermal boxes until arrival at the laboratory. The WWTP serves approximately 800,000 people and receives effluents from several hospitals in the region. The primary treatment is by decantation, the secondary treatment uses biofiltration and tertiary treatment consists of chlorination and UV irradiation processes. For solid phase extraction (Oasis HLB 200 mg, 6 mL, Waters), 250 mL of samples were previously filtered by nylon membrane (0.45 μm) and the pH was adjusted to 3 with acetic acid (2%). The samples were run in solid phase extraction cartridges in a stream of 5–8 mL/min previously conditioned with 5 mL of methanol and 5 mL of ultrapure water. Then, the cartridges were dried with nitrogen flow, eluted with 5 mL of methanol and 2 mL of acetone–methanol ratio of 1:1. For the reconstitution, 0.1 mL of water–methanol ratio of 4:1 was used, followed by storage at −80°C for further analysis. The method validation can be found in Appendix A Section S1 and Table S1.

1.5. Instrumentation

For identification purposes, an UHPLC Ultimate 3000 RSLCnano system (Thermo Fischer Scientific, Germany) coupled with a quadrupole time-of-flight (QTOF) Impact II mass spectrometer with an electrospray ion source (Bruker Daltonics, Germany) was used. The chromatographic column was a Kinetex 1.7 μm C18 100 Å, 150 × 2.1 mm (Phenomenex, USA). The mobile phase consisted of H_2O acidified with 0.1% formic acid (A) and the organic phase was acetonitrile (B) at the flow rate of 150 μL/min and volume injection of 10 μL. The gradient used was (%B): 0 min (20%); 1.5 min (30%); 10 min (75%); 13–17 min (100%) and 18–25 min (5%).

Samples were analyzed in broadband collision-induced dissociation (bbCID) and in product ion scan mode. In bbCID, low collision energy and high collision energy are applied simultaneously to generate fragments and precursor ions in a single run. The product ion scan mode (MS/MS) was used to confirm the fragment ions. Analysis was performed in positive electro-spray ionization (ESI+) mode operating in the high-resolution mode over the range *m/z* 50–1000 with

acquisition rate of 3 Hz. The mass spectrometer optimized parameters were as follows: ion spray voltage, 2.5 kV; end plate offset, −500 V; nebulizer gas (N_2), 2.8 bars; dry gas (N_2), 8 L/min; dry heater, 200°C. 20 μL of sodium formate 10 mmol/L was used for internal calibration on the high-precision calibration mode (HPC).

1.6. Data processing

Compass Data Analysis (Bruker Daltonics, Germany) was performed to analyze fragmentation patterns in order to identity possible TPs by the visual comparison of the chromatograms of the experimental samples with the blank samples (non-spiked). The suspected TP was analyzed in product ion scan mode (MS/MS mode) to obtain the structural information. Moreover, the elemental formulas were estimated by mass error of less than 5 ppm and the isotopic patterns were analyzed as to determine the presence of chlorine in the molecule, since the ^{35}Cl and ^{37}Cl have identifiable isotopic distributions.

2. Results and discussion

2.1. Degradation experiments

In the hydrolysis experiments, DUL showed stability over time in 4 days and no TP was detected. The non-detection of TPs may be attributed to the fact that was performed at room temperature. In the literature, one study reported that the DUL was degraded in 5%–16% at 80°C, with an acid solution, in 4 hr (0.5 mol/L HCl, 9 hr) and four TPs were detected (Datar and Waghmare, 2014). These TPs may have been formed by the high temperature of the experiment or/and by the presence of the acid in the solution. Another study showed that when the temperature was 60°C for 15 days, DUL also gave rise to 10 TPs (Sinha et al., 2009). Both works used HPLC as separation technique, being therefore not possible to identify the TPs because no mass measurement was available.

In the photodegradation experiment, DUL produced nine TPs, seven were elucidated through fragmentation patterns obtained from the MS/MS spectra analyses. The probable chemical structures assigned to these products may have been formed by different reactions. Nevertheless, two isomers of DUL, called DUL-ISO1 and DUL-ISO2 did not have their structures identified by the fact that they present fragmentation patterns similar to the DUL ones.

The time profile showing the formation and degradation of TPs is presented in Fig. 1a and b. As it can be seen, DUL was completely degraded after 30 min by UV irradiation (DUL-UV). Most of TPs formed had their maximum signal intensity in the first 10 min from the beginning of the experiment and after 45 min in contact with UV light, all TPs were degraded. The pathways for the formation of TPs were proposed (Fig. 2). Santoke et al. (2012) observed that DUL degraded about 72% under gamma irradiation and several TPs were identified using a TOF mass spectrometer. In comparison to our study only one TP identified by Santoke et al. (2012) has the same molecular mass, that is, TP-330 in this study, but with a different structure. It should be noted, however, that in the work of Santoke et al. (2012) there was no identification of the compound by fragmentation of the precursor ion and, moreover, gamma irradiation, rather than UV irradiation, was used to elucidate the mechanisms of TPs formation.

The contact of chlorine with DUL resulted in complete removal of the drug in 24 hr of reaction (DUL-CL) and two TPs were detected and identified (Fig. 1c). One TP detected, TP-332, had at least one chlorine atom attached to the molecule, probably bound to one of the aromatics rings. The MS spectra enabled to confirm the presence of chlorine by means of the ^{35}Cl and ^{37}Cl isotopic distribution. The most abundant TP was TP-332. The chromatograms of elucidated TPs can be found in Appendix A Fig. S1 and details on the identification are below.

2.2. Structure elucidation of TPs

2.2.1. DUL, DUL-ISO1 and DUL-ISO2

In MS/MS spectrum, two DUL isomers with similar fragmentation patterns were detected, only the *m/z* intensities varied (Appendix A Fig. S2). As such, and unfortunately, analysis of the fragmentation patterns, that were too similar, did not enable to identify the isomers formed.

The analysis of the fragmentation patterns in the MS/MS of DUL (Appendix A Fig. S3) showed that the parent ion lost methylamine (CH_3NH_2) to give *m/z* 267 ($C_{17}H_{15}OS^+$), which in turn lost ethylene (C_2H_4) to give the fragment ion at *m/z* 239 ($C_{15}H_{11}OS^+$). This latter fragment ion lost one water (H_2O) molecule at *m/z* 221 ($C_{15}H_9S^+$) and loss of thiophene (C_4H_4S) giving *m/z* 183 ($C_{13}H_{11}O^+$). Since the TPs chemical structures are similar to DUL it was to be expected that the TPs formed would have similar losses.

2.2.2. TP-312A, TP-312B and TP-312C

These TPs, although with the same molecular mass, have different fragmentation patterns observed in their MS/MS spectra (Fig. 3). Analysis of the MS/MS spectrum of TP-312A (Fig. 3a) led us to propose that it has been formed by an oxidation on the DUL aliphatic chain. Indeed, the MS/MS spectrum showed the neutral loss of CH_3NH_2 at *m/z* 281 ($C_{17}H_{13}O_2S^+$) and it may be concluded that the oxidation did not occur on the methyl group. The fragment ion *m/z* 197 ($C_{13}H_9O_2^+$) may be attributed to the elimination of C_4H_4S together with CH_3NH. It may therefore be concluded that oxidation also did not occur in thiophene. The elimination of H_2O at *m/z* 263 ($C_{17}H_{11}OS^+$) from *m/z* 281 resulted, probably, from an ether group present in the TP molecule, this loss occurred also on the DUL structure. The most intense peak at *m/z* 255 ($C_{15}H_{11}O_2S^+$) was due to the elimination of both CH_3NH_2 and C_2H_2, the latter one probably originating from the naphthalene or thiophene ring. The formation of the fragment ion *m/z* 253 ($C_{16}H_{13}OS^+$) reinforces the hypothesis of oxidation on α-carbon with the loss of *N*-methylformamide (C_2H_5NO).

TP-312B appears to have been formed by an epoxidation on naphthalene. This hypothesis is supported by the identification of fragment ions at *m/z* 253 ($C_{15}H_9O_2S^+$) and *m/z* 228 ($C_{14}H_{14}NO_2^+$) in its MS/MS spectrum (Fig. 3b). The former fragment ion indicated the neutral loss of C_3H_9N, possibly ethylmethylamine from the aliphatic chain with the amine group. The latter fragment ion, *m/z* 228, implied the loss of

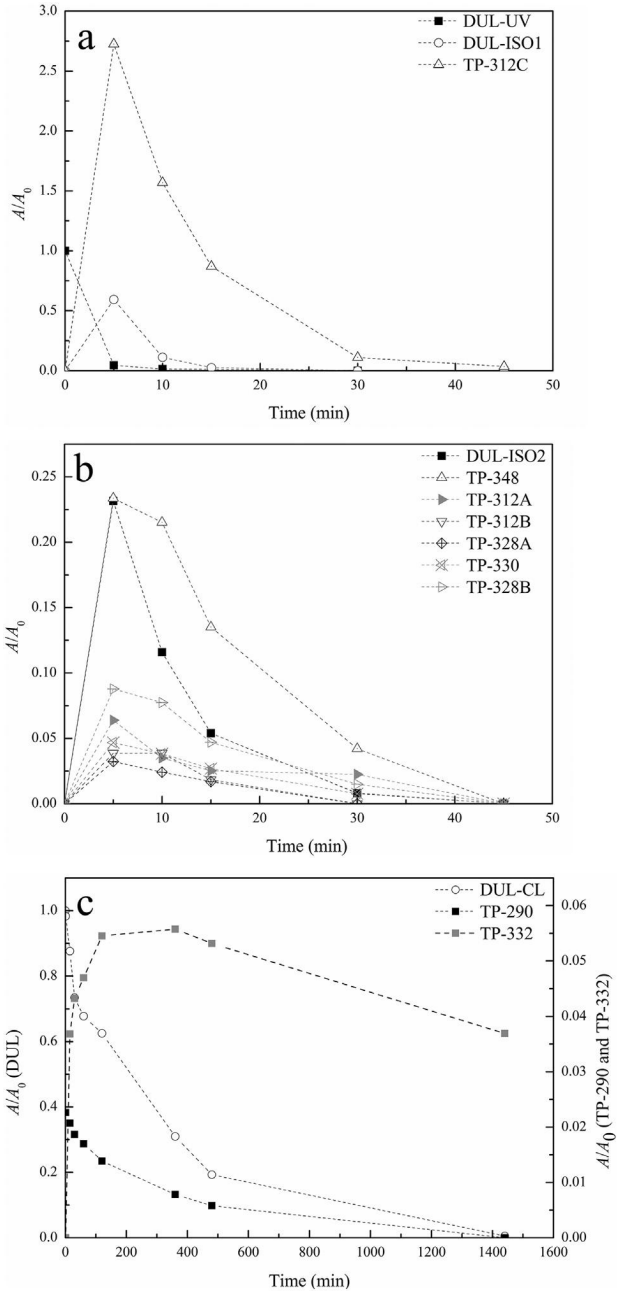

Fig. 1 – Time profile of DUL and TPs by (a) and (b) photodegradation and (c) chlorination. *A* is the peak area of the respective TP and A_0 is the peak area of DUL at t = 0 min.

C_4H_4S, the thiophene group, suggesting that no reaction occurred in this group Furthermore, only one loss of H_2O has been identified at *m/z* 263 ($C_{17}H_{11}OS^+$) from *m/z* 281 ($C_{17}H_{13}O_2S^+$) suggesting it to be related to the ether group of the TP structure, meaning that no hydroxylation occurred. To reinforce our assumption for the structure of this TP, studies of UV/chlorine degradation have identified the epoxidation process in carbamazepine (Wang et al., 2016; Zhou et al., 2016).

The analysis of the fragmentation patterns in the MS/MS spectrum of TP-312C (Fig. 3c), suggested a TP structure bearing an imine group, possible originating from the amide group of

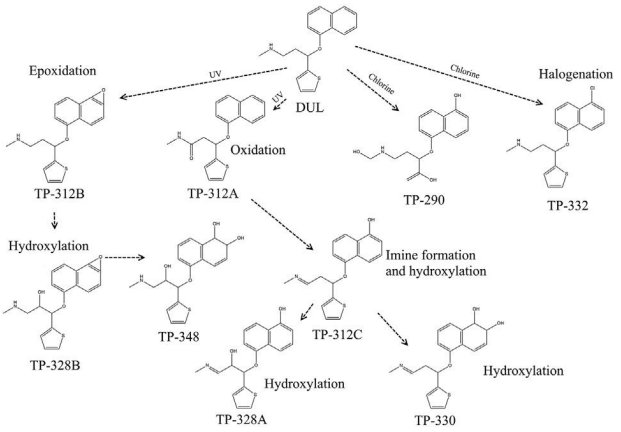

Fig. 2 – Proposed pathway of TPs formation.

TP-312A. The fragment ion *m/z* 269 ($C_{16}H_{13}O_2S^+$) supported this hypothesis by loss of a C_2H_5N radical from the parent ion, only possible with imine. According to the literature, the formation of imines and nitriles from amides by UV radiation and soft X-rays has been confirmed (Johnson et al., 2011). Furthermore, hydroxylation of naphthalene occurring in this TP structure was proposed by the fact that only one loss of H_2O was detected. This loss could be related to the ether group of the compound, same occurred on the structure of the DUL, the most likely position for hydroxylation being the 1-position

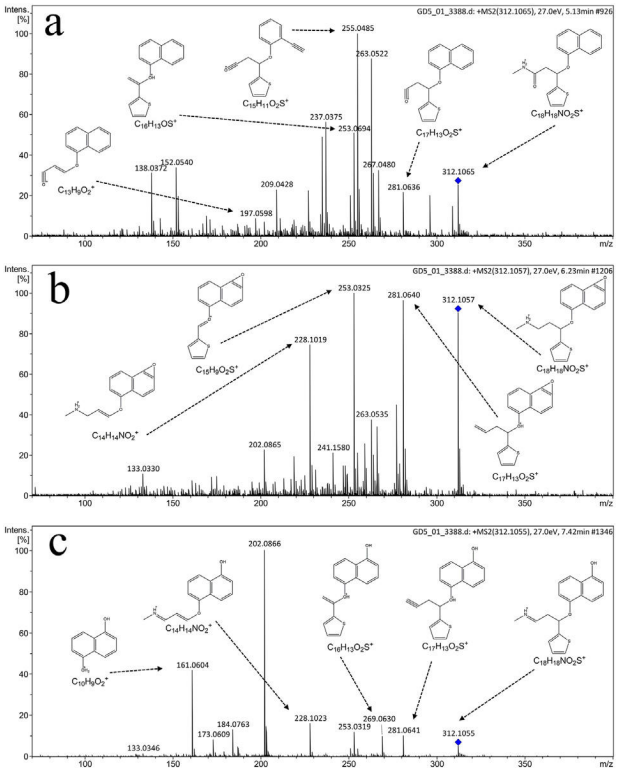

Fig. 3 – MS/MS spectra and proposed structures of (a) TP-312A, (b) TP-312B and (c) TP-312C.

because it is more stable and studies found in the literature indicated that the hydroxylation process may occur in compounds with aromatic rings (Vinu and Madras, 2011; Yuzawa et al., 2012) The loss of C_4H_4S, was identified by fragmentation from the parent ion resulting in *m/z* 228 ($C_{14}H_{14}NO_2^+$), proving that there was no hydroxylation of this group. The fragment ion *m/z* 202 ($C_{12}H_{12}NO_2^+$) resulting from *m/z* 228 by the loss of C_2H_2, probably occurred from the aromatic group. Another fragment ion that confirms a TP structure resulting from the formation of 1-naphthol was that at *m/z* 161 ($C_{10}H_9O_2^+$), formed by losses of thiophene and the aliphatic amine from the parent ion.

2.2.3. TP-328A and TP-328B

Two TPs with the same molecular mass were identified but with different MS/MS spectra. In the MS/MS spectrum of TP-328A (Appendix A Fig. S4), neutral losses of two H_2O molecules were identified, one at *m/z* 310 ($C_{18}H_{16}NO_2S^+$) from the parent ion and the other at *m/z* 234 ($C_{16}H_{12}NO^+$) from *m/z* 252 ($C_{16}H_{14}NO_2^+$). The former H_2O loss justifies the presence of one OH group on the TP structure that might be due to hydroxylation, probably in β-carbon because it is more stable. The other H_2O loss may result from the presence of an ether group. Another hydroxylation probably formed the 1-naphthol, since no other H_2O loss was detected.

Analysis of the MS/MS spectrum of TP-328B suggests a structure formed by hydroxylation and epoxidation processes. The loss of CH_3NH_2 at *m/z* 297 ($C_{17}H_{13}O_3S^+$) was identified in the MS/MS spectrum (Appendix A Fig. S5), arguing for no reactions on the methyl group and no imine formation. Hydroxylation probably occurred on β-carbon and, elimination from the parent ion of C_3H_9NO, resulting in *m/z* 269 ($C_{15}H_9O_3S^+$), suggests the fragmentation of the aliphatic amine group (*N*-Methylethanolamine), corroborating our hypothesis. The fragment ion at *m/z* 213 ($C_{13}H_9O_3^+$), the most intense peak in the spectrum, showed the neutral losses of C_4H_4S and CH_3NH_2, which may indicate that there was no reaction on the thiophene group. The *m/z* 185 ($C_{12}H_9O_2^+$) fragment ion could be due to the loss of CO from fragment ion *m/z* 213 (C_{13} $H_9O_3^+$), probably involving the oxygen formed by epoxidation.

2.2.4. TP-330

Based on the MS/MS spectrum of this TP (Appendix A Fig. S6), losses of two H_2O molecules at *m/z* 294 ($C_{18}H_{16}NOS^+$) from the parent ion were detected. We attribute the first loss of H_2O to the presence of OH on the naphthalene, whereas the second H_2O molecule loss could occur from the ether group by hydrogen rearrangement, in a process similar to the one that occurred in DUL. Two hydroxylation processes on the naphthalene group and formation of imine from TP-312A are proposed for the formation of TP-330. The peak at *m/z* 251 ($C_{16}H_{11}OS^+$) showed the losses of two H_2O molecules and of C_2H_5N from parent ion. The loss of C_2H_5N suggests that hydroxylation did not occur on β-carbon. Indeed, if hydroxylation had occurred on β-carbon C_2H_7N should have been eliminated, which was not the case. In theory, hydroxylation could occur on the methyl or α-carbon groups if there was no formation of imine. It should be noted that, on the α-carbon, it would be unlikely because it forms a hemiaminal group, which would be unstable and corroborating this assumption, in the MS/MS spectrum losses of CH_3NH_2O or H_2O + CH_3N at the methyl group, were not detected. The eliminations from the parent ion of two H_2O molecules and C_3H_7N giving rise to *m/z* 237 ($C_{15}H_9OS^+$) are in agreement with the formation of the imine, C_3H_7N representing the loss of the aliphatic imine. The fragment ion at *m/z* 223 ($C_{15}H_{11}S^+$) showed the elimination of CO from *m/z* 251 fragment ion, which may argue for a TP structure where 1-naphthol has been formed.

2.2.5. TP-348

Analysis of neutral losses in the MS/MS spectrum of this TP showed the loss of two water molecules, one from the parent ion to give fragment ion *m/z* 312 which, in turn, lost one H_2O molecule giving rise to fragment ion *m/z* 294 ($C_{18}H_{16}NOS^+$) (Appendix A Fig. S7). In view of these observations it seems likely that two hydroxylation reactions, one on β-carbon of aliphatic chain and the other on the naphthalene ring might have been responsible for the TP structure. The third loss of H_2O could be from an ether group. In theory, hydroxylation at the α-carbon of the aliphatic chain could occur, but it forms an unstable compound. Hydroxylation on the methyl group was not considered by the fact that elimination of CH_3NH_2OH or CH_3N were not found in the MS/MS spectrum. Two hydroxylations and dehydrogenation of naphthalene were considered to occur since, after losing one H_2O molecule, a naphthol group might have been formed. The hydroxylations are proposed to have been formed at the 1,2 positions of naphthalene in agreement with McConkey et al. (2002) that identified the formations of hydroxyl groups in these positions by degrading naphthene with natural sunlight. The fragment ion at *m/z* 235 ($C_{16}H_{11}S^+$), could be formed by the loss of the CH_3NH_2, 3 H_2O and CO molecules from *m/z* 312 ($C_{18}H_{18}NO_2S^+$). The loss of the CO molecule may confirm the hypothesis of a TP structure where formation of the naphthol group occurred.

2.2.6. TP-290

In the MS/MS spectrum (Appendix A Fig. S8), three consecutive losses of H_2O were identified, one from the parent ion to *m/z* 272 ($C_{16}H_{18}NO_3^+$), another from this one to *m/z* 254 ($C_{16}H_{16}NO_2^+$) and the other from the latter ion to *m/z* 236 ($C_{16}H_{14}NO^+$). One of these losses probably involves OH at the ether group after hydrogen rearrangement. The structure proposed is a molecule where the sulfur atom has been replaced by one oxygen atom to form an alcohol group being the other OH attached to the methyl group. The peak at *m/z* 211 ($C_{14}H_{11}O_2^+$) showed the neutral losses of H_2O and C_2H_7NO, either both directly from the parent ion, or H_2O from the parent ion and C_2H_7NO from *m/z* 272. The latter loss may indicate that OH was bound to methyl. In theory it could be bound to the α-carbon of the aliphatic chain, but if that was so, a hemiaminal group might have been formed, which would result in a less stable compound. The loss of CO at *m/z* 183 ($C_{13}H_{11}O^+$) from *m/z* 211, suggests a structure bearing a 1-naphthol group.

2.2.7. TP-332

The MS spectrum of this TP shows (Appendix A Fig. S9), based on the isotopic contribution of chlorine ($^{35}Cl/^{37}Cl$), that its structure bears one chlorine atom. This chlorine appears to be attached to the aromatic ring corroborated by the loss of $C_{10}H_6ClO$ from the parent ion giving rise to *m/z* 155 ion

JOURNAL OF ENVIRONMENTAL SCIENCES 82 (2019) 113–123

Table 1 – Transformation products (TPs) of duloxetine (DUL) after degradation process identified by their fragmentation patterns in the MS/MS spectra.

TP code	Retention time (min)	Structure	Theoretical mass $[M + H]^+$	Elemental formula $[M + H]^+$	Mass error (ppm)	Process
DUL	7.38	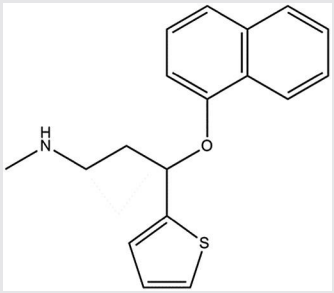	298.1260	$C_{18}H_{20}NOS^+$	−2.3	
			267.0838	$C_{17}H_{15}OS^+$	−3.7	
			239.0525	$C_{15}H_{11}OS^+$	0	
			221.0419	$C_{15}H_9S^+$	0.9	
			211.0576	$C_{14}H_{11}S^+$	−1.4	
			183.0804	$C_{13}H_{11}O^+$	−2.2	
			157.0648	$C_{11}H_9O^+$	−0.6	
TP-312A	5.13	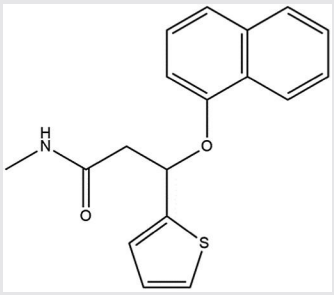	312.1053	$C_{18}H_{18}NO_2S^+$	3.8	UV
			281.0631	$C_{17}H_{13}O_2S^+$	1.7	
			267.0474	$C_{16}H_{11}O_2^+$	2.2	
			263.0525	$C_{17}H_{11}OS^+$	−1.1	
			255.0474	$C_{15}H_{11}O_2S^+$	4.3	
			253.0682	$C_{16}H_{13}OS^+$	4.7	
			237.0369	$C_{15}H_9OS^+$	2.5	
			209.0419	$C_{14}H_9S^+$	4.3	
			197.0597	$C_{13}H_9O_2^+$	0.5	
			152.0528	$C_8H_{10}NS^+$	−0.6	
			138.0372	$C_7H_8NS^+$	0	
TP-312B	6.23	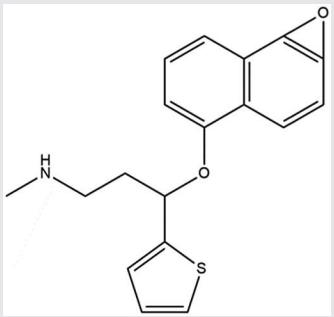	312.1053	$C_{18}H_{18}NO_2S^+$	1.3	UV
			281.0631	$C_{17}H_{13}O_2S^+$	3.2	
			263.0525	$C_{17}H_{11}OS^+$	3.8	
			253.0318	$C_{15}H_9O_2S^+$	2.8	
			228.1019	$C_{14}H_{14}NO_2^+$	0	
			202.0863	$C_{12}H_{12}NO_2^+$	1.0	
TP-312C	7.42	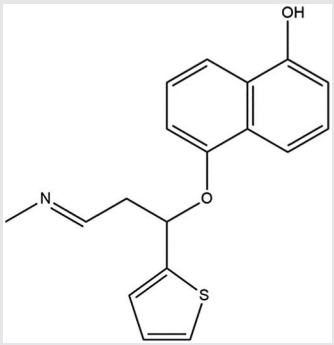	312.1053	$C_{18}H_{18}NO_2S^+$	0.6	UV
			281.0631	$C_{17}H_{13}O_2S^+$	3.5	
			269.0631	$C_{16}H_{13}O_2S^+$	−0.4	
			253.0318	$C_{15}H_9O_2S^+$	0.4	
			228.1019	$C_{14}H_{14}NO_2^+$	1.7	
			202.0863	$C_{12}H_{12}NO_2^+$	1.5	
			184.0757	$C_{12}H_{10}NO^+$	3.2	
			161.0597	$C_{10}H_9O_2^+$	4.3	
TP-328A	5.00	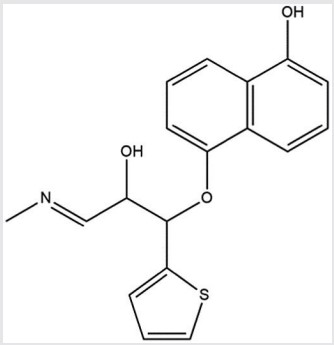	328.1002	$C_{18}H_{18}NO_3S^+$	3.6	UV
			310.0896	$C_{18}H_{16}NO_2S^+$	3.2	
			294.1125	$C_{18}H_{16}NO_3^+$	−1.0	
			276.1019	$C_{18}H_{14}NO_2^+$	0.7	
			266.1176	$C_{17}H_{16}NO_2^+$	1.1	
			252.1019	$C_{16}H_{14}NO_2^+$	3.7	
			238.0863	$C_{15}H_{12}NO_2^+$	2.1	
			234.0913	$C_{16}H_{12}NO^+$	4.7	

(continued on next page)

Table 1– (*continued*)

TP code	Retention time (min)	Structure	Theoretical mass $[M + H]^+$	Elemental formula $[M + H]^+$	Mass error (ppm)	Process
TP-328B	5.92	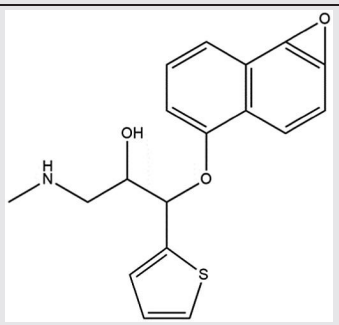	328.1002	$C_{18}H_{18}NO_3S^+$	3.0	UV
			297.0580	$C_{17}H_{13}O_3S^+$	−3.0	
			279.0474	$C_{17}H_{11}O_2S^+$	3.9	
			269.0267	$C_{15}H_9O_3S^+$	4.0	
			213.0542	$C_{13}H_9O_3^+$	0	
			185.0597	$C_{12}H_9O_2^+$	0	
			157.0648	$C_{11}H_9O^+$	0	
TP-330	7.98	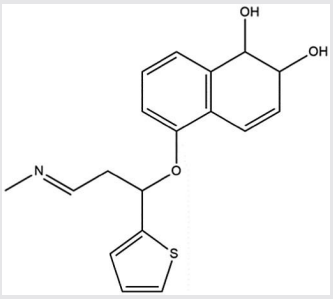	330.1158	$C_{18}H_{20}NO_3S^+$	3.3	UV
			312.1060	$C_{18}H_{18}NO_2S^+$	−4.5	
			294.0947	$C_{18}H_{16}NOS^+$	−1.4	
			270.0947	$C_{16}H_{16}NOS^+$	3.7	
			251.0525	$C_{16}H_{11}OS^+$	−0.8	
			237.0369	$C_{15}H_9OS^+$	−2.5	
			223.0576	$C_{15}H_{11}S^+$	3.1	
TP-348	4.23	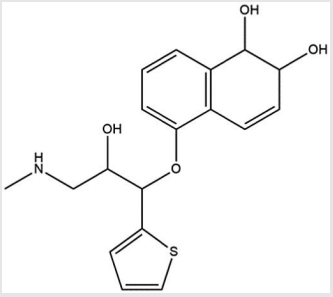	348.1264	$C_{18}H_{22}NO_4S^+$	3.3	UV
			312.1053	$C_{18}H_{18}NO_2S^+$	−4.7	
			294.0947	$C_{18}H_{16}NOS^+$	5.5	
			281.0631	$C_{17}H_{13}O_2S^+$	−1.2	
			270.0947	$C_{16}H_{16}NOS^+$	1.7	
			263.0525	$C_{17}H_{11}OS^+$	1.4	
			255.0474	$C_{15}H_{11}O_2S^+$	−2.1	
			237.0369	$C_{15}H_9OS^+$	3.8	
			235.0576	$C_{16}H_{11}S^+$	−0.6	
			227.0525	$C_{14}H_{11}OS^+$	−2.6	
			213.0369	$C_{13}H_9OS^+$	1.2	
TP-290	5.08	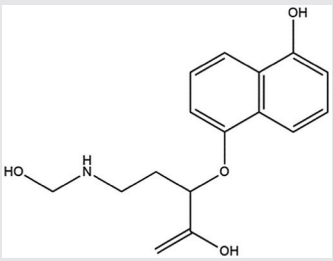	290.1387	$C_{16}H_{20}NO_4^+$	4.8	CL
			272.1281	$C_{16}H_{18}NO_3^+$	2.2	
			254.1176	$C_{16}H_{16}NO_2^+$	−1.2	
			236.1070	$C_{16}H_{14}NO^+$	−3.0	
			226.1225	$C_{15}H_{16}NO^+$	−1.3	
			211.0754	$C_{14}H_{11}O_2^+$	0	
			195.0804	$C_{14}H_{11}O^+$	−3.0	
			183.0804	$C_{13}H_{11}O^+$	−3.8	
TP-332	8.82	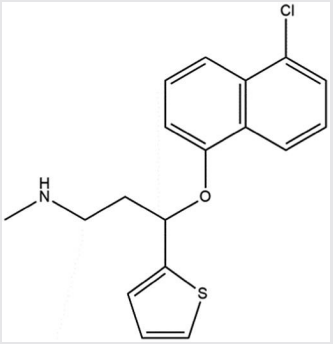	332.0870	$C_{18}H_{19}ClNOS^+$	−0.9	CL
			273.0140	$C_{15}H_{10}ClOS^+$	0	
			217.0415	$C_{13}H_{10}ClO^+$	3.7	
			191.0258	$C_{11}H_8ClO^+$	4.2	
			182.0731	$C_{10}H_{13}ClN^+$	2.2	
			155.0763	$C_8H_{13}NS^+$	4.5	

UV: Photodegradation; CL: Chlorination.

Table 2 – Ecotoxicity predicted by ECOSAR and TEST.

Compound	Fish LC_{50} 96 hr (mg/L)	Relative potency [a]	*D. magna* LC_{50} 48 hr (mg/L)	Relative potency [a]	Green algae EC_{50} 96 hr (mg/L)	Relative potency [a]	*T. pyriformis* IGC50 (mg/L)	Relative potency [a]
DUL	0.72	1.00	1.74	1.00	0.07	1.00	2.24	1.00
TP-312A	4.03	0.18	3.66	0.47	0.97	0.07	4.74	0.47
TP-312B	0.74	0.98	0.28	6.12	0.07	0.97	2.09	1.07
TP-312C	0.40	1.83	1.00	1.74	0.10	0.75	[b]	–
TP-328A	1.18	0.61	1.82	0.96	1.09	0.07	[b]	–
TP-328B	9.36	0.08	1.41	1.23	0.95	0.08	[b]	–
TP-330	1.25	0.58	2.00	0.87	1.79	0.04	[b]	–
TP-348	12.5	0.06	24.75	0.07	1.18	0.06	26.96	0.08
TP-290	7.31	0.10	4.32	0.40	0.60	0.12	30.45	0.07
TP-332	0.28	2.59	0.74	2.36	0.03	2.57	0.57	3.93

[a] Toxicity ratio between DUL and TP formed.
[b] Prediction out of applicability domain.

$C_8H_{13}NS^+$ (Appendix A Fig. S10). The neutral loss from the parent ion of C_3H_9N at *m/z* 273 ($C_{15}H_{10}ClOS^+$) corroborates that there was no reaction on the aliphatic amine. The fragment ion at *m/z* 217 ($C_{13}H_{10}ClO^+$) showed the losses of both C_4H_4S and CH_3NH_2 from the parent ion. This means that the chlorine is bound to the aromatic ring, possibly on the 1-position, forming 1-chloronaphthalene group, considering that the 1-position is more reactive than 2-position, which can be explained by the high stability of the resonance structure for the reactive intermediate (arenium ion) (Sorrell, 2005).

2.3. Summary of fragmentation patterns

Table 1 shows the retention time, fragmentation patterns, mass error and DBE of the TPs detected after the degradation processes.

2.4. Toxicity prediction

Ecotoxicity of DUL and their identified TPs were predicted by QSAR models from ECOSAR and from T.E.S.T (Details of these models were described in Section 1.6). The DUL-ISO1 and DUL-ISO2 toxicity predictions were not performed because the chemical structures were not elucidated. Most of the results for the 96-hr F. minnow LC_{50} endpoint from TEST were outside the AD, so they were not considered. For the 48-hr *D. magna* LC_{50} endpoint of both tools was carried out the consensus method. The relative potency was calculated by the ratio between DUL and TPs formed (Table 2).

Most of TPs presented low ecotoxicity at all endpoints parameters in comparison with DUL. Only TP-332 showed toxicity by at least two-fold higher than the parent compound for all endpoints and this TP was formed by the halogenation of benzene in the chlorination process, which eliminated about 40% during the experiment. The TP-312C and TP-312B had higher toxicities in at least two endpoints.

For comparison criteria, Di Poi et al. (2014) investigated the ecotoxicity of DUL and other antidepressants on two early life stages on Pacific oysters and in the embryonic stage alterations in larval development occur at concentration of at least 200 μg/L of DUL. Another study analyzed the toxicity of DUL by 48-hr *D. magna* LC_{50} tests and it was verified that it had toxicity between 2.45 and 4.33 mg/L (in the *in silico* method was 1.74 mg/L) and presented high risk in the environmental risk assessment methodology in marine waters (Minguez et al., 2016).

The mutagenicity predictions of DUL and their TPs were performed using T.E.S.T, VEGA SARpy and VEGA KNN/read-across (Table 3). In this work, the prediction of mutagenicity was performed in three prediction models to avoid false positive results. Preclinical studies showed that DUL was not mutagenic in the AMES test, which corroborates with *in silico* predictions and most of the results of VEGA SARpy and VEGA KNN/read-across presented predictions that may be outside the AD ($0.9 > ADI \geq 0.65$). The QSAR analysis for mutagenicity resulted in one TP with positive mutagenicity prediction for all methods, TP-330, which was formed by UV irradiation. All TPs with positive mutagenicity prediction were formed and completely degraded in less than 90 min in contact with UV light.

2.5. Wastewater analysis

Samples from a wastewater effluent were analyzed by UHPLC Q-TOF/MS in MS full scan mode to detect the TPs previously elucidated by the laboratory experiments. In MS/MS mode, DUL showed poor fragmentation at low concentrations. In

Table 3 – Mutagenicity predicted by VEGA platform and TEST, (+) indicates mutagenic potential and (–) indicates non-mutagenic.

Compound	SARpy	AD index	KNN/Read-Across	AD index	TEST
DUL	–	0.743	–	0.843	–
TP-312A	–	0.739	–	0.846	+
TP-312B	–	0.737	–	0.782	+
TP-312C	+	0.68	–	0.833	+
TP-328A	–	0.729	–	0.835	+
TP-328B	–	0.813	–	0.843	–
TP-330	+	0.908	+	0.909	+
TP-348	+	0.685	–	0.785	–
TP-290	[a]	0	–	0.869	–
TP-332	–	0.731	–	0.892	–

[a] Prediction out of applicability domain.

MS mode, DUL was quantified (Appendix A Fig. S11a) at concentrations of 95.5 ng/L in the influent and 79.6 ng/L in the effluent, removal of 17% and TP-332 was detected in the effluent (Appendix A Fig. S11b). This TP was probably formed in the chlorination process of the WWTP and presented more ecotoxicity than DUL in the *in silico* prediction. The TPs of this work were identified under controlled conditions. In wastewater samples they might have been degraded, not being detected due to low concentrations or having not even been formed. Moreover, complex interactions with biotic and abiotic processes may occur. It would be necessary to analyze more effluents samples from different sources such as hospitals wastewater.

3. Conclusions

In the present work, the experiments showed that DUL reacts with chlorine and under UV irradiation, producing 11 TPs under controlled laboratory conditions, nine of them were elucidated and to the best of our knowledge, this is the first work that identifies the TPs of DUL by processes that may occur in the environment and in wastewater treatment plants. UHPLC Q-TOF/MS showed to be a powerful tool to elucidate TPs by analyzing the fragmentation patterns in MS/MS mode.

It could be concluded that DUL was completely degraded in both processes. In the hydrolysis process the drug presented stability over 4 days and no TP was detected. In photodegradation all TPs have been degraded after 45 min of experiment and in chlorination, TP-290 was degraded until the end of the experiment (after 24 hr) and TP-332 was partially eliminated.

QSARs assessments revealed six TPs with positive results for mutagenicity. Concerning ecotoxicity prediction, only TP-332 showed to be more toxic than the parent compound for all endpoints. In wastewater samples, it was concluded that DUL was not totally removed at WWTP and the TP-332 was formed, possibly during chlorination process. For future research, the possible formation of these TPs should be investigated in studies of emerging contaminants. Another fact to be considered is to verify the toxicity of these TPs by *in vitro* and *in vivo* assays.

Acknowledgments

The authors are grateful to Águas de Portugal for providing samples. This work was supported by Brazilian Federal Agency Coordenação de Aperfeiçoamento de Pessoal de Nível Superior (CAPES) for PhD grants (No. 99999.000845/2014-00) and Fundação para a Ciência e a Tecnologia (FCT) Portugal (Projects UID/MULTI/00612/2013, PEst-OE/QUI/UI0612/2013 and LISBOA-01-0145-FEDER-022125).

Appendix A. Supplementary data

Supplementary data to this article can be found online at https://doi.org/10.1016/j.jes.2019.02.025.

REFERENCES

Acuña, V., Ginebreda, A., Mor, J.R., Petrovic, M., Sabater, S., Sumpter, J., et al., 2015. Balancing the health benefits and environmental risks of pharmaceuticals: diclofenac as an example. Environ. Int. 85, 327–333.

Beretsou, V.G., Psoma, A.K., Gago-Ferrero, P., Aalizadeh, R., Fenner, K., Thomaidis, N.S., 2016. Identification of biotransformation products of citalopram formed in activated sludge. Water Res. 103, 205–214.

Bletsou, A.A., Jeon, J., Hollender, J., Archontaki, E., Thomaidis, N.S., 2015. Targeted and non-targeted liquid chromatography-mass spectrometric workflows for identification of transformation products of emerging pollutants in the aquatic environment. TrAC Trends Anal. Chem. 66, 32–44.

Carpinteiro, I., Rodil, R., Quintana, J.B., Cela, R., 2017. Reaction of diazepam and related benzodiazepines with chlorine. Kinetics, transformation products and in-silico toxicological assessment. Water Res. 120, 280–289.

Chadha, R., Bali, A., Bansal, G., 2016. Characterization of stress degradation products of duloxetine hydrochloride employing LC–UV/ PDA and LC–MS/TOF studies. J. Pharm. Biomed. Anal. 121, 39–55.

Chhalotiya, U.K., Bhatt, K.K., Shah, D.A., Baldania, S.L., 2010. Development and validation of a stability-indicating RP-HPLC method for duloxetine hydrochloride in its bulk and tablet dosage form. Sci. Pharm. 78 (4), 857–868.

Datar, P.A., Waghmare, R.U., 2014. Development and validation of an analytical method for the stability of duloxetine hydrochloride. J. Taibah. Univ. Sci. 8 (4), 357–363.

DGS (Directorate-General of Health), 2016. A Saúde dos Portugueses. Direção de Serviços de Informação e Análise. Portugal. Available at. https://comum.rcaap.pt/bitstream/10400.26/18278/1/A%20Sa%C3%BAde%20dos%20Portugueses%202016.pdf (Accessed September 09, 2018).

Di Poi, C., Evariste, L., Serpentini, A., Halm-Lemeille, M.P., Lebel, J. M., Costil, K., 2014. Toxicity of five antidepressant drugs on embryo – larval development and metamorphosis success in the Pacific oyster, *Crassostrea gigas*. Environ. Sci. Pollut. Res. Int. 21 (23), 13302–13314.

Directive, 2013. Directive 2013/39/EU of the European Parliament and of the Council of 12 August 2013 amending Directives 2000/60/EC and 2008/105/EC as regards priority substances in the field of water policy. Off. J. Eur. Union 226, 1–17 /39/EU., 2013.

El Najjar, N.H., Deborde, M., Journel, R., Vel Leitner, N.K., 2013. Aqueous chlorination of levofloxacin: kinetic and mechanistic study, transformation product identification and toxicity. Water Res. 47 (1), 121–129.

Fick, J., Lindberg, R.H., Kaj, L., Brorström-Lundén, E., 2011. Results from the Swedish National Screening Programme 2010. Subreport 3. Pharmaceuticals. Swedish Environmental Research Institute, p. 56 IVL Report B2014.

Johnson, P.S., Cook, P.L., Liu, X., Yang, W., Bai, Y., Abbott, N.L., et al., 2011. Universal mechanism for breaking amide bonds by ionizing radiation. J. Chem. Phys. 135, 44702–44709.

Kumar, N., Sangeetha, D., Vaghela, B., Reddy, P.S., Raghav, A., 2012. Development and validation of a stability indicating RP-LC method for the estimation of process related impurities and degradation products of duloxetine hydrochloride and phthalic acid in duloxetine hydrochloride delayed release capsules. J. Liq. Chromatogr. Relat. Technol. 35 (7), 867–881.

Mcconkey, B.J., Hewitt, L.M., Dixon, D.G., Greenberg, B.M., 2002. Natural sunlight induced photooxidation of naphthalene in aqueous solution. Water Air Soil Pollut. 136 (1–4), 347–359.

Minguez, L., Pedelucq, J., Farcy, E., Ballandonne, C., Budzinski, H., Halm-Lemeille, M.P., 2016. Toxicities of 48 pharmaceuticals and their freshwater and marine environmental assessment

in northwestern France. Environ. Sci. Pollut. Res. 23 (6), 4992–5001.

Pinto da Costa, J., Girão, A.V., Monteiro, O.C., Trindade, T., Costa, M.C., 2015. Biotechnologically obtained nanocomposites: a practical application for photodegradation of safranin-T under UV-vis and solar light. J. Environ. Sci. Health A Tox. Hazard. Subst. Environ. Eng. 50 (10), 996–1010.

Santoke, H., Song, W., Cooper, W.J., Peake, B.M., 2012. Advanced oxidation treatment and photochemical fate of selected antidepressant pharmaceuticals in solutions of Suwannee River humic acid. J. Hazard. Mater. 217–218, 382–390.

Schultz, M.M., Furlong, E.T., 2008. Trace analysis of antidepressant pharmaceuticals and their select degradates in aquatic matrixes by LC/ESI/MS/MS. Anal. Chem. 80 (5), 1756–1762.

Silva, L.J.G., Pereira, A.M.P.T., Meisel, L.M., Lino, C.M., Pena, A., 2015. Reviewing the serotonin reuptake inhibitors (SSRIs) footprint in the aquatic biota: uptake, bioaccumulation and ecotoxicology. Environ. Pollut. 197, 127–143.

Sinha, V.R., Anamika, Kumria, R., Bhinge, J.R., 2009. Stress degradation studies on duloxetine hydrochloride and development of an RP-HPLC method for its determination in capsule formulation. J. Chromatogr. Sci. 47 (7), 589–593.

Sorrell, T.M. (Ed.), 2005. Organic Chemistry, second ed. University Science Books, California.

Subedi, B., Kannan, K., 2015. Occurrence and fate of select psychoactive pharmaceuticals and antihypertensives in two wastewater treatment plants in New York State, USA. Sci. Total Environ. 514, 273–280.

Taylor, D., Senac, T., 2014. Human pharmaceutical products in the environment – the "problem" in perspective. Chemosphere 115, 95–99.

Trawiński, J., Skibiński, R., 2017. Photolytic and photocatalytic degradation of tandospirone: determination of kinetics, identification of transformation products and in silico estimation of toxicity. Sci. Total Environ. 591, 775–798.

US EPA (United States Environmental Protection Agency), 2016. User's Guide for T.E.S.T. (Toxicity Estimation Software Tool): A Program to Estimate Toxicity from Molecular Structure. version 4.2. Available at. www.epa.gov/sites/production/files/2016-05/documents/600r16058.pdf, Accessed date: 20 October 2018.

US EPA (United States Environmental Protection Agency), 2017a. The third unregulated contaminant monitoring rule (UCMR3): Data summary, January 2017. EPA 815-S-17-001. Office of Water (MS-140).

US EPA (United States Environmental Protection Agency), 2017b. Methodology document for the ECOlogical Structure-Activity Relationship Model (ECOSAR) Class Program (Ecological Structure Activity Relationships). version 2.0. Available at. www.epa.gov/tsca-screening-tools/ecological-structure-activity-relationships-program-ecosar-methodology-document, Accessed date: 15 October 2018.

Vinu, R., Madras, G., 2011. Photocatalytic degradation of water pollutants using nano-TiO_2. Energy efficiency and renewable energy through nanotechnology. In: Zang, L. (Ed.), Green Energy and Technology. Springer, London, pp. 626–677.

Wang, W.L., Wu, Q.Y., Huang, N., Wang, T., Hu, H.Y., 2016. Synergistic effect between UV and chlorine (UV/chlorine) on the degradation of carbamazepine: influence factors and radical species. Water Res. 98, 190–198.

Wilde, M.L., Menz, J., Trautwein, C., Leder, C., Kümmerer, K., 2016. Environmental fate and effect assessment of thioridazine and its transformation products formed by photodegradation. Environ. Pollut. 213, 658–670.

Worth, A.P., van Leeuwen, C.J., Hartung, T., 2004. The prospects for using (Q)SARs in a changing political environment: high expectations and a key role for the Commission's Joint Research Centre. SAR QSAR Environ. Res. 15 (5–6), 331–343.

Writer, J.H., Ferrer, I., Barber, L.B., Thurman, E.M., 2013. Widespread occurrence of neuro-active pharmaceuticals and metabolites in 24 Minnesota rivers and wastewaters. Sci. Total Environ. 461–462, 519–527.

Yin, J., Niu, Y., Shao, B., 2017. Products of methotrexate during chlorination. J. Environ. Sci. 55, 100–108.

Yuzawa, H., Aoki, M., Otake, K., Hattori, T., Itoh, H., Yoshida, H., 2012. Reaction mechanism of aromatic ring hydroxylation by water over platinum-loaded titanium oxide photocatalyst. J. Phys. Chem. C 116 (48), 25376–25387.

Zhou, S., Xia, Y., Li, T., Yao, T., Shi, Z., Zhu, S., et al., 2016. Degradation of carbamazepine by UV/chlorine advanced oxidation process and formation of disinfection by-products. Environ. Sci. Pollut. Res. 23 (16), 16448–16455.

Appendix A. Supplementary data

Degradation of duloxetine: Identification of transformation products by UHPLC-ESI(+)-HRMS/MS, *in silico* toxicity and wastewater analysis

S1. Method validation

For the validation of the method the following parameters were studied: Linearity, limit of detection and quantification, precision, recovery and matrix effects. The validation of the method was performed in MS mode. The linearity of the DUL was obtained by linear regression, which resulted in a determination coefficient (r^2) of 0.995 in concentrations between 0.01 and 25 ng/ml. Limits of quantification (L.D) and detection (L.Q) were calculated by signal-to-noise ratio (S/N) in MS mode (full scan), for L.D, S/N = 3 and for L.Q, S/N = 10, resulting in L.D = 3.5 ng/L and L.Q = 10 ng/L. Recoveries for SPE were determined by spiked samples at low (40 ng/L) and high concentrations (400 ng/L) in triplicate that resulted in recoveries of 96.4 and 110.4%, respectively. and the relative standard deviations were less than 20% (Table S1). Matrix effects (M.E) may significantly influence the analyte signals in complex matrices, especially when using electrospray ionization (ESI), because it may result in the increase or suppression of the signal of the target compound, causing a poor accuracy. The M.E was estimated by the difference of analyte peak area of the sample with the standard added after the extraction (100 ng/L) and the analyte peak area of the non-spiked sample.

Table S1 Recoveries, matrix effect (M.E), limits of detection (L.D) and quantification (L.Q) and correlation coefficient (r^2) of DUL

Compound	Re (RSD %) n=3 (40 ng/L)	Re (RSD %) n=3 (400 ng/L)	M.E (RSD %) n=3 (100 ng/L)	L.D (ng/L)	L.Q (ng/L)	r^2
DUL	96.4 (2.0)	110.4 (0.8)	103.9 (11.6)	3.5	10	0.995

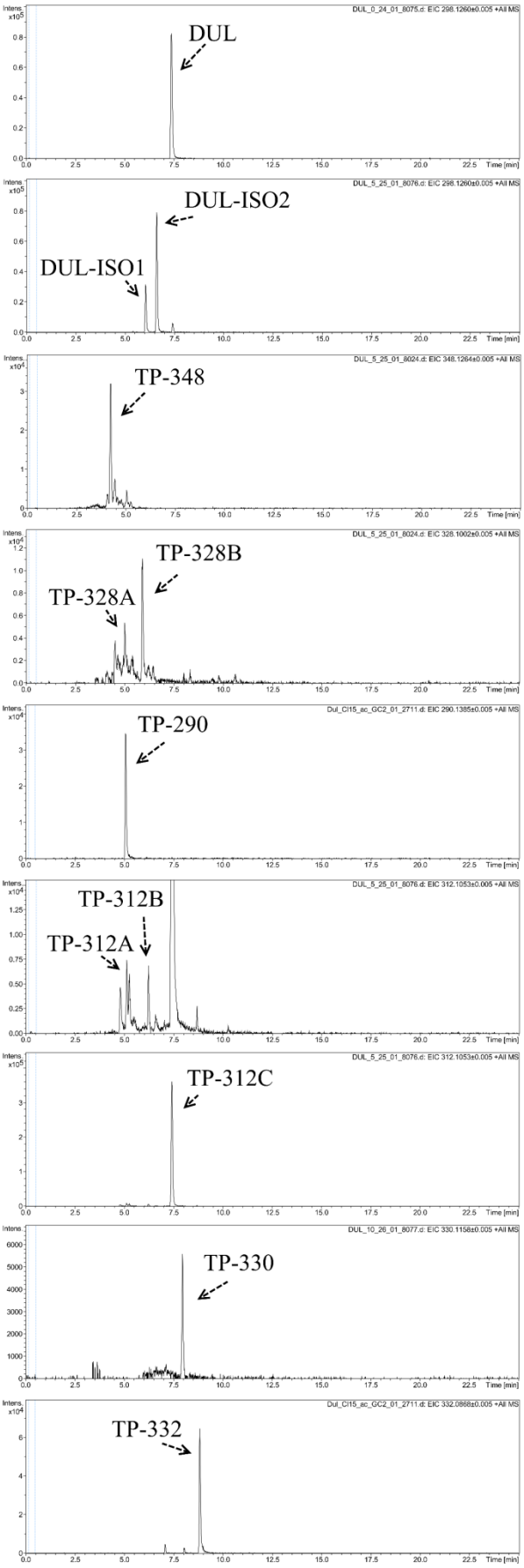
DUL
DUL-ISO2
DUL-ISO1
TP-348
TP-328B
TP-328A
TP-290
TP-312B
TP-312A
TP-312C
TP-330
TP-332
Time [min]

Fig. S1 Chromatograms (MS mode) of DUL and TPs.

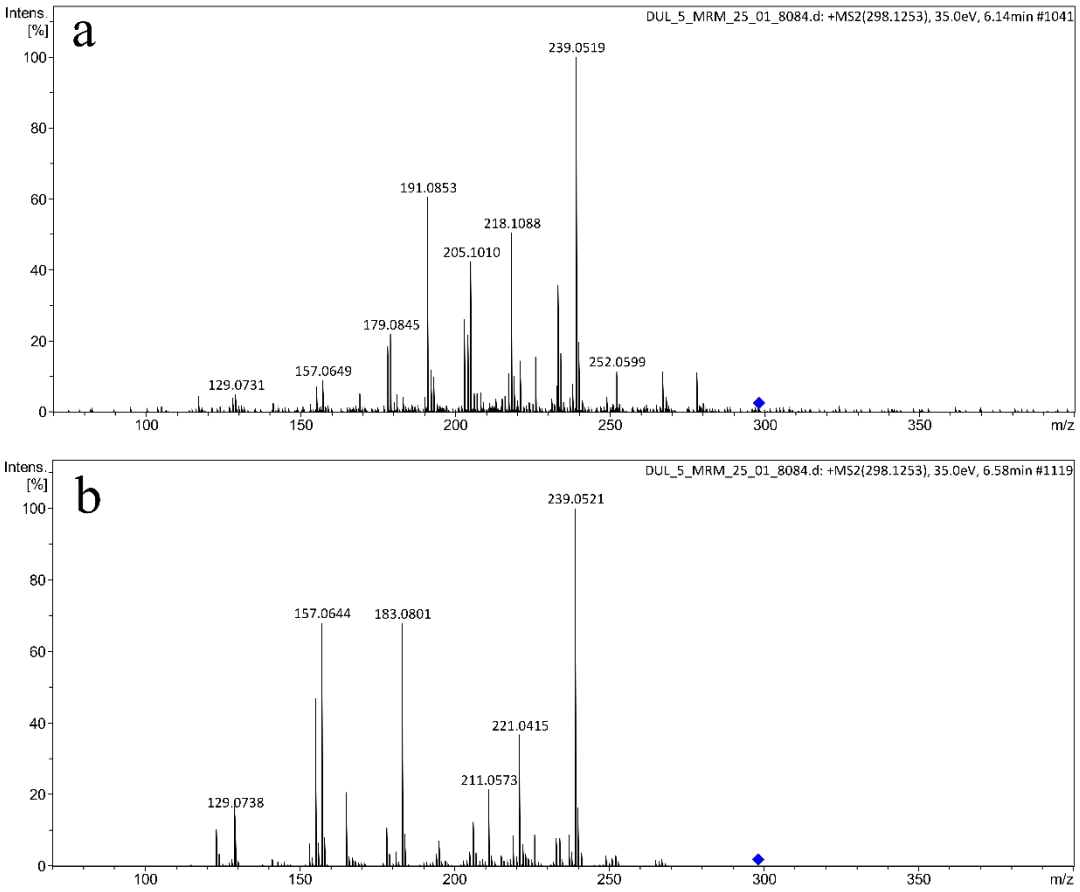

Fig. S2 MS/MS spectra of (a) DUL-ISO1 and (2) DUL-ISO2.

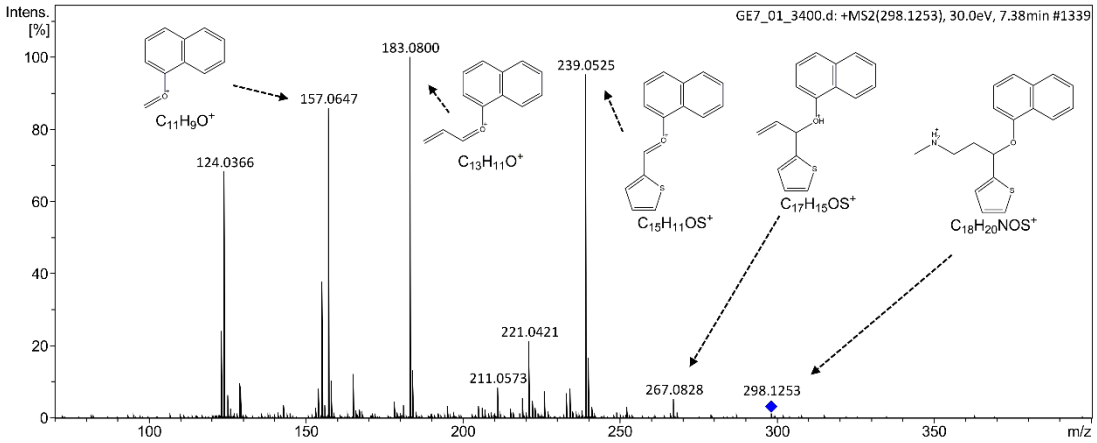

Fig. S3 MS/MS spectrum of DUL.

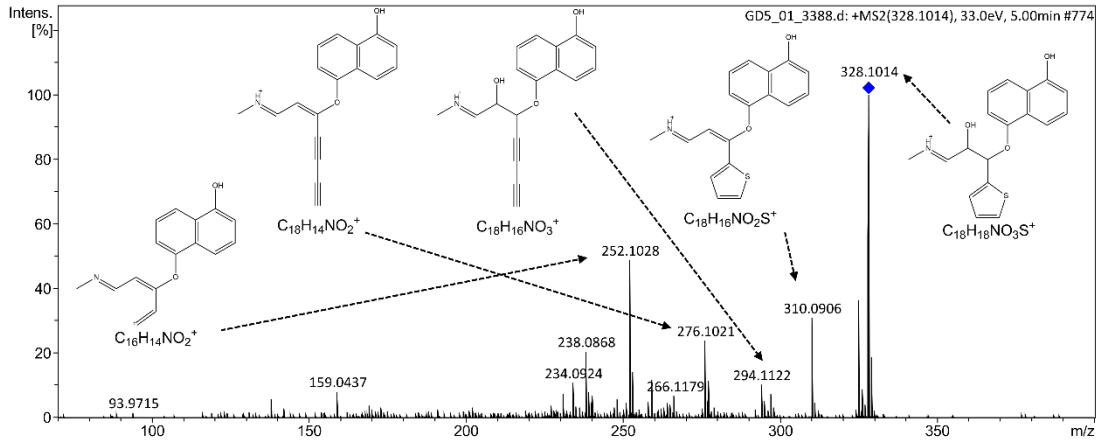

Fig. S4 MS/MS spectrum of TP-328A.

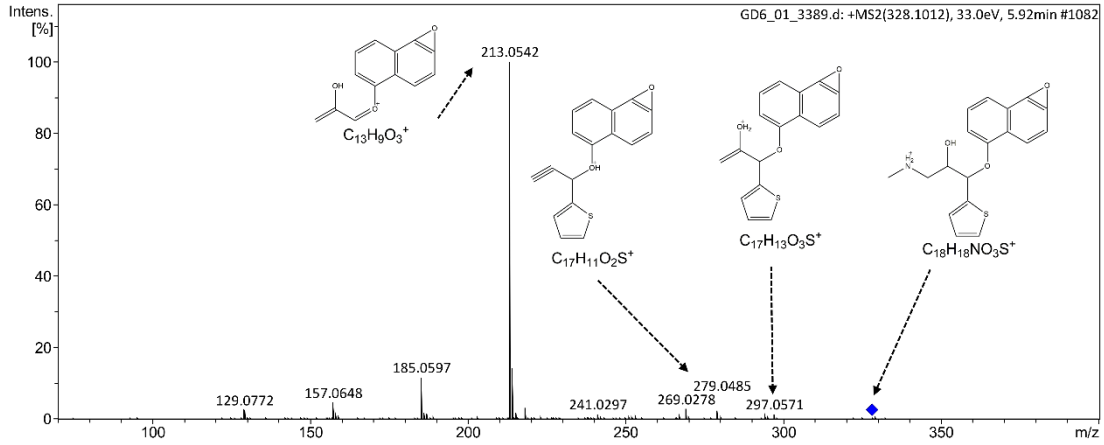

Fig. S5 MS/MS spectrum of TP-328B.

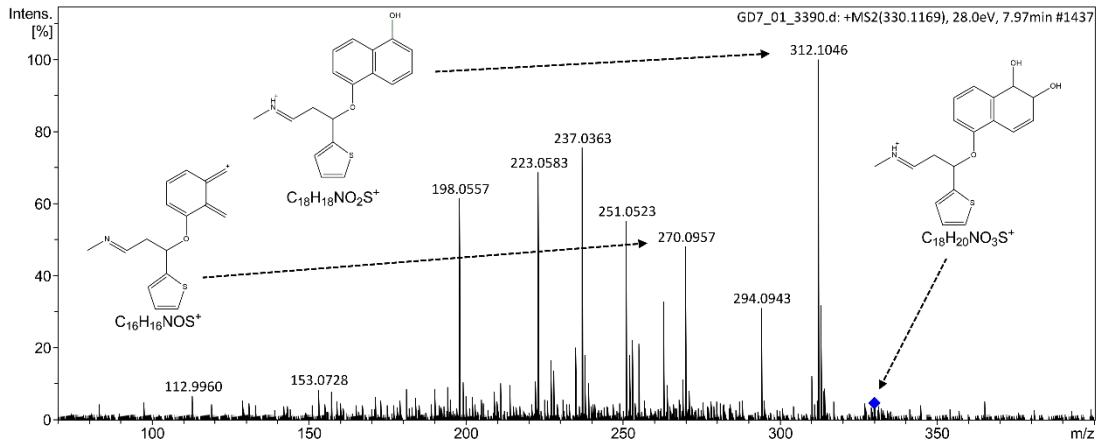

Fig. S6 MS/MS spectrum of TP-330.

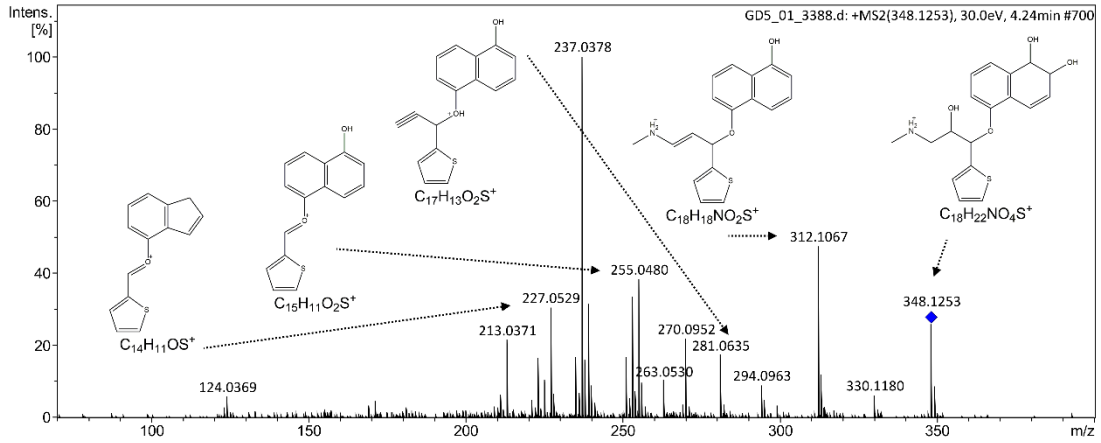

Fig. S7 MS/MS spectrum of TP-348.

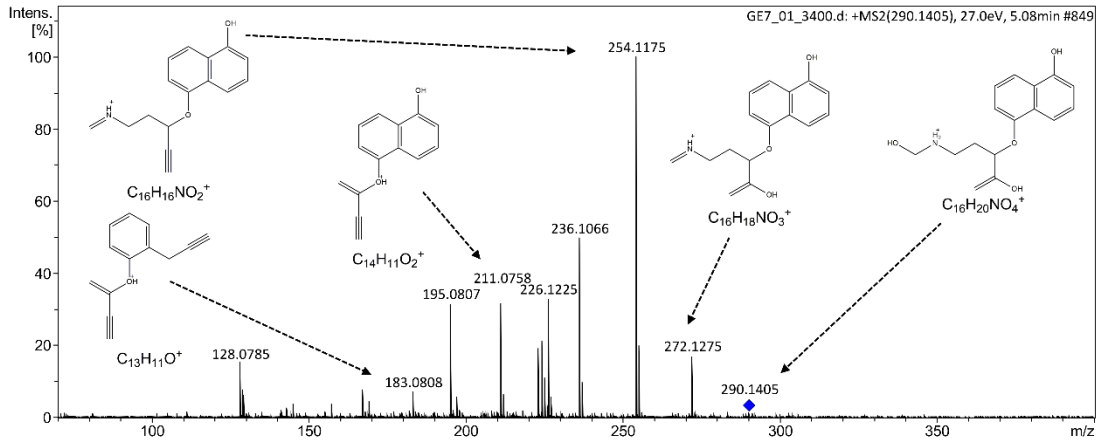

Fig. S8 MS/MS spectrum of TP-290.

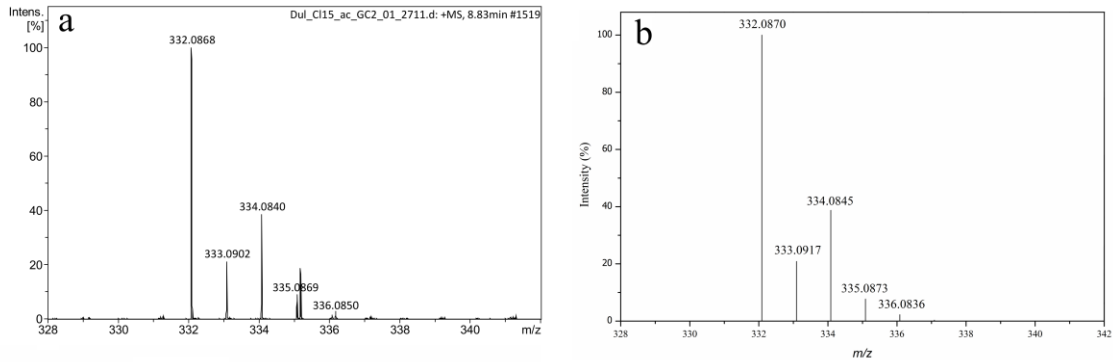

Fig. S9 Isotopic patterns in MS mode of (a) TP-332 and (b) theoretical

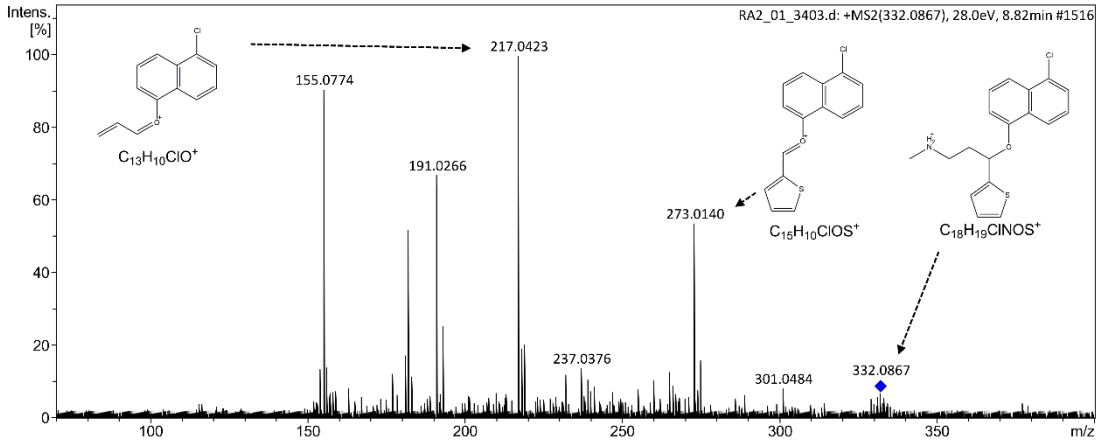

Fig. S10 MS/MS spectrum of TP-332.

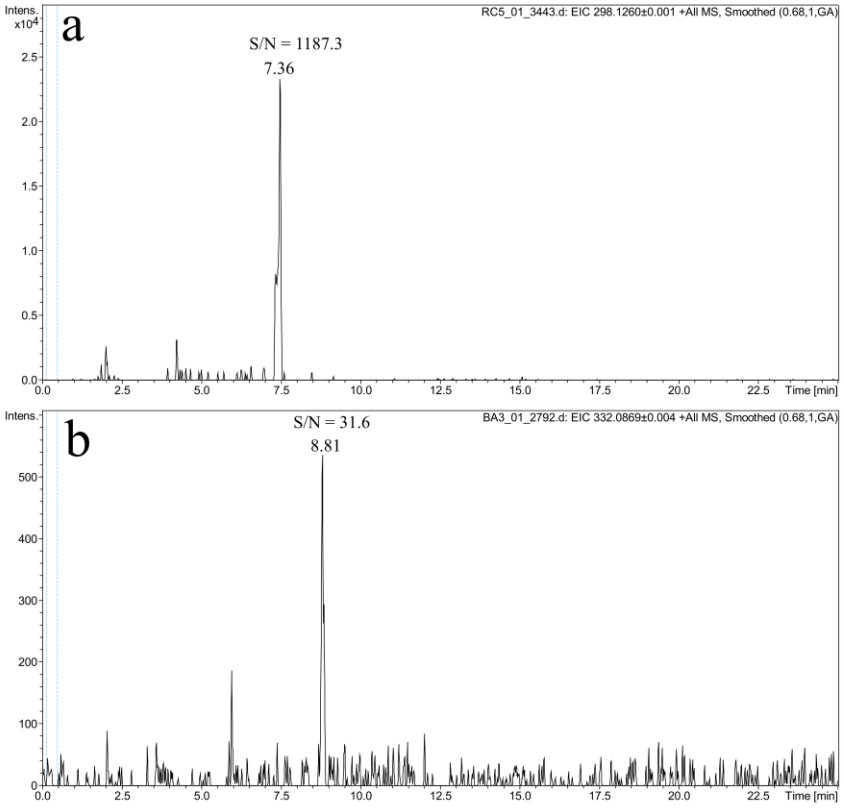

Fig. S11 MS spectrum of (a) DUL and (b) TP-332 in wastewater effluent.

4.2. Conclusões

Este trabalho elucidou onze TPs proveniente do DUL pelos processos de hidrólise, fotólise e cloração em condições laboratoriais utilizando água superficial como matriz. O uso do UHPLC-QTOF-MS se mostrou uma ferramenta poderosa para a elucidação das estruturas químicas dos TPs. Adicionalmente, nove destes TPs nunca foram discutidos anteriormente. Na hidrólise, o DUL apresentou estabilidade em quatro dias e não foi detetado TPs durante este processo. Ao longo da fotólise foram gerados nove TPs e após 30 min, o DUL foi completamente eliminado assim como todos os TPs, foi observado também a formação de dois isómeros do DUL, porém não foi possível identificar as estruturas devido à semelhança dos padrões de fragmentação obtidos nos espectros MS/MS. Na cloração, o DUL foi degradado após 24 h e somente dois TPs foram formados.

As predições *in silico* foram realizados com quatro parâmetros de ecotoxicidade: 96-hr F. minnow LC_{50}, 48-hr *D. magna* LC_{50} and T*. pyriformis* IGC_{50} e 96-hr green algae EC_{50}. A maioria dos TPs resultou em uma menor toxicidade em comparação com o DUL, porém o TP-332 mostrou ser mais tóxico que o composto parente para todos estes parâmetros. A mutagenicidade foi realizada em três métodos QSARs no qual somente o TP-330 (formado somente pela radiação UV−Vis) apresentou mutagenicidade positiva para todos os métodos.

Amostras de efluentes foram extraídas por SPE e validadas. O DUL foi quantificado nas concentrações de 95,5 ng L^{-1} no influente e 79,6 ng L^{-1} no efluente, ou seja, houve uma remoção de 17%. O TP-332, que em nosso experimento foi formado durante a cloração, foi detetado no efluente. Para futuras pesquisas, é essencial analisar em efluentes de diferentes fontes e realizar ensaios *in vivo* ou *in vitro* para verificar o potencial tóxico destes TPs.

4.3. Referências

1. Fick, J., Lindberg, R.H., Kaj, L., Brorström-Lundén, E., 2011. Results from the Swedish National Screening Programme 2010. Subreport 3. Pharmaceuticals. Swedish Environmental Research Institute, p. 56 IVL Report B2014.

2. Schultz, M.M., Furlong, E.T., 2008. Trace analysis of antidepressant pharmaceuticals and their select degradates in aquatic matrixes by LC/ESI/MS/MS. *Anal. Chem*. 80 (5), 1756–1762. doi:10.1021/ac702154e

3. Santoke, H., Song, W., Cooper, W.J., Peake, B.M., 2012. Advanced oxidation treatment and photochemical fate of selected antidepressant pharmaceuticals in solutions of Suwannee River humic acid. *J. Hazard. Mater*. 217–218, 382–390. doi:10.1016/j.jhazmat.2012.03.049

Capítulo 5

Degradação fotocatalítica da amitriptilina, trazodona e venlafaxina por nanofios de titanato dopados com cobalto

5.1. Introdução

A fotocatálise é uma das tecnologias mais promissoras para a degradação de contaminantes em matrizes ambientais, técnica que consiste em decompor o poluente por fotões através de um catalisador. O fotocatalisador mais amplamente utilizado é o TiO_2 [1] por apresentar estabilidade química e baixo custo porém, é limitado pela baixa capacidade de absorção de luz visível. Contudo, métodos como sensibilização, dopagem ou formação de nanocompósitos com semicondutores têm como objetivo melhorar a capacidade de absorção do fotocatalisador [2,3,4]. Nanofios de titanato foram modificados com 1% de dopagem com cobalto (Co-TNW), desenvolvido anteriormente pelo grupo de pesquisa da Prof. Dr. Olinda C. Monteiro do Centro de Química e Bioquímica da Faculdade de Ciências da Universidade de Lisboa. Este fotocatalisador foi utilizado na remoção de vários poluentes sob radiação UV-Vis [5].

Este trabalho teve como objetivo avaliar a eficiência do Co-TNW na remoção de três fármacos antidepressivos (AMI, TRA e VEN) sob radiação UV-Vis. Estes fármacos são frequentemente detectados no meio ambiente, o que mostra que não há uma total eliminação em sistemas de tratamento de efluentes. Estudos mostraram que a AMI teve uma remoção de aproximadamente 85% na ETAR [6], seguida da VEN, com 50% [7] e TRA, com 35% de eficiência [8]. Adicionalmente, TPs foram elucidados pelas análises de padrões de fragmentação em modo MS/MS obtidos pela cromatografia líquida de ultra alto desempenho acoplada a espectrometria de massa do tipo quadrupolo/tempo de voo. Por último, a toxicidade dos TPs foi avaliada por modelos de relações quantitativas estrutura-atividade.

Para o complemento deste trabalho, foi realizado um experimento de degradação do AMI sob outra radiação, a visível, com o objetivo de simular a radiação solar utilizando o Co-TNW como catalisador para identificar a formação dos TPs sob este tipo de radiação.

Este capítulo é uma representação integral dos artigos:

Osawa, R.A., Barrocas, BT., Monteiro, O.C., Oliveira, M.C., Florêncio, M.H., 2019. Photocatalytic degradation of amitriptyline, trazodone and venlafaxine using modified cobalt-titanate nanowires under UV−Vis radiation: Transformation products and in silico toxicity. *Chem. Eng. J*. 373, 1338−1347. doi:10.1016/j.cej.2019.05.137

Osawa, R.A., Barrocas, BT., Monteiro, O.C., Oliveira, M.C., Florêncio, M.H., 2019. Visible light photocatalytic degradation of amitriptyline using cobalt doped titanate nanowires: Kinetics and degradation pathways (Artigo submetido)

Chemical Engineering Journal 373 (2019) 1338–1347

Contents lists available at ScienceDirect

Chemical Engineering Journal

journal homepage: www.elsevier.com/locate/cej

Photocatalytic degradation of amitriptyline, trazodone and venlafaxine using modified cobalt-titanate nanowires under UV–Vis radiation: Transformation products and *in silico* toxicity

Rodrigo A. Osawa[a,b,*], Beatriz T. Barrocas[a,c], Olinda C. Monteiro[a,c], M. Conceição Oliveira[d], M. Helena Florêncio[a,b]

[a] Centro de Química e Bioquímica, Faculdade de Ciências, Universidade de Lisboa, 1749-016 Lisboa, Portugal
[b] Laboratório de FTICR e Espectrometria de Massa Estrutural, Faculdade de Ciências, Universidade de Lisboa, 1749-016 Lisboa, Portugal
[c] Centro de Química Estrutural, Faculdade de Ciências, Universidade de Lisboa, 1749-016 Lisboa, Portugal
[d] Centro de Química Estrutural, Instituto Superior Técnico, Universidade de Lisboa, 1049-001 Lisboa, Portugal

HIGHLIGHTS

- Photolysis and photocatalysis using Co-TNW of three antidepressants was investigated.
- Amitriptyline and venlafaxine showed high degradation rate in photocatalysis.
- The structures of twenty TPs were elucidated and degradation pathway were proposed.
- Trazodone TPs showed mutagenic potential according to *in silico* toxicity prediction.

GRAPHICAL ABSTRACT

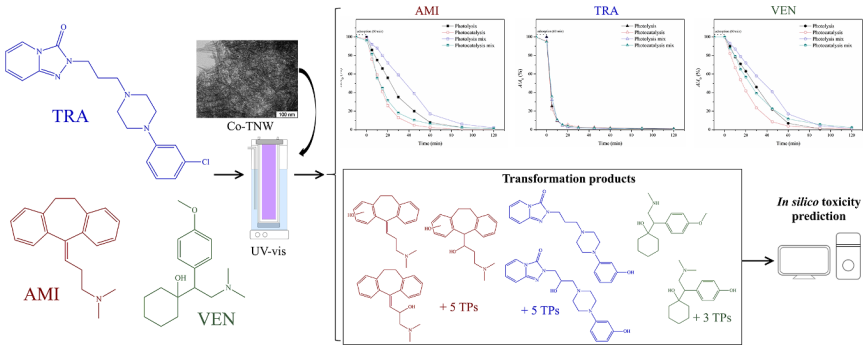

ARTICLE INFO

Keywords:
UV – Vis photocatalysis
Modified cobalt-titanate nanowire
Antidepressants
UHPLC-QTOF-MS/MS
Transformation products
In silico toxicity prediction

ABSTRACT

This work investigated the catalytic ability of modified cobalt-titanate nanowires (Co-TNW) on photodegradation of three antidepressants: amitriptyline (AMI), trazodone (TRA) and venlafaxine (VEN). The experiments were carried out with spiked tap water under UV–Vis radiation in the presence of Co-TNW as catalyst. The transformation products (TPs) were elucidated by ultra-high performance liquid chromatography coupled to quadrupole time-of-flight mass spectrometry. Degradation pathways were proposed and *in silico* toxicity assessment (ecotoxicity and mutagenicity) were performed. The results showed an enhancement in the AMI and VEN removal efficiency due to the photocatalyst use. The TRA showed a similar degradation rate in photolysis and photocatalysis. Moreover, it was verified that in the photocatalytic assisted processes, more AMI and VEN TPs were formed. Overall, the structures of twenty TPs were proposed (eight from AMI, seven from TRA and five from VEN) and to the best of found knowledge, fourteen of them have never been described before. Some of these TPs had a higher ecotoxicity than parent compound by the *in silico* analyses. Regarding of TRA, all TPs resulted in positive mutagenicity in at least one prediction model. Therefore, it is necessary to consider the formation of TPs in photocatalytic degradation of contaminants since they may impose toxicity to aquatic organisms.

* Corresponding author at: Centro de Química e Bioquímica, Faculdade de Ciências, Universidade de Lisboa, 1749-016 Lisboa, Portugal.
E-mail address: raosawa@fc.ul.pt (R.A. Osawa).

https://doi.org/10.1016/j.cej.2019.05.137
Received 18 March 2019; Received in revised form 27 April 2019; Accepted 20 May 2019
Available online 22 May 2019

1. Introduction

Pharmaceutical compounds have frequently been detected in the environment in recent decades. Several studies quantified drugs in a variety of environmental matrices at concentrations of the order of ng/L up to μg/L [1–5]. The main source of drugs comes from effluent treatment plants since conventional treatments are not intended to remove these contaminants. In the environment, pharmaceutical compounds may cause various ecotoxicological effects on aquatic biota such as genotoxicity, endocrine interference and development of resistance in microorganisms and, consequently, may affect humans [6–8].

Another fact to be considered is the production of transformation products (TPs) which, by definition, are products formed from abiotic (chemical and physical factors) and biotic (biological factor) processes of a parent compound. These processes may occur in the environment and in the water and wastewater treatment plants (WWTPs) [9,10]. Some studies have identified the TPs of pharmaceutical compounds in effluents and surface waters by high- resolution mass spectrometry [11,12]. In other words, the TPs may present persistence and affect aquatic biota and human health, since their ecotoxicological effects are mostly unknown. Therefore, the identification of these TPs represents a challenge since for most of them there are no analytical standards and the mechanisms of degradation and environmental interaction are complex and unknown. Nevertheless, with the improvement of mass spectrometry technologies such as advances in the characteristics of mass resolution, mass accuracy, mass range, sensitivity, selectivity and data processing it is now possible to elucidate many of these molecular structures. Mass analysers such as Orbitrap, time-of-flight (TOF) and Fourier transform-ion cyclotron resonance (FT-ICR) have been used for a wide range of applications, including food safety testing, pharmaceutical research, metabolomics and proteomics applications and environmental analyses [13–15].

One way to predict toxicity is by *in silico* toxicity assessments, which are computation models, based on molecular descriptors. This method aims to complement the *in vivo* and *in vitro* toxicity tests and has the advantages of predicting the toxicity of unknown compounds and reduce the time and the cost of the assays [16]. The limitations of the models used for *in silico* toxicity determinations are defined by applicability domain (AD), which aims to give reliability in the prediction results.

Antidepressants are one of the groups of drugs frequently found in the environment, these drugs are used to treat major depression and other mental health conditions such as anxiety disorders, attention-deficit/hyperactivity disorder, chronic pain and neuropathic pain. According to literature, the drug amitriptyline (AMI) had a removal of approximately 85% in WWTP [17], followed by venlafaxine (VEN), with 50% [18] and trazodone (TRA), with 35% of efficiency [19]. Therefore, it is essential to study new ways of removing these drugs, as well as to elucidate the formed TPs.

One of the removal methods that has been highlighted is photocatalysis that consists in decomposing the pollutant by photons through a catalyst [20,21]. The titanate nanostructures, such as titanate nanowires (TNW) and nanotubes (TNT), are materials used for photocatalysis; they are semiconductors and combine the characteristics of the TiO_2 nanoparticles with the properties of lamellar titanates. Nevertheless, these materials have low radiation absorptive capacity in the visible light spectrum but, this disadvantage can be overcome by metal doping, sensitization or formation of nanocomposites with other semiconductors [22–24]. These methods of modifying the nanomaterial structure have been demonstrated as one of the most promising techniques for produce photocatalysts to be used for the degradation of organic pollutants in environmental samples. In our previous study, TNW modified with 1% of cobalt doping (Co-TNW) was developed and tested with success in the removal of several pollutants under UV–Vis radiation [25].

The aim of this work was to estimate the efficiency of Co-TNW, previously described as a promising and versatile photocatalyst [25] to degrade VEN, TRA and AMI in tap water under UV–Vis radiation. This photocatalyst was selected based on previous studies [25,26]. In this work, it was demonstrated that pristine titanate nanoparticles were a better photocatalyst for pollutants degradation than nanocrystalline TiO_2. Recently, we prepared several Co-containing titanate samples were prepared and evaluated their photocatalytic performance using distinct model pollutants. All the Co-modified materials were found to be better catalysts than the pristine powder, being the sample with 1% of Co the best one. This sample was used in the present work.

The TPs formed by these processes were also elucidated by analyses of fragmentation patterns in the MS/MS mode obtained using ultra-high performance liquid chromatography coupled to quadrupole time-of-flight mass spectrometry (UHPLC-QTOF-MS/MS) and the possible pathway formations were described. Lastly, the toxicity of the TPs was assessed by *in silico* predictions of their ecotoxicity and mutagenicity by quantitative structure–activity relationships (QSARs) models.

2. Materials and methods

2.1. Standards and reagents

Venlafaxine hydrochloride (> 98%) was purchased from TCI Chemicals (Belgium). Amitriptyline hydrochloride (≥98%) and trazodone hydrochloride (≥99%) were obtained from Sigma-Aldrich (USA). LC-MS grade acetonitrile (ACN), formic acid and water were purchased from Fisher Scientific (USA). Ultrapure water was obtained with the Milli-Q ultrapure system (Barnstead International, Dubuque, USA). Stock solutions of 1000 mg/L of each compound were prepared in ultrapure water and stored at a temperature of −80 °C.

2.2. Synthesis and characterization of Co-TNW

The Co-TNW sample was prepared by a hydrothermal approach previously reported using a Co-doped amorphous precursor [25]. This precursor was prepared using a $TiCl_3$ solution (20 wt% in 20–30 wt% HCl) diluted in a ratio of 1:2 in 2 M HCl solution with the required molar amount (1%) of cobalt. To this solution, a 4 M NH_4OH solution was added drop-by-drop under vigorous stirring, until complete solid precipitation. This suspension was kept overnight at room temperature. The precipitate was filtered and washed with distilled water several times. The greenish grey precursor thus obtained was used to produce the Co-TNW sample, using a hydrothermal approach. The synthesis was performed in an autoclave system (160 °C, 24 h) using 10 g of amorphous precursor in *ca.* 70 mL of a 10 M NaOH aqueous solution. After cooling to room temperature, the powder was washed several times with water, until pH 7 of the filtrate solution, and was afterwards dried at 60 °C.

The catalyst characterization was discussed in our previous work [25]. Briefly, the specific surface area (B.E.T. method) was 267.22 m^2/g and the optical bandgap energy was 2.43 ± 0.05 eV.

2.3. Experiments

For UV–Vis photodegradation experiments, a 250 mL refrigerated photoreactor (Ace Glass, USA) was used [27] and the source of radiation was a 450 W medium-pressure mercury-vapor lamp (Hanovia, UK).

Tap water samples were collected from the Lisbon water supply and the physico-chemical parameters were analysed by the Portuguese Environment Agency (Table S1). The water samples (100 mL) were spiked with AMI, VEN and TRA in the concentration of 10 mg/L in single and mixture solutions. This high concentration was used to facilitate the identification of TPs. The pH of water was neither modified nor buffered to avoid any possible influence on the formation of TPs. For photocatalysis experiments, 15 mg of powder were added to 100 mL of the aqueous solutions.

Before irradiation, the samples with the catalyst were left in dark conditions for 1 h to reach the adsorption equilibrium. In all experiments, magnetic stir bars were used. Aliquots were withdrawn at regular intervals: 0, 5 min, 10 min, 15 min, 20 min, 30 min, 45 min, 1 h, 1.5 h and 2 h, centrifuged and frozen at −80 °C for further analyses.

2.4. Instrumentation

The analyses were performed with a Thermo Scientific UltiMate 3000 LC system (Thermo Fischer Scientific, Germany) coupled to a Bruker Impact II QTOF mass spectrometer equipped with an electrospray source (Bruker Daltonics, Germany). A Kinetex C18 column (1.7 µm particle size; 2.1 × 150 mm) (Phenomenex, USA) was used for chromatography separation. The volume injection was 7 µL with a flow rate of 150 µL/min. The mobile phase A was ultrapure water with 0.1% of formic acid and B was ACN. The elution conditions were as follows: 0–1.5 min, 5% B; 1.5–13 min, 75% B; 13–18 min, 100% B; 18–21 min, 100% B; 21–23 min, 5% B and finally 23–30 min, 5% B. The column and the sampler were maintained at 35 °C and 10 °C, respectively. The operation conditions of the mass spectrometer were published in our previous study [28].

2.5. Transformation products elucidation

Data analysis was carried out using Compass DataAnalysis 4.1 software (Bruker Daltonics, Germany). The suspect TPs were identified in the MS mode by manual observation of peaks (signal-to-noise ratio 10:1) of precursor ions between spiked and non-spiked samples and were listed to later obtain the fragmentation patterns in the product ion scan mode (MS/MS mode). The criterion for the determination of molecular formulas was to consider the mass error of less than 5 ppm for the precursor ions as well as products ions.

2.6. In silico toxicity

For *in silico* toxicity predictions two freely available software were used: Toxicity Estimation Software Tool (T.E.S.T, version 4.2.1) from US Environmental Protection Agency and VEGA platform (version 1.1.4) from Istituto di Ricerche Famacologiche Mario Negri, which includes several QSARs models. Both tools use simplified molecular-input line entry system (SMILES) to represent the chemical structure of the molecule.

For T.E.S.T, the following endpoints were used: 96-h fathead minnow LC_{50}, 48-h *D. magna* LC_{50}, 48-h *T. pyriformis* IGC_{50} and mutagenicity. The first three endpoints represent the acute toxicity, in other words, the concentration of the chemical in water at which 50% of the target organism dies after the respective hour. The mutagenicity is predicted by the AMES test, where positive results indicate mutagenic potential. T.E.S.T has several prediction methods including hierarchical clustering, single model, FDA, nearest neighbor and consensus-based methods. Details of these models and molecular descriptors are described in T.E.S.T User's Guide [29]. This work used the consensus method which is the average of predicted toxicities of other QSARs models to result in a more accurate prediction. The AD is calculated for each QSAR model and if the prediction result is outside the AD, the model is not included in the consensus method.

In VEGA platform, the QSARs models KNN/Read-Across and SarPy/IRFMN were used for mutagenicity. The AD of VEGA platform is based on the Applicability Domain Index (ADI), which is a result of 0 to 1. The ADI is calculated by other parameters such as similar molecules with known experimental value, model descriptors range check and concordance for similar molecules. Details of the parameters can be found in http://www.vega-qsar.eu/. Values between 0.9 and 1 result in a prediction within the AD, values between 0.65 and 0.9 result in a prediction that may be inside the AD and values below 0.65 result in a prediction outside the AD. This work considered the results above 0.65 as within the AD.

3. Results and discussion

3.1. Photodegradation studies

After 1 h in the dark, the catalyst adsorbed approximately 3% of the total AMI present in solution. As Fig. 1a shows, the AMI removal efficiency is higher for the Co-TNW catalyzed process than for photolysis, independently of have the pollutant in a single or in a mixture solution. In our previous study [25], a mechanism proposal for the light-activated electron-hole transfer processes in the catalyst was presented and discussed. It was concluded that the pollutant degradation is a result of a combined action of holes and other highly oxidant species, mainly HO•. During this present work, and concerning the degradation process, a total of eight AMI TPs were identified, the structures elucidations of which were described in Section 3.2. Only the time profiles of the TPs formed in the single compound solutions were considered. All of those TPs were detected in the samples during AMI photocatalytic degradation, and only four of them were formed during photolysis.

Fig. 1b–c shows the formation profiles of AMI TPs in the single compound solution in the presence or absence of Co-TNW. The TPs peak areas were normalized with respect to their parent compound at $t = 0$ min (A/A_0). It was verified that the TP_{ami}-294c degraded more rapidly in the presence of Co-TNW than in photolysis conditions. This suggests that Co-TNW is also catalytic for this TP degradation process. Nevertheless, the TP_{ami}-296 was not completely eliminated after 120 min of irradiation. At the same time, we consider that TP_{ami}-296 is photocatalytic degraded and originates three other TPs: TP_{ami}-312a, TP_{ami}-312b and TP_{ami}-314, as shown in Fig. 2, which represents the AMI degradation pathway proposed. It was observed that more hydroxylation reactions occurred during the photocatalysis because only the TP_{ami}-310, TP_{ami}-294a, TP_{ami}-312a and TP_{ami}-312b were identified in this process. We believe that this is due to the formation of more

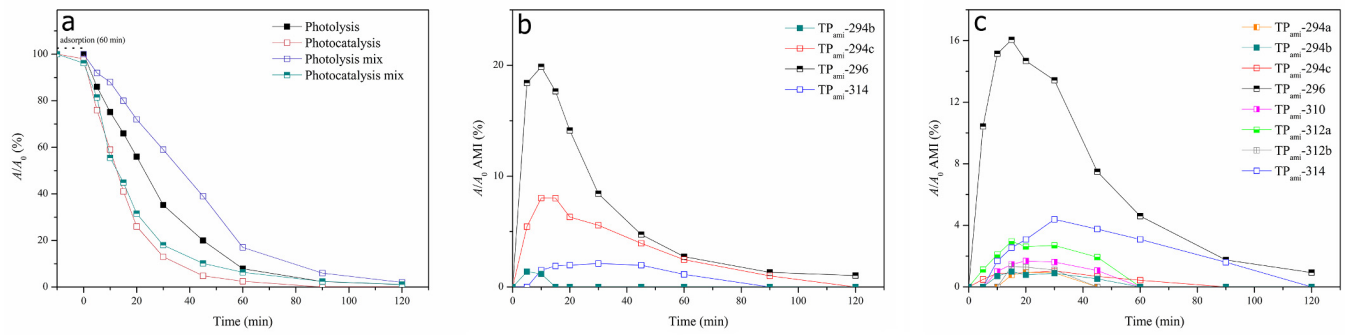

Fig. 1. (a) AMI photodegradation in a single and mixture solution, (b) time profiles of AMI TPs during photolysis and (c) time profiles of AMI TPs in photocatalysis.

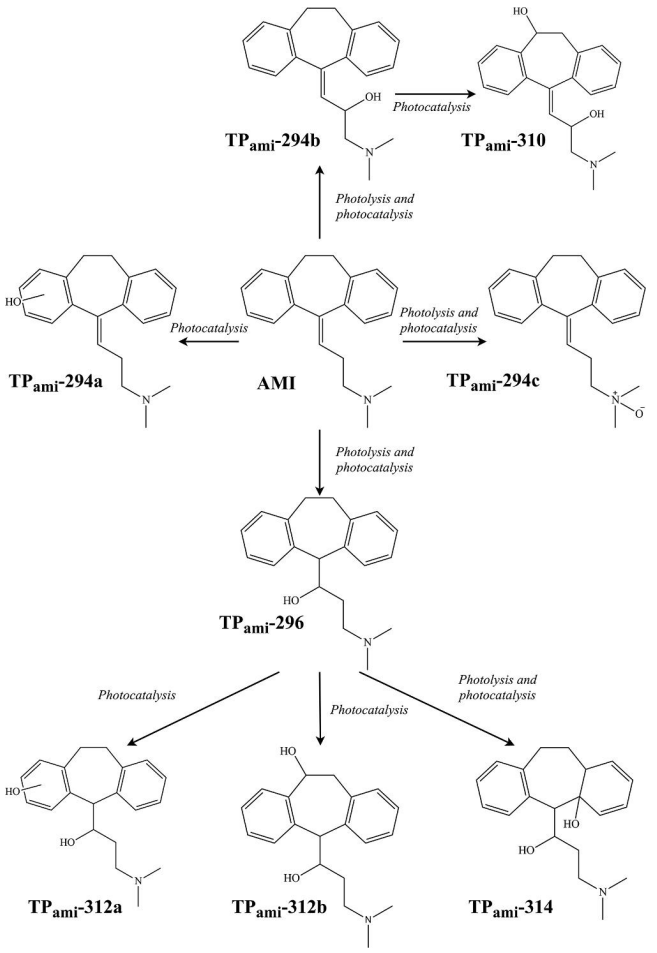

Fig. 2. Degradation pathways proposed for AMI photolysis and photocatalysis.

hydroxyl radicals under UV–Vis radiation.

Considering the TRA removal studies, the catalyst used (Co-TNW) adsorbed about 5% of the initial pollutant. In less than 15 min, about 90% of the TRA was removed in the single and mixture based experiments (Fig. 3a). Seven TRA TPs were identified during photolysis and photocatalysis and, as observed in Fig. 3b–c, these TPs presented low photocatalytic activity and therefore there was no major difference in the time profile of the TRA TPs.

The TP with the highest peak area was the TP_{tra}-354 (51% of A_0 TRA) and it was not completely degraded during photolysis and photocatalysis after 120 min, in other words, although TRA was rapidly eliminated, this TP showed higher resistance to degradation under UV–Vis light and even in the presence of the catalyst. We believe that this product gave rise to the other six TRA TPs (Fig. 4).

Considering the VEN degradation process, it was observed that Co-TNW did not adsorb this pollutant. After 90 min of irradiation and without any catalyst, the drug was degraded by about 99% in the single compound solution. This value decreases for about 85% when VEN is in a mixture of the three antidepressants. This indicates that this compound, when in complex matrices, may exhibit lower removal efficiency. Although, with the use of Co-TNW as photocatalyst, a higher removal rate, than that of photolysis (Fig. 5a), was observed.

Five VEN TPs were elucidated by the MS/MS spectra analyses during the photocatalyzed process. It is interesting that two of them were detected only in the photolysis experiments (Fig. 5b–c), one by an hydroxylation and one by demethylation process. Considering the intermediates degradation, it was observed that with the use of Co-TNW as photocatalyst, the TP_{ven}-294 was degraded faster, in less than 45 min compared to time needed to degradate this TP formed only during photolysis, which took twice as long to eliminate them. A proposal for the VEN degradation pathway is presented in Fig. 6.

3.2. Structure elucidation of TPs

3.2.1. AMI TPs formed by hydroxylation

The TPs formed by hydroxylation processes exhibited, in the MS/MS spectrum, the elimination of H_2O as their main characteristic when the hydroxylation occurred on a saturated carbon. When no H_2O elimination was detected, hydroxylation possibly occurred in an aromatic ring.

Three TPs (TP_{ami}-294a, TP_{ami}-294b and TP_{ami}-294c) are isomers, although showing different fragmentation patterns (Fig. 7). The first two were presumably generated by hydroxylation processes. Analysis of the ion fragments in the MS/MS spectrum of TP_{ami}-294a did not show any elimination of H_2O (Fig. 7a) therefore, hydroxylation may have occurred in the aromatic ring and, unfortunately, it is not possible to identify the position of the OH group.

As can be seen in Fig. 7b, the MS/MS spectrum of TP_{ami}-294b showed two characteristic neutral losses, C_2H_7N at *m/z* 249 ($C_{18}H_{17}O^+$) which further eliminates H_2O to give *m/z* 231 ($C_{18}H_{15}^+$). The loss of C_2H_7N suggests that there was no formation of the N-oxide group. Therefore, the hydroxylation reaction was possibly on the β-carbon of the aliphatic chain, since at the α-carbon the reaction forms a hemiaminal group, which is unstable. The fact that *m/z* 231 loses C_2H_2 f to form *m/z* 205 ($C_{16}H_{13}^+$) corroborates that the hydroxylation was on the aliphatic chain rather than on the cycloheptane. Chen et al. [30] also identified this TP in the photodegradation of AMI in aqueous fulvic acids solutions. Other TPs proposed by Chen et al. [30] were not detected in this study, we assume that the matrix influences the formation of the AMI TPs.

MS/MS spectrum of TP_{ami}-310 (Fig. S1) showed two eliminations of H_2O to give *m/z* 292 ($C_{20}H_{22}NO^+$) and *m/z* 274 ($C_{20}H_{20}N^+$), respectively, which may indicate one hydroxylation of the aliphatic chain, probably on β-carbon of tertiary amine, and another on the cycloheptane. Moreover, the elimination of C_2H_7N to give *m/z* 265 ($C_{18}H_{17}O_2^+$), corroborate that there were no hydroxylation reactions on the tertiary carbon of the amine.

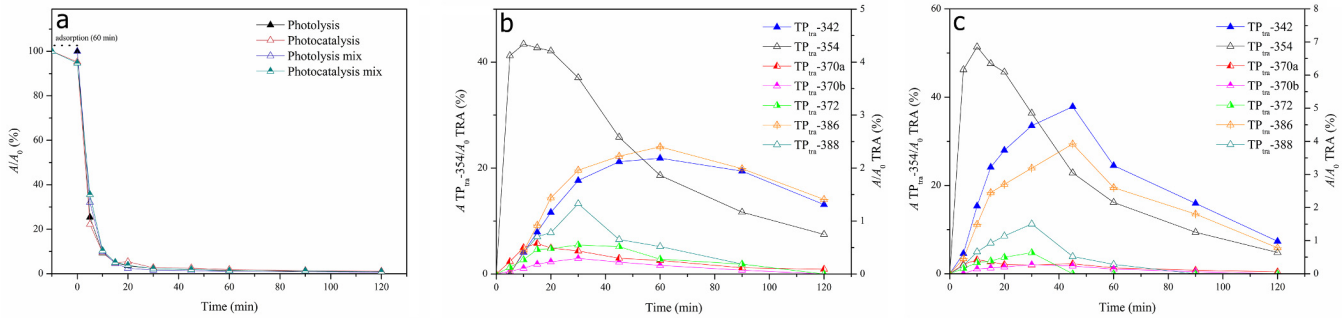

Fig. 3. (a) TRA photodegradation in a single and mixture solution, (b) time profiles of TRA TPs during photolysis and (c) time profiles of TRA TPs in photocatalysis.

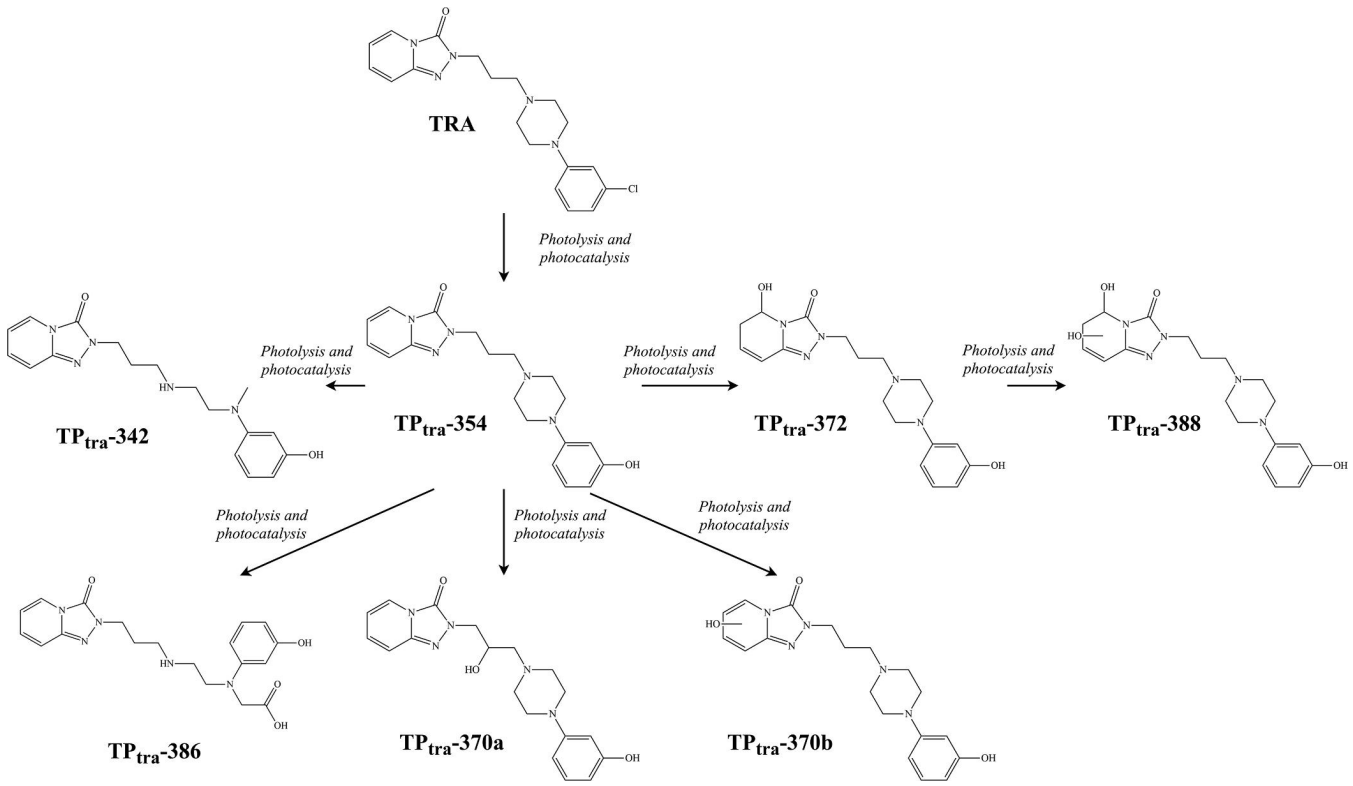

Fig. 4. Degradation pathways proposed for TRA photolysis and photocatalysis.

3.2.2. AMI TP formed by N-oxidation

The TP_{ami}-294c appears to have been formed by an oxidation of the tertiary amine, forming the *N*-oxide group. The peak at *m/z* 233 ($C_{18}H_{17}^{+}$) reinforces this hypothesis, due to the fact that this fragment ion was detected by the elimination of dimethylamine oxide (C_2H_7NO) from the precursor ion ($C_{20}H_{24}NO^{+}$). Also, no H_2O elimination was detected in the MS/MS spectrum (Fig. 7c), which excludes the hypothesis that hydroxylation could have occurred either at the carbon of the tertiary amine or at the aliphatic chain. This TP is named amitriptylinoxide and is a metabolite of AMI. The study by Li et al. [31] identified this TP in agricultural soils and Wan et al. [32] described three TPs generated by AMI photodegradation in Fe(III)-citrate-oxalate binary system. None of these were elucidated in this present work however, TP_{ami}-294c was proposed in the degradation pathway.

3.2.3. AMI TPs formed by hydration and hydration-hydroxylation

Analysis of TP_{ami}-296 MS/MS spectrum (Fig. S2) suggests that this TP was formed by hydration of alkene in the AMI structure and the elimination of H_2O at *m/z* 278 ($C_{20}H_{24}N^{+}$) from precursor ion ($C_{20}H_{26}NO^{+}$) corroborates this statement. Unfortunately, the spectrum does not allow to identify the position of the hydroxy group (OH). We proposed that the hydration of alkene occurred on the γ-carbon of tertiary amine of AMI, in accordance with Khaleel et al. [33]. They have suggested the same position of the OH group when elucidating the TPs formed by photodegradation of desipramine, an antidepressant of the same AMI class of medication, a tricyclic antidepressant.

The TP_{ami}-312a and TP_{ami}-312b have the same monoisotopic mass and it seems reasonable to suggest that both were formed by hydroxylation of TP_{ami}-296 (hydration of alkene and hydroxylation processes). The TP_{ami}-312a was probably generated by one hydroxylation at the aromatic ring of TP_{ami}-296 due to the elimination of only one H_2O from the precursor ion ($C_{20}H_{26}NO_2^{+}$) and detected in the MS/MS spectrum at *m/z* 294 ($C_{20}H_{24}NO^{+}$) (Fig. S3). We believe that this elimination occurred with the OH group on the γ-carbon of tertiary amine.

The MS/MS spectrum of TP_{ami}-312b (Fig. S4) showed two neutral eliminations of H_2O, one at *m/z* 294 ($C_{20}H_{24}NO^{+}$) from precursor ion ($C_{20}H_{26}NO_2^{+}$) and the other at *m/z* 231 ($C_{18}H_{15}^{+}$) from *m/z* 249 ($C_{18}H_{17}O^{+}$). These water molecules eliminations may suggest that two hydroxylations have occurred, possibly one on the unsaturation of the

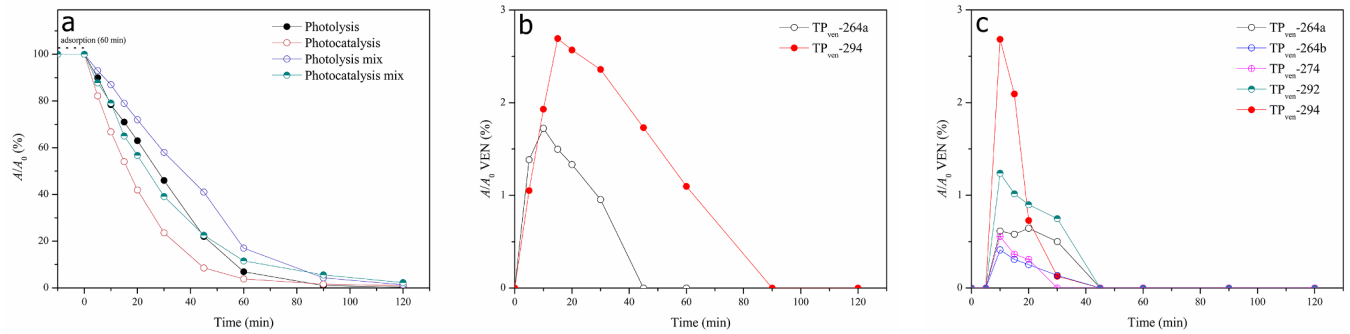

Fig. 5. (a) VEN photodegradation in a single and mixture solution, (b) time profiles of VEN TPs during photolysis and (c) time profiles of VEN TPs in photocatalysis.

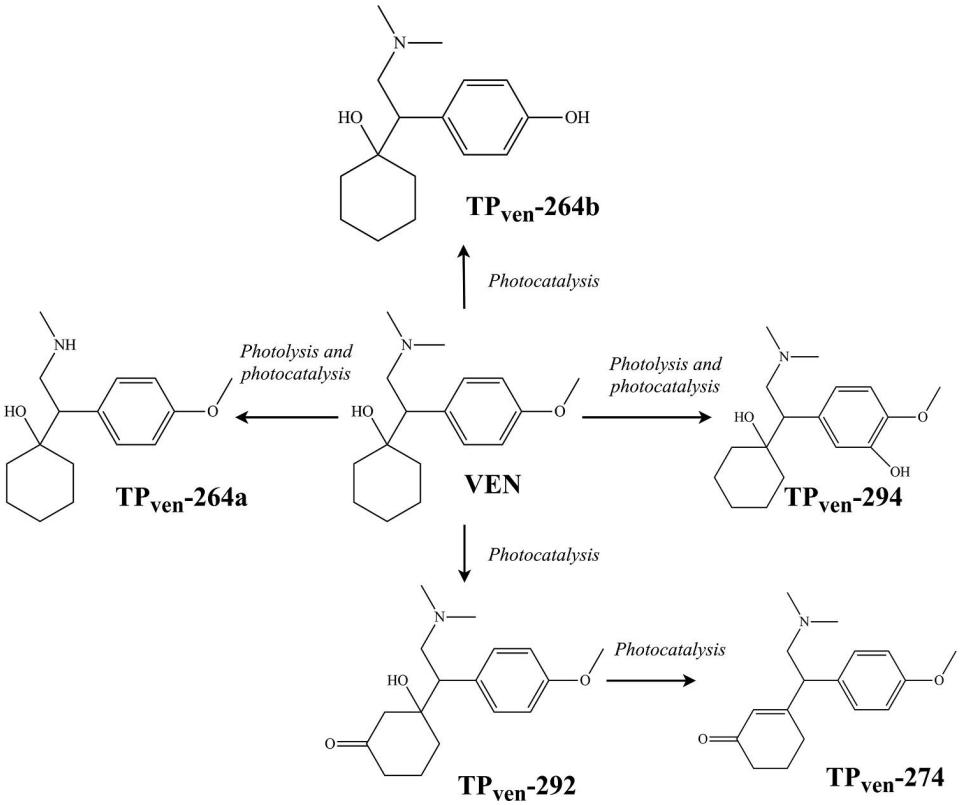

Fig. 6. Degradation pathways proposed for VEN photolysis and photocatalysis.

aliphatic chain and the other on the cycloheptane.

Based on the MS/MS spectrum of TP$_{ami}$-314 (Fig. S5), eliminations of two H_2O molecules from the precursor ion ($C_{20}H_{28}NO_2^+$) led to *m/z* 296 ($C_{20}H_{26}NO^+$) and *m/z* 278 ($C_{20}H_{24}N^+$) fragment ions, which may mean that there were two hydrations of alkene. Elimination of C_2H_7NO was not identified, which may indicate that there was no formation of the N-oxide group. One of the hydration sites may have been similar to the formation of TP$_{ami}$-296 and the other, possibly occurred on the cycloheptane. Nevertheless, by analysing the fragmentation patterns it was not possible to identify the position of the OH group. We consider therefore a structure similar to the one proposed for an AMI photodegradation study in purified water [34]. But, when compared to what was proposed by Nassar et al. [34] on the δ-carbon of the tertiary amine, we believe that the other OH group was bound to the γ-carbon of tertiary amine because it was formed from the TP$_{ami}$-296. In addition, Nassar et al. [34] suggested two more AMI TPs, which were not detected in the present study.

3.2.4. TRA TPs formed by dehalogenation-hydroxylation

The TP$_{tra}$-354 has been formed by substitution of chlorine by one OH group in the aromatic ring, forming a phenol group. To support this hypothesis, the losses of heterocyclic and pyridine groups from *m/z* 354 were identified at *m/z* 219 ($C_{13}H_{19}N_2O^+$) (Fig. S6). To note that a study on the photodegradation of TRA identified a product, which resulted in the substitution of chlorine by an OH group [35]. Overall, three TPs were identified by DellaGreca et al. [35] and only one of them was not identified in the present study. The explanation may be related to the radiation source since DellaGreca et al. [35] used UV-B irradiation in the experiments.

It has been proposed that TP$_{tra}$-370a was generated from a dehalogenation and a hydroxylation process. Analysis of MS/MS spectrum (Fig. S7) identified the elimination of H_2O at *m/z* 352 ($C_{19}H_{22}N_5O_2^+$) from precursor ion ($C_{19}H_{24}N_5O_3^+$). This suggested that hydroxylation occurred on β-carbon of aliphatic chain, since on α-carbon it would form an unstable group. The identification of a fragment ion at *m/z* 191 ($C_{11}H_{15}N_2O^+$), involving the phenol and piperazine groups excludes the occurrence of the hydroxylation in piperazine.

The TP$_{tra}$-370b was formed by a dehalogenation and a hydroxylation process, possibly from the TP$_{tra}$-354. Nevertheless, unlike TP$_{tra}$-370a, hydroxylation possibly occurred in the pyridine group since the elimination of H_2O was not detected in the MS/MS spectrum (Fig. S8). The formation of the fragment ion *m/z* 164 ($C_7H_6N_3O_2^+$) corroborates this assumption. Nonetheless, it was not possible to identify the OH group position.

3.2.5. TRA TPs formed by dehalogenation-hydroxylation-hydration

The fragmentation pattern of the TP$_{tra}$-372 (Fig. S9) was similar to the one of TP$_{tra}$-354, which suggested the substitution of chlorine for OH and we believe that TP$_{tra}$-372 was formed by hydration of alkene of TP$_{tra}$-354, possibly in the pyridine group. The eliminations of one H_2O molecule leading to fragment ion *m/z* 354 ($C_{19}H_{24}N_5O_2^+$) and of piperazine plus phenol ($C_{10}H_{14}N_2O_2$) leading to the *m/z* 194 ($C_9H_{12}N_3O_2^+$), both from the precursor ion ($C_{19}H_{26}N_5O_3^+$), corroborate this hypothesis. The fragment ion *m/z* 166 ($C_7H_8N_3O_2^+$) showed that the hydroxylation occurred in the pyridine group. This TP is in agreement with the TRA photodegradation study by DellaGreca et al. [35].

It has been proposed that TP$_{tra}$-388 was generated by a hydroxylation of TP$_{tra}$-372, in other words, the chlorine was replaced by an OH group and hydration of alkene occurred in a process similar to the formation of TP$_{tra}$-372. The fragment ion *m/z* 182 ($C_7H_8N_3O_3^+$) (Fig. S10) showed that the two OH groups were bound to the pyridine group. Nevertheless, it was not possible to unequivocally determine the position of the other OH group.

3.2.6. TRA TPs formed by dehalogenation-hydroxylation-demethylation and dehalogenation-hydroxylation-oxidation

The TP$_{tra}$-342 was probably formed by demethylation of the

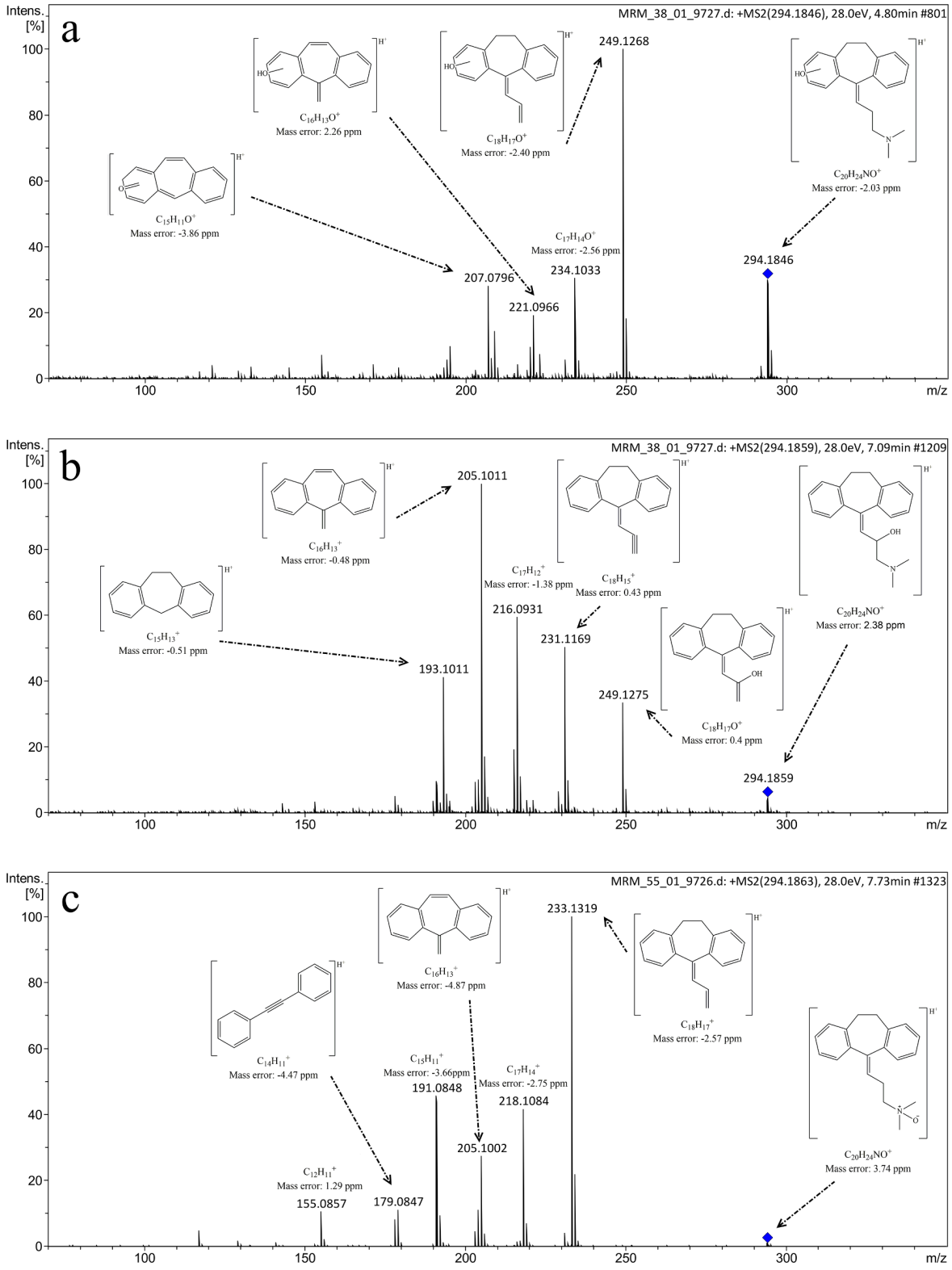

Fig. 7. MS/MS spectrum and proposed fragmentation of (a) TP_{ami}-294a, (b) TP_{ami}-294b and (c) TP_{ami}-294c.

piperazine group from TP_{tra}-354. The demethylation occurred after ring opening. To corroborate this proposal, the fragment ion at *m/z* 207 ($C_{12}H_{19}N_2O^+$) (Fig. S11) exhibited neutral losses of pyrazolone and pyridine from the precursor ion ($C_{18}H_{24}N_5O_2^+$), which means that there were no reactions in these groups. Trawiński and Skibiński [36] and Wen et al. [37] also proposed products in which the ring opening in the piperazine group occurred in studies of photodegradation of drugs.

The TP_{tra}-386 was assumed to have been generated by a dehalogenation to form a phenol group and also that a carboxylic acid functional group was produced on the piperazine group. This hypothesis is reinforced by the MS/MS spectrum analysis (Fig. S12). In this spectrum the *m/z* 342 ($C_{18}H_{24}N_5O_2^+$) was generated by the neutral loss of CO_2 from the precursor ion ($C_{19}H_{24}N_5O_4^+$), that may represent the formation of the carboxylic acid. The fragment ion *m/z* 176 ($C_9H_{10}N_3O^+$)

represents pyridine and pyrazolone with aliphatic chain, which may confirm that there are no reactions in this group. Therefore, the formation of a carboxylic acid in the piperazine group is proposed. In the literature, the products of the photodegradation of levofloxacin, a compound containing the piperazine group, were studied and a piperazine oxidation reaction was proposed by ring opening [37]. Wang et al. [38] showed that piperazine may form a carboxylic acid group through the ring opening reaction by oxidative degradation.

3.2.7. VEN TP formed by hydroxylation

Analysis of MS/MS spectrum of TP_{ven}-294 (Fig. S13) showed only one neutral loss of H_2O, from precursor ion ($C_{17}H_{28}NO_3^+$) to *m/z* 276 ($C_{17}H_{26}NO_2^+$), this loss was also found in the MS/MS spectrum of VEN, which suggests that the hydroxylation occurred in the aromatic ring. Nevertheless, it was not possible to identify the position of the OH group in the aromatic ring. We consider that the OH is attached at the 2-position of the ring, according to Khunphonoi et al. [39] who studied the photocatalytic degradation of *p*-cresol and identified the formation of 4-methylcatechol, in other words, the hydroxylation may have occurred at position 2 of *p*-cresol.

3.2.8. VEN TPs formed by demethylation

Analysis of MS/MS spectrum of TP_{ven}-264a (Fig. S14) showed the elimination of methanamine (CH_5N) at *m/z* 215 ($C_{15}H_{19}O^+$) from *m/z* 246 ($C_{16}H_{24}NO^+$). This elimination led to the belief that TP_{ven}-264a was formed by a process of demethylation of the tertiary amine, resulting in a secondary amine. And, indeed, Lambropoulou et al. [40] identified the same structure when studying photodegradation of VEN. It was noted that the study of VEN degradation by Lambropoulou et al. [40] generated more than 20 TPs. We assumed that the highest amount of TPs was due to a higher concentration of catalyst, up to 800 mg/L, whereas in the present study 150 mg/L was used.

The TP-264b was probably also formed by a demethylation process of VEN, but being different from TP-264a, that is, the demethylation occurred in the methoxy group, thus forming the phenol. In the MS/MS spectrum (Fig. S15), the fragment ion at *m/z* 201 ($C_{14}H_{17}O^+$) from the *m/z* 246 ($C_{16}H_{24}NO^+$) showed the loss of C_2H_7N, which corroborates that the demethylation did not occur in this tertiary amine group. Several studies have also identified this TP in photodegradation processes [40,41]. The study conducted by García-Galán et al. [41] elucidated other TPs that were not identified in this study, we assume that this was due to the fact that they used H_2O_2 as oxidant.

3.2.9. VEN TPs formed by dehydration-oxidation

TP_{ven}-292 was possibly formed by an oxidation process. In theory, oxidation could have occurred on the aliphatic chain or on cyclohexane. Nonetheless, when analysing the MS/MS spectrum (Fig. S16) the fragment ion at *m/z* 229 ($C_{15}H_{17}O_2^+$), which was formed from the neutral losses of H_2O plus C_2H_7N of the precursor ion, eliminated CO to form the fragment ion at *m/z* 201 ($C_{14}H_{17}O^+$). The loss of CO was possible due to the oxidation of cyclohexane, probably in 3-position. According to Gonzalez et al. [42], the methylcyclohexane may form 3-methylcyclohexanone by photocatalytic oxidation using in TiO_2-suspended water.

We believe that the TP_{ven}-274 was generated from dehydration of alcohol to form an alkene from TP_{ven}-292. This hypothesis is supported by the elimination of CO from *m/z* 229 ($C_{15}H_{17}O_2^+$) to form *m/z* 201 ($C_{14}H_{17}O^+$) (Fig. S17), this elimination was also found in TP_{ven}-292.

3.3. In silico toxicity assessment

For TPs in which it was not possible to identify the position of the hydroxylation reaction, an average of the ecotoxicity values of all possible positions was performed and the mutagenicity was considered positive if at least one of the positions shows a positive result.

The ecotoxicity predictions of AMI TPs showed that most have low toxic relative potential compared to AMI (Table 1), with the exceptions of the TP_{ami}-294a, TP_{ami}-312a and TP_{ami}-314 for the endpoint 48-h *T. pyriformis* IGC_{50} with relative potencies of 1.22, 1.74 and 3.58, respectively. Although the TPs have low toxic relative potential for endpoint 96-h f. minnow LC_{50}, most of the values were classified as very toxic (< 1 mg/L). The TP_{ami}-294a and TP_{ami}-312a were only generated in photocatalysis, however, these TPs have low intensity relative areas and were completely degraded in 60 min and the TP_{ami}-314, after

Table 1
In silico ecotoxicity and mutagenicity of AMI, TRA, VEN and TPs, (+) represents mutagenic potential and (−) represents non-mutagenic potential.

Compound	96-h f. minnow LC_{50} (mg/L)	Relative potency	48-h *D. magna* LC_{50} (mg/L)	Relative potency	48-h *T. pyriformis* IGC_{50} (mg/L)	Relative potency	Mutagenicity		
							T.E.S.T	KNN/Read-Across	SarPy/IRFMN
AMI	0.12	1	2.1	1	17.27	1	−	−	−
TP_{ami}-294a	0.49	0.24	2.68	0.78	14.20	1.22	−	−	−
TP_{ami}-294b	0.65	0.18	14.63	0.14	24.62	0.70	−	−	−
TP_{ami}-294c	[a]	–	[a]	–	[a]	–	−	−	−
TP_{ami}-296	0.53	0.23	3.83	0.55	18.56	0.93	−	−	−
TP_{ami}-310	0.41	0.29	25.55	0.08	27.84	0.62	−	−	[a]
TP_{ami}-312a	0.39	0.31	6.96	0.30	9.95	1.74	−	+	−
TP_{ami}-312b	1.07	0.11	5.34	0.39	27.94	0.62	−	−	−
TP_{ami}-314	3.11	0.04	7.94	0.26	4.82	3.58	−	−	−
TRA	[a]	–	32.57	1.00	[a]	–	−	+	+
TP_{tra}-342	[a]	–	92.15	0.35	[a]	–	+	+	+
TP_{tra}-354	[a]	–	114.16	0.29	[a]	–	+	+	+
TP_{tra}-370a	[a]	–	312.42	0.10	[a]	–	+	+	+
TP_{tra}-370b	[a]	–	96.12	0.34	[a]	–	+	+	+
TP_{tra}-372	[a]	–	99.93	0.33	[a]	–	−	+	[a]
TP_{tra}-386	[a]	–	263	0.12	[a]	–	+	+	+
TP_{tra}-388	[a]	–	151.59	0.21	[a]	–	+	+	[a]
VEN	6.96	1.00	10.34	1.00	12.63	1.00	−	−	−
TP_{ven}-264a	6.57	1.06	13.4	0.77	15.8	0.80	−	−	−
TP_{ven}-264b	6.09	1.14	5.84	1.77	17.59	0.72	−	−	−
TP_{ven}-274	4.3	1.62	5.64	1.83	1.01	12.50	−	−	−
TP_{ven}-292	24.67	0.28	33.5	0.31	12.85	0.98	−	−	−
TP_{ven}-294	12.39	0.56	16.61	0.62	16.53	0.76	−	−	−

[a] Prediction outside of the applicability domain.

90 min was degraded only in photolysis and after 120 min in the presence of the catalyst. Only TP_{ami}-312a had a mutagenic potential for a model KNN/Read-Across and was only formed in photocatalysis. In the literature, it was demonstrated that the AMI altered the physiological and biochemical parameters of the zebrafish in concentrations in the order of ng/L, which represented a high potential of toxicity in aquatic organisms [43].

The endpoints 96-h fathead minnow LC_{50} and 48-h *T. pyriformis* IGC_{50} of the TRA TPs were outside of the applicability domain in the consensus method and the relative potencies of the TPs with the 48-h parameter *D. magna* LC_{50} were all below the TRA (Table 1). Nevertheless, all TPs resulted in positive mutagenicity in at least one model and as previously described, these TPs were formed in the experiments in photolysis and photocatalysis. Four of them were not completely removed after 120 min (TP_{tra}-342, TP_{tra}-354, TP_{tra}-370a and TP_{tra}-386), however, the use of the catalyst for photodegradation had a slightly higher removal efficiency of these TPs. To the best of our knowledge, there are no ecotoxicity studies of the TRA and TPs.

The results of the *in silico* prediction for the TPs of the VEN showed that only the TP_{ven}-274 had a greater relative potential for the three ecotoxicity endpoints (Table 1). This TP was only formed in photocatalysis but presented relatively low relative area and in less than 30 min was completely degraded. All VEN TPs presented negative results in the predictions of mutagenicity (Table 1). According to the literature, VEN was toxic when exposed to the oyster larvae with $EC_{50} < 1$ mg/L [44].

4. Conclusions

In this study, Co-TNW was used as photocatalyst in the photodegradation process of three antidepressants, AMI, VEN, and TRA. The formation of the correspondent TPs and sub-sequential degradation was also analysed. The results indicated that both, AMI and VEN were faster degradate when Co-TNW was used as photocatalyst, in both single and mixed solutions.

For the photocatalyzed process, eight AMI TPs were identified in comparison with only four TPs recognized during photolysis. Although most of the AMI TPs were totally degraded in less than 90 min, with the exception of TP_{ami}-296. Overall, the *in silico* ecotoxicity predictions of AMI TPs showed they had low toxic potential compared to the one of the parent compound.

During the VEN photocatalytic degradation, five TPs were elucidated compared to the two formed under UV–Vis radiation but with no catalyst. Analysing the VEN TPs photodegradation, it was possible to conclude that they were degraded faster when in contact with the catalyst. Regarding *in silico* ecotoxicity, only TP_{ven}-274 presented a relative potency of toxicity higher than VEN itself and none of the VEN TPs resulted in positive mutagenicity.

The time of TRA degradation was identical for photolysis and using the Co-TNW as photocatalyst. In additional, the seven identified TRA TPs showed low photocatalytic activity and four were not removed even after 120 min of irradiation. All TRA TPs showed positive results for mutagenicity in at least one model but, unfortunately, the prediction of two ecotoxicity models (96-h f. minnow LC_{50} and 48-h *D. magna* LC_{50}) resulted in values outside of the AD.

To the best of our knowledge, fourteen TPs have never been described in degradation studies and the proposals in this work may contribute to better understand the photodegradation pathways for AMI, TRA and VEN. These results may, therefore, highlight the importance of considering the formation of TPs in the presence of a photocatalyst since, as shown in this study, more TPs may be formed, and they may present more toxicity than the parent compounds. Future studies should include the *in vitro* or *in vivo* toxicity assays as well as photodegradation under artificial sunlight.

Acknowledgments

This work was supported by Brazilian Federal Agency Coordenação de Aperfeiçoamento de Pessoal de Nível Superior (CAPES) for PhD grant (99999.000845/2014-00) and Fundação para a Ciência e a Tecnologia (FCT) for PhD grant (SFRH/BD/101220/2014) and Projects (UID/MULTI/00612/2019, PEst-OE/QUI/UI0612/2013, IF/01210/2014, and LISBOA-01-0145-FEDER-022125).

Appendix A. Supplementary data

Supplementary data to this article can be found online at https://doi.org/10.1016/j.cej.2019.05.137.

References

[1] E. Vulliet, L. Wiest, R. Baudot, M.F. Grenier-Loustalot, Multi-residue analysis of steroids at sub-ng/L levels in surface and ground-waters using liquid chromatography coupled to tandem mass spectrometry, J. Chromatogr. A 1210 (2008) 84–91, https://doi.org/10.1016/j.chroma.2008.09.034.
[2] J. Wu, X. Qian, Z. Yang, L. Zhang, Study on the matrix effect in the determination of selected pharmaceutical residues in seawater by solid-phase extraction and ultra-high-performance liquid chromatography-electrospray ionization low-energy collision-induced dissociation tandem mass spectrometry, J. Chromatogr. A 1217 (2010) 1471–1475, https://doi.org/10.1016/j.chroma.2009.12.074.
[3] P. Wang, T. Yuan, J. Hu, Y. Tan, Determination of cephalosporin antibiotics in water samples by optimised solid phase extraction and high performance liquid chromatography with ultraviolet detector, Int. J. Environ. Anal. Chem. 91 (2011) 1267–1281, https://doi.org/10.1080/03067311003778649.
[4] R. Aznar, C. Sánchez-Brunete, B. Albero, J.A. Rodríguez, J.L. Tadeo, Occurrence and analysis of selected pharmaceutical compounds in soil from Spanish agricultural fields, Environ. Sci. Pollut. Res. 21 (2014) 4772–4782, https://doi.org/10.1007/s11356-013-2438-7.
[5] M. Caban, E. Lis, J. Kumirska, P. Stepnowski, Determination of pharmaceutical residues in drinking water in Poland using a new SPE-GC-MS(SIM) method based on Speedisk extraction disks and DIMETRIS derivatization, Sci. Total Environ. 538 (2015) 402–411, https://doi.org/10.1016/j.scitotenv.2015.08.076.
[6] E. Geiger, R. Hornek-Gausterer, M.T. Saçan, Single and mixture toxicity of pharmaceuticals and chlorophenols to freshwater algae *Chlorella vulgaris*, Ecotoxicol. Environ. Saf. 129 (2016) 189–198, https://doi.org/10.1016/j.ecoenv.2016.03.032.
[7] M.R. Pino-Otín, S. Muñiz, J. Val, E. Navarro, Effects of 18 pharmaceuticals on the physiological diversity of edaphic microorganisms, Sci. Total Environ. 595 (2017) 441–450, https://doi.org/10.1016/j.scitotenv.2017.04.002.
[8] S. Rainieri, A. Barranco, M. Primec, T. Langerholc, Occurrence and toxicity of musks and UV filters in the marine environment, Food Chem. Toxicol. 104 (2017) 57–68, https://doi.org/10.1016/j.fct.2016.11.012.
[9] D. Fatta-Kassinos, M.I. Vasquez, K. Kümmerer, Transformation products of pharmaceuticals in surface waters and wastewater formed during photolysis and advanced oxidation processes – degradation, elucidation of byproducts and assessment of their biological potency, Chemosphere 85 (2011) 693–709, https://doi.org/10.1016/j.chemosphere.2011.06.082.
[10] O. Golovko, V. Kumar, G. Fedorova, T. Randak, R. Grabic, Seasonal changes in antibiotics, antidepressants/psychiatric drugs, antihistamines and lipid regulators in a wastewater treatment plant, Chemosphere 111 (2014) 418–426, https://doi.org/10.1016/j.chemosphere.2014.03.132.
[11] M. Hörsing, T. Kosjek, H.R. Andersen, E. Heath, A. Ledin, Fate of citalopram during water treatment with O_3, ClO_2, UV and fenton oxidation, Chemosphere 89 (2012) 129–135, https://doi.org/10.1016/j.chemosphere.2012.05.024.
[12] C. Boix, M. Ibáñez, R. Bagnati, E. Zuccato, J.V. Sancho, F. Hernández, S. Castiglioni, High resolution mass spectrometry to investigate omeprazole and venlafaxine metabolites in wastewater, J. Hazard. Mater. 302 (2016) 332–340, https://doi.org/10.1016/j.jhazmat.2015.09.059.
[13] J. Aceña, S. Stampachiacchiere, S. Pérez, D. Barceló, Advances in liquid chromatography – high-resolution mass spectrometry for quantitative and qualitative environmental analysis, Anal. Bioanal. Chem. 407 (2015) 6289–6299, https://doi.org/10.1007/s00216-015-8852-6.
[14] I. Ferrer, J.A. Zweigenbaum, E.M. Thurman, Identification of pesticide transformation products in food applying high-resolution mass spectrometry, in: R. Romero-González, A.G. Frenich (Eds.), Applications in High Resolution Mass Spectrometry Food Safety and Pesticide Residue Analysis, Elsevier, 2017, pp. 315–335, , https://doi.org/10.1016/B978-0-12-809464-8.00010-5.
[15] N. Iwamoto, T. Shimada, Recent advances in mass spectrometry-based approaches for proteomics and biologics: Great contribution for developing therapeutic antibodies, Pharmacol. Ther. 185 (2018) 147–154, https://doi.org/10.1016/j.pharmthera.2017.12.007.
[16] S. Ekins, J. Mestres, B. Testa, *In silico* pharmacology for drug discovery: applications to targets and beyond, Br. J. Pharmacol. 152 (2007) 21–37, https://doi.org/10.1038/sj.bjp.0707306.
[17] B. Kasprzyk-Hordern, R.M. Dinsdale, A.J. Guwy, The removal of pharmaceuticals, personal care products, endocrine disruptors and illicit drugs during wastewater treatment and its impact on the quality of receiving waters, Water Res. 43 (2009)

363–380, https://doi.org/10.1016/j.watres.2008.10.047.
[18] E. Gracia-Lor, J.V. Sancho, R. Serrano, F. Hernández, Occurrence and removal of pharmaceuticals in wastewater treatment plants at the Spanish Mediterranean area of Valencia, Chemosphere 87 (2012) 453–462, https://doi.org/10.1016/j.chemosphere.2011.12.025.
[19] N. Collado, S. Rodriguez-Mozaz, M. Gros, A. Rubirola, D. Barceló, J. Comas, I. Rodriguez-Roda, G. Buttiglieri, Pharmaceuticals occurrence in a WWTP with significant industrial contribution and its input into the river system, Environ. Pollut. 185 (2014) 202–212, https://doi.org/10.1016/j.envpol.2013.10.040.
[20] M.A. Gondal, A.A. Adesida, S.G. Rashid, S. Shi, R. Khan, Z.H. Yamani, K. Shen, Q. Xu, Z.S. Seddigi, X. Chang, Preparation of WO_3/g-C_3N_4 composites and their enhanced photodegradation of contaminants in aqueous solution under visible light irradiation, React. Kinet. Mech. Catal. 114 (2015) 357–367, https://doi.org/10.1007/s11144-014-0787-y.
[21] S. Li, X. Hao, X. Dai, T. Tao, Rapid photocatalytic degradation of pollutant from water under UV and sunlight via cellulose nanofiber aerogel wrapped by TiO_2, J. Nanomater. 2018 (2018) 1–12, https://doi.org/10.1155/2018/8752015.
[22] B. Barrocas, T.J. Entradas, C.D. Nunes, O.C. Monteiro, Titanate nanofibers sensitized with ZnS and Ag_2S nanoparticles as novel photocatalysts for phenol removal, Appl. Catal. B Environ. 218 (2017) 709–720, https://doi.org/10.1016/j.apcatb.2017.06.089.
[23] B. Barrocas, M.C. Neves, M. Conceição Oliveira, O.C. Monteiro, Enhanced photocatalytic degradation of psychoactive substances using amine-modified elongated titanate nanostructures, Environ. Sci. Nano. 5 (2018) 350–361, https://doi.org/10.1039/C7EN00882A.
[24] B.T. Barrocas, M.C. Oliveira, H.I.S. Nogueira, S. Fateixa, O.C. Monteiro, Ruthenium-modified titanate nanowires for the photocatalytic oxidative removal of organic pollutants from water, ACS Appl. Nano Mater. 2 (2019) 1341–1349, https://doi.org/10.1021/acsanm.8b02215.
[25] B. Barrocas, A.J. Silvestre, A.G. Rolo, O.C. Monteiro, The effect of ionic Co presence on the structural, optical and photocatalytic properties of modified cobalt–titanate nanotubes, Phys. Chem. Chem. Phys. 18 (2016) 18081–18093, https://doi.org/10.1039/C6CP01889K.
[26] E.K. Ylhäinen, M.R. Nunes, A.J. Silvestre, O.C. Monteiro, Synthesis of titanate nanostructures using amorphous precursor material and their adsorption/photocatalytic properties, J. Mater. Sci. 47 (2012) 4305–4312, https://doi.org/10.1007/s10853-012-6281-x.
[27] A. Franco, M.C. Neves, M.M.L.R. Carrott, M.H. Mendonça, M.I. Pereira, O.C. Monteiro, Photocatalytic decolorization of methylene blue in the presence of TiO_2/ZnS nanocomposites, J. Hazard. Mater. 161 (2009) 545–550, https://doi.org/10.1016/j.jhazmat.2008.03.133.
[28] R.A. Osawa, A.P. Carvalho, O.C. Monteiro, M.C. Oliveira, M.H. Florêncio, Transformation products of citalopram: identification, wastewater analysis and *in silico* toxicological assessment, Chemosphere 217 (2019) 858–868, https://doi.org/10.1016/j.chemosphere.2018.11.027.
[29] T. Martin, User's Guide for T.E.S.T. (version 4.2) (Toxicity Estimation Software Tool) A Program to Estimate Toxicity from Molecular Structure, U.S. Environmental Protection Agency, 2016, Washington, DC.
[30] Y. Chen, J. Liang, L. Liu, X. Lu, J. Deng, I.P. Pozdnyakov, Y. Zuo, Photosensitized degradation of amitriptyline and its active metabolite nortriptyline in aqueous fulvic acid solution, J. Environ. Qual. 46 (2017) 1081–1087, https://doi.org/10.2134/jeq2017.05.0181.
[31] H. Li, M.W. Sumarah, E. Topp, Persistence of the tricyclic antidepressant drugs amitriptyline and nortriptyline in agriculture soils, Environ. Toxicol. Chem. 32 (2013) 509–516, https://doi.org/10.1002/etc.2112.
[32] D. Wan, J. Zuo, Y. Chen, Q. Chen, Y. Zuo, Photodegradation of amitriptyline in Fe(III)-citrate-oxalate binary system: synergistic effect and mechanism, Chemosphere 210 (2018) 224–231, https://doi.org/10.1016/j.chemosphere.2018.07.006.
[33] N.D.H. Khaleel, W.M.M. Mahmoud, O. Olsson, K. Kümmerer, UV-photodegradation of desipramine: impact of concentration, pH and temperature on formation of products including their biodegradability and toxicity, Sci. Total Environ. 566–567 (2016) 826–840, https://doi.org/10.1016/j.scitotenv.2016.05.095.
[34] R. Nassar, A. Trivella, S. Mokh, M. Al-Iskandarani, H. Budzinski, P. Mazellier, Photodegradation of sulfamethazine, sulfamethoxypiridazine, amitriptyline, and clomipramine drugs in aqueous media, J. Photochem. Photobiol. A Chem. 336 (2017) 176–182, https://doi.org/10.1016/j.jphotochem.2016.12.008.
[35] M. Dellagreca, M. Rosaria, L. Previtera, M. Rubino, V. Barone, O. Crescenzi, Phototransformation of the drug trazodone in aqueous solution, J. Photochem. Photobiol. A Chem. 199 (2008) 353–357, https://doi.org/10.1016/j.jphotochem.2008.06.018.
[36] J. Trawiński, R. Skibiński, Photolytic and photocatalytic degradation of tandospirone: determination of kinetics, identification of transformation products and *in silico* estimation of toxicity, Sci. Total Environ. 590–591 (2017) 775–798, https://doi.org/10.1016/j.scitotenv.2017.03.050.
[37] X. Wen, C. Niu, H. Guo, L. Zhang, C. Liang, G. Zeng, Photocatalytic degradation of levofloxacin by ternary Ag_2CO_3/CeO_2/AgBr photocatalyst under visible-light irradiation: degradation pathways, mineralization ability, and an accelerated interfacial charge transfer process study, J. Catal. 358 (2018) 211–223, https://doi.org/10.1016/j.jcat.2017.12.005.
[38] T. Wang, K.-J. Jens, Oxidative degradation of aqueous PZ solution and AMP/PZ blends for post-combustion carbon dioxide capture, Int. J. Greenh. Gas Control. 24 (2014) 98–105, https://doi.org/10.1016/j.ijggc.2014.03.003.
[39] R. Khunphonoi, N. Grisdanurak, Mechanism pathway and kinetics of p-cresol photocatalytic degradation over titania nanorods under UV–visible irradiation, Chem. Eng. J. 296 (2016) 420–427, https://doi.org/10.1016/j.cej.2016.03.117.
[40] D. Lambropoulou, E. Evgenidou, V. Saliverou, C. Kosma, I. Konstantinou, Degradation of venlafaxine using TiO_2/UV process: kinetic studies, RSM optimization, identification of transformation products and toxicity evaluation, J. Hazard. Mater. 323 (2017) 513–526, https://doi.org/10.1016/j.jhazmat.2016.04.074.
[41] J.J. García-Galán, A. Anfruns, R. Gonzalez-Olmos, S. Rodríguez-Mozaz, J. Comas, UV/H_2O_2 degradation of the antidepressants venlafaxine and O-desmethylvenlafaxine: elucidation of their transformation pathway and environmental fate, J. Hazard. Mater. 311 (2016) 70–80, https://doi.org/10.1016/j.jhazmat.2016.02.070.
[42] M.A. Gonzalez, S.G. Howell, S.K. Sikdar, Photocatalytic selective oxidation of hydrocarbons in the aqueous phase, J. Catal. 183 (1999) 159–162, https://doi.org/10.1006/jcat.1999.2395.
[43] M. Yang, W. Qiu, J. Chen, J. Zhan, C. Pan, X. Lei, M. Wu, Growth inhibition and coordinated physiological regulation of zebrafish (*Danio rerio*) embryos upon sublethal exposure to antidepressant amitriptyline, Aquat. Toxicol. 151 (2014) 68–76, https://doi.org/10.1016/j.aquatox.2013.12.029.
[44] C. Di Poi, K. Costil, V. Bouchart, M.P. Halm-Lemeille, Toxicity assessment of five emerging pollutants, alone and in binary or ternary mixtures, towards three aquatic organisms, Environ. Sci. Pollut. Res. 25 (2018) 6122–6134, https://doi.org/10.1007/s11356-017-9306-9.

Appendix A. Supplementary data

Photocatalytic degradation of amitriptyline, trazodone and venlafaxine using modified cobalt-titanate nanowires under UV−Vis radiation: Transformation products and *in silico* toxicity

Table S1. Physico-chemical parameters of tap water.

Parameters	Value
Alkalinity (mg/L $CaCO_3$)	46
pH	7.3
Conductivity (µS/cm, 20 ºC)	$1.7e^2$
DOC (mg/L)	1.0
[NH_3] (mg/L)	< 0.13[a]
[NO_3^-] (mg/L)	2.2
[PO_4^{3-}] (mg/L)	< 0.020[a]
[Cl^-] (mg/L)	21
[SO_4^{2-}] (mg/L)	20

[a]Below the limit of quantification

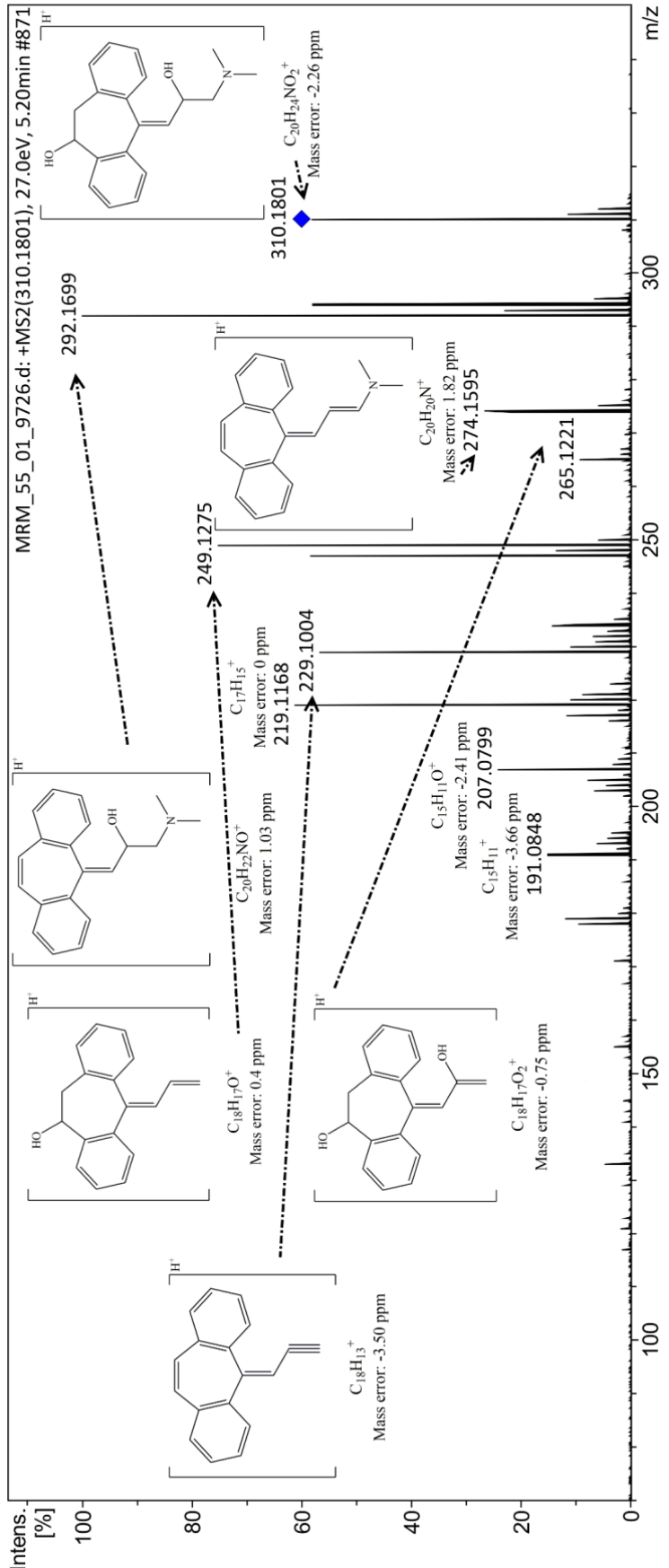

Figure S1. MS/MS spectrum of TP_{ami}-310.

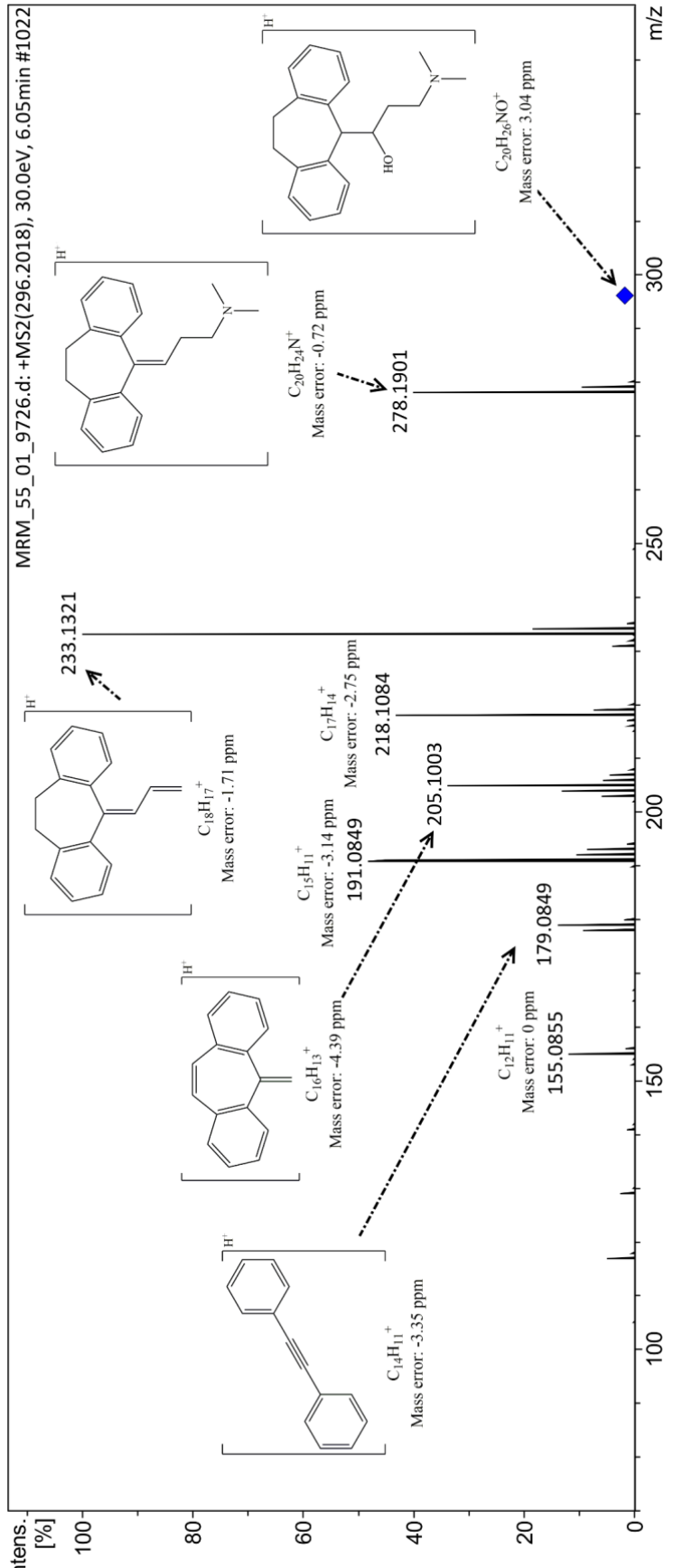

Figure S2. MS/MS spectrum of TP_{ami}-296.

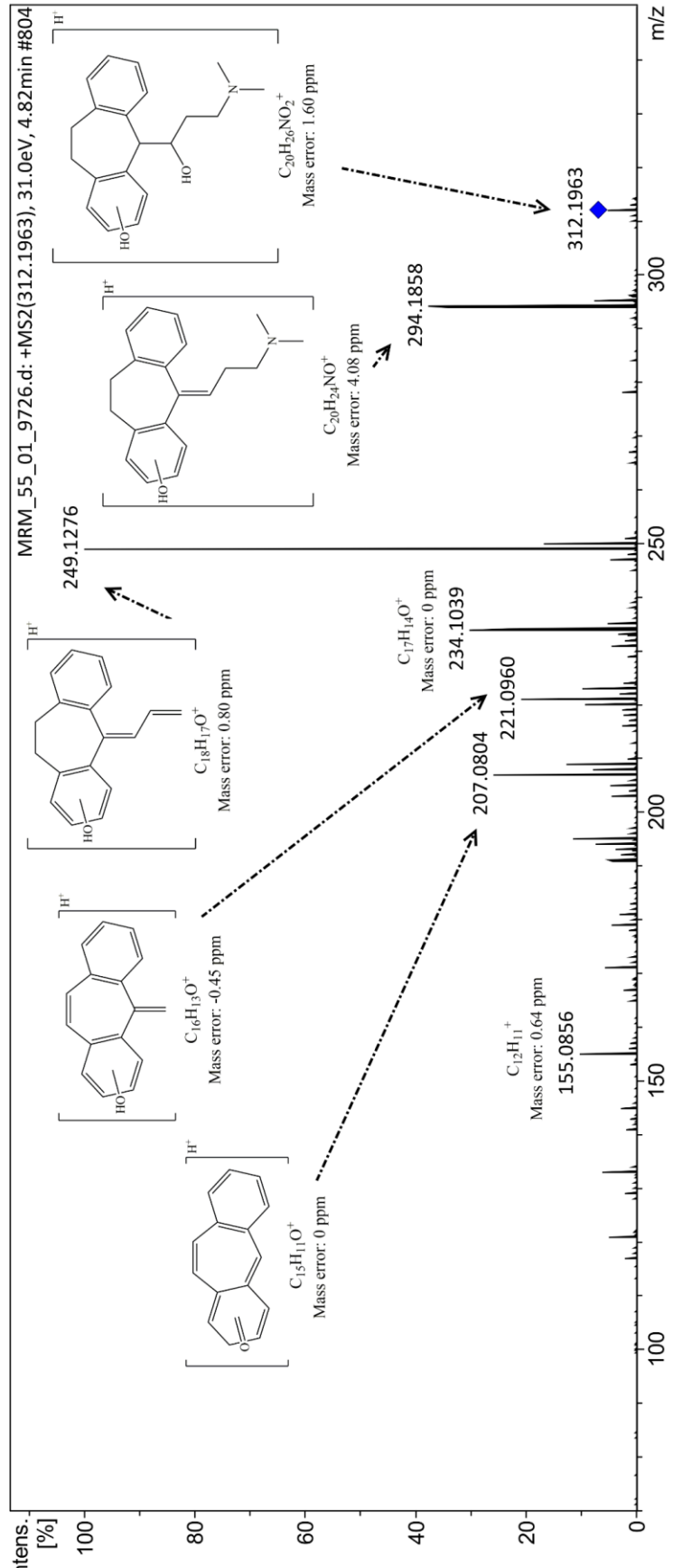

Figure S3. MS/MS spectrum of TP_{ami}-312a.

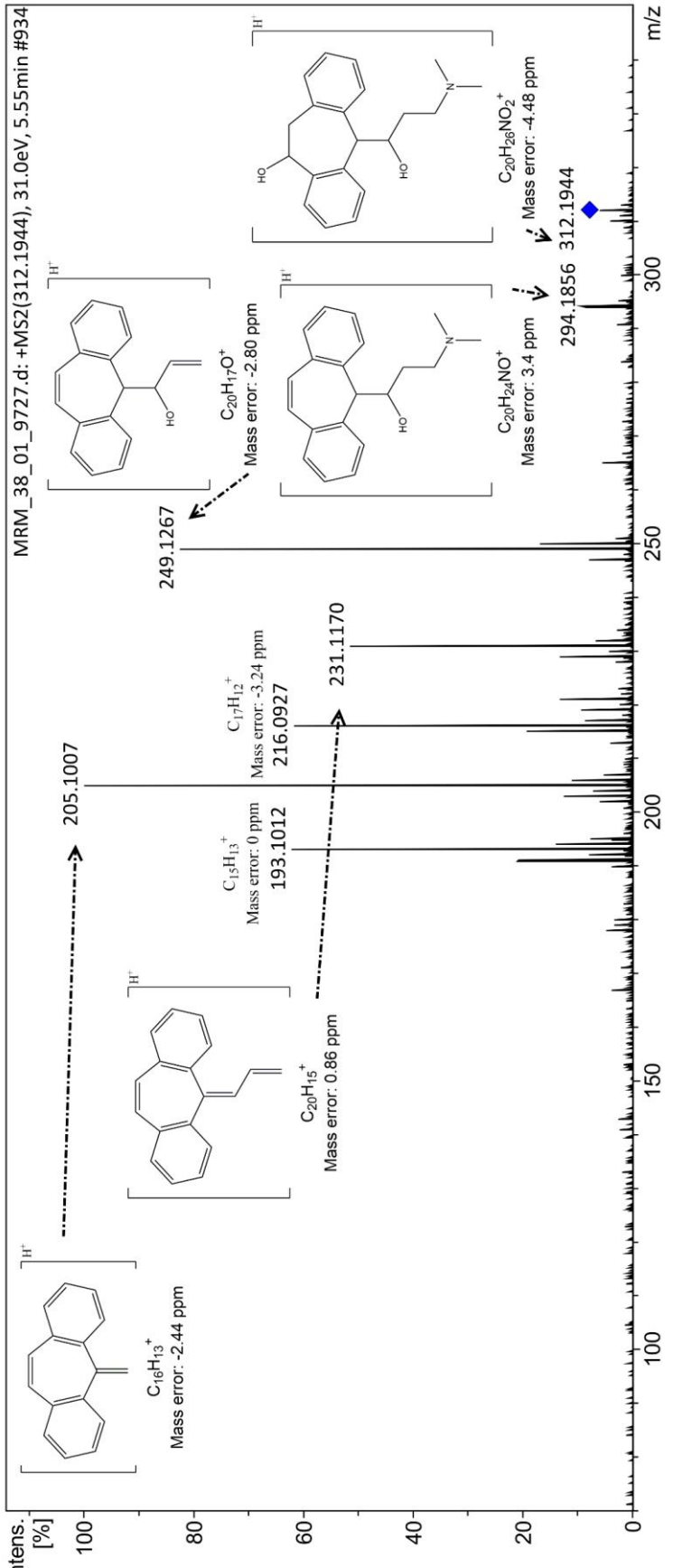

Figure S4. MS/MS spectrum of TP_{ami}-312b.

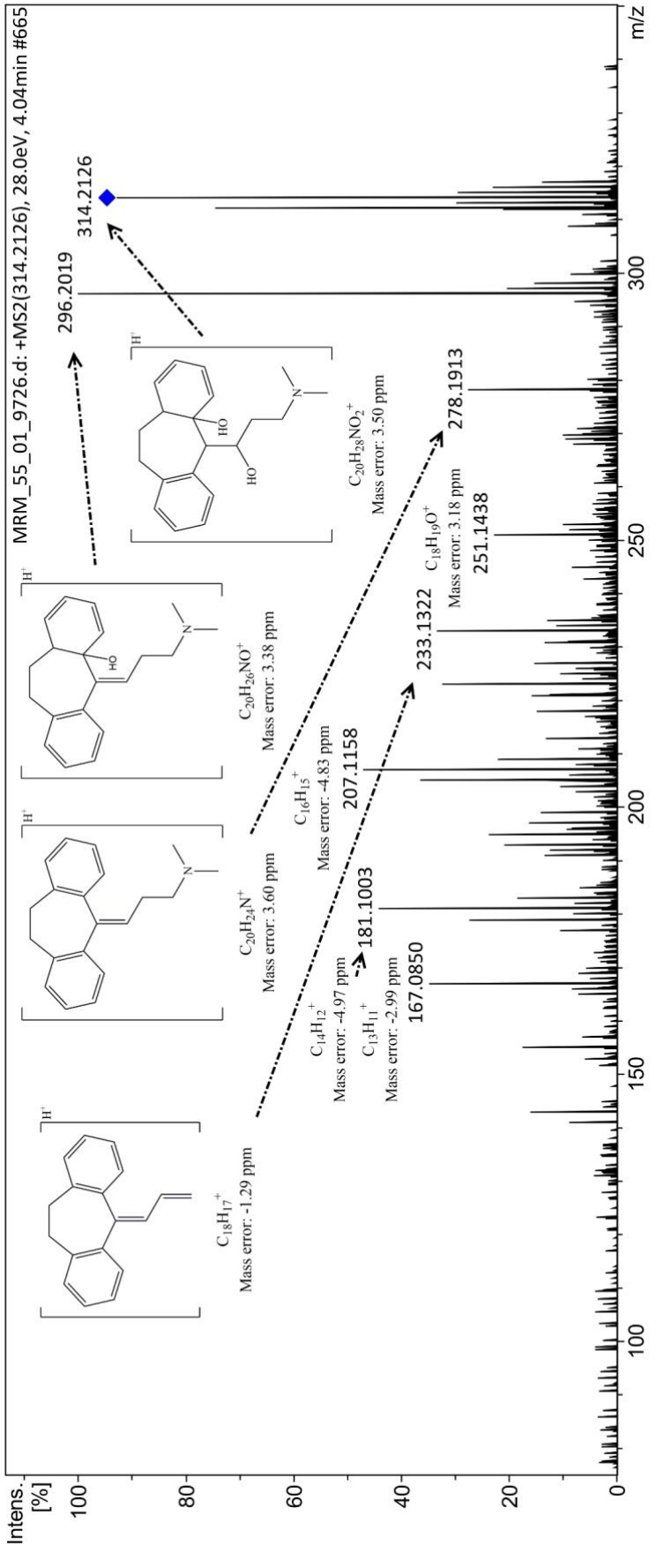

Figure S5. MS/MS spectrum of TP_{ami}-314.

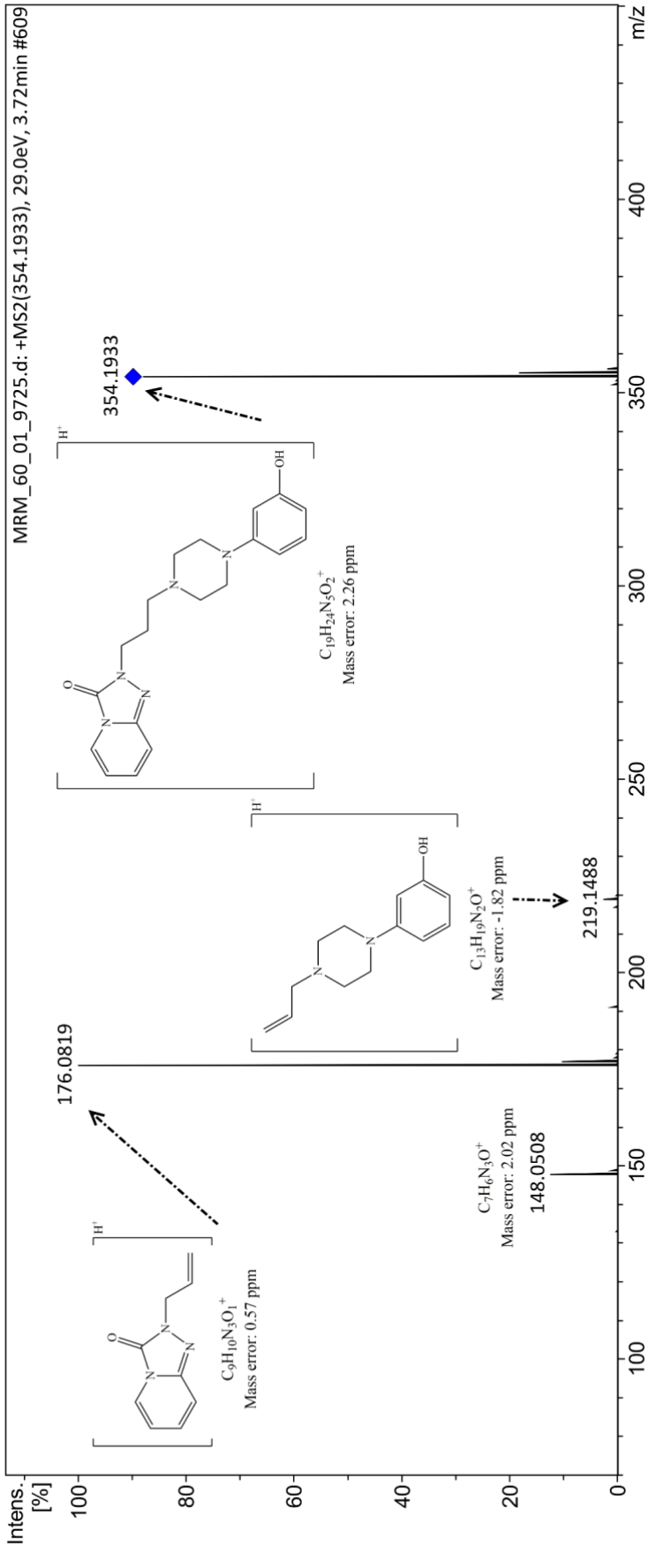

Figure S6. MS/MS spectrum of TP_{tra}-354.

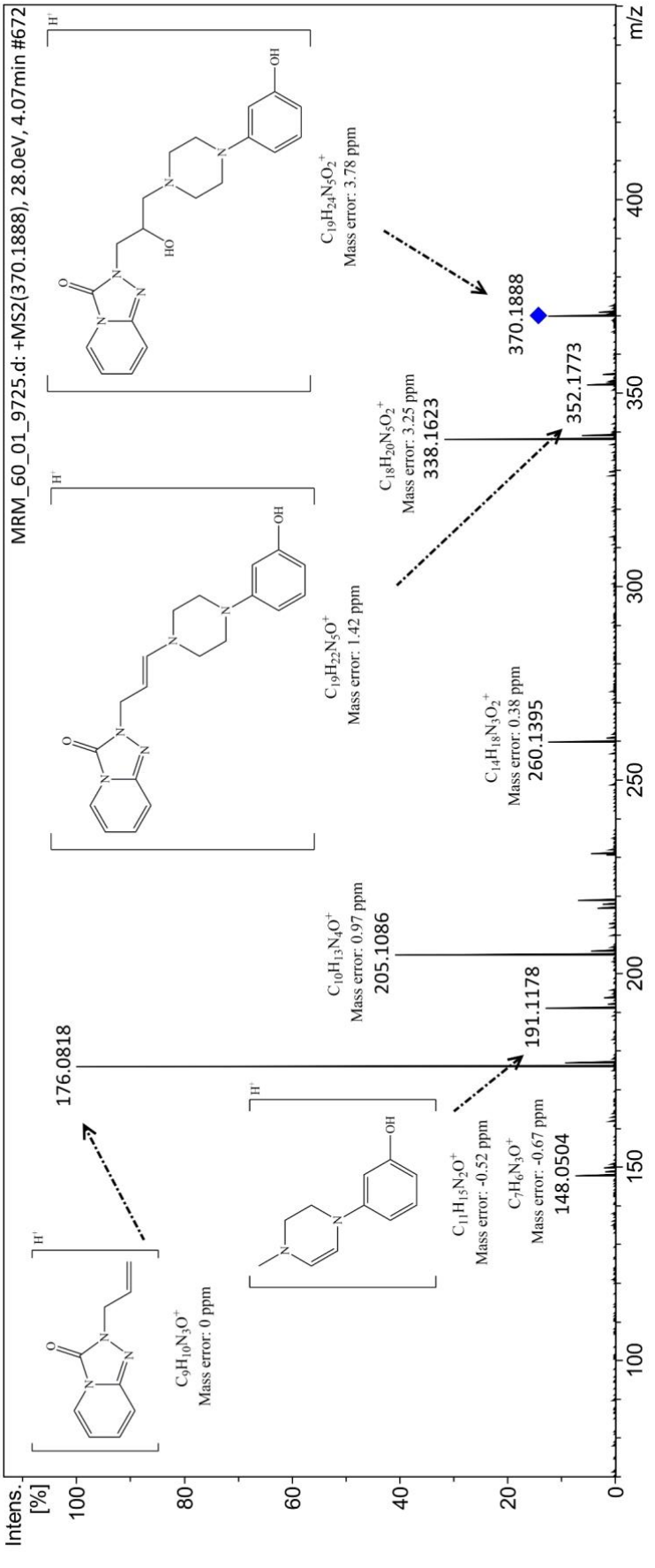

Figure S7. MS/MS spectrum of TP_{tra}-370a.

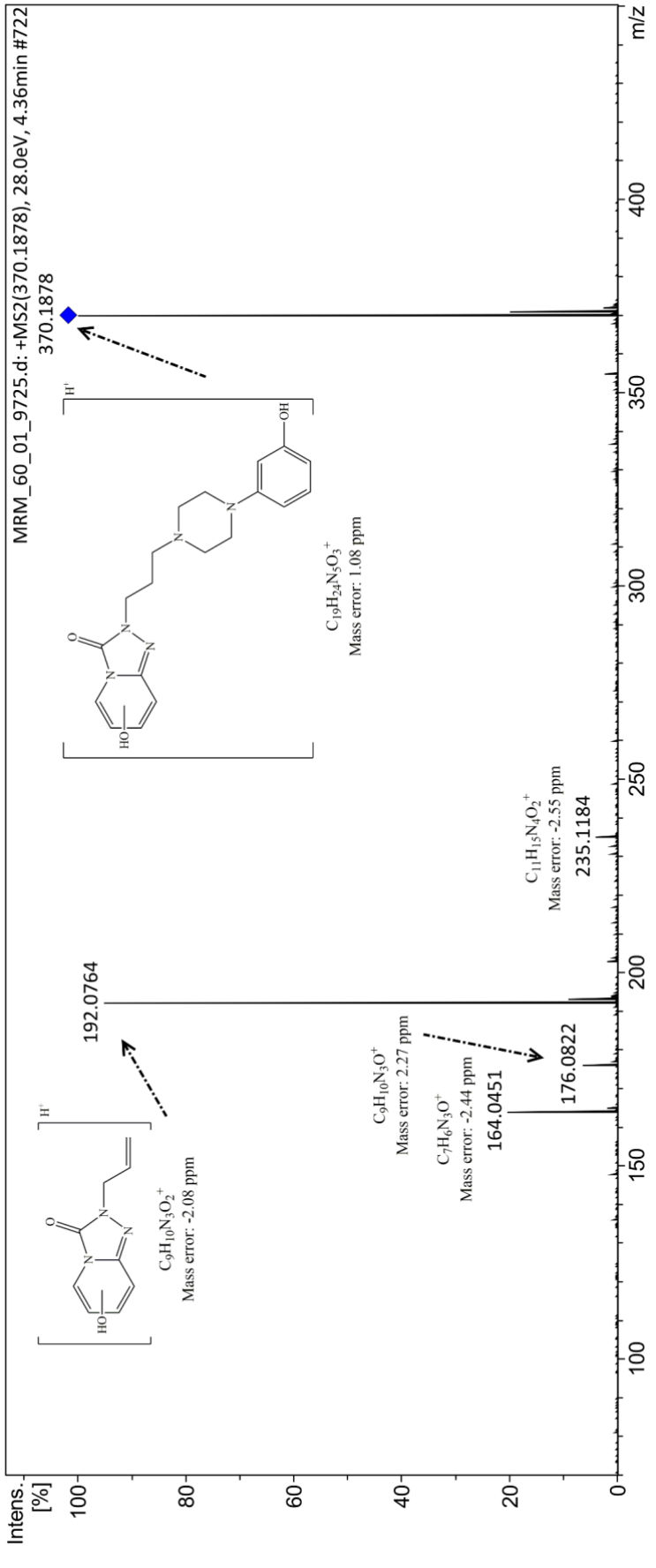

Figure S8. MS/MS spectrum of TP_{tra}-370b.

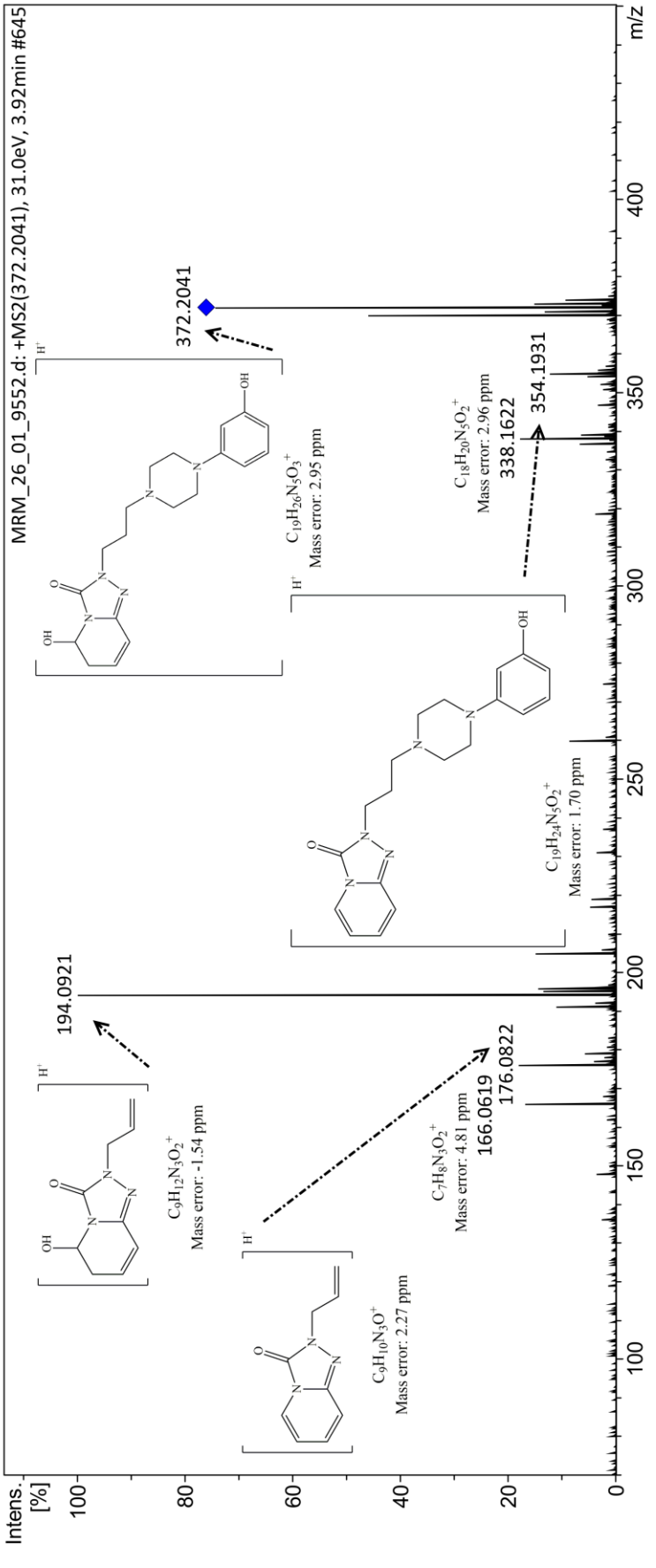

Figure S9. MS/MS spectrum of TP_{tra}-372.

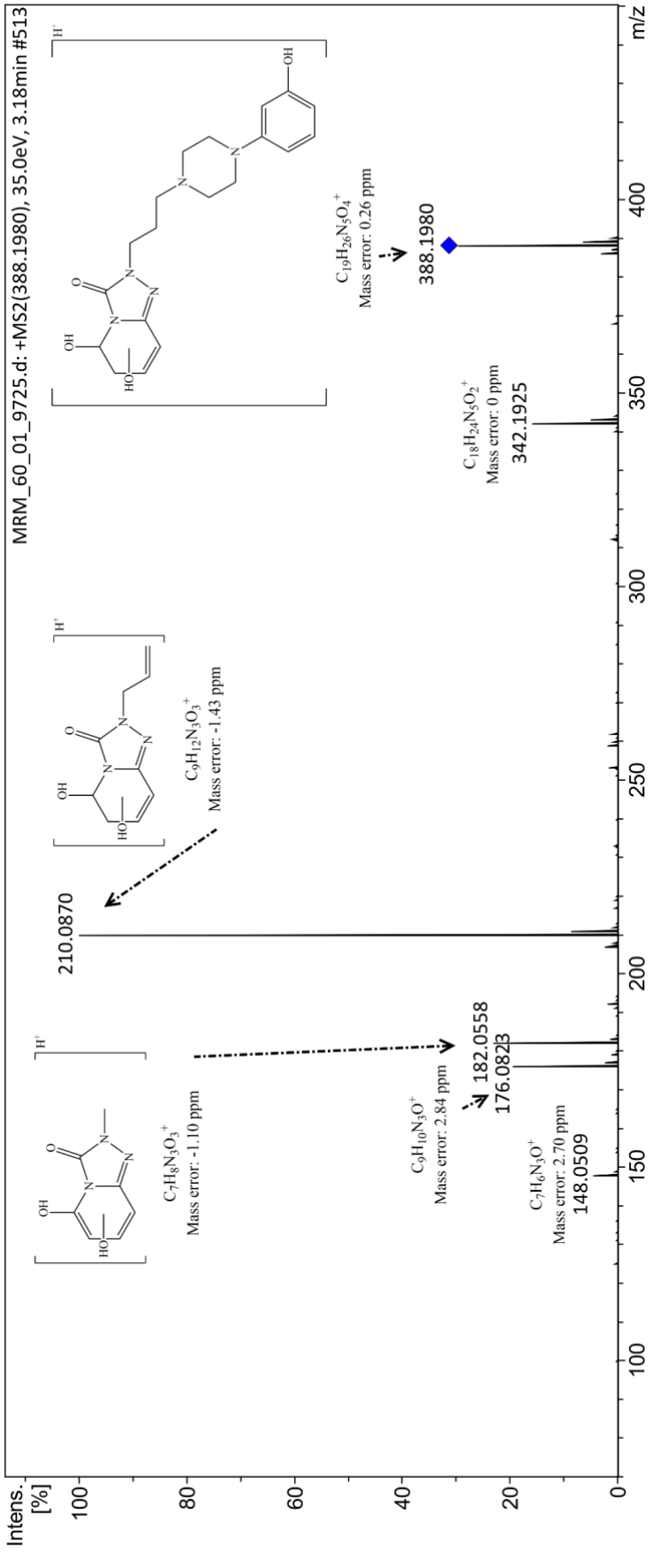

Figure S10. MS/MS spectrum of TP_{tra}-388.

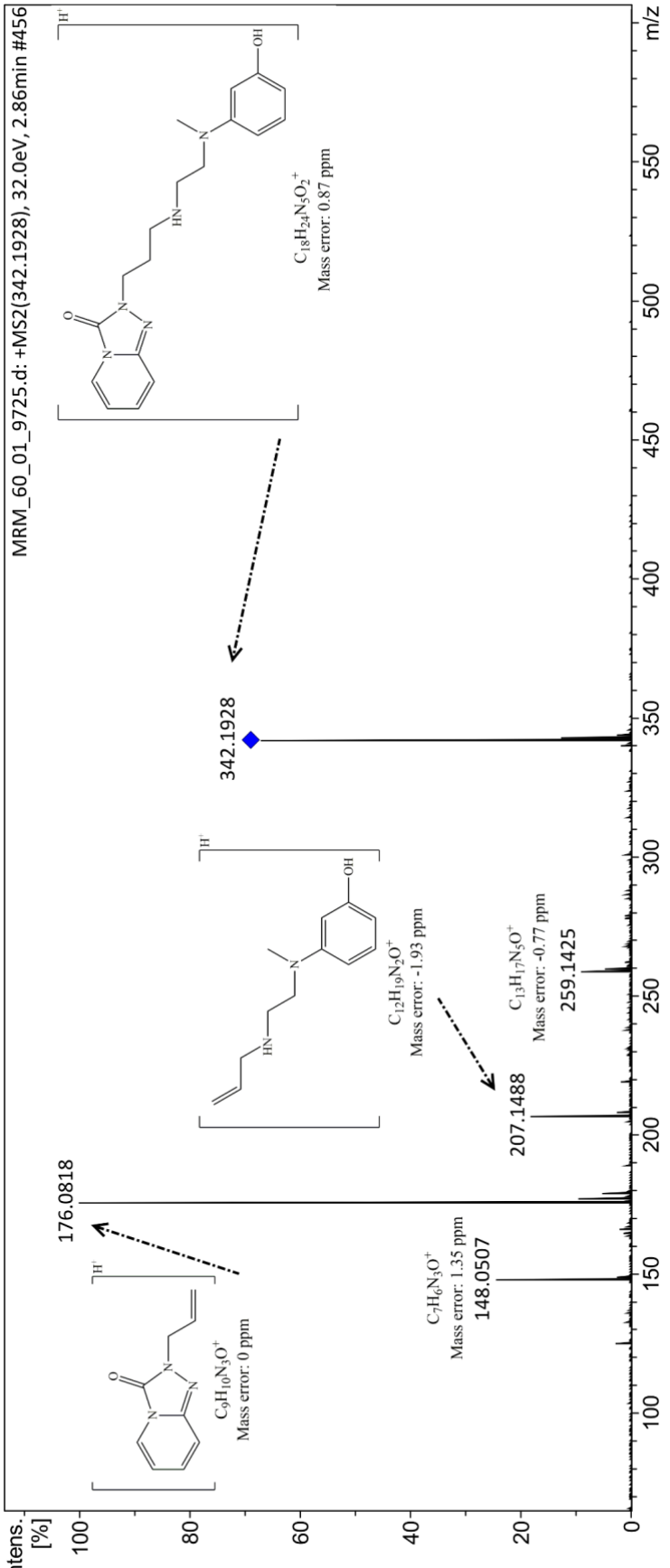

Figure S11. MS/MS spectrum of TP_{tra}-342.

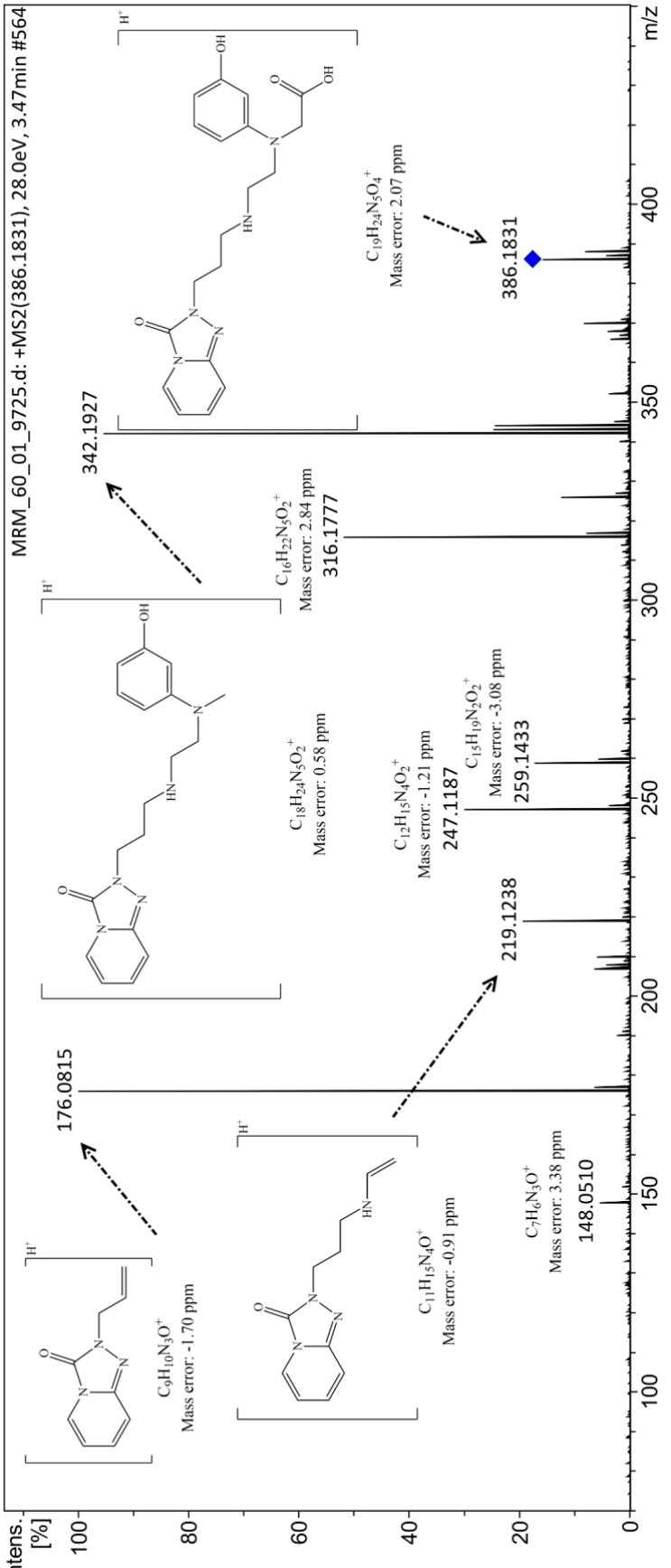

Figure S12. MS/MS spectrum of TP_{tra}-386.

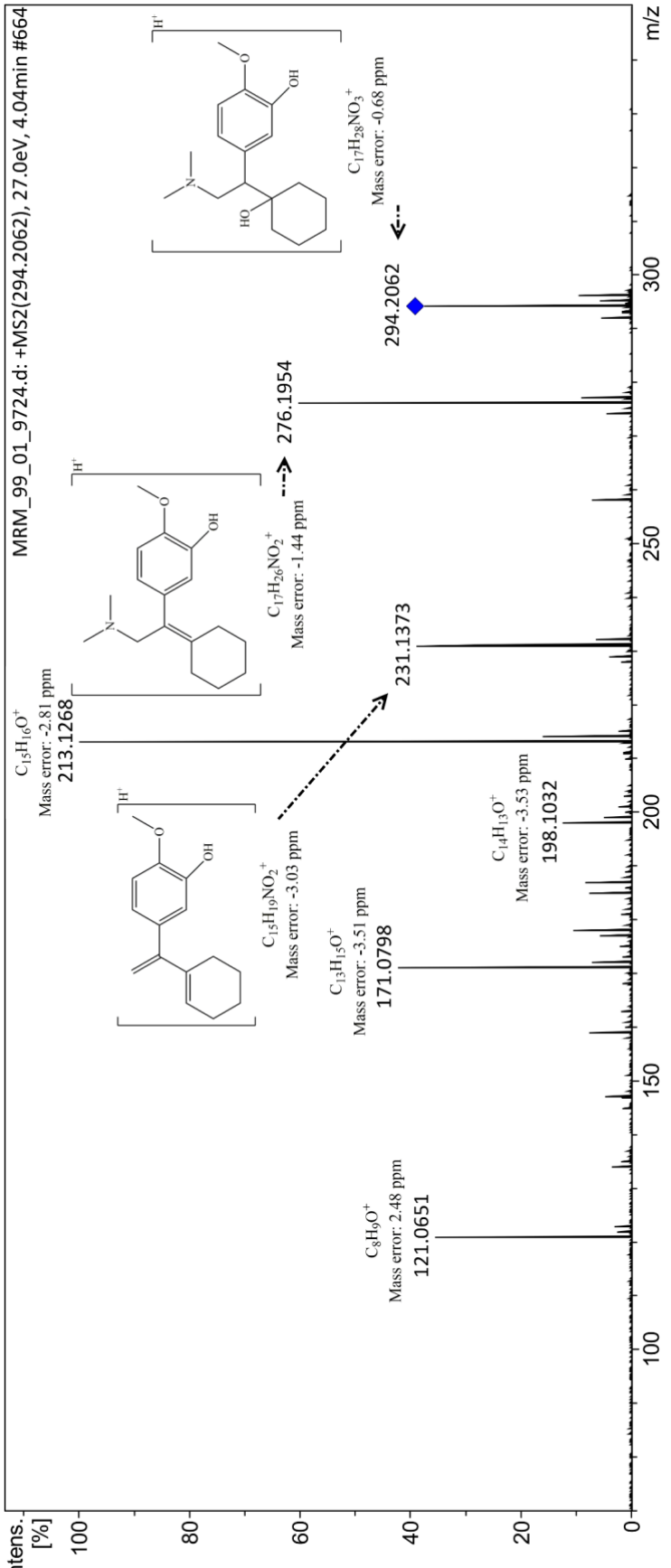

Figure S13. MS/MS spectrum of TP_{ven}-294.

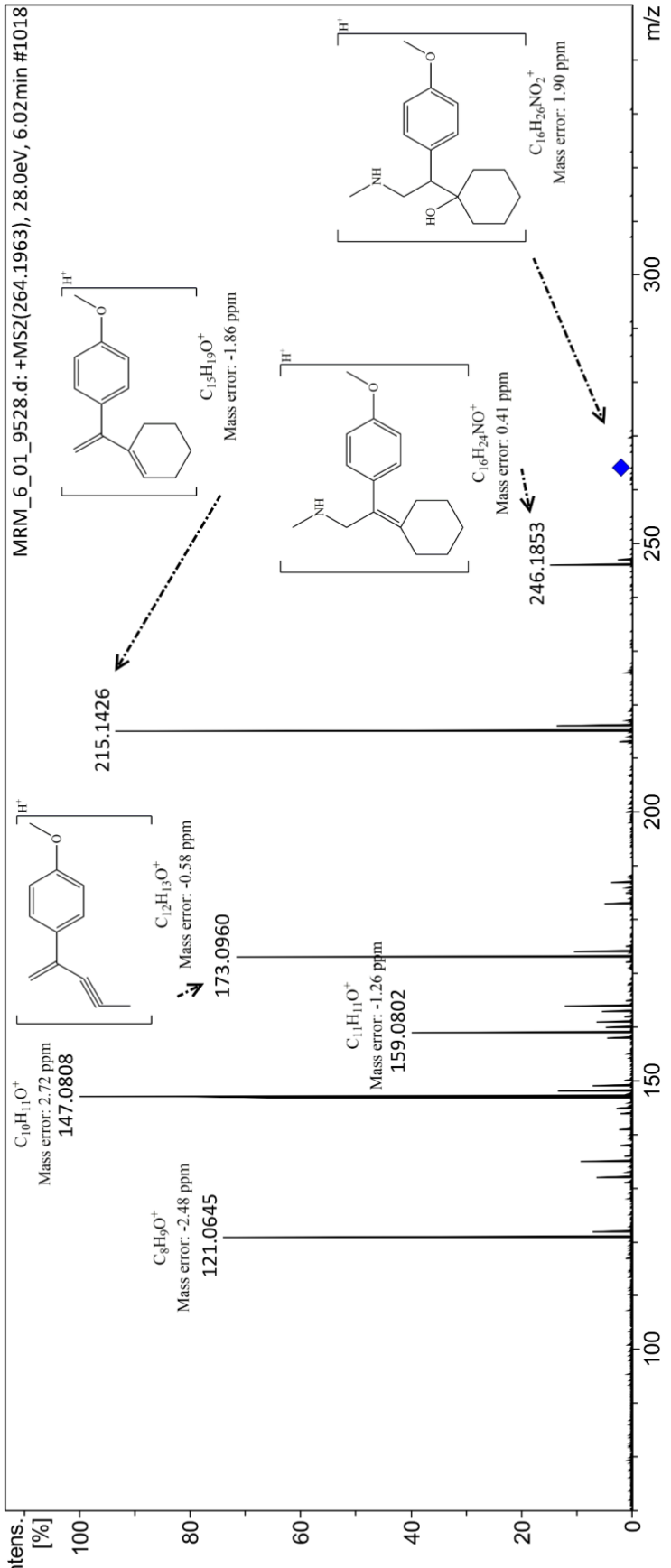

Figure S14. MS/MS spectrum of TP_{ven}-264a.

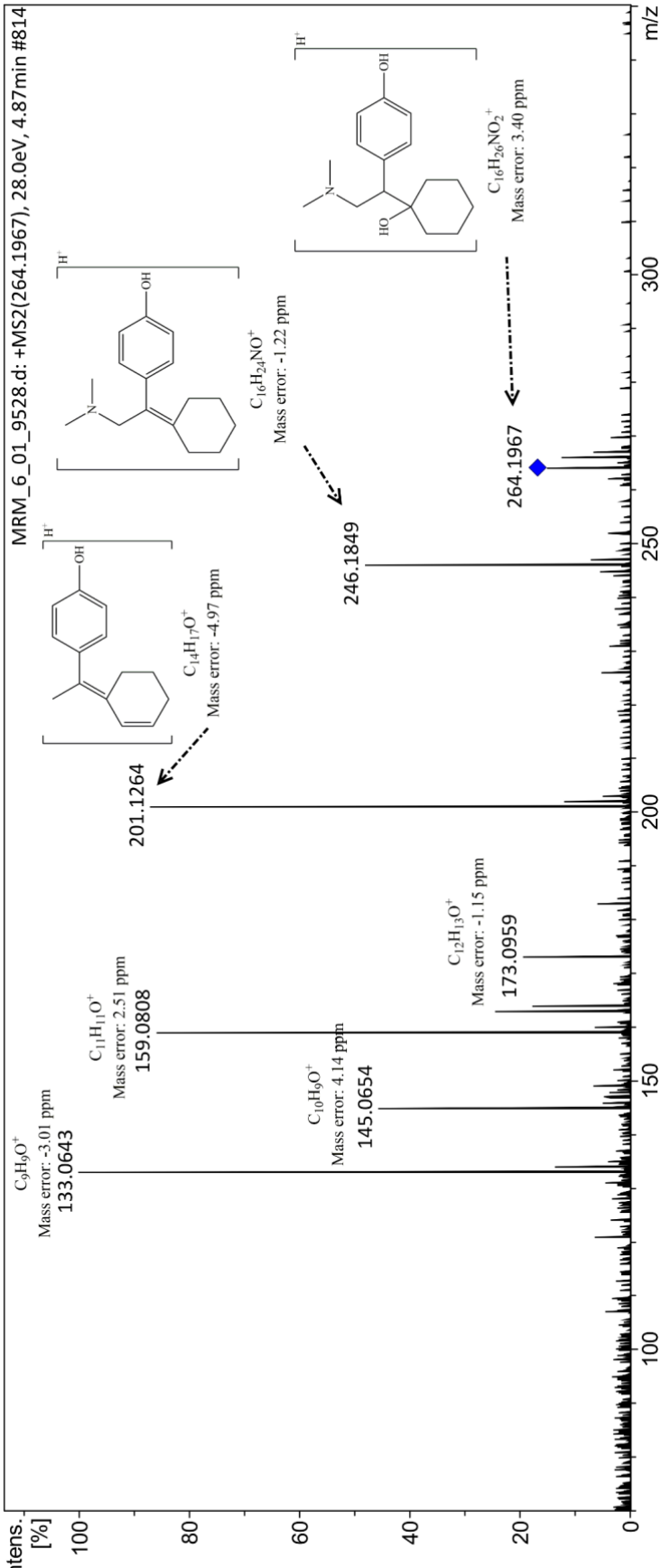

Figure S15. MS/MS spectrum of TP_{ven}-264b.

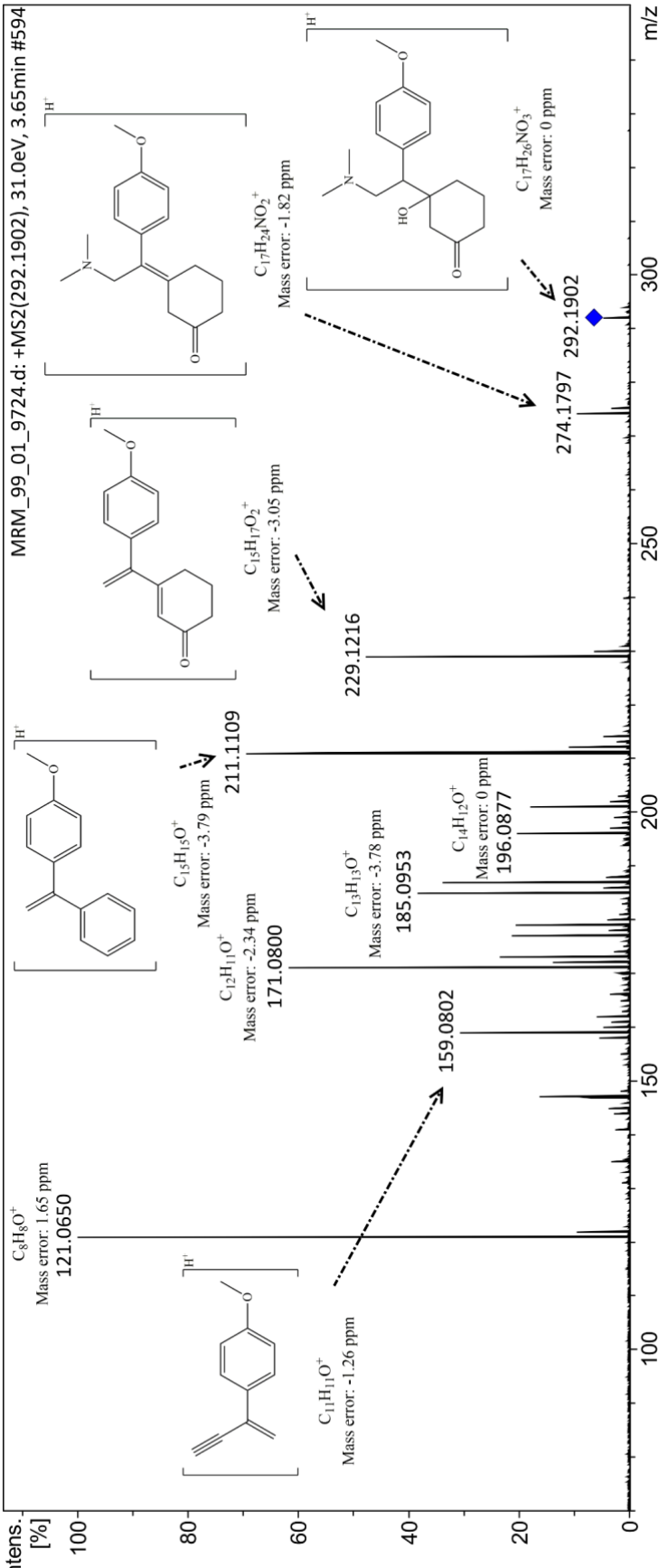

Figure S16. MS/MS spectrum of TP_{ven}-292.

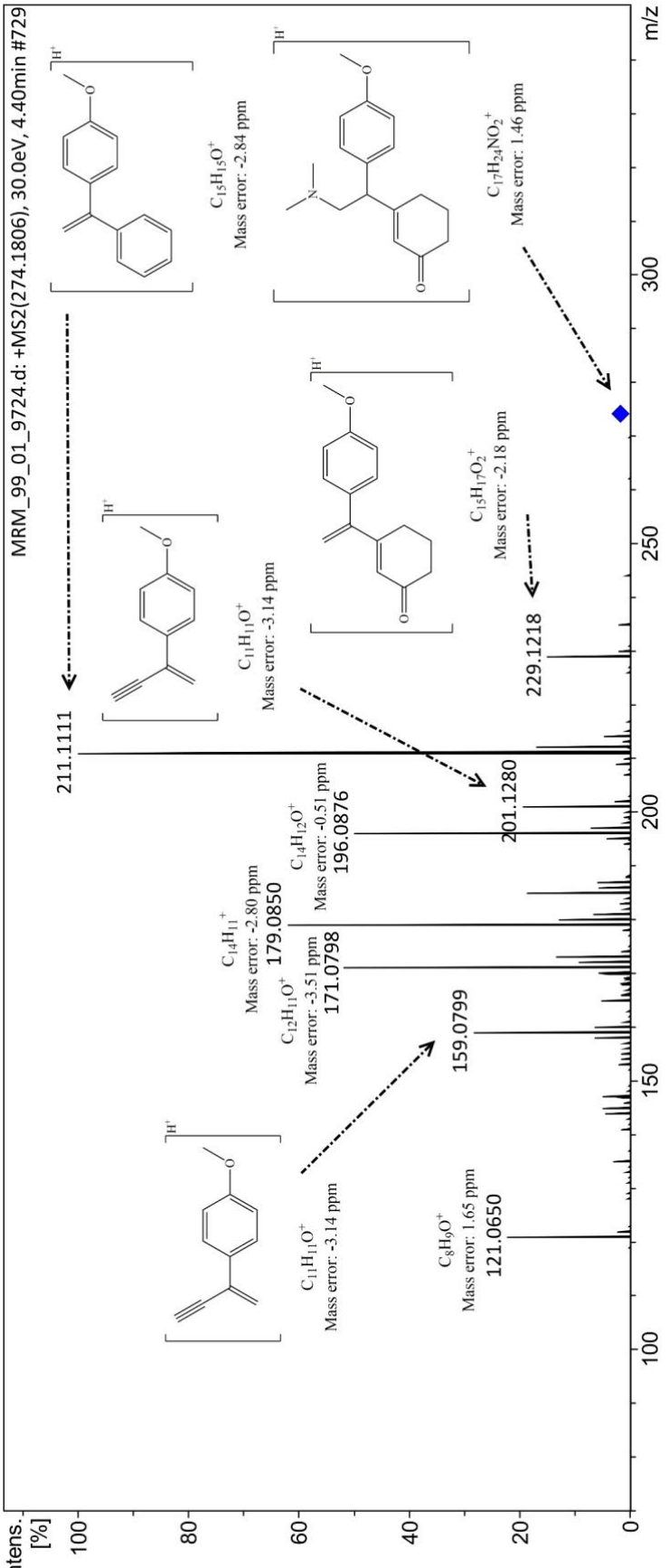

Figure S17. MS/MS spectrum of TP_{ven}-274.

Visible light photocatalytic degradation of amitriptyline using cobalt doped titanate nanowires: Kinetics and degradation pathways

Abstract

Pharmaceutical compounds have been frequently detected in environmental matrices such as effluents, surface water and drinking water which is a matter of concern. Because of this, the use of photocatalysis has been highlighted as a way to remove these contaminants from water systems and several photocatalysts have been developed for this purpose. In this study, cobalt-doped titanate nanowires (Co-TNW) were used as a catalyst for the degradation of amitriptyline (AMI) in tap water under artificial sunlight. The kinetic was monitored and additionally, the transformation products (TPs) were elucidated by high-resolution mass spectrometry. When comparing to AMI photolysis, the results demonstrated that the degradation rate of AMI was nearly twice with the catalyst. As a result of the photocatalytic degradation process, nine TPs were generated and their degradation pathways were proposed. Three of these TPs have never been described in the literature. In the photocatalytic studies, the Co-TNW presented low catalytic activity under visible light for TPs which shows that their formation may be relevant for toxicity and photodegradation studies.

Keywords: Photocatalysis; Cobalt-doped titanate nanowires; Visible light radiation; Amitriptyline; Transformation products; High-resolution mass spectrometry

1. Introduction

Amitriptyline (AMI) is a tricyclic antidepressant mainly used to treat major depressive and anxiety disorders. After consumption, the drug is excreted mostly by urine, thus reaching the wastewater treatment plant (WWTP) and consequently the surface waters, since conventional wastewater treatments are not effective for the removal of these contaminants. Several studies revealed that AMI had a removal between 65%−85% in WWTPs (Kasprzyk-Hordern et al. 2009; Baker and Kasprzyk-Hordern 2013); and were detected in surface water and tap water in concentrations of 71.6 ng/L (Baker and Kasprzyk-Hordern 2011) and 1.4 ng/L (Togola and Budzinski 2008), respectively.

Additionally, there is a concern about the transformation products (TPs), which are products generated in the environment and in the WWTP by biological or physical-chemical processes of the parent compound. Some studies have noticed the presence of TPs in different environmental matrices, including effluents wastewater (Aymerich et al. 2016; Beretsou et al. 2016; Li et al. 2016), surface waters (Aymerich et al. 2016; Boix et al. 2016; Li et al. 2016) and soil (Li et al. 2013). The TPs may present persistence or toxicity superior than the parent compound (Escher et al. 2011). Therefore, new technologies are needed to remove these contaminants and their TPs in order for them to do not affect the aquatic biota and human health.

Photocatalysis is one pollutant degradation method that has been outstanding in the last decades. Most of the photocatalytic studies use nanocrystalline TiO_2 as catalyst for the removal of pollutants since this material presents low cost, long-term stability and it is environment-friendly. However, it has the limitation of having low radiation absorptive capacity under visible light spectrum and high photo-generated charge carriers recombination rate. Nevertheless, methods of metal doping, sensitization or formation of nanocomposites with other semiconductors have been proposed to overcome this disadvantage by enhancing the photocatalytic activity (Gnanasekaran et al. 2016; Bomila et al. 2018; Barrocas et al. 2019). These methods have been showing higher efficiency toward pollutant removal in environmental samples.

In our previous study, titanate nanowires modified by cobalt doping (Co-TNW) were synthesized and an increase of the visible radiation absorption, together with a decrease on the recombination rate was noticed. Overall, the use of Co-TNW as a photocatalytic has proved to be effective in the removal of pollutants under UV−Vis radiation (Barrocas et al. 2016; Osawa et al. 2019).

The objective of this work was to evaluate the degradation of AMI using Co-TNW as a photocatalyst under artificial solar light. In addition, the elucidation of the TPs using the high-resolution mass spectrometry enabling us to, finally, propose, the corresponding degradation pathways.

2. Experimental

2.1. Materials

The amitriptyline hydrochloride (≥ 98%) analytical standard was purchased from Sigma-Aldrich (USA). Acetonitrile, formic acid and water were obtained from Fisher

Scientific (USA). The photocatalyst was synthesized by hydrothermal approach previously described applying a Co-doped amorphous precursor, in which its characterization has already been discussed (Barrocas et al. 2016).

2.2. Photocatalysis study

Tap water was collected from the local drinking water supply and the physico-chemical parameters were previously reported (Osawa et al. 2019). The water samples (150 mL) were spiked with the target compound AMI with the concentration of 10 mg/L. Additionally, 15 mg of the Co-TNW powder were used for the photocatalysis experiments and the samples under study were firstly left for 1 h in the darkness for adsorption equilibrium and then they were irradiated with artificial solar light. Aliquots were withdrawn from the photoreactor at designated time intervals: 0 min, 15 min, 30 min, 1 h, 1.5 h, 2 h, 3 h, 5 h and 8 h, after which they were centrifuged and stored at −80 °C for further analyses.

Photodegradation experiments were performed using an arc lamp housing with xenon arc lamp power supply (Newport, USA). The radiation source was a 500 W mercury-xenon arc lamp (Newport, USA), emitting radiation in the visible and near UV range. A 250 mL borosilicate glass with recirculation of water for cooling was employed to cut off the UV radiation emitted by the lamp to simulate solar radiation, and the photoreactor was placed 30 cm away from the source of radiation.

2.3. Instrumentation

AMI and its TPs were analyzed by an UHPLC UltiMate 3000 LC system (Thermo Fischer Scientific, Germany) coupled to a mass spectrometer QTOF Impact II (Bruker Daltonics, Germany). Details of the instrumentation parameters were previously described elsewhere (Osawa et al. 2019). The TPs were elucidated by the analysis of the MS and MS/MS spectra, with a mass error of less than 5 ppm, enabled to identify the monoisotopic mass of the parental ion and its fragments, respectively.

3. Results and discussion

3.1. Photodegradation experiments

In the photocatalysis experiments, AMI showed a removal rate of 41%, with respect to the initial concentration whereas when photolysis was used it showed a 22% removal within 8 h of the experiment (**Fig. 1a**). This may indicates that in environmental

matrices such as surface waters this drug exhibits a certain removal under solar radiation. The result is in agreement with Chen et al. (2017) who demonstrated that the AMI degraded in a solution of fulvic acid. Just for a matter of comparison, our previous study reported the removal of 90 % of AMI under UV−Vis radiation in 30 min using Co-TNW as catalyst (Osawa et al. 2019).

The analyses of AMI photodegradation rates discussed in this report allowed us to study the kinetics of removal of this drug. As shown in **Fig. 1b**, the photocatalytic degradation rate followed the pseudo-first order kinetics as given by Eq. 1:

$$\ln \frac{C_0}{C} = k_r t \quad (1)$$

where C_0 and C are the concentration of AMI at time zero and at time t, respectively, and k_r is the degradation rate constant. The pseudo-first order constants in photocatalysis and photolysis were k_r = 0.0617 h^{-1} and k_r = 0.0366 h^{-1}, respectively.

Our experiment revealed nine TPs in the photolysis and photocatalysis processes. The amount of TPs increases with the time of irradiation, and it is higher when Co-TNW was used as catalyst, which makes sense since the degradation rate of AMI was higher in photocatalysis (**Fig. 1c−d**). The peaks areas of TPs were normalized from the peak area of AMI at time 0 min. The TPs that presented larger relative areas were TP-8 and TP-9, in both processes after 8 h of experiment. Nevertheless, it was observed that no degradation occurred with most TPs during the 8 h of irradiation, Analyses of the MS/MS spectra for elucidation of TPs can be found in **section 3.2.** Overall, since TPs seems to be not eliminated under the experimental conditions used, their formation during AMI degradation should be relevant and should be considered. The main reactions for the formation of these TPs are hydroxylations and oxidations, as shown in **Fig. 2**, in which a degradation pathway is proposed.

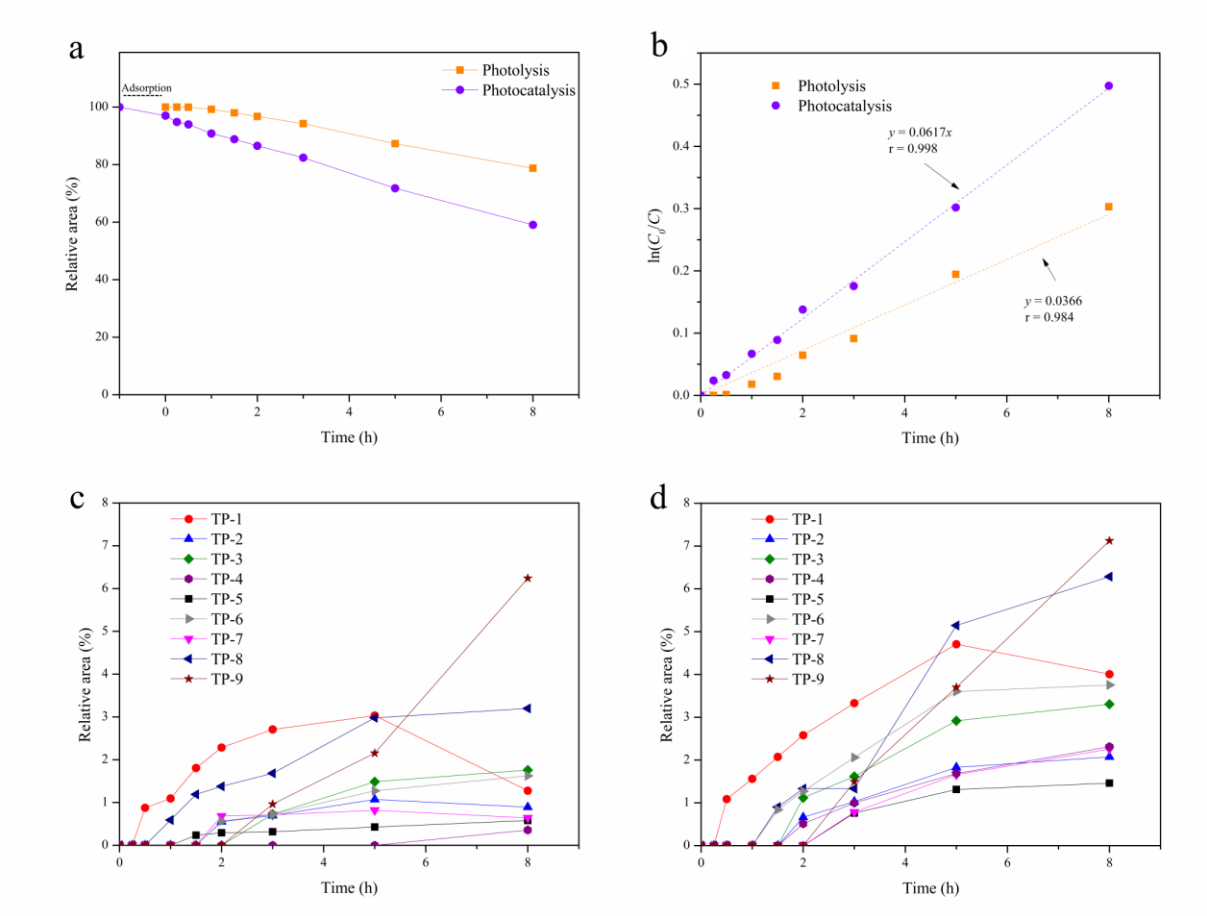

Fig. 1 (a) Photolysis and photocatalysis of amitriptyline (AMI); (b) pseudo-first order kinetics; evolution profiles of transformation products (TPs) during photolysis (c) and during photocatalysis (d).

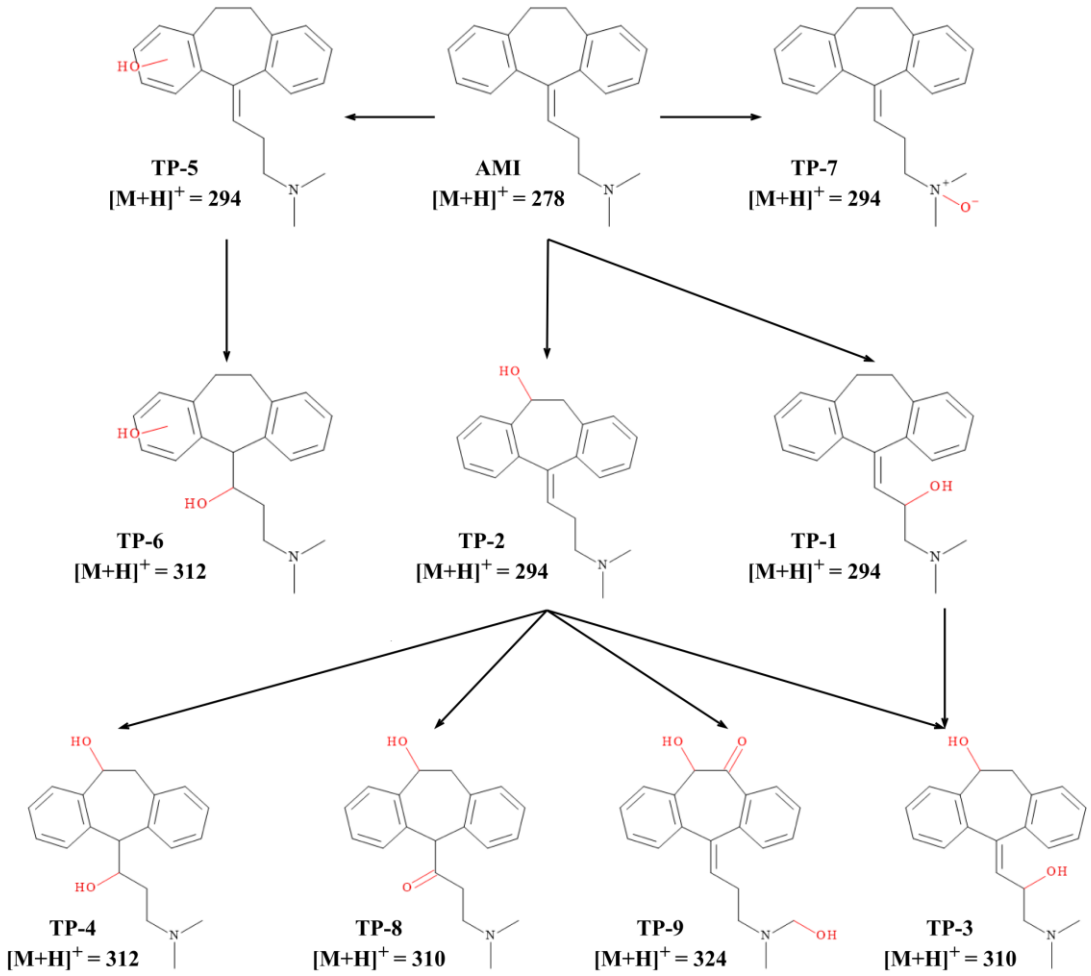

Fig. 2 Proposed degradation pathways of amitriptyline (AMI).

3.2. Elucidation of TPs

For identification of the chemical structures of TPs, in the fragmentation patterns obtained from MS/MS spectra, some neutral losses were monitored. **Table 1** shows the high-resolution mass data, the elemental formula of product ions from the parent compound and the relative mass errors (ppm). Neutral loss of H_2O may indicate the formation of one OH group by an hydroxylation process and we suggest that four TPs (TP-1, TP-2, TP-3 and TP-4) were formed only by this processes. Three of these TPs (TP-1, TP-3 and TP-4) have already been identified and discussed in our previous work in which AMI was degraded by UV−Vis radiation (Osawa et al. 2019). Briefly, TP-1 was generated by hydroxylation of the β-carbon of the aliphatic chain because the loss of H_2O was identified in the fragment ion at *m/z* 249 ($C_{18}H_{17}O^+$) from which the fragment ion at *m/z* 231 ($C_{18}H_{15}^+$) resulted. TP-2 had the OH group attached to cyclohexane

because neutral loss of H_2O was detected from the *m/z* 294 ($C_{20}H_{24}NO^+$) to *m/z* 276 ($C_{20}H_{22}N^+$). Finally, we suppose TP-3 could have been originated from the hydroxylation of TP-1 or TP-2 because two eliminations of H_2O were detected in the fragmentation pattern of MS/MS spectrum, firstly from the parent ion at *m/z* 310 ($C_{20}H_{24}NO_2^+$) to *m/z* 292 ($C_{20}H_{22}NO^+$) and, subsequently, to *m/z* 274 ($C_{20}H_{20}N^+$). Two H_2O eliminations were detected in the MS/MS spectra of TP-4, however, unlike TP-3, we believe that hydration of the alkene of the aliphatic chain occurred.

TP-5 was most probably generated by a hydroxylation process, however, elimination of H_2O has not been identified in the MS/MS spectrum, therefore, the OH group may be attached to the aromatic ring. TP-6 was presumably formed from hydration of alkene of TP-5. Both TPs were also elucidated in our previously published work (Osawa et al. 2019).

The neutral loss of dimethylamine oxide (C_2H_7NO) may demonstrate the formation of *N*-oxide group. That elimination was observed in the MS/MS spectrum of TP-7, the discussion of which was previously reported (Osawa et al. 2019). The elimination of carbon monoxide (CO) may determine the formation of ketone, possibly by an oxidation process. Therefore, we believe that TP-8 was formed by an oxidation of alkene from TP-2, Zhang et al. (2016) demonstrated the process of oxidation of alkenes by photocatalysis and proton-reduction catalysis using visible light. The fragment ion at *m/z* 209 ($C_{15}H_{13}O^+$) showed the elimination of *N*,*N*-dimethylethanamine ($C_4H_{11}N$) plus CO, which supports the hypothesis of oxidation of alkene, and the fragment ion at *m/z* 191 ($C_{15}H_{11}^+$) exhibited the loss of H_2O, which indicates the presence of the OH group, possibly bound to cycloheptane.

The MS/MS spectrum of TP-9 showed the elimination of CO at *m/z* 195 ($C_{14}H_{11}O^+$) resulting from *m/z* 233 ($C_{15}H_{11}O_2^+$) in which the oxidation reaction probably occurred in cycloheptane, Calza et al. (2008) identified oxidation in the heterocyclic group of imipramine (compound similar to the AMI) in the photocatalysis process. Additionally, losses of C_2H_7NO plus H_2O at *m/z* 245 were identified. We believe that these were two hydroxylation reactions, one at the tertiary amine carbon and the other at cycloheptane, respectively. This hypothesis is reinforced through the fragment at *m/z* 223 ($C_{15}H_{11}O_2^+$) from parent ion ($C_{20}H_{22}NO_3^+$), that indicates the loss of $C_5H_{11}NO$, which may represent the [methyl(prop-2-enyl)amino]methanol.

Table 1. AMI TPs, retention times (Tr), fragment ions and mass error.

Compound name	Tr (min)	Theoretical mass $[M+H]^+$	Elemental formula $[M+H]^+$	Relative error (ppm)
TP-1	7.13	294.1852	$C_{20}H_{24}NO^+$	2.72
		249.1274	$C_{18}H_{17}O^+$	1.60
		231.1168	$C_{18}H_{15}^+$	-2.16
		216.0934	$C_{17}H_{12}^+$	-1.85
		205.1012	$C_{16}H_{13}^+$	-3.90
		193.1012	$C_{15}H_{13}^+$	-0.51
TP-2	6.65	294.1852	$C_{20}H_{24}NO^+$	1.36
		276.1747	$C_{20}H_{22}N^+$	-1.08
		231.1168	$C_{18}H_{15}^+$	-2.16
		216.0934	$C_{17}H_{12}^+$	-3.70
		205.1012	$C_{16}H_{13}^+$	0
TP-3	5.24	310.1808	$C_{20}H_{24}NO_2^+$	-2.58
		292.1696	$C_{20}H_{22}NO^+$	-0.34
		274.1590	$C_{20}H_{20}N^+$	0
		249.1274	$C_{18}H_{17}O^+$	-2.40
		229.1012	$C_{18}H_{13}^+$	-2.62
		219.1168	$C_{17}H_{15}^+$	-2.74
		207.0804	$C_{15}H_{11}O^+$	-2.90
TP-4	5.57	312.1958	$C_{20}H_{26}NO_2^+$	-4.48
		294.1846	$C_{20}H_{24}NO^+$	3.40
		249.1274	$C_{18}H_{17}O^+$	-2.80
		231.1168	$C_{18}H_{15}^+$	0.86
		216.0934	$C_{17}H_{12}^+$	-3.24
		205.1012	$C_{16}H_{13}^+$	-2.44
		193.1012	$C_{15}H_{13}^+$	0
TP-5	4.80	294.1852	$C_{20}H_{24}NO^+$	-2.04
		249.1274	$C_{18}H_{17}O^+$	-2.40
		234.1039	$C_{17}H_{14}O^+$	-2.56
		221.0961	$C_{16}H_{13}O^+$	2.26
		207.0804	$C_{15}H_{11}O^+$	-3.86
TP-6	4.82	312.1958	$C_{20}H_{26}NO_2^+$	-1.28
		294.1846	$C_{20}H_{24}NO^+$	1.02
		249.1274	$C_{18}H_{17}O^+$	-2.41
		221.0961	$C_{16}H_{13}O^+$	-4.07
		207.0804	$C_{15}H_{11}O^+$	-2.41
		155.0855	$C_{12}H_{11}^+$	-1.29
TP-7	7.74	294.1852	$C_{20}H_{24}NO^+$	2.04

		233.1325	$C_{18}H_{17}^+$	-2.57
		218.1090	$C_{17}H_{14}^+$	-2.30
		205.1012	$C_{16}H_{13}^+$	-4.38
		191.0855	$C_{15}H_{11}^+$	-2.61
		179.0855	$C_{14}H_{11}^+$	-0.56
TP-8	6.10	310.1808	$C_{20}H_{24}NO_2^+$	0.32
		209.0961	$C_{15}H_{13}O^+$	-1.43
		191.0855	$C_{15}H_{11}^+$	-1.04
TP-9	5.14	324.1594	$C_{20}H_{22}NO_3^+$	-0.30
		245.0961	$C_{18}H_{13}O^+$	-0.81
		233.0597	$C_{16}H_9O_2^+$	-2.57
		223.0754	$C_{15}H_{11}O_2^+$	-1.34
		195.0804	$C_{14}H_{11}O^+$	-2.56
		177.0699	$C_{14}H_9^+$	-2.82

4. Conclusions

This study demonstrated that AMI was not completely degraded in tap water after 8 hours under artificial solar light. More precisely AMI was removed at about 41% of the initial concentration by photocatalysis when compared to 22% in the absence of the catalyst. In other words, AMI may exhibit persistence in the environment when exposed to solar radiation, which may be a matter of concern. In addition, nine TPs were identified by analyses of MS/MS spectra and to the best of our knowledge, three of them have never been reported in the literature and most of them presented low photocatalytic activity. Despite the fact that photocatalysis is a promising technology for the removal of contaminants, it is essential to consider the TPs formed by this process, since they may be potentially toxic to aquatic organisms and humans.

Acknowledgments

Rodrigo A. Osawa acknowledges Brazilian Federal Agency Coordenação de Aperfeiçoamento de Pessoal de Nível Superior (CAPES) for his PhD Grant (99999.000845/2014-00). The authors also thank Fundação para a Ciência e Tecnologia (Projects UID/MULTI/00612/2019, IF/01210/2014, and LISBOA-01-0145-FEDER-022125). Beatriz T. Barrocas acknowledges FCT for her PhD Grant (SFRH/BD/101220/2014).

References

Aymerich I, Acuña V, Barceló D, et al (2016) Attenuation of pharmaceuticals and their transformation products in a wastewater treatment plant and its receiving river ecosystem. Water Res 100:126–136. doi: 10.1016/j.watres.2016.04.022

Baker DR, Kasprzyk-Hordern B (2013) Spatial and temporal occurrence of pharmaceuticals and illicit drugs in the aqueous environment and during wastewater treatment: new developments. Sci Total Environ 454–455:442–56. doi: 10.1016/j.scitotenv.2013.03.043

Baker DR, Kasprzyk-Hordern B (2011) Multi-residue analysis of drugs of abuse in wastewater and surface water by solid-phase extraction and liquid chromatography-positive electrospray ionisation tandem mass spectrometry. J Chromatogr A 1218:1620–31. doi: 10.1016/j.chroma.2011.01.060

Barrocas B, Silvestre AJ, Rolo AG, Monteiro OC (2016) The effect of ionic Co presence on the structural, optical and photocatalytic properties of modified cobalt–titanate nanotubes. Phys Chem Chem Phys 18:18081–18093. doi: 10.1039/C6CP01889K

Barrocas BT, Oliveira MC, Nogueira HIS, et al (2019) Ruthenium-Modified Titanate Nanowires for the Photocatalytic Oxidative Removal of Organic Pollutants from Water. ACS Appl Nano Mater acsanm.8b02215. doi: 10.1021/acsanm.8b02215

Beretsou VG, Psoma AK, Gago-ferrero P, et al (2016) Identi fi cation of biotransformation products of citalopram formed in activated sludge. Water Res 103:205–214. doi: 10.1016/j.watres.2016.07.029

Boix C, Ibáñez M, Sancho J V., et al (2016) Biotransformation of pharmaceuticals in surface water and during waste water treatment: Identification and occurrence of transformation products. J Hazard Mater 302:175–187. doi: 10.1016/j.jhazmat.2015.09.053

Bomila R, Srinivasan S, Gunasekaran S, Manikandan A (2018) Enhanced photocatalytic degradation of methylene blue dye, opto-magnetic and antibacterial behaviour of pure and la-doped ZnO nanoparticles. J Supercond Nov Magn 31:855–864. doi: 10.1007/s10948-017-4261-8

Calza P, Sakkas VA, Villioti A, et al (2008) Multivariate experimental design for the photocatalytic degradation of imipramine. Determination of the reaction pathway and identification of intermediate products. Appl Catal B Environ 84:379–388. doi: 10.1016/j.apcatb.2008.04.015

Chen Y, Liang J, Liu L, et al (2017) Photosensitized Degradation of Amitriptyline and Its Active Metabolite Nortriptyline in Aqueous Fulvic Acid Solution. J Environ Qual 46:1081–1087. doi: 10.2134/jeq2017.05.0181

Escher BI, Baumgartner R, Koller M, et al (2011) Environmental toxicology and risk assessment of pharmaceuticals from hospital wastewater. Water Res 45:75–92. doi: 10.1016/j.watres.2010.08.019

Gnanasekaran L, Hemamalini R, Saravanan R, et al (2016) Intermediate state created by dopant ions (Mn, Co and Zr) into TiO2 nanoparticles for degradation of dyes under visible light. J Mol Liq 223:652–659. doi: 10.1016/j.molliq.2016.08.105

Kasprzyk-Hordern B, Dinsdale RM, Guwy AJ (2009) The removal of pharmaceuticals, personal care products, endocrine disruptors and illicit drugs during wastewater treatment and its impact on the quality of receiving waters. Water Res 43:363–80. doi: 10.1016/j.watres.2008.10.047

Li H, Sumarah MW, Topp E (2013) Persistence of the tricyclic antidepressant drugs amitriptyline and nortriptyline in agriculture soils. Environ Toxicol Chem 32:509–516. doi: 10.1002/etc.2112

Li Z, Sobek A, Radke M (2016) Fate of Pharmaceuticals and Their Transformation Products in Four Small European Rivers Receiving Treated Wastewater. Environ Sci Technol 50:5614–5621. doi: 10.1021/acs.est.5b06327

Osawa RA, Barrocas BT, Monteiro OC, et al (2019) Photocatalytic degradation of amitriptyline, trazodone and venlafaxine using modified cobalt-titanate nanowires under UV–Vis radiation: Transformation products and in silico toxicity. Chem Eng J 373:1338–1347. doi: 10.1016/j.cej.2019.05.137

Togola A, Budzinski H (2008) Multi-residue analysis of pharmaceutical compounds in aqueous samples. J Chromatogr A 1177:150–158. doi: 10.1016/j.chroma.2007.10.105

Zhang G, Hu X, Chiang CW, et al (2016) Anti-Markovnikov Oxidation of β-Alkyl Styrenes with H2O as the Terminal Oxidant. J Am Chem Soc 138:12037–12040. doi: 10.1021/jacs.6b07411

5.2. Conclusões

O estudo demonstrou que o uso do Co-TNW como fotocatalisador apresentou atividade fotocatalítica para o AMI e o VEN, tanto para misturas como para soluções únicas. Foi notado que o Co-TNW adsorveu o AMI na solução em cerca de 3% da concentração inicial e, durante a fotocatálise do AMI, houve a formação de oito TPs. Estes foram elucidados pela análise dos espectros MS/MS enquanto que na fotólise, somente quatro TPs foram identificados. A maior parte destes TPs foram degradados em menos de 90 min e apresentaram baixo potencial tóxico relativo em comparação com o AMI porém, a maioria dos valores para o parâmetro 96-h f. minnow LC_{50} foram classificados como altamente tóxicos.

Não foi observado o processo de adsorção do VEN no catalisador. Na degradação, foram formados cinco TPs durante a fotocatálise em comparação com somente dois durante a fotólise. Nas análises *in silico*, nenhum TP apresentou potencial mutagénico e somente um mostrou um maior potencial ecotóxico em comparação com o fármaco.

Para o TRA, o catalisador adsorveu aproximadamente 5% da concentração inicial, porém, não houve diferenças entre a fotocatálise e a fotólise. Sete TPs foram identificados, tendo apresentado baixa atividade fotocatalítica. Quatro TPs permaneceram presentes na solução após 2 horas de radiação UV−Vis, o que mostra que estes TPs são persistentes em processos de fotodegradação. Na análise in silico, todos os TPs resultaram em um potencial mutagénico positivo.

O experimento complementar da degradação do AMI sob radiação visível identificou nove TPs, sendo quatro somente foram identificados sob esse tipo de radiação. O AMI foi degradado em aproximadamente 40% sob a fotocatálise em comparação com 20% sob fotólise em 8 horas de radiação.

Estes estudos demonstraram a importância de analisar os TPs ao estudar processos de degradação, já que muitos podem apresentar persistência, mesmo após o poluente já ter sido eliminado no sistema. Catorze TPs nunca foram descritos na literatura e podem apresentar uma alta toxicidade logo, é essencial estudar possíveis complicações do ponto de vista ecotoxicológico.

5.3. Referências

1. Li, S., Hao, X., Dai, X., Tao, T., 2018. Rapid photocatalytic degradation of pollutant from water under uv and sunlight via cellulose nanofiber aerogel wrapped by TiO_2. *J. Nanomater*. 2018, 1–12. doi:10.1155/2018/8752015

2. Barrocas, B., Entradas, T.J., Nunes, C.D., Monteiro, O.C., 2017. Titanate nanofibers sensitized with ZnS and Ag_2S nanoparticles as novel photocatalysts for phenol removal. *Appl. Catal. B Environ.* 218, 709–720. doi:10.1016/j.apcatb.2017.06.089

3. Barrocas, B., Neves, M.C., Conceição Oliveira, M., Monteiro, O.C., 2018. Enhanced photocatalytic degradation of psychoactive substances using amine-modified elongated titanate nanostructures. *Environ. Sci. Nano*. 5, 350–361. doi:10.1039/C7EN00882A

4. Barrocas, B.T., Oliveira, M.C., Nogueira, H.I.S., Fateixam S., Monteiro, O.C., 2019. Ruthenium-modified titanate nanowires for the photocatalytic oxidative removal of organic pollutants from water. *ACS Appl. Nano Mater*. 2 (3), 1341–1349. doi:10.1021/acsanm.8b02215

5. Barrocas, B., Silvestre, A.J., Rolo, A.G., Monteiro, O.C., 2016. The effect of ionic Co presence on the structural, optical and photocatalytic properties of modified cobalt–titanate nanotubes. *Phys. Chem. Chem. Phys*. 18, 18081–18093. doi:10.1039/C6CP01889K

6. Kasprzyk-Hordern B., Dinsdale, R.M., Guwy, A.J., 2009. The removal of pharmaceuticals, personal care products, endocrine disruptors and illicit drugs during wastewater treatment and its impact on the quality of receiving waters. *Water Res*. 43, 363–80. doi:10.1016/j.watres.2008.10.047

7. Gracia-Lor, E., Sancho, J.V., Serrano, R., Hernández, F., 2012. Occurrence and removal of pharmaceuticals in wastewater treatment plants at the Spanish Mediterranean area of Valencia. *Chemosphere*. 87, 453–462. doi:10.1016/j.chemosphere.2011.12.025

8. Collado, N., Rodriguez-Mozaz, S., Gros, M., Rubirola, A., Barceló, D., Comas, J., Rodriguez-Roda, I., Buttiglieri, G., 2014. Pharmaceuticals occurrence in a WWTP with significant industrial contribution and its input into the river system. *Environ. Pollut*. 185, 202–212. doi:10.1016/j.envpol.2013.10.040

Capítulo 6

Degradação fotocatalítica da ciclofosfamida e ifosfamida em efluente por nanofios de titanato dopados com ruténio

6.1. Introdução

IF e CP são fármacos frequentemente prescritos para o tratamento do cancro e doenças auto-imunes. Por conta dos mecanismos farmacodinâmicos, estes fármacos apresentam genotoxicidade, mutagenicidade, citotoxicidade e teratogenicidade [1,2,3]. Como consequência são altamente perigosos no ambiente já que o seu consumo faz com que sejam detetados no meio ambiente. Vários estudos quantificaram estes fármacos em águas superficiais, efluentes domésticos e efluentes hospitalares [4,5,6], o que mostra que não são completamente eliminados nos sistemas de tratamento de efluentes.

Este estudo visa avaliar a eficácia da fotocatálise com nanofios de titanato modificados com ruténio (Ru-TNW) na remoção do IF e CP, utilizando efluente do tratamento secundário como matriz, coletado na ETAR de Alcântara, em Lisboa. Adicionalmente, os TPs formados foram elucidados por espectrometria de massa de alta resolução e foram realizadas predições de toxicidade por métodos QSARs. O fotocatalisador foi sintetizado e caracterizado pelo grupo de pesquisa liderado pela Prof. Dr. Olinda C. Monteiro do Centro de Química e Bioquímica da Faculdade de Ciências da Universidade de Lisboa [7]. Este fotocatalisador apresenta uma área de superfície específica (método B.E.T.) de 232,20 m^2 g^{-1} e energia de bandgap óptico de 3,64 eV. Os ensaios demonstraram que o RU-TNW apresentou alta atividade fotocatalítica para a remoção de cafeína e seus TPs.

Este capítulo é uma representação integral do artigo:

Osawa, R.A., Barrocas, BT., Monteiro, O.C., Oliveira, M.C., Florêncio, M.H., 2019. Photocatalytic degradation of cyclophosphamide and ifosfamide: Effects of wastewater matrix, transformation products and *in silico* toxicity prediction. *Sci. Total Environ*. 692, 503−510. doi:10.1016/j.scitotenv.2019.07.247

Science of the Total Environment 692 (2019) 503–510

Contents lists available at ScienceDirect

Science of the Total Environment

journal homepage: www.elsevier.com/locate/scitotenv

Photocatalytic degradation of cyclophosphamide and ifosfamide: Effects of wastewater matrix, transformation products and *in silico* toxicity prediction

Rodrigo A. Osawa [a,b,*], Beatriz T. Barrocas [a,c], Olinda C. Monteiro [a,c], M. Conceição Oliveira [d], M. Helena Florêncio [a,b]

[a] Centro de Química e Bioquímica, Faculdade de Ciências, Universidade de Lisboa, 1749-016 Lisboa, Portugal
[b] Laboratório de FTICR e Espectrometria de Massa Estrutural, Faculdade de Ciências, Universidade de Lisboa, 1749-016 Lisboa, Portugal
[c] Centro de Química Estrutural, Faculdade de Ciências, Universidade de Lisboa, 1749-016 Lisboa, Portugal
[d] Centro de Química Estrutural, Instituto Superior Técnico, Universidade de Lisboa, 1049-001 Lisboa, Portugal

HIGHLIGHTS

- Ru-TNW demonstrated photocatalytic activity for removal of alkylating agents.
- The degradation of alkylating agents followed the pseudo-first order kinetics.
- Four cyclophosphamide TPs and six ifosfamide TPs were proposed by HRMS.
- Toxicities of TPs were assessed by computation methods.

GRAPHICAL ABSTRACT

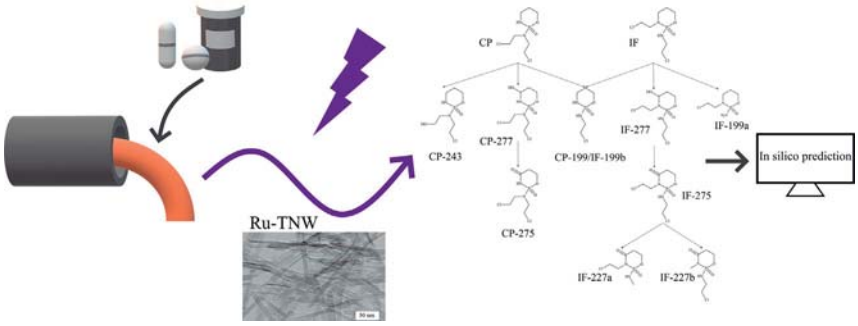

ARTICLE INFO

Article history:
Received 10 May 2019
Received in revised form 24 June 2019
Accepted 16 July 2019
Available online xxxx

Editor: Paola Verlicchi

Keywords:
Cytotoxic drugs
Photocatalysis
Wastewater
High-resolution mass spectrometry
Transformation products
In silico toxicity

ABSTRACT

Antineoplastic drugs have been identified in surface water and effluents from wastewater treatment and, once in the environment, may be harmful to aquatic organisms, as these compounds are possibly mutagenic, genotoxic, cytotoxic, carcinogenic and teratogenic. This work investigated the photodegradation of cyclophosphamide (CP) and ifosfamide (IF) using ruthenium doped titanate nanowires (Ru-TNW) in distilled water (DW) and in wastewater (WW) from secondary wastewater treatment, under UV–Vis radiation. The results indicated that Ru-TNW showed photocatalytic activity for the two cytotoxic drugs with the half-life ($t_{1/2}$) of 15.1 min for CP and 12.9 min for IF in WW. Four CP transformation products (TPs) and six IF TPs from the photodegradation process are here reported. These TPs were elucidated by high-resolution mass spectrometry. For both pollutants, the results showed different time profiles for the TPs when WW and DW were used as matrix. Overall, in the WW there was a higher production of TPs and two of them were detected only in this matrix. In other words, environmental matrices may produce different TPs. Degradation pathways were proposed and both drugs bear similarities. Additionally, *in silico* toxicity were performed by quantitative structure-activity relationship models. The predictions indicated that the TPs, with the exception of one IF TP, presented high mutagenic potential.

* Corresponding author at: Centro de Química e Bioquímica, Faculdade de Ciências, Universidade de Lisboa, 1749-016 Lisboa, Portugal.
E-mail address: raosawa@fc.ul.pt (R. A. Osawa).

https://doi.org/10.1016/j.scitotenv.2019.07.247
0048-9697/

1. Introduction

Pharmaceutical compounds have been detected in several environmental matrices. The main sources of these contaminations are effluents from domestic and hospital sewage treatment plants due to the inefficient removal of conventional wastewater treatment. Many of these contaminants may affect the aquatic ecosystem and consequently human health *via* drinking water or bioaccumulation in the food chain since they may present mutagenicity, genotoxicity, endocrine interference and development of resistance in microorganisms (Farré et al., 2008; Lai et al., 2015; Lonappan et al., 2016; Pereira et al., 2015; Wei et al., 2015). A group of drugs that have high toxic potential are antineoplastic agents, which are chemotherapeutic drugs that present genotoxicity, mutagenicity, cytotoxicity and teratogenicity (Ellenberger and Mohn, 1975; Witt and Bishop, 1996), which makes them highly hazardous in the environment (Besse et al., 2012; Kümmerer and Al-Ahmad, 2010).

Ifosfamide (IF) and cyclophosphamide (CP) are the most commonly prescribed alkylating agents for the treatment of cancers and autoimmune diseases that act directly on the DNA, causing inhibition of cell division and consequently cell death (Besse et al., 2012). The use of these drugs is reflected in their detection in environmental matrices, since pharmacokinetic studies have shown that the IF and CP are excreted unchanged in the urine in 61% and 10–20%, respectively (Wishart et al., 2018). Studies have identified IF and CP in surface waters (up to 41 ng L^{-1} for IF and up to 64 ng L^{-1} for CP), domestic wastewater (WW) (up to 2900 ng L^{-1} for IF and up to 17 ng L^{-1} for CP) and hospital WW (up to 6800 ng L^{-1} for IF and up to 22,000 for CP ng L^{-1}), in other words, the wastewater treatment plants (WWTPs) do not completely remove these drugs and thus they may reach the aquatic ecosystem (Česen et al., 2016b; Moldovan, 2006; Ternes et al., 1998; Valcárcel et al., 2011).

In the literature, several treatment technologies for the removal of these contaminants can be found. Lin et al. (2015) showed that ozonation can rapidly remove anticancer compounds at basic pH. Other study reported the low efficiency of removal of the IF and CP in a UV/H_2O_2 process (Wols et al., 2013). Kovalova et al. (2012) demonstrated poor CP removal using a membrane bioreactor in a hospital WWTP. Lai et al. (2015) demonstrated high IF removal efficiency using TiO_2 as a photocatalyst. Nevertheless, only few of these studies were focused on the formation of transformation products (TPs), compounds generated from the degradation of the parent compound by abiotic and biotic processes in WWTP and the environment. Thus, it is necessary to study new technologies for removal of these compounds and their TPs.

Photocatalysis is one of the most promising methods for the effective removal of contaminants in the environment. The use of TiO_2 as catalyst has been studied in the past because it is photoactive, chemically stable and inexpensive. However, its use is limited due to its low visible light absorption capacity. To overcome this limitation and to improve TiO_2 base materials photocatalytic performance, several studies have been reported, including methods of sensitization, doping or formation of nanocomposites (Ahmed et al., 2017; Barrocas et al., 2017; Senthilnathan and Philip, 2011; Zyoud et al., 2010).

Another important concern that is extremely relevant in pollutants removal processes is the toxicity of TPs that are formed during degradation. There are many studies on the behavior and toxicity effects of the antineoplastic drugs, while few are known regarding the TPs. And the fact is that TPs may exhibit different toxicity or persistence regarding the parent compound. One way of assessing toxicity is by the *in silico* method, which are computational tools to predict toxicity. The *in silico* method aims to complement *in vitro* and *in vivo* tests and has the advantage of not requiring the chemical standard since many TPs have limited available standards (Bakhtyari et al., 2013; Cao et al., 2018). One of the *in silico* models is based on quantitative structure-activity relationship (QSAR), which uses experimental or theoretical molecular descriptors to search for a relationship between chemical structure and biological activity. These models have limitations, which consists of parameters called applicability domain (AD).

This work aims to evaluate the efficiency of crystalline titanate nanowires modified with ruthenium (Ru-TNW) as photocatalyst in WW effluent samples for the removal of IF and CP under UV–Vis radiation, as well as to elucidate the TPs formed. According to our previous studies (Barrocas et al., 2019; Ylhäinen et al., 2012), the pristine titanate nanoparticles showed better results in the catalytic degradation of organic pollutants compared to nanocrystalline TiO_2. In addition, Ru-TNW demonstrated enhanced photocatalytic activity for the removal of caffeine and their TPs compared to pristine TNW. These studies demonstrated that this material can be seen as an excellent candidate to substitute TiO2 as photocatalyst. The TPs elucidation is based on the analysis of a mass spectrum obtained using an ultra-high performance liquid chromatography coupled to quadrupole time-of-flight mass spectrometry (UHPLC-QTOF). Toxicity was also predicted by means of QSARs models.

2. Materials and methods

2.1. Standards and reagents

The analytical standards of ifosfamide and cyclophosphamide monohydrate were purchased from Fluka (Buchs, Switzerland). LC-MS grade acetonitrile, formic acid and water were obtained from Fisher Scientific (Hampton, USA). Stock solutions were prepared using ultrapure water (Milli-Q ultrapure system, Barnstead International, Dubuque, USA) and stored at −80 °C.

2.2. Synthesis and characterization of Ru-TNW

The Ru-TNW sample was prepared by a hydrothermal approach using a Ru-containing amorphous precursor, as previously reported (Barrocas et al., 2019). This precursor was prepared using a $TiCl_3$ solution (20 wt% in 20–30 wt% HCl) diluted in a ratio of 1:2 in 2 M HCl solution with the required molar amount (1%) of ruthenium (as $RuCl_3$). To this solution, a 4 M ammonia solution was added drop-by-drop under vigorous stirring, until complete solid precipitation. This suspension was kept overnight at room temperature. The precipitate was filtered and washed with distilled water (DW) several times. The dark grey precursor thus obtained was used to produce the Ru-TNW sample. The synthesis was performed in an autoclave system (160 °C, 24 h) using 10 g of amorphous precursor in *ca.* 70 mL of a 10 M NaOH aqueous solution. After cooling to room temperature, the powder was washed several times with DW, until pH 7 of the filtrate solution, and it was afterward dried at 60 °C. The catalyst characterization was discussed in our previous work (Barrocas et al., 2019). This Ru-TNW sample has a specific surface area (B.E.T. method) of 232.20 $m^2\ g^{-1}$ and the optical bandgap energy of 3.64 eV. Furthermore, the photoluminescence characterization showed that the presence of Ru in this sample reduces the recombination rate due to effective electron-hole separation.

2.3. Photodegradation experiments

The experiments were conducted using a refrigerated photoreactor (Ace Glass, Vineland, USA). The radiation source was a 450 W medium-pressure mercury-vapor lamp (Hanovia, Slough, UK) with the total irradiated energy being 40–48% in the ultraviolet range and 40–43% in the visible region (Franco et al., 2009).

150 mL of working solution (DW or WW effluent from the secondary treatment) were spiked with 10 mg L^{-1} in single and mixture solutions of IF and CP. The WW stock solution was collected from the WWTP of Lisbon in amber bottles and stored at a temperature of 4 °C. The analysis of the physicochemical parameters of this solution (Table 1) was carried out in the laboratory of the Portuguese Environment Agency. The photodegradation experiments were initiated immediately after WW sampling. The pH of the DW samples was adjusted to 7.5 to be

equal to the WW samples. To evaluate the efficiency of the catalyst, 20 mg of the powder was added to the solution and in both matrices.

Before irradiation, the samples with catalyst were stirred in dark conditions for 1 h to reach the adsorption equilibrium. During irradiation, aliquots were withdrawn at regular intervals and the samples were centrifuged and filtered (nylon syringe filter, 0.22 μm) before being frozen for further analyses.

2.4. Instrumentation

Analyses were performed by Elute UHPLC system (Bruker Daltonics, Bremen, Germany) tandem Impact II QTOF mass spectrometer (Bruker Daltonics, Bremen, Germany) with electrospray ion source (ESI). The chromatographic separation was achieved using a Halo® C18 (5 μm particle size; 4.6 × 150 mm) (Advanced Materials Technology, Waltham, USA) reverse phase column at flow rate of 400 μL min^{-1} and injection volume of 10 μL. Ultrapure water acidified with 0.1% formic acid (A) and acetonitrile (B) were used as mobile phase and the gradient was: 0–1.5 min, 20% B; 1.5–10 min, 30% B; 10–13 min, 100% B; 13–17 min, 100% B; 17–18 min, 20% B and 18–25 min, 20% B.

The samples were ionized in positive ion mode mass spectra, with the following parameters being applied: nebulizer gas pressure (N_2), 2.8 bars; dry gas flow (N_2), 8 L min^{-1}; ion spray voltage, 2.5 kV; end plate offset, −500 V and dry heater temperature, 200 °C. Sodium formate 10 mM was used for internal calibration in the high-precision calibration mode (HPC) before each analysis. Compass DataAnalysis 4.1 software (Bruker Daltonics, Bremen, Germany) was used for data analysis.

For detection and identification of possible and suspicious TPs, a non-target approach was initially performed in full scan mode (MS) from 70 to 550 *m/z*. Then, the product ion scanning mode (MS/MS) was performed to obtain the structural information of the TPs.

2.5. In silico toxicity

The prediction of *in silico* toxicity was carried out by following free available tools: Ecological Structure-Activity Relationship (ECOSAR v1.1) to estimate ecotoxicity and VEGA platform (v1.1.4) to predict the mutagenic potential. ECOSAR is based on prediction of the toxicity by linear mathematical relationship between log K_{ow} values and toxicity values of a training set for each class, and our study considered the neutral organic values. Three endpoints were selected: fish 96-h LC_{50}, daphnid 48-h LC_{50} and green algae 96-h EC_{50}. The AD of this tool relates the log K_{ow} value to the solubility of the chemical compound. If log K_{ow} exceeds the set value, the compound is outside the AD. In VEGA platform the consensus method for the prediction of mutagenicity (Ames test) was adopted, this method consists in performing the prediction based on four QSARs models (CAESAR, SarPy, ISS and KNN). The AD ranges from 0 to 1, where values equal to 1 indicate positive mutagenicity as demonstrated by experimental data, above 0.9 have high reliability of being mutagenic and above 0.6 results in medium reliability. In this present study values of AD below 0.6 were considered as outside the AD.

Table 1
Physico-chemical parameters from WWTP secondary effluent.

Parameters	Value
pH	7.5
DOC (mg L^{-1})	11
NH_3 (mg L^{-1})	32
NO_3^- (mg L^{-1})	20
PO_4^{3-} (mg L^{-1})	1.3
SO_4^{2-} (mg L^{-1})	162

3. Results and discussion

3.1. Photodegradation kinetics of IF and CP

There was no adsorption of CP and IF on the surface of the photocatalyst during 1 h of exposure in the dark. This statement is in agreement with other studies, Ofiarska et al. (2016) demonstrated that there was no adsorption on the surface of the Pt-TiO_2 as a catalyst and Lai et al. (2015) also indicated that no adsorption of IF on TiO_2 occurred under dark conditions.

The photo-assisted degradation profiles of CP and IF, using DW and WW are presented in Fig. 1a—b. The photocatalytic experiments performed using DW were here used only to compare the degradation rates and the formation of TPs with the WW ones. A clear improvement on the degradation of CP and IF was observed using Ru-TNW as catalyst, especially when WW was used for solutions preparation. As expected, the results are better when the pollutants were used as single solutions. Considering 30 min as a time reference and using WW as matrix, an increase of 10% of CP degradation was observed for the photocatalysis when compared photolysis. For the same period but using a CP and IF mixture, this value increases to 14%.

Even considering that Ru-TNW is also catalytic for IF photo-assisted removal, the improvements on the degradation due to the catalyst presence are slightly lower for this pollutant compared to CP. For the single solution in WW conditions, there was an increase of 9% on IF degradation for the catalytic process. This value raises to 10.7% when a mixture solution was used.

These results are interesting since they indicate that Ru-TNW is catalytic for CP and IF photo-assisted degradation processes. More relevant is the fact that an enhancement on the relative catalytic performance of this catalyst was observed when a mixture of pollutants was used. Although we expected a better efficiency of the catalyst, as seen in our previous study (Barrocas et al., 2019), we believe that it was due the presence of dissolved organic matter, which may act as scavengers, by reacting with the oxidizing species in surface of the catalyst, reducing the efficiency of the rate of removal of the pollutants. As a matter of fact, Ye et al. (2019) reported a decrease in performance of photocatalytic degradation of pollutant using TiO_2 nanotube array with the addition of dissolved organic matter, however at certain concentrations of phosphate and bicarbonates the inhibitory effect of organic matter may be attenuated. Other studies have shown the effects of complex matrices on the photocatalysis of pollutants for which there was a lower removal rate when compared to the one of pure water (Antonopoulou et al., 2016; Rioja et al., 2016).

In order to evaluate the efficiency of Ru-TNW as a photocatalyst, the photodegradation kinetics parameters were calculated for CP and IF in single and mixture solutions in the two different matrices (DW and WW effluent from the secondary treatment). CP and IF degradations experiments followed the pseudo-first order kinetics and the degradation rate constant was obtained according to the Eq. (1):

$$\ln\frac{C}{C_0} = -k_r t \tag{1}$$

where C_0 is the initial concentration of the analyte, C is the concentration of the compound at time t and k_r is the degradation rate constant.

The half-lives ($t_{1/2}$) were determined from the Eq. (2):

$$t_{1/2} = \frac{\ln 2}{k_r} \tag{2}$$

Although the experiments lasted 2 h under UV–Vis radiation, for comparison purposes the pseudo-first order kinetic model was applied up to 1 h. Thus, both pharmaceutical compounds presented a correlation coefficient (r) above 0.99 (Table 2), which confirms that the pseudo-first order model fits into the photodegradation kinetics of

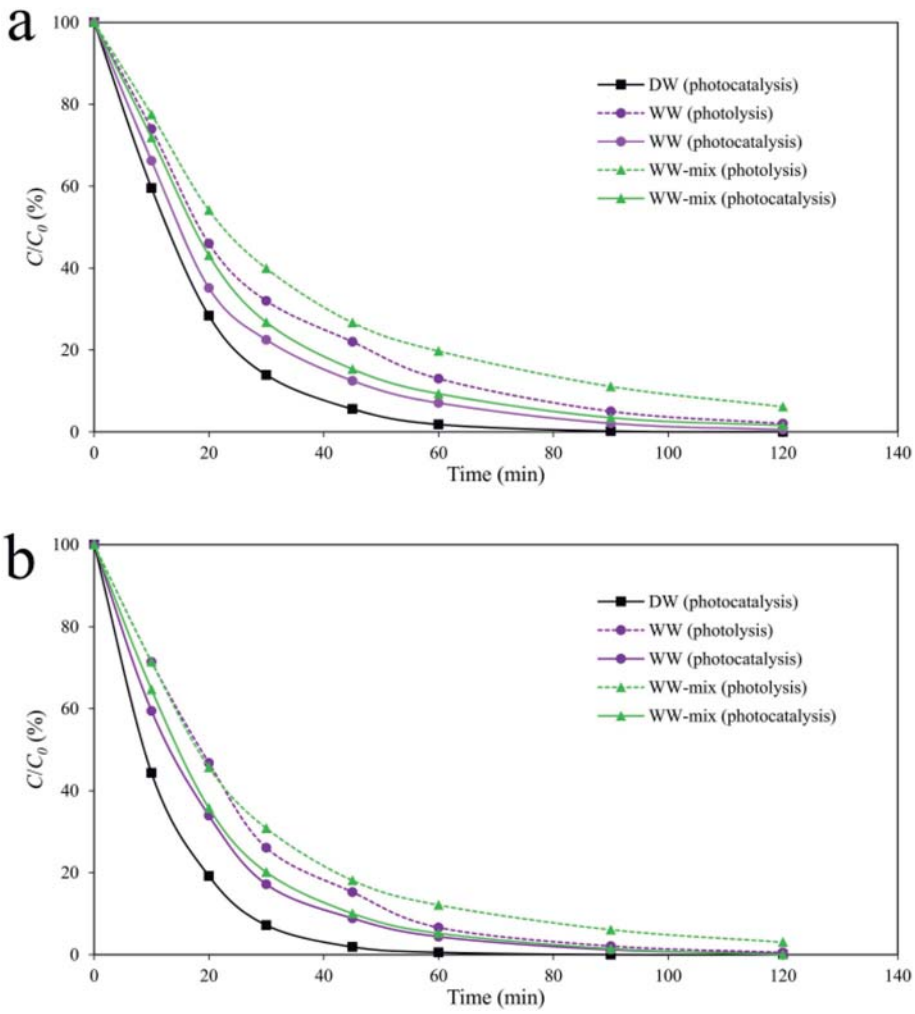

Fig. 1. Degradation profiles of (a) cyclophosphamide (CP) and (b) ifosfamide (IF) using distilled water (DW) and wastewater (WW) as matrices in single and mixture (mix) solutions.

these compounds. Therefore, it was found that for both matrices the IF had a rate of degradation higher than the CP one. The $t_{1/2}$ photodegradation of IF ranges from 8.0 min under photocatalysis for the single solution in DW to 18.9 min under photolysis for the mixture solution in WW. CP, $t_{1/2}$ photodegradation ranged from 10.6 to 24.4 min, for photocatalysis in DW and for photolysis in mixture solution in WW, respectively.

The results described above show the influence of the matrix in the degradation of both compounds. The complexity of a matrix as effluent may explain the degradation efficiency of the target compounds. In addition to determining the photodegradation of CP and IF, the study of the formation of their TPs during photolysis and photocatalysis was carried out.

Table 2
Photodegradation rate constants (k_r), correlation coefficients (r) and half-lives ($t_{1/2}$) of CP and IF in single and mixture solutions.

Compound	Degradation	Matrix	r	k_r (min^{-1})	$t_{1/2}$ (min)
CP	Photolysis	WW	0.992	0.0346	20.0
	Photocatalysis	DW	0.997	0.0655	10.6
		WW	0.992	0.0459	15.1
IF	Photolysis	WW	0.992	0.0436	15.9
	Photocatalysis	DW	0.999	0.0867	8.0
		WW	0.995	0.0536	12.9
CP -Mixture	Photolysis	WW	0.992	0.0284	24.4
	Photocatalysis	WW	0.994	0.0408	17.0
IF -Mixture	Photolysis	WW	0.994	0.0367	18.9
	Photocatalysis	WW	0.997	0.0503	13.8

3.2. Identification of CP and IF TPs

The results here discussed are about TPs formed in single solutions. Overall, four TPs originating from CP and six TPs from IF were identified. Using DW as matrix, the influence of Ru-TNW as catalyst was determined. All of CP TPs were identified in both processes: photolysis and photocatalysis, these TPs had a slightly higher degradation rate during photocatalysis with exception of CP-277, we believe that this TP was formed from CP. The analysis of the fragmentation patterns to elucidate the chemical structures is found in Section 3.2. In the degradation experiments using the WW as a matrix, CP-243 was not detected in photolysis and photocatalysis. Although CP-243 was not formed, the other TPs were not fully degraded in 2 h under UV–Vis radiation (Fig. 2a). In other words, besides the fact that the photodegradation rate of the parent compound is less effective in real matrices, the TPs may also be less degraded (Fig. 2b). In addition, CP-275 and CP-199 were found in hospital WW samples at concentrations up to 2100 ng L^{-1} and 178 ng L^{-1}, respectively, these TPs being metabolites of CP (Česen et al., 2016b).

The IF TPs identified in the experiments with DW under photolysis and under photocatalysis showed similar time profiles in both processes. Almost all TPs were degraded after 2 h with the exception of IF-275 as shown in Fig. 2c. Both IF-275 and CP-275, which are isomers, did not exhibit complete removal in these experiments. Furthermore,

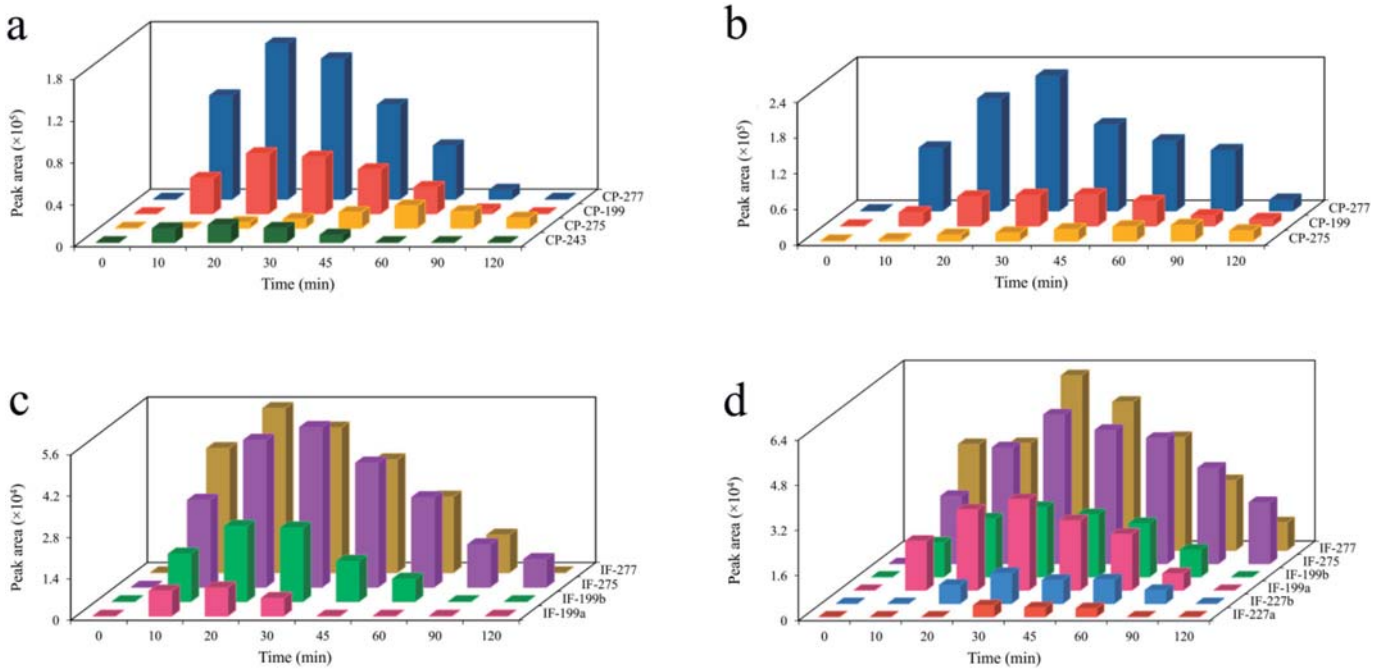

Fig. 2. Time profile of TPs during photocatalytic degradation of CP in (a) DW, (b) CP in WW, (c) IF in DW and (d) IF in WW.

two TPs were detected only in the experiments with WW: IF-227a and IF-227b (Fig. 2d).

Fig. 3 shows the degradation pathways we proposed for IF and CP. We believe that CP photodegraded into three TPs: CP-277, CP-243 and CP-199. Finally, CP-275 was formed from dehydrogenation of hydroxy group connect with the heterocyclic ring from CP-277. To the best of our knowledge, CP-243 has never been reported. The other three TPs (CP-199, CP-275 and CP-277) have already been identified in other works such as in (Lai et al., 2015) that when studying the photocatalysis with TiO_2 of CP detected five TPs, two of which are reported in the present study (CP-199 and CP-275). Another study (Lutterbeck et al., 2015) elucidated four TPs with experimental conditions similar to Lai et al. (2015) and two of those were detected in our study (CP-275 and CP-277). Ofiarska et al. (2016) identified two TPs when performing photocatalysis with Pt-TiO_2 but only one of them CP-275 was identified in the present study.

It has been proposed that IF photodegraded into three TPs: IF-277, IF-199a and IF-199b. Additionally, IF-277 degraded to IF-275 by dehydrogenation of hydroxy group. In the WW samples, we believe that IF-227a and IF-227b were generated from IF-275. In the literature, Česen et al. (2016b) identified four TPs by photodegradation under UV radiation, but in our study, we only identified two of these (IF-275 and IF-199). It is presumed that this difference can be due to the type of lamp used by Česen et al. (2016b), a low-pressure cooper UV lamp. One study reported eight IF TPs (Lai et al., 2015), three of which were identified in our study. It was noted that the studies by Lai et al. (2015) and Ofiarska et al. (2016) identified one TP of *m/z* 227, whereas in the present study two isomers were identified with *m/z* 227: IF-227a and IF-227b, however, we proposed different structures for these TPs. These studies have demonstrated that the type of photocatalyst and matrix should be regarded since they may generate different TPs. Table 3 shows the products ions in the MS/MS spectra, which are analysed in below for the identification of the structures of the TPs.

It has been suggested that CP-243 was formed by replacing the chlorine atom with the hydroxy group from the CP molecule. In the MS/MS spectrum (Fig. S1), loss of H_2O was detected at *m/z* 225 ($C_7H_{15}ClN_2O_2P^+$) from precursor ion at *m/z* 243 ($C_7H_{17}ClN_2O_3P^+$), which corroborates the formation of a hydroxy group. In theory, the OH group could be bound in the heterocyclic group, but this possibility is improbable due to the loss of ethanol (C_2H_6O) leading to *m/z* 197 ($C_5H_{11}ClN_2O_2P^+$) from *m/z* 243, which is only plausible after replacing the chlorine atom by the OH group.

The CP-277 was generated by hydroxylation of CP. The elimination of H_2O at *m/z* 259 ($C_7H_{14}Cl_2N_2O_2^+$) from precursor ion at *m/z* 277 ($C_7H_{16}Cl_2N_2O_3P^+$), it was verified in the MS/MS spectrum (Fig. S2), confirm that a hydroxylation reaction occurred. Hypothetically, hydroxylation could have occurred in the chloroethane groups but no loss of chloroethene or chloroethanol were detected. Therefore, it was assumed that the OH group was attached to the heterocyclic group. However, it was not possible to predict the exact position of the hydroxylation process. It was assumed that this TP is a metabolite, named 4-hydroxycyclophosphamide (Li et al., 2010), thus, the OH was linked to 4-position of the heterocyclic group.

It was assumed that CP-275 was generated from dehydrogenation of the hydroxy group of CP-277. To corroborate this assumption, neutral losses of C_2H_4 plus CO were identified from the precursor ion at *m/z* 275 ($C_7H_{14}Cl_2N_2O_3^+$) to *m/z* 221 ($C_4H_{12}Cl_2N_2O_2P^+$) (Fig. S3), the loss of CO may indicate oxidation, possibly in the heterocyclic ring. The CP-277 is a metabolite (4-Ketocyclophosphamide) as reported by Liu et al. (2005) and Li et al. (2010).

It was considered that CP-199 was formed by loss of the chloroethane group from CP This TP is a CP metabolite named N-dechloroethylcyclophosphamide and along with IF-199a and IF-199b are isomers. We believe that IF-199a and IF-199b lost the chloroethane group from the parent compound and, as observed, the IF has two chloroethane groups in its chemical structure. By the analysis of the fragments, it was not possible to identify the structures of these TPs (Figs. S4 and S5). However, it was concluded that IF-199b has the same structure as CP-199 because it has the same chromatographic retention time. Both TPs were reported as IF metabolites (Li et al., 2010).

IF-277 was generated from the hydroxylation of IF and is an isomer of CP-277 thus, the fragmentation patterns were similar to the ones of CP-275. Analysis of the MS/MS spectrum (Fig. S6) allows identifying the loss of H_2O at *m/z* 259 ($C_7H_{14}Cl_2N_2O_2P^+$) from precursor ion, *m/z* 277 ($C_7H_{16}Cl_2N_2O_3P^+$), which is an indication of the addition of OH in the structure of the molecule. IF-277 is a metabolite named 4-Hydroxyifosfamide (Li et al., 2010).

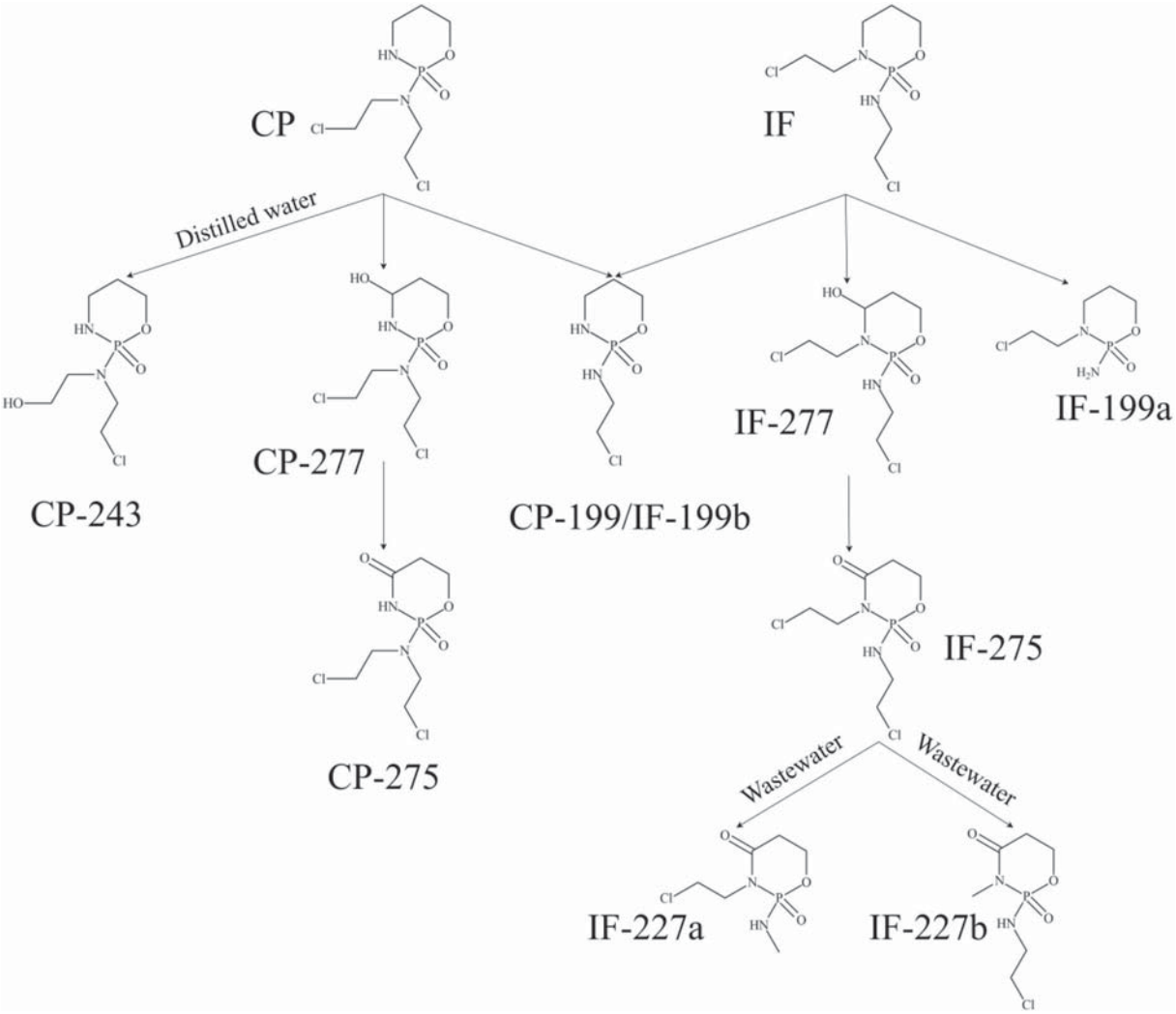

Fig. 3. Proposed photodegradation pathways for IF and CP.

The IF-275 has the same molecular mass as CP-275 and presents similar fragmentation patterns in MS/MS spectrum (Fig. S7) thus, it has been suggested that IF-275 was produced by dehydrogenation of the hydroxy group of IF-277. The loss of CO of *m/z* 213 ($C_5H_{11}ClN_2O_3P^+$) to *m/z* 185 ($C_4H_{11}ClN_2O_2P^+$) may corroborate this assumption and IF-275 is a metabolite (4-Ketoifosfamide) (Li et al., 2010).

IF-227a and IF-227b are isomers and in the MS/MS spectra, both showed similar ion fragmentation (Figs. S8 and S9). It was assumed that these TPs were formed from the loss of chloromethane from IF-275. The main characteristic to elucidate these TPs structures was through the *m/z* 141 ($C_2H_6ClNO_2P^+$) of IF-227b since this fragment ion shows the loss of C_4H_7NO from precursor ion ($C_6H_{13}ClN_2O_3P^+$), which is only possible with the loss of chloromethane from the aliphatic chain attached to oxazaphosphinane. Therefore, IF-227a formed with loss of chloromethane that is bound to the aliphatic chain with nitrogen. *In silico* toxicity was applied to elucidated TPs to identify their toxic potential in the environment (Section 3.3).

3.3. In silico toxicity

In silico ecotoxicity was performed by ECOSAR tool using three endpoints: fish 96-h LC_{50}, daphnid 48-h LC_{50} and green algae 96-h EC_{50} (Table 4). The toxicity values of each endpoint were classified according to the functional groups of the compound. In this study, the choice of functional group was based on the closest values found in the literature, not necessarily in the group with lowest values. Białk-Bielińska et al. (2017) reported concentrations up to 100 mg L^{-1} of IF and CP that were non-toxic to *V. fischeri* 30-min EC_{50}, *R. supcapitata* 72-h EC_{50} and *D. magna* 48-h EC_{50}. Another study concluded that CP presented EC_{50} values above 1000 mg L^{-1} for *P. putida* (16-h) and *D. magna* (48-h) and value of 930 mg L^{-1} for *P. subcapitata* (96-h) (Zounková et al., 2007). Russo et al. (2018) demonstrated that CP metabolites (CP-275 and CP-199/IF-199b) had no toxic effects at concentrations up to 100 mg L^{-1} for *C. dubia*, *B. calyciflorus* and *T. platyurus* whereas CP and IF were toxic to these organisms at concentrations above 986 mg L^{-1} and 196 mg L^{-1}, respectively. Based on these data, where concentrations to cause some toxic effect were above 100 mg L^{-1}, the values estimated by the *in silico* tool ranged from 139 to 4210 mg L^{-1} for fish endpoint, 322 to 12,800 mg L^{-1} for daphnid endpoint and for the green algae endpoint, the predictions were 161–9500 mg L^{-1}. It was noted that the TPs had lower toxic potential than parent compounds. However, in environmental matrices, these contaminants may have toxic effects potentiated, a study showing that a mixture of CP, IF and some metabolites resulted in an EC_{50} of 11.5 mg L^{-1} for *S. leopoliensis* (Česen et al., 2016a).

CP and IF are mutagenic, genotoxic and teratogenic (Ellenberger and Mohn, 1975; Witt and Bishop, 1996) and in the literature, it has been reported that some metabolites also have potential mutagenicity, according to Hales (1982) and Winckler et al. (1984), CP-277 and CP-275 demonstrated high mutagenic potential. However, Česen et al.

Table 3
Product ions identified in the MS/MS spectra of TPs with retention time (Rt) and relative error (ppm).

TP	Rt	Molecular mass (*m/z*)	Elemental formula $[M + H]^+$	Relative error (ppm)
CP-199/IF-199b	4.57	199.0398	$C_5H_{13}ClN_2O_2P$	−4.5
		171.0085	$C_3H_9ClN_2O_2P$	0
		141.9819	$C_2H_6ClNO_2P$	−3.5
CP-243	4.47	243.0660	$C_7H_{17}ClN_2O_3P$	−2.0
		225.0554	$C_7H_{15}ClN_2O_2P$	0.4
		197.0241	$C_5H_{11}ClN_2O_2P$	−2.0
		186.0081	$C_4H_{10}ClNO_3P$	0.5
		167.9976	$C_4H_8ClNO_2P$	−1.2
CP-275	5.81	275.0114	$C_7H_{14}Cl_2N_2O_3P$	−0.7
		259.0164	$C_7H_{14}Cl_2N_2O_2P$	−2.3
		221.0008	$C_4H_{12}Cl_2N_2O_2P$	−1.8
		213.0190	$C_5H_{11}ClN_2O_3P$	−1.4
		203.9742	$C_4H_9Cl_2NO_2P$	−2.4
		141.9821	$C_3H_6Cl_2NO$	1.4
CP-277	5.67	277.0270	$C_7H_{16}Cl_2N_2O_3P$	4.0
		259.0164	$C_7H_{14}Cl_2N_2O_2P$	−1.5
		221.0008	$C_4H_{12}Cl_2N_2O_2P$	−0.4
		203.9742	$C_4H_9Cl_2NO_2P$	0
		159.0086	$C_3H_9Cl_2N_2O$	0.6
IF-199a	4.37	199.0398	$C_5H_{13}ClN_2O_2P$	−3.5
		171.0085	$C_3H_9ClN_2O_2P$	−4.6
		153.9819	$C_3H_6ClNO_2P$	3.2
IF-227a	4.46	227.0347	$C_6H_{13}ClN_2O_3P$	0
		200.0238	$C_5H_{12}ClNO_3P$	0.5
		171.9925	$C_3H_8ClNO_3P$	2.9
		153.9819	$C_3H_6ClNO_2P$	−0.6
IF-227b	4.61	227.0347	$C_6H_{13}ClN_2O_3P$	0
		200.0238	$C_5H_{12}ClNO_3P$	−0.5
		171.9925	$C_3H_8ClNO_3P$	−0.6
		159.9928	$C_6H_5ClO_3$	−0.6
		141.9819	$C_2H_6ClNO_2P$	4.9
IF-275	6.04	275.0114	$C_7H_{14}Cl_2N_2O_3P$	2.9
		239.0347	$C_7H_{13}ClN_2O_3P$	−0.8
		221.0008	$C_4H_{12}Cl_2N_2O_2P$	0.9
		213.0190	$C_5H_{11}ClN_2O_3P$	−0.5
		185.0241	$C_4H_{11}ClN_2O_2P$	1.6
		141.9821	$C_3H_6Cl_2NO$	3.5
IF-277	5.47	277.0270	$C_7H_{16}Cl_2N_2O_3P$	−1.4
		259.0164	$C_7H_{14}Cl_2N_2O_2P$	3.8
		221.0008	$C_4H_{12}Cl_2N_2O_2P$	0.4
		182.0132	$C_5H_{10}ClNO_2P$	−3.8
		159.9922	$C_6H_5ClO_3$	3.1

(2016a) reported that there were no genotoxic effects without metabolic activation in IF, CP and most metabolites when single or in a mixture. In contrast, a mixture of fourteen cytotoxic drugs showed positive results for mutagenicity, assuming a synergistic effect (Chouquet et al., 2018). In our *in silico* result, all TPs showed mutagenic potential with the exception of IF-199a. To summarize, TPs formed by photodegradation may also be harmful to aquatic organisms, as synergies between contaminants may occur.

Table 4
Ecotoxicity and mutagenicity prediction of CP, IF and their TPs. The mutagenicity value of 1 indicates mutagenic prediction by experimental data.

Compound	Fish 96-h LC_{50} (mg L^{-1})	Daphnid 48-h LC_{50} (mg L^{-1})	Green algae 96-h EC_{50} (mg L^{-1})	Mutagenicity
CP	139	322	161	1
CP-243	1300	3630	2390	0.82
CP-275	572	[a]	870	1
CP-277	1170	3190	2040	1
CP-199/IF-199b	600	1600	983	0.82
IF	139	322	161	1
IF-199a	600	1600	983	[a]
IF-227a	1280	3600	2380	0.82
IF-227b	1280	3600	2380	0.82
IF-275	4210	12,800	9500	0.82
IF-277	1170	3190	2040	0.82

[a] Prediction outside the AD.

4. Conclusions

Photocatalytic degradation of CP and IF under UV–Vis radiation in two different matrices were studied. Using Ru-TNW as photocatalyst, the degradation of both compounds presented a higher removal rate independently on the matrix used, DW and WW from secondary treatment. In the mixture with the WW, the $t_{1/2}$ of the CP was 24.4 min during photolysis and 17.0 min in the photocatalysis whereas for the IF it was 18.9 min in the photolysis and 13.8 min during the photocatalysis.

In addition, four CP TPs and six IF TPs were elucidated by analyses of their MS/MS spectra obtained by UHPLC-QTOF. To the best of our knowledge, four TPs have never been described in degradation studies (CP-243, IF-199a, IF-227a and IF-227b). Pathways of their degradation are here proposed. The TPs showed different time profiles under photocatalytic conditions due to the matrices. Some of these TPs are human metabolites and can also be formed by abiotic processes. In addition, IF-227a and IF-227b were only detected in this matrix whereas CP-243 was only formed when DW was used. In other words, it is fundamental that in photodegradation studies, the experimental conditions approach the ones of environmental systems, to better understand the degradation pathways of pollutants.

Finally, *in silico* toxicity was performed for the two drugs and their TPs. The ecotoxicity prediction showed that TPs had low toxic potential on aquatic organisms. However, most of TPs resulted in positive mutagenicity, thus experimental data (*in vivo* assays) in environmental conditions are essential to confirm these predictions. For future studies, we intend to perform the photocatalytic experiments under solar radiation, verify if the same TPs are formed in this condition and analyze the nutrient removal in the effluent.

Acknowledgments

Rodrigo A. Osawa acknowledges Brazilian Federal Agency Coordenação de Aperfeiçoamento de Pessoal de Nível Superior (CAPES) for your PhD Grant (BEX 0845/14-0). Beatriz T. Barrocas acknowledges Fundação para a Ciência e a Tecnologia (FCT) for her PhD Grant (SFRH/BD/101220/2014). The authors also thank FCT (Projects UID/MULTI/00612/2019, PEst-OE/QUI/UI0612/2013, IF/01210/2014, and LISBOA-01-0145-FEDER-022125).

Appendix A. Supplementary data

Supplementary data to this article can be found online at https://doi.org/10.1016/j.scitotenv.2019.07.247.

References

Ahmed, M.A., Abou-Gamra, Z.M., Medien, H.A.A., Hamza, M.A., 2017. Effect of porphyrin on photocatalytic activity of TiO_2 nanoparticles toward Rhodamine B photodegradation. J. Photochem. Photobiol. B Biol. 176, 25–35. https://doi.org/10.1016/j.jphotobiol.2017.09.016.

Antonopoulou, M., Hela, D., Konstantinou, I., 2016. Photocatalytic degradation kinetics, mechanism and ecotoxicity assessment of tramadol metabolites in aqueous TiO_2 suspensions. Sci. Total Environ. 545–546, 476–485. https://doi.org/10.1016/j.scitotenv.2015.12.088.

Bakhtyari, N.G., Raitano, G., Benfenati, E., Martin, T., Young, D., 2013. Comparison of in silico models for prediction of mutagenicity. J. Environ. Sci. Health C Environ. Carcinog. Ecotoxicol. Rev. 31, 45–66. https://doi.org/10.1080/10590501.2013.763576.

Barrocas, B., Entradas, T.J., Nunes, C.D., Monteiro, O.C., 2017. Titanate nanofibers sensitized with ZnS and Ag_2S nanoparticles as novel photocatalysts for phenol removal. Appl. Catal. B Environ. 218, 709–720. https://doi.org/10.1016/j.apcatb.2017.06.089.

Barrocas, B.T., Oliveira, M.C., Nogueira, H.I.S., Fateixa, S., Monteiro, O.C., 2019. Ruthenium-modified titanate nanowires for the photocatalytic oxidative removal of organic pollutants from water. ACS Appl. Nano Mater. 2, 1341–1349. https://doi.org/10.1021/acsanm.8b02215.

Besse, J.-P., Latour, J.-F., Garric, J., 2012. Anticancer drugs in surface waters: what can we say about the occurrence and environmental significance of cytotoxic, cytostatic and

endocrine therapy drugs? Environ. Int. 39, 73–86. https://doi.org/10.1016/j.envint.2011.10.002.
Białk-Bielińska, A., Mulkiewicz, E., Stokowski, M., Stolte, S., Stepnowski, P., 2017. Acute aquatic toxicity assessment of six anti-cancer drugs and one metabolite using biotest battery – biological effects and stability under test conditions. Chemosphere 189, 689–698. https://doi.org/10.1016/j.chemosphere.2017.08.174.
Cao, Q., Liu, L., Yang, H., Cai, Y., Li, W., Liu, G., Lee, P.W., Tang, Y., 2018. In silico estimation of chemical aquatic toxicity on crustaceans using chemical category methods. Environ. Sci.: Processes Impacts 20, 1234–1243. https://doi.org/10.1039/c8em00220g.
Česen, M., Eleršek, T., Novak, M., Žegura, B., Kosjek, T., Filipič, M., Heath, E., 2016a. Ecotoxicity and genotoxicity of cyclophosphamide, ifosfamide, their metabolites/transformation products and their mixtures. Environ. Pollut. 210, 192–201. https://doi.org/10.1016/j.envpol.2015.12.017.
Česen, M., Kosjek, T., Busetti, F., Kompare, B., Heath, E., 2016b. Human metabolites and transformation products of cyclophosphamide and ifosfamide: analysis, occurrence and formation during abiotic treatments. Environ. Sci. Pollut. Res. 23, 11209–11223. https://doi.org/10.1007/s11356-016-6321-1.
Chouquet, T., Acramel, A., Sauvageon, H., Plé, A., Jourdan, N., Madelaine, I., Faure, P., Mourah, S., Goldwirt, L., 2018. Mutagenicity assessment of environmental contaminations in a hospital centralized reconstitution unit. Ecotoxicol. Environ. Saf. 165, 174–181. https://doi.org/10.1016/j.ecoenv.2018.09.002.
Ellenberger, J., Mohn, G., 1975. Mutagenic activity of cyclophosphamide, ifosfamide, and trofosfamide in different genes of Escherichia coli and Salmonella typhimurium after biotransformation through extracts of rodent liver. Arch. Toxikol. 33, 225–240. https://doi.org/10.1007/BF00311275.
Farré, M. la, Pérez, S., Kantiani, L., Barceló, D., 2008. Fate and toxicity of emerging pollutants, their metabolites and transformation products in the aquatic environment. TrAC Trends Anal. Chem. 27, 991–1007. https://doi.org/10.1016/j.trac.2008.09.010.
Franco, A., Neves, M.C., Carrott, M.M.L.R., Mendonça, M.H., Pereira, M.I., Monteiro, O.C., 2009. Photocatalytic decolorization of methylene blue in the presence of TiO_2/ZnS nanocomposites. J. Hazard. Mater. 161, 545–550. https://doi.org/10.1016/j.jhazmat.2008.03.133.
Hales, B.F., 1982. Comparison of the mutagenicity and teratogenicity of cyclophosphamide and its active metabolites, 4-Hydroxycyclophosphamide, phosphoramide mustard, and acrolein. Cancer Res. 42, 3016–3021.
Kovalova, L., Siegrist, H., Singer, H., Wittmer, A., McArdell, C.S., 2012. Hospital wastewater treatment by membrane bioreactor: performance and efficiency for organic micropollutant elimination. Environ. Sci. Technol. 46, 1536–1545. https://doi.org/10.1021/es203495d.
Kümmerer, K., Al-Ahmad, A., 2010. Estimation of the cancer risk to humans resulting from the presence of cyclophosphamide and ifosfamide in surface water. Environ. Sci. Pollut. Res. 17, 486–496. https://doi.org/10.1007/s11356-009-0195-4.
Lai, W.W.P., Lin, H.H.H., Lin, A.Y.C., 2015. TiO_2 photocatalytic degradation and transformation of oxazaphosphorine drugs in an aqueous environment. J. Hazard. Mater. 287, 133–141. https://doi.org/10.1016/j.jhazmat.2015.01.045.
Li, F., Patterson, A.D., Höfer, C.C., Krausz, K.W., Gonzalez, F.J., Idle, J.R., 2010. Comparative metabolism of cyclophosphamide and ifosfamide in the mouse using UPLC-ESI-QTOFMS-based metabolomics. Biochem. Pharmacol. 80, 1063–1074. https://doi.org/10.1016/j.bcp.2010.06.002.
Lin, A.Y.-C., Hsueh, J.H.-F., Hong, P.K.A., 2015. Removal of antineoplastic drugs cyclophosphamide, ifosfamide, and 5-fluorouracil and a vasodilator drug pentoxifylline from wastewaters by ozonation. Environ. Sci. Pollut. Res. 22, 508–515. https://doi.org/10.1007/s11356-014-3288-7.
Liu, Z., Chan, K.K., Wang, J.J., 2005. Tandem mass spectrometric analysis of cyclophosphamide, ifosfamide and their metabolites. Rapid Commun. Mass Spectrom. 19, 2581–2590. https://doi.org/10.1002/rcm.2099.
Lonappan, L., Brar, S.K., Das, R.K., Verma, M., Surampalli, R.Y., 2016. Diclofenac and its transformation products: environmental occurrence and toxicity - a review. Environ. Int. 96, 127–138. https://doi.org/10.1016/j.envint.2016.09.014.
Lutterbeck, C.A., Machado, Ê.L., Kümmerer, K., 2015. Photodegradation of the antineoplastic cyclophosphamide: a comparative study of the efficiencies of UV/H_2O_2, UV/Fe^{2+}/H_2O_2 and UV/TiO_2 processes. Chemosphere 120, 538–546. https://doi.org/10.1016/j.chemosphere.2014.08.076.
Moldovan, Z., 2006. Occurrences of pharmaceutical and personal care products as micropollutants in rivers from Romania. Chemosphere 64, 1808–1817. https://doi.org/10.1016/j.chemosphere.2006.02.003.
Ofiarska, A., Pieczyńska, A., Fiszka Borzyszkowska, A., Stepnowski, P., Siedlecka, E.M., 2016. Pt-TiO_2-assisted photocatalytic degradation of the cytostatic drugs ifosfamide and cyclophosphamide under artificial sunlight. Chem. Eng. J. 285, 417–427. https://doi.org/10.1016/j.cej.2015.09.109.
Pereira, L.C., de Souza, A.O., Bernardes, M.F.F., Pazin, M., Tasso, M.J., Pereira, P.H., Dorta, D.J., 2015. A perspective on the potential risks of emerging contaminants to human and environmental health. Environ. Sci. Pollut. Res. 22, 13800–13823. https://doi.org/10.1007/s11356-015-4896-6.
Rioja, N., Zorita, S., Peñas, F.J., 2016. Effect of water matrix on photocatalytic degradation and general kinetic modeling. Appl. Catal. B Environ. 180, 330–335. https://doi.org/10.1016/j.apcatb.2015.06.038.
Russo, C., Lavorgna, M., Česen, M., Kosjek, T., Heath, E., Isidori, M., 2018. Evaluation of acute and chronic ecotoxicity of cyclophosphamide, ifosfamide, their metabolites/transformation products and UV treated samples. Environ. Pollut. 233, 356–363. https://doi.org/10.1016/j.envpol.2017.10.066.
Senthilnathan, J., Philip, L., 2011. Photodegradation of methyl parathion and dichlorvos from drinking water with N-doped TiO_2 under solar radiation. Chem. Eng. J. 172, 678–688. https://doi.org/10.1016/j.cej.2011.06.035.
Ternes, T.A., Hirsch, R., Mueller, J., 1998. Methods for the determination of neutral drugs as well as betablockers and 2-sympathomimetics in aqueous matrices using GC/MS and LC/MS/MS. Fresenius J. Anal. Chem. 362, 329–340. https://doi.org/10.1007/s002160051083.
Valcárcel, Y., González Alonso, S., Rodríguez-Gil, J.L., Gil, A., Catalá, M., 2011. Detection of pharmaceutically active compounds in the rivers and tap water of the Madrid region (Spain) and potential ecotoxicological risk. Chemosphere 84, 1336–1348. https://doi.org/10.1016/j.chemosphere.2011.05.014.
Wei, G.L., Li, D.Q., Zhuo, M.N., Liao, Y.S., Xie, Z.Y., Guo, T.L., Li, J.J., Zhang, S.Y., Liang, Z.Q., 2015. Organophosphorus flame retardants and plasticizers: sources, occurrence, toxicity and human exposure. Environ. Pollut. 196, 29–46. https://doi.org/10.1016/j.envpol.2014.09.012.
Winckler, K., Madle, S., Nau, H., 1984. Metabolites in Salmonella typhimurium, human peripheral lymphocytes and Chinese hamster ovary cells. Mutat. Res. 129, 47–55.
Wishart, D.S., Feunang, Y.D., Guo, A.C., Lo, E.J., Marcu, A., Grant, J.R., Sajed, T., Johnson, D., Li, C., Sayeeda, Z., Assempour, N., Iynkkaran, I., Liu, Y., Maciejewski, A., Gale, N., Wilson, A., Chin, L., Cummings, R., Le, D., Pon, A., Knox, C., Wilson, M., 2018. DrugBank 5.0: a major update to the DrugBank database for 2018. Nucleic Acids Res. 46, D1074–D1082. https://doi.org/10.1093/nar/gkx1037.
Witt, K.L., Bishop, J.B., 1996. Mutagenicity of anticancer drugs in mammalian germ cells. Mutat. Res. Fundam. Mol. Mech. Mutagen. 355, 209–234. https://doi.org/10.1016/0027-5107(96)00029-2.
Wols, B.A., Hofman-Caris, C.H.M., Harmsen, D.J.H., Beerendonk, E.F., 2013. Degradation of 40 selected pharmaceuticals by UV/H_2O_2. Water Res. 47, 5876–5888. https://doi.org/10.1016/j.watres.2013.07.008.
Ye, Y., Bruning, H., Liu, W., Rijnaarts, H., Yntema, D., 2019. Effect of dissolved natural organic matter on the photocatalytic micropollutant removal performance of TiO_2 nanotube array. J. Photochem. Photobiol. A Chem. 371, 216–222. https://doi.org/10.1016/j.jphotochem.2018.11.012.
Ylhäinen, E.K., Nunes, M.R., Silvestre, A.J., Monteiro, O.C., 2012. Synthesis of titanate nanostructures using amorphous precursor material and their adsorption/photocatalytic properties. J. Mater. Sci. 47, 4305–4312. https://doi.org/10.1007/s10853-012-6281-x.
Zounková, R., Odráška, P., Dolealová, L., Hilscherová, K., Maršálek, B., Bláha, L., 2007. Ecotoxicity and genotoxicity assessment of cytostatic pharmaceuticals. Environ. Toxicol. Chem. 26, 2208–2214. https://doi.org/10.1897/07-137R.1.
Zyoud, A.H., Zaatar, N., Saadeddin, I., Ali, C., Park, D.H., Campet, G., Hilal, H.S., 2010. CdS-sensitized TiO_2 in phenazopyridine photo-degradation: catalyst efficiency, stability and feasibility assessment. J. Hazard. Mater. 173, 318–325. https://doi.org/10.1016/j.jhazmat.2009.08.093.

Appendix A. Supplementary data

Photocatalytic degradation of cyclophosphamide and ifosfamide: Effects of wastewater matrix, transformation products and *in silico* toxicity prediction

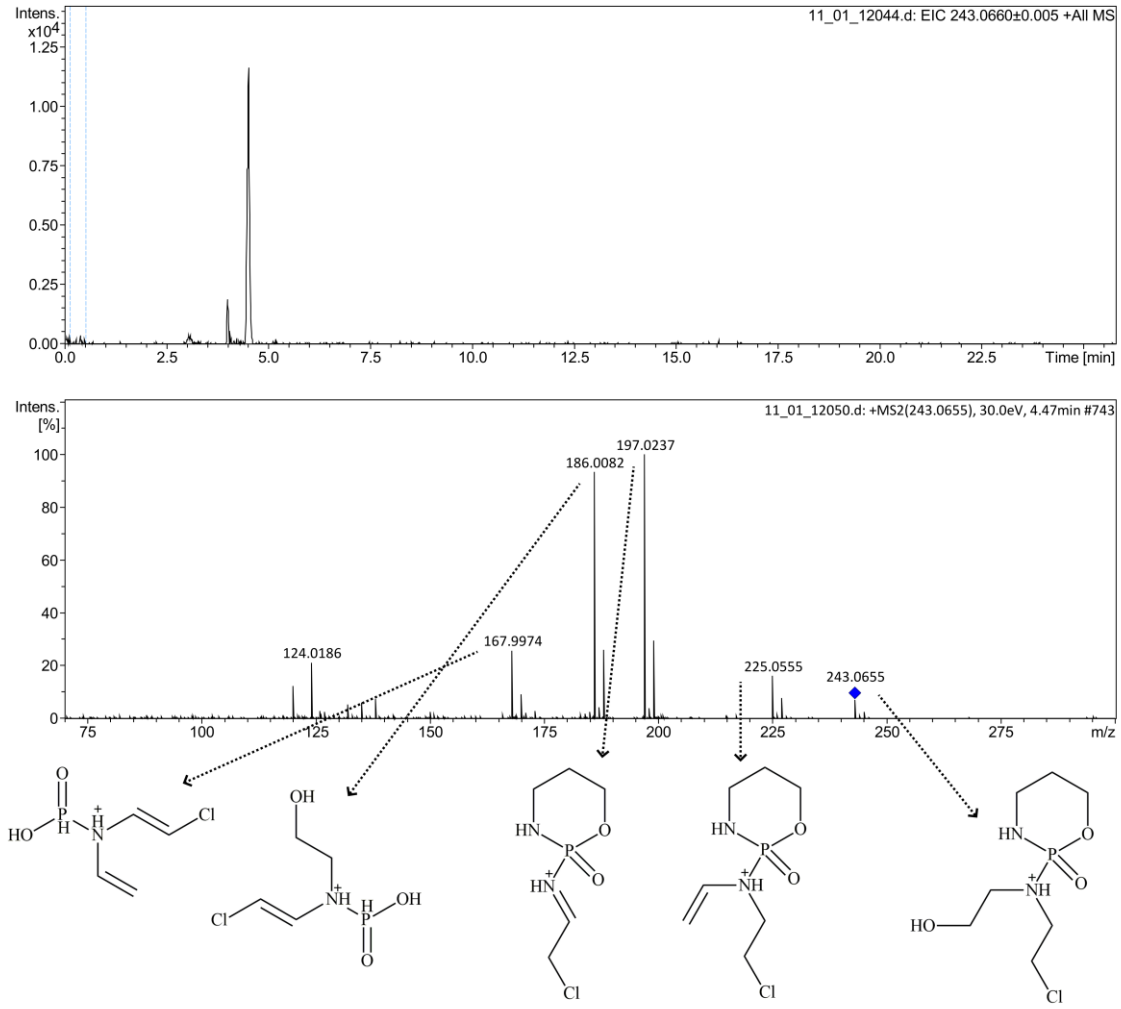

Fig. S1. Chromatogram and MS/MS spectrum of CP-243.

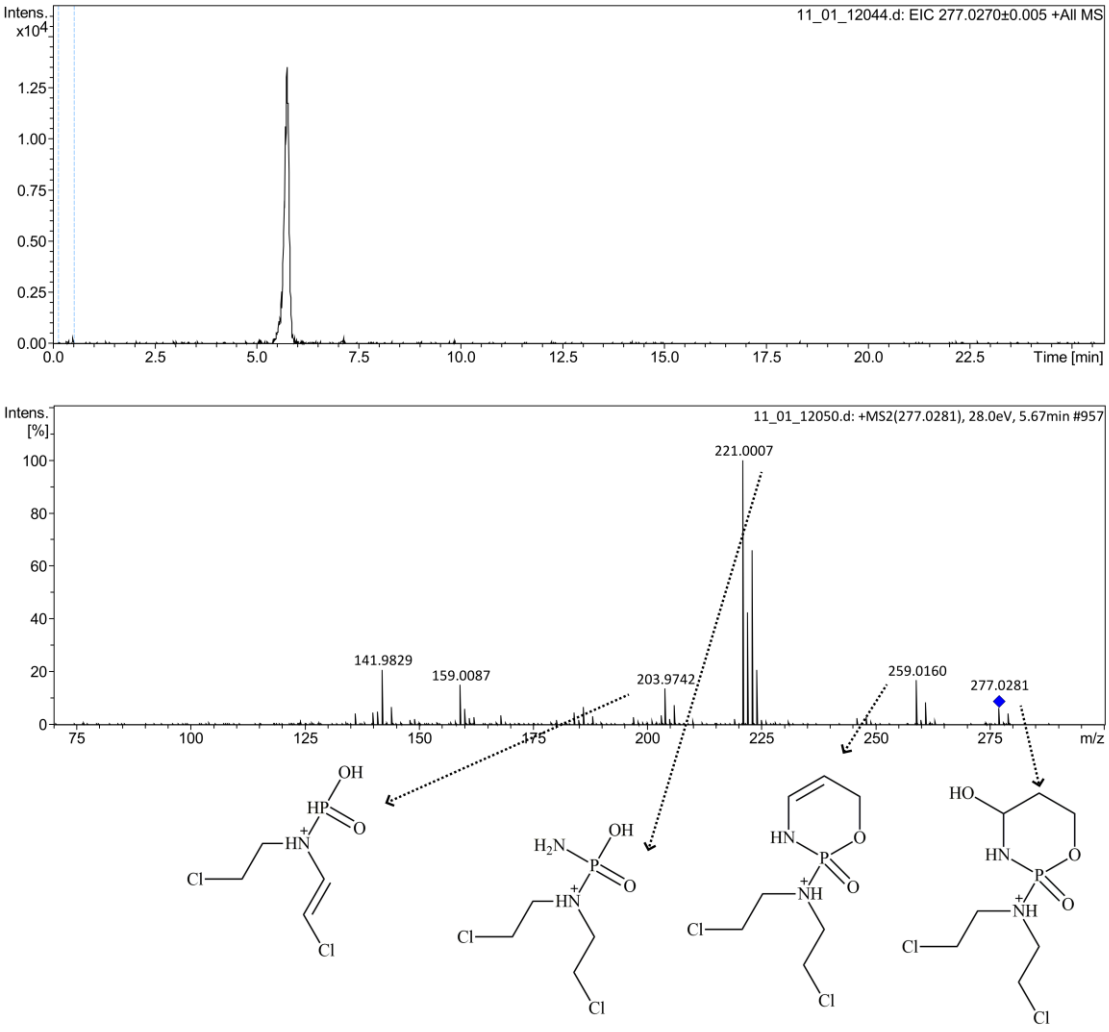

Fig. S2. Chromatogram and MS/MS spectrum of CP-277.

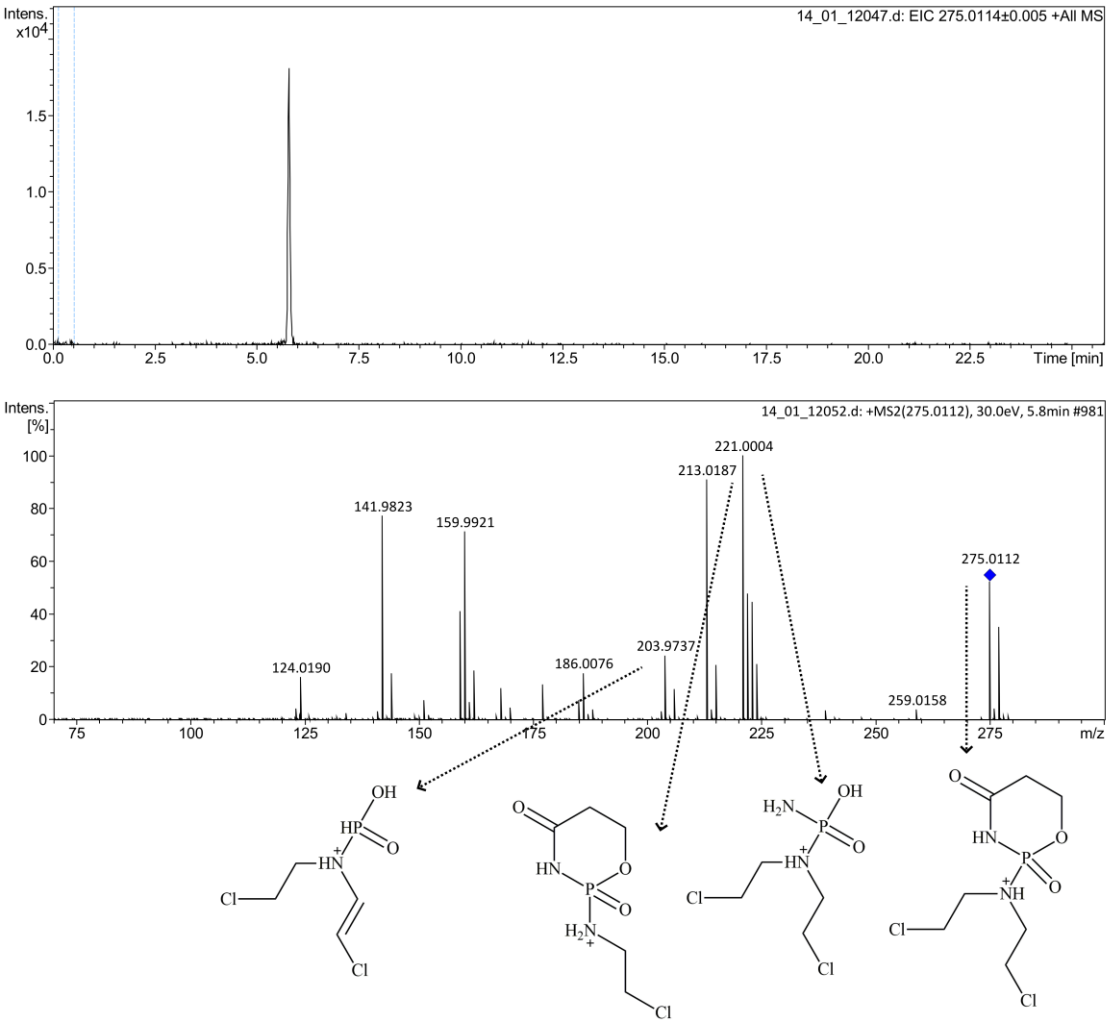

Fig. S3. Chromatogram and MS/MS spectrum of CP-275.

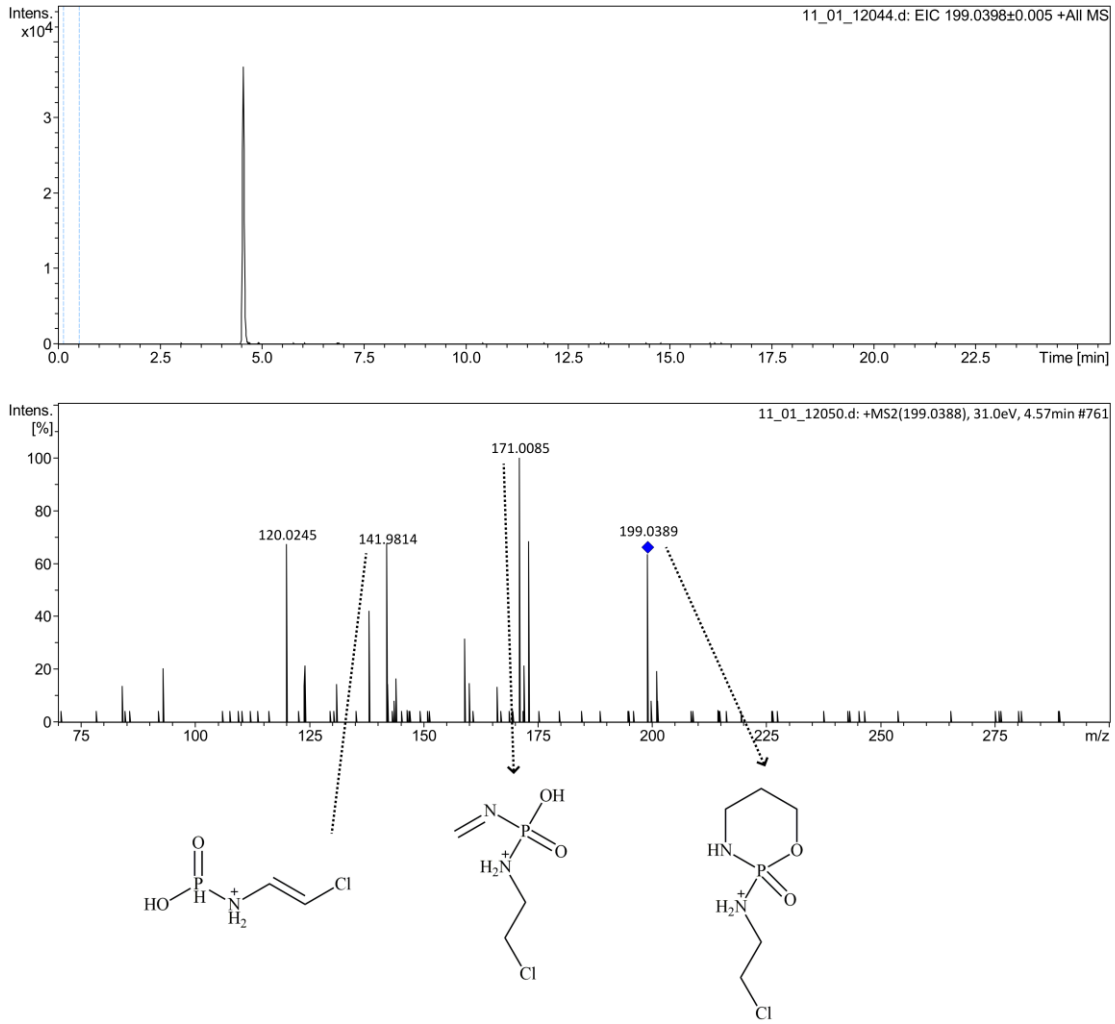

Fig. S4. Chromatogram and MS/MS spectrum of CP-199 and IF-199b.

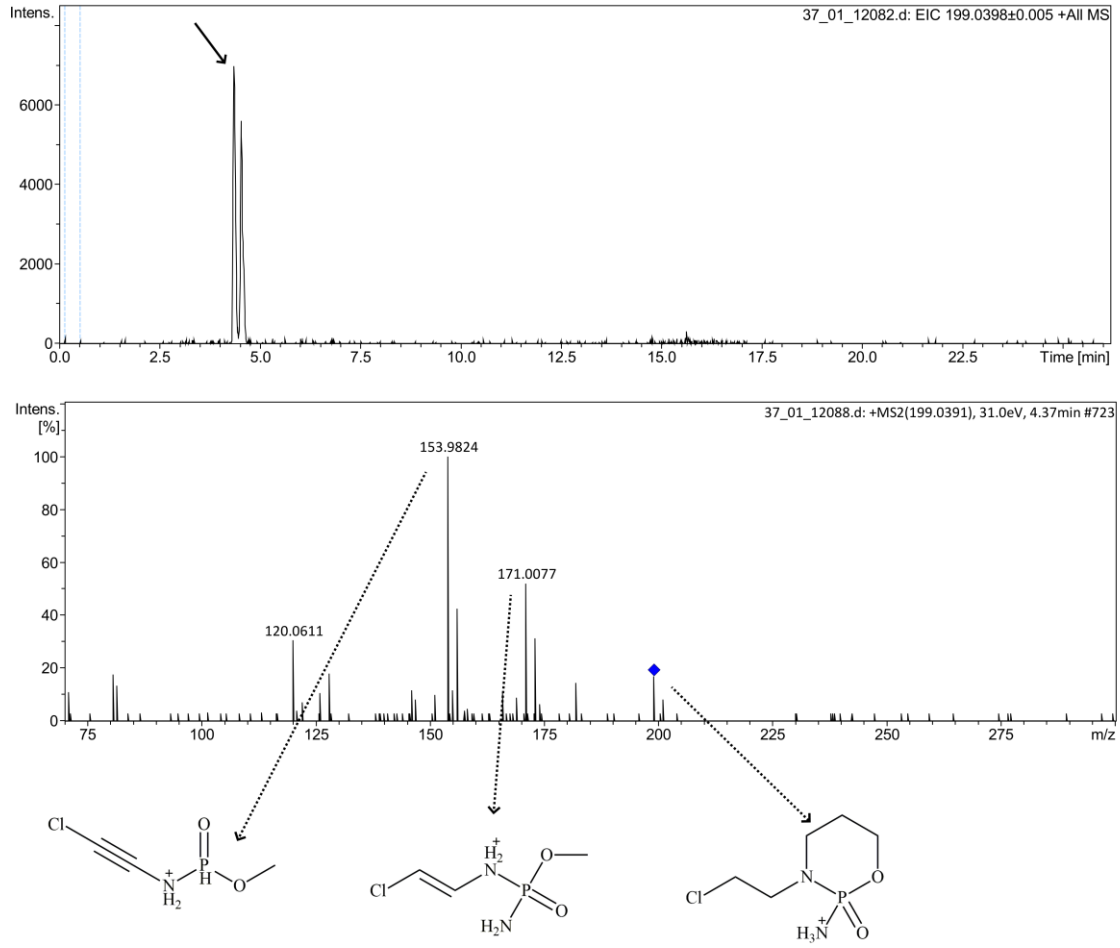

Fig. S5. Chromatogram and MS/MS spectrum of IF-199a.

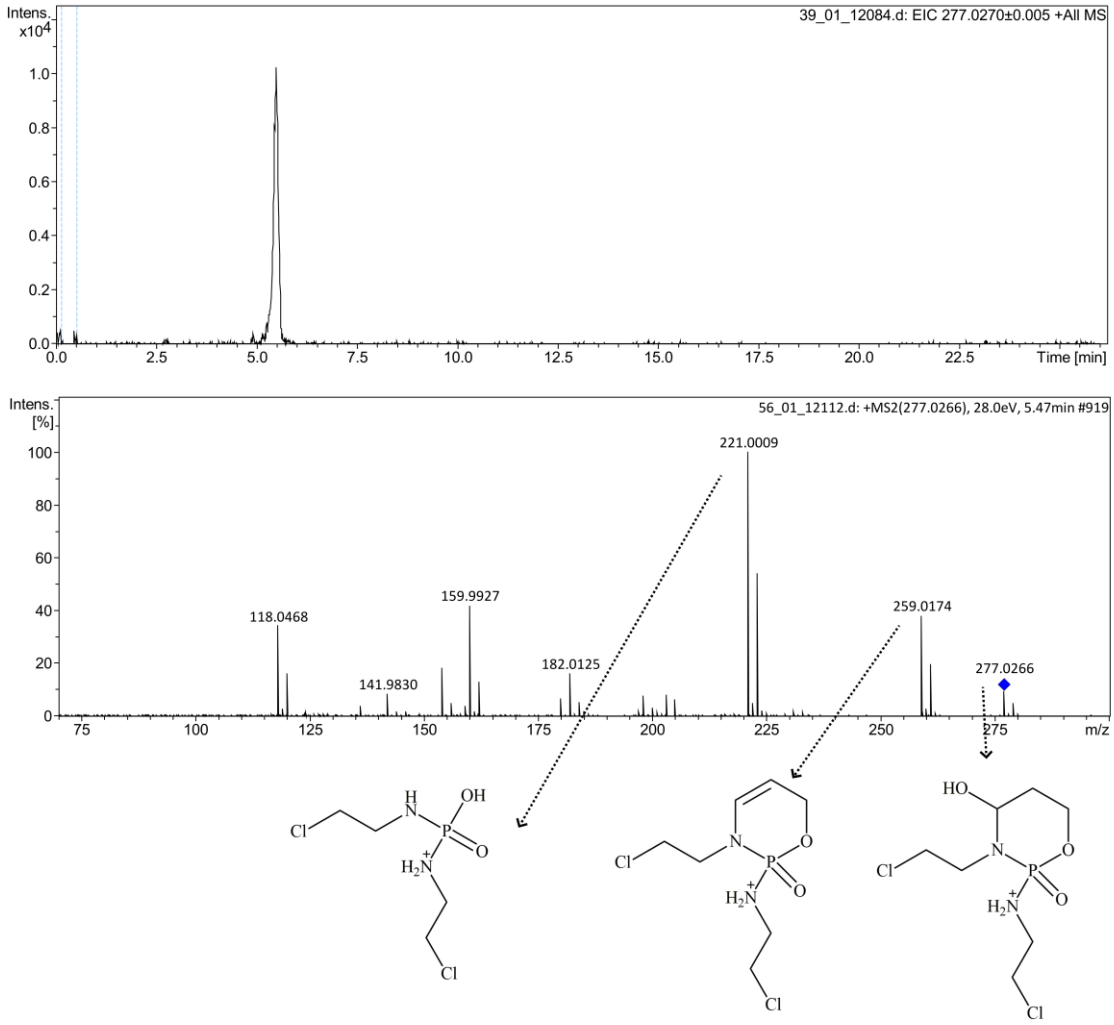

Fig. S6. Chromatogram and MS/MS spectrum of IF-277.

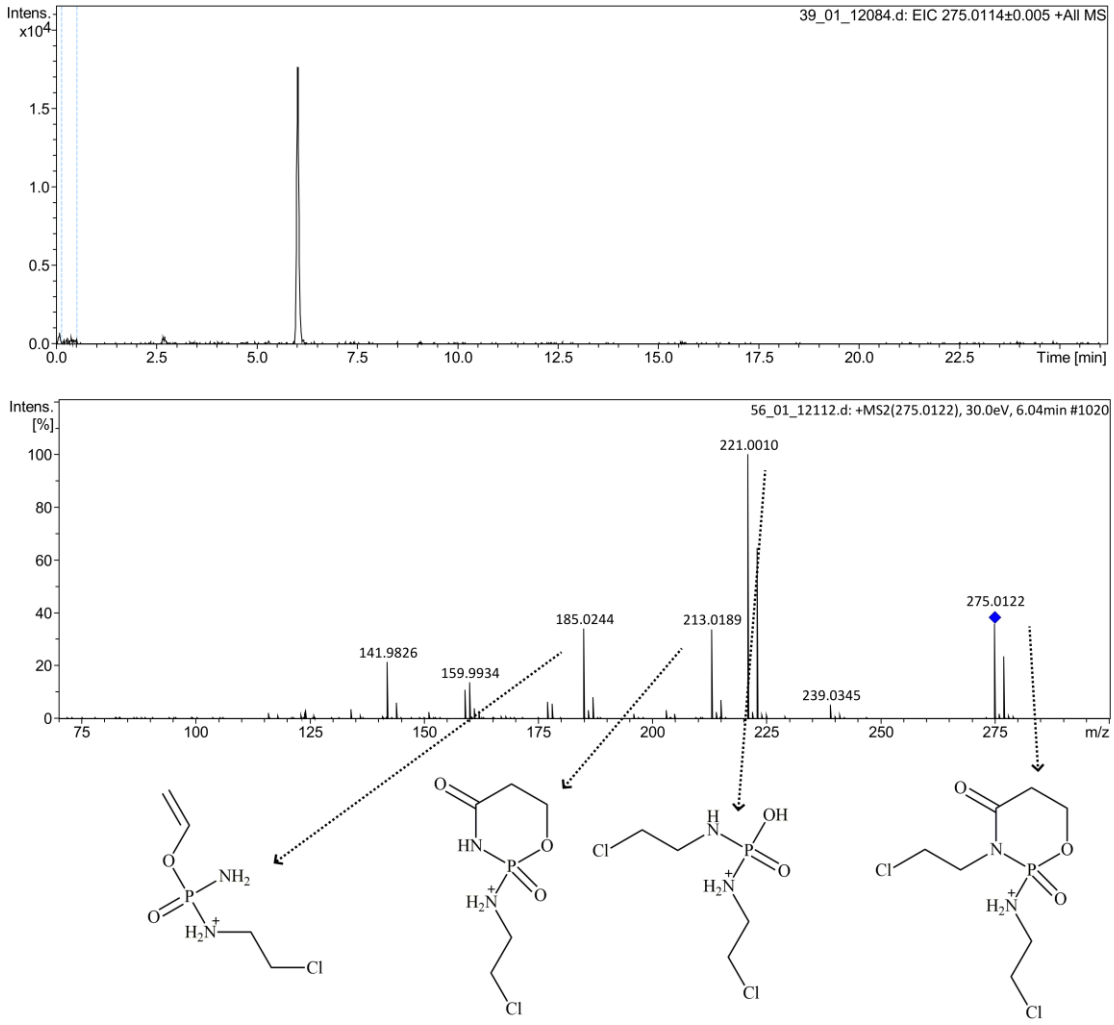

Fig. S7. Chromatogram and MS/MS spectrum of IF-275.

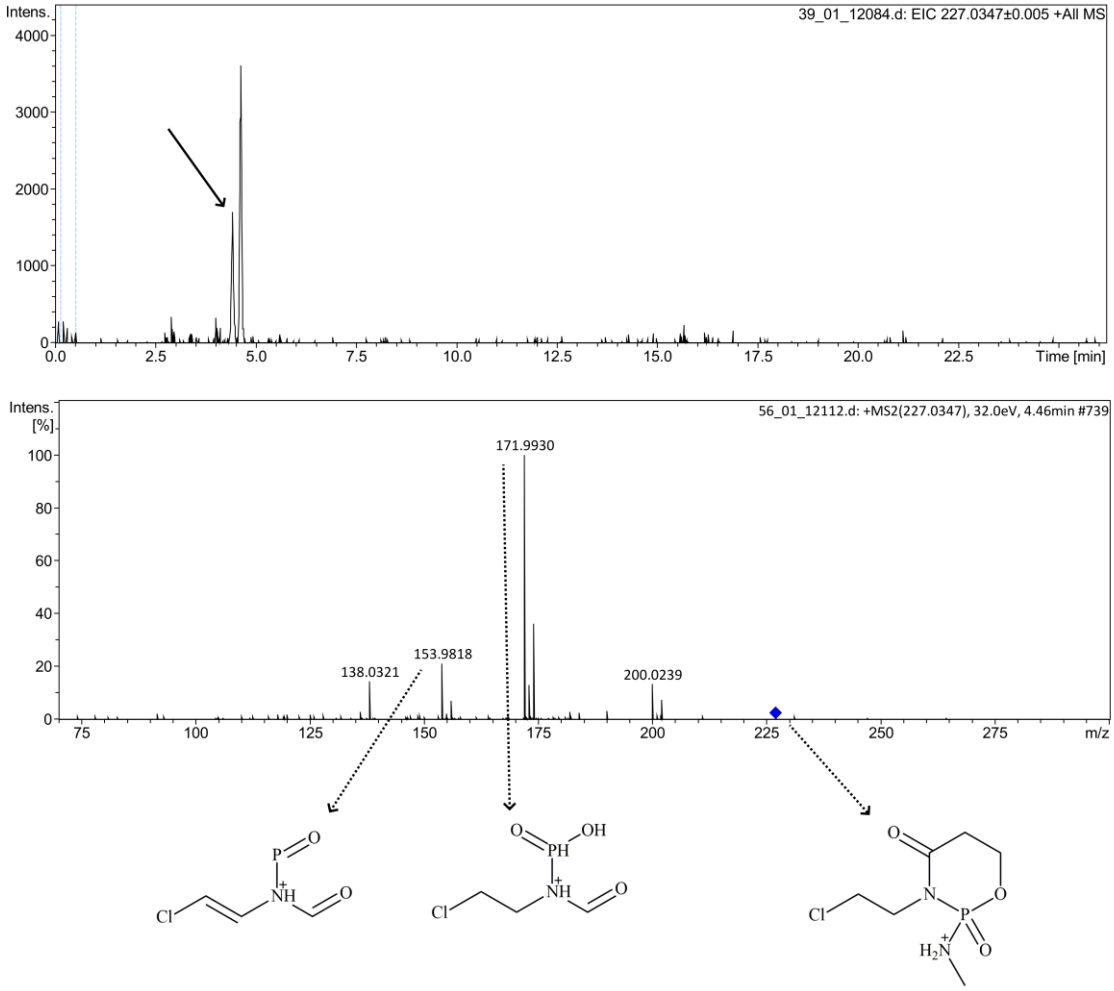

Fig. S8. Chromatogram and MS/MS spectrum of IF-227a.

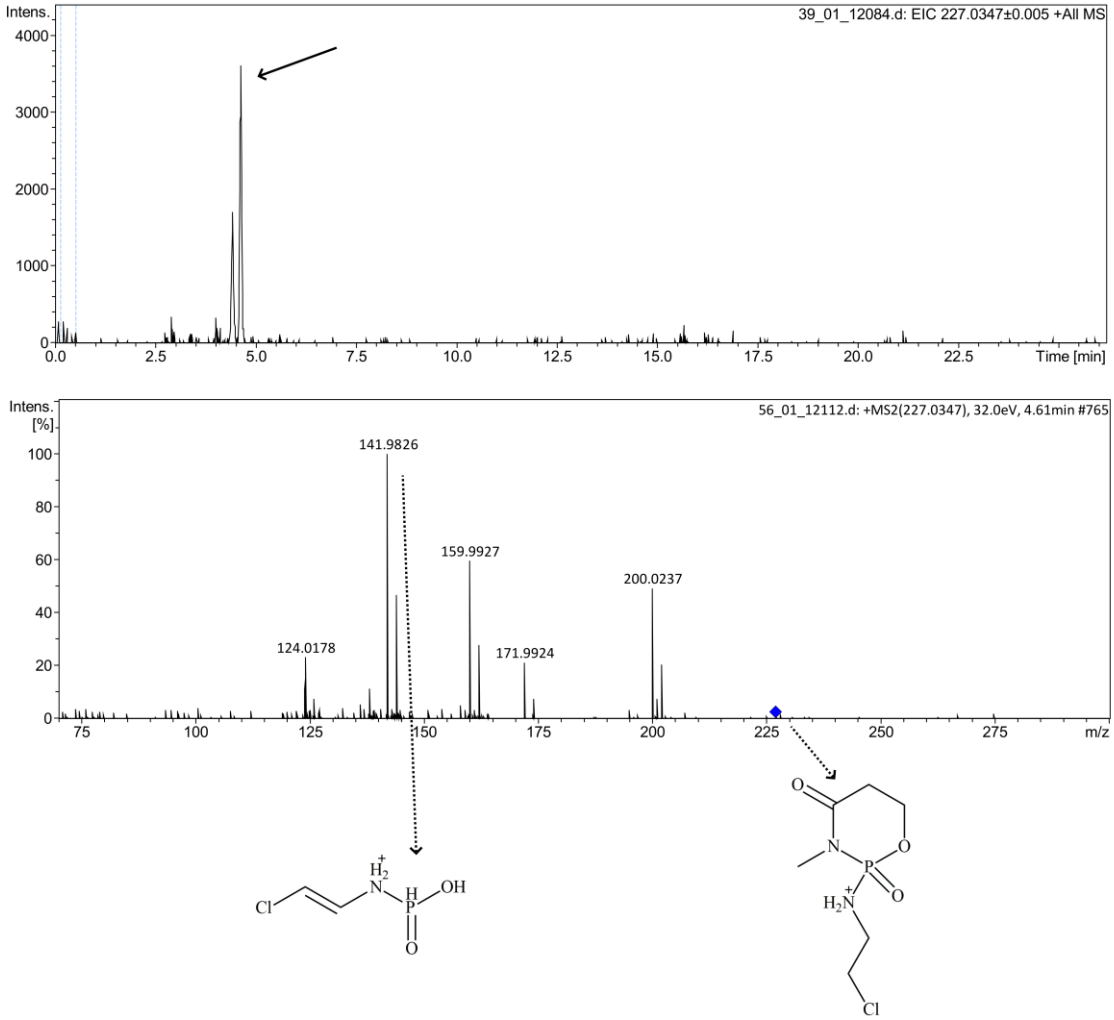

Fig. S9. Chromatogram and MS/MS spectrum of IF-227b.

6.2. Conclusões

Foram observadas maiores taxas de remoção usando o Ru-TNW em comparação com a fotólise tanto em matriz de água destilada quanto em efluente. As degradações seguiram a cinética de pseudo-primeira ordem. Na degradação do CP o tempo de meia vida ($t_{1/2}$) variou de 24.4 min em uma solução mista em efluente durante a fotólise a 10 min durante a fotocatálise em água destilada em uma solução única e para o IF, o $t_{1/2}$ foi de 18,9 min a 8 min para fotólise em solução mista em efluente e para fotocatálise em água destilada, respetivamente.

Durante as fotodegradações, foram constatadas a formação de quatro TPs do CP e seis TPs do IF. Adicionalmente, foi detetado um TP a mais ao degradar o CP em água destilada e dois TPs do IF ao usar o efluente. Alguns TPs formados são considerados metabolitos humanos, o que evidencia que estes TPs também podem ser formados por processos físicos. Este resultado mostrou que há influências na formação dos TPs em relação as matrizes usadas. Ou seja, é essencial estudar os processos de fotodegradações em matrizes mais próximas do real para assim ser possível aplicar em condições ambientais reais.

Para as análises de toxicidade *in silico*, os TPs apresentaram mutagenicidade positiva, sendo que em relação ao CP, IF, CP-275 e CP-277 já existem estudos experimentais que confirmam o potencial mutagénico. Os TPs também mostraram ser potencialmente perigosos para os organismos aquáticos, porém são necessários estudos *in vitro* e *in vivo* para confirmar estas predições.

6.3. Referências

1. Witt, K.L., Bishop, J.B., 1996. Mutagenicity of anticancer drugs in mammalian germ cells. Mutat. Res. - Fundam. *Mol. Mech. Mutagen*. 355, 209–234. doi:10.1016/0027-5107(96)00029-2

2. Besse, J.-P., Latour, J.-F., Garric, J., 2012. Anticancer drugs in surface waters: what can we say about the occurrence and environmental significance of cytotoxic, cytostatic and endocrine therapy drugs? *Environ. Int*. 39, 73–86. doi:10.1016/j.envint.2011.10.002

3. Kümmerer, K., Al-Ahmad, A., 2010. Estimation of the cancer risk to humans resulting from the presence of cyclophosphamide and ifosfamide in surface water. *Environ. Sci. Pollut. Res*. 17, 486–496. doi:10.1007/s11356-009-0195-4

4. Česen, M., Kosjek, T., Busetti, F., Kompare, B., Heath, E., 2016b. Human metabolites and transformation products of cyclophosphamide and ifosfamide: analysis, occurrence and formation during abiotic treatments. *Environ. Sci. Pollut. Res*. 23, 11209–11223. doi:10.1007/s11356-016-6321-1

5. Moldovan, Z., 2006. Occurrences of pharmaceutical and personal care products as micropollutants in rivers from Romania. *Chemosphere* 64, 1808–1817. doi:10.1016/j.chemosphere.2006.02.003

6. Ternes, T.A., Hirsch, R., Mueller, J., 1998. Methods for the determination of neutral drugs as well as betablockers and 2-sympathomimetics in aqueous matrices using GC/MS and LC/MS/MS. *Fresenius J. Anal. Chem*. 362, 329–340. doi:10.1007/s002160051083

7. Barrocas, B.T., Oliveira, M.C., Nogueira, H.I.S., Fateixa, S., Monteiro, O.C., 2019. Ruthenium-modified titanate nanowires for the photocatalytic oxidative removal of organic pollutants from water. *ACS Appl. Nano Mater*. 2, 1341–1349. doi:10.1021/acsanm.8b02215

Capítulo 7

Degradação fotocatalítica da trazodona por diferentes catalisadores sob luz solar artificial

7.1. Introdução

Conforme visto nos capítulos 5 e 6, onde os catalisadores Co-TNW e Ru-TNW foram testados sob radiação UV−Vis na degradação de diferentes fármacos, neste capítulo foi usada radiação do espectro do visível para a degradação do TRA. A escolha deste fármaco deveu-se ao facto de ser rapidamente degradado durante a fotocatálise e a fotólise sob a radiação UV−Vis [1]. Este estudo tem como objetivo avaliar a remoção do poluente utilizando diferentes catalisadores sob a radiação visível para simular a luz solar, assim como analisar os TPs formados. Os catalisadores selecionados foram: nanofios de titânio não dopados (undoped-TNW), nanofios de titânio dopados com ferro (Fe-TNW), além dos dois previamente testados, Co-TNW e Ru-TNW. Consoante dito anteriormente, todos os catalisadores foram sintetizados e devidamente caracterizados pelo grupo de pesquisa da Prof. Dr. Olinda C. Monteiro do Centro de Química e Bioquímica da Faculdade de Ciências da Universidade de Lisboa [2,3]. As principais características encontram-se resumidas na **Tabela 7.1.**

Tabela 7.1. Características dos catalisadores

Catalisador	Área superficial (BET) ($m^2\,g^{-1}$)	Energia ótica do *bandgap* (eV)
Undoped-TNW	288,60	3,27
Co-TNW	267,22	2,43
Fe-TNW	124,74	3,42
Ru-TNW	232,20	3,64

Prevê-se que a degradação do TRA sob radiação visível apresente uma taxa menor em comparação com radiação UV−Vis já que a energia da radiação do espectro visível é inferior. A formação dos TPs também pode apresentar alterações com novos TPs sendo gerados conforme observado no capítulo 5, no qual foram identificados diferentes TPs do AMI nestes dois tipos de radiação.

Este capítulo é uma representação integral do artigo em preparo:

Osawa, R.A., Barrocas, B.T., Monteiro, O.C., Oliveira, M.C., Florêncio, M.H., Photodegradation of trazodone under visible light radiation: A comparative study using different metal-doped titanate nanowires.

Photodegradation of trazodone under visible light radiation: A comparative study using different metal-doped titanate nanowires

Abstract

Titanate nanomaterials have been outstanding in the removal of emerging contaminants by the photocatalysis process since they have advantages over TiO_2, especially in the region of visible light, when modified through techniques such as doping with metals. In this work, the photocatalytic performance of four catalysts were compared for the removal of the antidepressant trazodone (TRA), undoped titanate nanowires (undoped-TNW), cobalt modified titanate nanowires (Co-TNW), iron modified titanate nanowires (Fe-TNW), and ruthenium modified titanate nanowires (Ru-TNW) under visible light radiation. It was verified that Ru-TNW presented the highest adsorption capacity of the TRA, with 14% of the initial concentration. In the photodegradation, Fe-TNW was the one that presented the best catalytic activity per surface area. Thirteen transformation products (TPs) were identified by high resolution mass spectrometry with distinct time profiles for each catalyst. In addition, toxicity assessment by computational methods showed that TPs presented toxicity to aquatic organisms with mutagenic potential and were not readily biodegradable. These findings reinforce the importance of considering TPs during the removal of pollutants, since many may be toxic and can be produced only in photocatalysis.

Keywords: Titanate nanowires; Metal doping; High-resolution mass spectrometry; Degradation pathways; *In silico* toxicity

1. Introduction

The detection of pharmaceuticals in surface water, groundwater, drinking water and effluents has been a matter of concern from the point of view of public and environmental health (Kapelewska et al., 2018; Riva et al., 2019; Starling et al., 2019). Several studies have concluded that the main source of pharmaceuticals contamination comes from wastewater treatment plants (WWTPs), since conventional processes are not intended to remove these contaminants which are mostly resistant to biodegradation (Blum et al., 2018; Collado et al., 2014; Giebułtowicz et al., 2014). Once in the environment, pharmaceutical compounds may cause adverse effects on

aquatic organisms and human health (Geiger et al., 2016; Önlü and Saçan, 2018). This work is focus on the photodegradation of trazodone (TRA), an antidepressant medication belonging to the serotonin antagonist and reuptake inhibitor class. Recent works have shown that TRA had not been totally eliminated in effluent treatment; Paíga et al. (2019) detected TRA in influent of WWTP in Portugal at an average concentration of 294 ng L^{-1} and of 234 ng L^{-1} in the effluent. Other investigation quantified TRA in influent at average concentration of 60 ng L^{-1} and effluent 30 ng L^{-1} in the WWTP in the United States (Oliveira et al., 2015).

Therefore, new technologies have emerged with the aim of removing these contaminants such as photocatalytic degradation. This technique proves to be promising due to the low cost, chemical stability and no mass transfer limitations. Studies have demonstrated the efficiency in the use of TiO_2 as a catalyst for the photodegradation of contaminants (Mohapatra et al., 2014; Pugazhenthiran et al., 2014). However, the main disadvantage of using TiO_2 is the wide band gap which represents low energy efficiency under solar irradiation. In recent years, alternative materials, including titanate elongated nanostructures, have been used to improve these catalytic processes. Nanotubular titanates combine the attributes of TiO_2 like photocatalytic activity, with the attributes of lamellar titanates, as ion-exchange ability. In addition, it has been shown that the use of doped nanomaterials can increases the efficiency of these catalysts in the photodegradation of contaminants, when compared to pristine nanomaterials, especially in the region of visible radiation. In our previous studies, three catalysts were developed from crystalline titanate nanowires (TNW) by doping with different transition metals: cobalt (Co-TNW), iron (Fe-TNW) and ruthenium (Ru-TNW). All of them presented high photocatalytic activity for the removal of pollutants (Barrocas et al., 2016; Barrocas et al., 2019).

Additionally, there is a concern about transformation products (TPs), which are products formed by physical, chemical or biological processes from the parent compound. The TPs may present greater toxicity and/or greater persistence in the environment than the parent compound (Han et al., 2019; Ma et al., 2017). There is a difficulty in identifying the TPs, since they are mostly unknown compounds, in other words, there are no analytical standards available. Nevertheless, hybrid high-resolution mass spectrometry (HRMS), a powerful tool because of high mass accuracy and high resolution, has been used in order to elucidate the TPs, and to determine the exact masses for non-target compounds. Several publications reported the formation

of TPs from emerging contaminants by photolysis and photocatalysis under UV−Vis radiation, visible light and natural sunlight (Li et al., 2016; Osawa et al., 2019; Vulava et al., 2016). However, there is limited research on TPs from TRA, DellaGreca et al. (2008) identified three of the TPs formed under sunlight and to the best of our knowledge, there are no studies related to the detection of TPs from TRA in environmental matrices and toxicity in aquatic organisms. Nevertheless, the clastogenic, mutagenic and cytotoxic effects of TRA were demonstrated in human peripheral blood lymphocytes *in vitro* assays (Yilmaz et al. 2016). One way to study toxicity is to perform *in silico* predictions, which consist of computational methods to analyse the toxicity potential of pollutants on specific endpoints such as aquatic organisms. This method is intended to complement the *in vivo* or *in vitro* toxicity analyses and is suitable when there are no analytical standards available for testing in organisms. Other advantages are the low cost of application and reduced analysis time (Melnikov et al., 2016; Raies and Bajic, 2016). There are several *in silico* models and each has its limitations, these limitations are denominated applicability domain (AD), which determines the reliability of the prediction values (Bakhtyari et al., 2013; Golbamaki et al., 2014)

The objective of this work was to investigate the degradation rates of TRA under photolysis and photocatalysis using different catalysts (undoped-TNW, Co-TNW, Fe-TNW and Ru-TNW) under visible light and to identify the formation of TPs. The elucidation of the TP structures was performed by ultra-high performance liquid chromatography coupled to quadrupole flight time spectrometry (UHPLC/Q-TOF). In addition, *in silico* predictions were performed for ecotoxicity, mutagenicity and biodegradability.

2. Experimental

2.1. Chemicals

Trazodone hydrochloride (CAS Number 25332-39-2) was purchased from Sigma-Aldrich (USA), purity ≥ 99%. LC-MS grades acetonitrile, formic acid and water were obtained from Fisher Scientific (USA). Ultrapure water (Milli-Q ultrapure system, USA) was used for stock solutions.

2.2. TNW synthesis

The synthesis and characterization of the photocatalysts were published in previous works (Barrocas et al., 2016; Barrocas et al., 2019). **Table 1** shows the summary of the main characteristics of each catalyst.

Table 1. main characteristics of catalyst.

Catalyst	BET surface area ($m^2\ g^{-1}$)	optical bandgap energy (eV)
Undoped-TNW	288.60	3.27
Co-TNW	267.22	2.43
Fe-TNW	124.74	3.42
Ru-TNW	232.20	3.64

2.3. Photodegradation experiments

The photodegradation experiments were performed using arc lamp housing with 300 W xenon lamp as visible light source of radiation (Newport, USA). A 250 mL borosilicate glass with recirculation of water for cooling was placed 30 cm away from the radiation source.

Distilled water samples (150 mL) were spiked with 5 mg L^{-1} of TRA. The high concentration of the drug was used to facilitate the identification of the TPs. 20 mg of catalyst were added to TRA solutions and the suspensions were stirred throughout the experiments. Prior to the radiation, the suspension was placed in the dark for 1 h to verify the adsorption of the compound on the catalyst surface. Finally, aliquots were withdrawn (1 mL) at given time intervals (0, 15 min, 30 min, 1 h, 2.5 h, 5 h and 8 h), centrifuged to remove the catalyst and frozen at −80 °C for later analysis. The experiment was repeated for each catalyst.

2.4. Instrumentation

Analysis was performed on an Elute UHPLC system (Bruker Daltonics, Bremen, Germany) coupled with a QTOF Impact II mass spectrometer with an electrospray ion source (Bruker Daltonics, Bremen, Germany). A Halo® C18 (5 µm particle size; 4.6 × 150 mm) (Advanced Materials Technology, Waltham, USA) was used as separation column with the flow rate at 400 µL min^{-1} and the volume injection was 10 µL. The gradient program was set as follows, ultrapure water acidified with 0.1% formic acid (A) and acetonitrile (B) were used as the mobile phase: 0 min (20% B), −1.5 min (20%

B), −10 min (30% B), −13 min (100% B), −17 min (100% B), −18 min (20% B), –25 min (20% B). The mass spectrometer operated in a high-resolution mode in the positive ion mode, details of the operational conditions can be found in (Osawa et al., 2019).

2.5. *In silico* predictions

In silico toxicity was assessed by ECOSAR (v2.0, US EPA) for ecotoxicity endpoints and T.E.S.T (v4.2.1, US EPA) for mutagenicity endpoint. ECOSAR uses log k_{ow} values to estimate toxicity and these values are calculated according to the chemical classes of the compound. In this study, it was considered the class with the lowest value, which corresponds to the highest toxicity. The AD of this model is based on the log k_{ow} values where the compound is no longer soluble and does not result in toxicity to aquatic organisms. Three endpoints were chosen: fish 96-h LC_{50}, daphnid 48-h LC_{50} and green algae 96-h EC_{50}. In T.E.S.T, the consensus method for mutagenicity was adopted, which consists of the average values estimated by other QSARs methods and each method uses a generic algorithm technique to define a descriptor set in a given cluster. The ecotoxicity endpoints from T.E.S.T were not applied because most of the estimated values were outside the AD.

In silico biodegradability was predicted by Biowin tool, which is part of the EPI Suite (v4.1, EPA). The tool contains seven models with different methodologies and this work considered the models Biowin5 (linear model) and Biowin6 (nonlinear model) based on the biodegradation test (OECD 301C) using the Japanese Ministry of International Trade and Industry (MITI) data. These models presented good accuracy results under REACH (Registration Evaluation Authorization and restriction of Chemicals) legislation (Devillers et al., 2013; Pizzo et al., 2013). The predicted values range from 0 to 1, where above 0.5 indicates that the compound is not readily biodegradable, however, the AD is not defined in this tool.

3. Results and discussion

3.1. Degradation profiles rate

First of all, the adsorption capacity of the catalysts was verified, in which the suspension was stirred for 1 h in the dark before being exposed to light. The adsorption of the pollutant on the surface of the catalyst is highly relevant for heterogeneous photocatalytic reactions since it may increase the removal rate However, excessive adsorption may decrease the removal efficiency due to modifications in the optical

absorption capacity of the catalyst (Liu et al., 2013). In this work, Ru-TNW was the sample with the highest adsorption rate, 14% of the TRA was adsorbed after 1 h. Undoped-TNW and Co-TNW presented similar results, 7% of TRA decreased after 1 h in contact with the respective catalysts Fe-TNW showed only 4% adsorption of the initial pollutant present in solution.

Concerning TRA photodegradation, the use of the undoped-TNW sample as a photocatalyst showed that apparently it was the one presenting the highest rate of degradation (**Fig. 1a**). After 5 h under artificial solar radiation, about 98% of the initial amount was removed, followed by Fe-TNW with 88% of TRA removal. On the other side, the photolysis eliminated approximately 57% of the TRA. In summary, the order of the degradation rate should be: undoped-TNW> Fe-TNW> Co-TNW> Ru-TNW> Photolysis. However, if it should be considered the influence of the surface area of the catalysts, since this it is a heterogeneous process. In fact, the surface area of the samples tested is quite different, with TNW possessing the highest value (288.6 m^2/g), with decreases of 7, 20 and 57% for Co-TNW, Ru-TNT and Fe-TNW respectively. Considering this parameter in the photocatalytic performance of the samples, Fe-TNW will present the best photocatalytic results followed by TNW, Ru-TNW and Co-TNW (**Fig. 1b**).

Although the undoped-TNW and doped samples presented a greater efficiency of degradation, it is essential to identify the TPs since many of them can be toxic and not be removed during the TRA photocatalytic process. In this work, predictions were made using computational models, which can be found in **section 3.3**. Thirteen TPs from TRA were identified, which were formed by different processes. The ratio of TP area at a given irradiation time and the initial area of the TRA, in percentage, were used to estimate the relative peak area of TPs. Two TPs were of greater relevance (TP-354 and TP-402), because of their high amount in solution and because they may have influenced the degradation of the TRA. The other eleven TPs are not relevant once they resulted in a relative area smaller than 4%.

After 8 h of photolysis, the TP-354 had a relative intensity of 26%, in other words, about a quarter of TRA was transformed into this product that was not degraded during this same period. This indicates that in real matrices, TP-354 may be formed and it does not degrade under solar radiation (**Fig. 2a**). However, during photocatalytic experiments, this TP was produced and afterwards degraded, highlighting Fe-TNW

and TNW as the catalysts that at the end of 8 h of irradiation allow the almost complete removal of TP-354.

We believe that the high amount of TP-354 formation in the presence of the doped photocatalysts it may have induced lower rates of TRA removal due to the direct competition of the two compounds, TP-354 and TRA, for the same active sites of the catalyst. Supporting this hypothesis, it is the fact that for 1 h of irradiation, a similar amount of TP-354 was observed for photolysis and photocatalysis (doped and undoped TNW).

The TP-402 was the intermediate product with the second highest expression; after 5 h under radiation and using TNW as photocatalyst, this value was 9%. As shown in **Fig. 2b**, after 8 h of photolysis less than 1% of TP-402 was present in solution, whereas for photocatalysis this production only increases, until the end of the experiments. The time profile of the TP-402 showed that it is necessary to evaluate the formation of the TPs when studying the processes of degradation of the pollutants, because they may persist in the environment even with the parent compound eliminated. The analysis concerning the elucidation of the chemical structures of the TPs, acquired by the MS/MS spectra can be found in the section below.

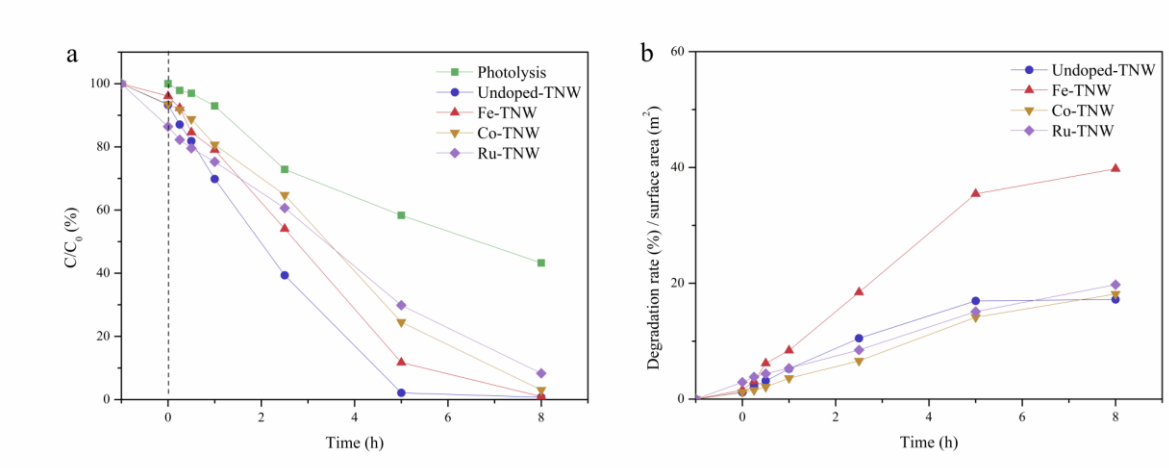

Fig. 1. Time profile of (a) photodegradation of trazodone (TRA) and (b) degradation rate by surface area of catalyst.

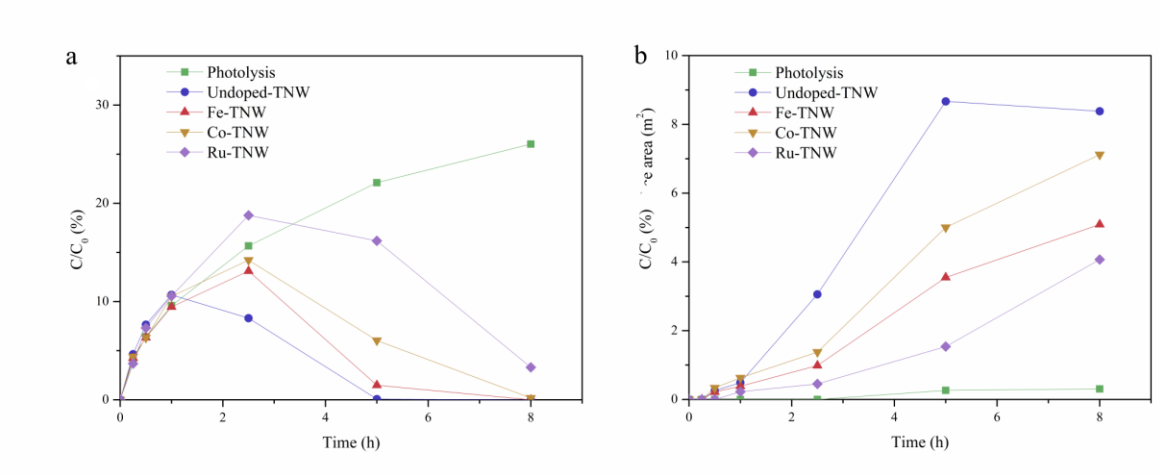

Fig. 2. Time profile of transformation products (a) TP-354 and (b) TP-402.

3.2. Elucidation of TPs

The TP-354 was elucidated in our previous findings on the degradation of TRA under UV−Vis radiation. In summary, it was assumed that this TP was generated by the dehalogenation of the chlorobenzene group to form a phenol group from TRA. In the MS/MS spectrum analysis, no loss of H_2O was identified, which may mean that the hydroxylation occurred on the benzene ring to form the phenol. The identification of fragment ion at *m/z* 176 ($C_9H_{10}N_3O^+$) corroborates this assumption, since this fragment represents the heterocyclopyridine group, in other words, the addition of the OH was not detected in this group.

TP-342, TP-370 and TP-386 were also identified and discussed in our previous work using UV−Vis radiation. In brief, these TPs were formed from the TP-354 by hydroxylation on the β-carbon of the aliphatic chain to form TP-370 and, demethylation of the piperazine group generated TP-342. It was observed that the presence of the catalysts determined the production of TPs, emphasizing that during photolysis the TP-342 were not detected or, put in another way, photocatalysis process may generate other TPs.

The time profile of TP-404 showed that that in the photolysis there was no degradation and in the photocatalysis, all the catalysts had catalytic activity in the removal of this product, whereas undoped-TNW as catalyst generated less TP-404 (**Fig. S**). The chemical structure of this TP was formed from two hydroxylations of TRA, these hydroxylations possibly occurred in the pyridine group, since no H_2O losses were detected, presuming that the OH groups were attached to the aromatic ring. Additionally, the fragment ion at *m/z* 208 ($C_9H_{10}N_3O_3^+$) was identified in the MS/MS

spectrum, representing the pyrazolone, the alkane and the pyridine bound to two OH groups. Unfortunately, it was not possible to determine the positions of the OH groups. The TP-404 generated the TP-420, which was detected both in photolysis and photocatalysis processes and, after 5 h of radiation, only with the undoped-TNW and Fe-TNW catalysts this TP was eliminated. By analyzing the MS/MS spectrum of TP-420: The fragment ion at *m/z* 224 ($C_9H_{10}N_3O_4^+$) endorses this statement, wherein the OH groups have been detected. Nevertheless, one H_2O loss was detected in the spectrum from *m/z* 224 to *m/z* 206 ($C_9H_8N_3O_3^+$), which may represent that this OH was attached to the alkane group.

The TP-406 was identified during photolysis and photocatalysis and it has not been completely eliminated only with Ru-TNW. The chemical structure of TP-406 was elucidated by the loss of H_2O, which was found in the fragmentation patterns indicating a hydroxylation process, from precursor ion to *m/z* 388, It was therefore assumed that there was hydration of the alkene in the aromatic ring to form a hydroxyl (OH) group. DellaGreca identified the same process when studying the TRA photodegradation. The fragment ion at *m/z* 210 showed the loss of $C_{10}H_{13}ClN_2$ from precursor ion, which corroborates that the OH groups were added to the heterocyclic ring. TP-394 was formed by opening of the piperazine ring from TP-406, in other words, simultaneously with an hydroxylation and an hydration of alkene, the fragment ion at *m/z* 198 ($C_8H_{12}N_3O_3$) may confirm that the hydroxylation and hydration of the alkene occurred on the pyridine ring.

TP-388 was generated by hydroxylation process from TRA, however, no loss of H_2O was found in the MS/MS spectrum, which may argue that OH group was bound to the aromatic ring. In theory, hydroxylation could have occurred on chlorobenzene or on the heterocyclic group. However, the ion fragment at *m/z* 176 was formed by the loss of piperidine plus chlorophenol from precursor ion, which corroborates that hydroxylation occurred in chlorobenzene forming chlorophenol. Nonetheless, it was impossible to identify the position of OH group. All catalysts showed catalytic activity for TP-388, as seen in **Table 2.** We believe that TP-402 was produced by oxidation process of TP-388, the oxidation having occurred on the piperazine group, due to the identification of the fragment ion at *m/z* 247 from precursor ion, which showed the loss of chloro-(methyleneamino) phenol (C_7H_6ClNO) and the following fragment ion was at *m/z* 219 which represents the loss of CO on the piperazine group, in other words, validates the oxidation process. Nevertheless, it was not possible to determine the site

of the oxidation process in the piperazine. In addition, Baena-Nogueras et al (2017) investigated the photodegradation of ciprofloxacin (drug having a piperazine group in the chemical structure) under simulated sunlight irradiation and identified a TP that was formed by oxidation of the piperazine group.

The photoproduct TP-346 was detected in all experiment conditions, which was generated by the opening of the piperazine ring from TRA. Other works have also reported different TPs formed by the opening of the piperazine ring in photodegradation of tandospirone and sildenafil (Eichhorn et al., 2012; Trawiński and Skibiński, 2017).

We believe that TP-374 was formed by hydroxylation, dehydrogenation and ring opening, all of these reactions occurring in the piperazine group. The loss of H_2O in the MS/MS spectrum from parent ion to fragment *m/z* 356 ($C_{18}H_{19}ClN_5O$) justifies the hydroxylation and the fragment ion at *m/z* 182 (C_9H_9ClNO) is only possible if these reactions occurred in the piperazine ring. To reinforce this statement, Trawiński Skibiński (2017) also observed the dehydrogenation of piperazine during the photodegradation of an anxiolytic drug. It was assumed that the TP-356 was generated from dehydroxylation of piperazine group from TP-374 to form dihydroimidazole. **Table 2** summarizes the main fragments obtained by analyzing the MS/MS spectra of the TPs with the monoisotopic mass with their respective mass errors and the time profile and **Fig. 3.** shows the proposed TRA degradation pathway.

Table 2. Main fragments from MS/MS spectra of TRA transformation products (TPs) with their respective time profiles.

Compound	Elemental formula $[M+H]^+$	Theoretical mass $[M+H]^+$	Error (ppm)	Time profile				
				Photolysis	Undoped-TNW	Co-TNW	Fe-TNW	Ru-TNW
TP-342	$C_{18}H_{24}N_5O_2^+$	342.1925	0.86	-	↗↘	-	↗↘	↗
	$C_{12}H_{19}N_2O^+$	207.1492	0.96					
	$C_9H_{10}N_3O^+$	176.0818	1.70					
	$C_7H_6N_3O^+$	148.0505	3.38					

TP-346	$C_{17}H_{21}ClN_5O^+$	346.1429	−1.15					
	$C_{11}H_{15}N_4O^+$	219.1240	−0.46	↗↘	↗↘	↗↘	↗↘	↗↘
	$C_9H_{10}N_3O^+$	176.0818	0					
	$C_7H_6N_3O^+$	148.0505	3.38					
TP-354	$C_{19}H_{24}N_5O_2^+$	354.1925	−0.56					
	$C_{13}H_{19}N_2O^+$	219.1492	−2.28	↗	↗↘	↗↘	↗↘	↗↘
	$C_9H_{10}N_3O^+$	176.0818	−1.13					
	$C_7H_6N_3O^+$	148.0505	2.03					
TP-356	$C_{18}H_{19}ClN_5O^+$	356.1273	−0.56					
	$C_9H_{10}N_3O^+$	176.0818	1.13	↗→	↗↘	↗↘	↗↘	↗
	$C_7H_6N_3O^+$	148.0505	4.73					
TP-370	$C_{19}H_{24}N_5O_3^+$	370.1874	0.54					
	$C_{19}H_{22}N_5O_2^+$	352.1768	0.57					
	$C_{18}H_{20}N_5O_2^+$	338.1612	0.29	↗	-	↗↘	-	↗
	$C_{10}H_{13}N_4O^+$	205.1084	−1.46					
	$C_9H_{10}N_3O^+$	176.0818	−2.27					
TP-374	$C_{18}H_{21}ClN_5O_2^+$	374.1378	-0.53					
	$C_{18}H_{19}ClN_5O^+$	356.1273	0.84					
	$C_9H_9ClNO^+$	182.0367	1.64	↗	↗↘	↗↘	↗↘	↗↘
	$C_9H_{10}N_3O^+$	176.0818	0.57					
	$C_7H_6N_3O^+$	148.0505	4.05					
TP-386	$C_{19}H_{24}N_5O_4^+$	386.1823	1.03					
	$C_{18}H_{24}N_5O_2^+$	342.1925	−2.34	↗	-	↗	-	-
	$C_{16}H_{22}N_5O_2^+$	316.1768	−3.48					
	$C_{15}H_{19}N_2O_2^+$	259.1441	−1.54					

	$C_9H_{10}N_3O^+$	176.0818	−2.84					
	$C_7H_6N_3O^+$	148.0505	2.70					
TP-388	$C_{19}H_{23}ClN_5O_2^+$	388.1535	0.77					
	$C_{18}H_{19}ClN_5O^+$	356.1273	−0.28					
	$C_{14}H_{17}ClN_3O^+$	278.1055	0.36	↗	↗↘	↗↘	↗↘	↗↘
	$C_{10}H_{13}N_4O^+$	205.1084	−4.39					
	$C_9H_{10}N_3O^+$	176.0818	−1.70					
	$C_7H_6N_3O^+$	148.0505	0.67					
TP-394	$C_{18}H_{25}ClN_5O_3^+$	394.1640	1.77					
	$C_8H_{12}N_3O_3^+$	198.0873	3.53	↗	↗↘	↗↘	↗↘	↗
	$C_8H_{10}N_3O_2^+$	180.0768	1.11					
TP-402	$C_{19}H_{21}ClN_5O_3^+$	402.1327	−0.25					
	$C_{18}H_{19}ClN_5O^+$	356.1273	0.84					
	$C_{12}H_{15}N_4O_2^+$	247.1190	−0.81	↗	↗↘	↗	↗	↗
	$C_{11}H_{15}N_4O^+$	219.1240	−1.37					
	$C_9H_{10}N_3O^+$	176.0818	−1.13					
	$C_7H_6N_3O^+$	148.0505	2.03					
TP-404	$C_{19}H_{23}ClN_5O_3^+$	404.1484	−0.74					
	$C_{13}H_{14}ClN_2^+$	233.0840	−1.72	↗	↗↘	↗↘	↗↘	↗↘
	$C_9H_{10}N_3O_3^+$	208.0717	−1.44					
	$C_{10}H_{11}ClN_2^+$	194.0605	−2.58					
TP-406	$C_{19}H_{25}ClN_5O_3^+$	406.1640	0					
	$C_{19}H_{23}ClN_5O_2^+$	388.1566	−3.35	↗	↗↘	↗↘	↗↘	↗↘
	$C_9H_{12}N_3O_3^+$	210.0873	−0.95					
	$C_9H_{10}N_3O_2^+$	192.0768	−1.56					

TP-420	$C_{19}H_{23}ClN_5O_4^+$	420.1433	1.90					
	$C_9H_{10}N_3O_4^+$	224.0666	−0.89					
	$C_9H_8N_3O_3^+$	206.0560	0.48	↗↘	↗↘	↗↘	↗↘	↗↘
	$C_7H_6N_3O_4^+$	196.0353	0.51					
	$C_7H_4N_3O_3^+$	178.0247	0					

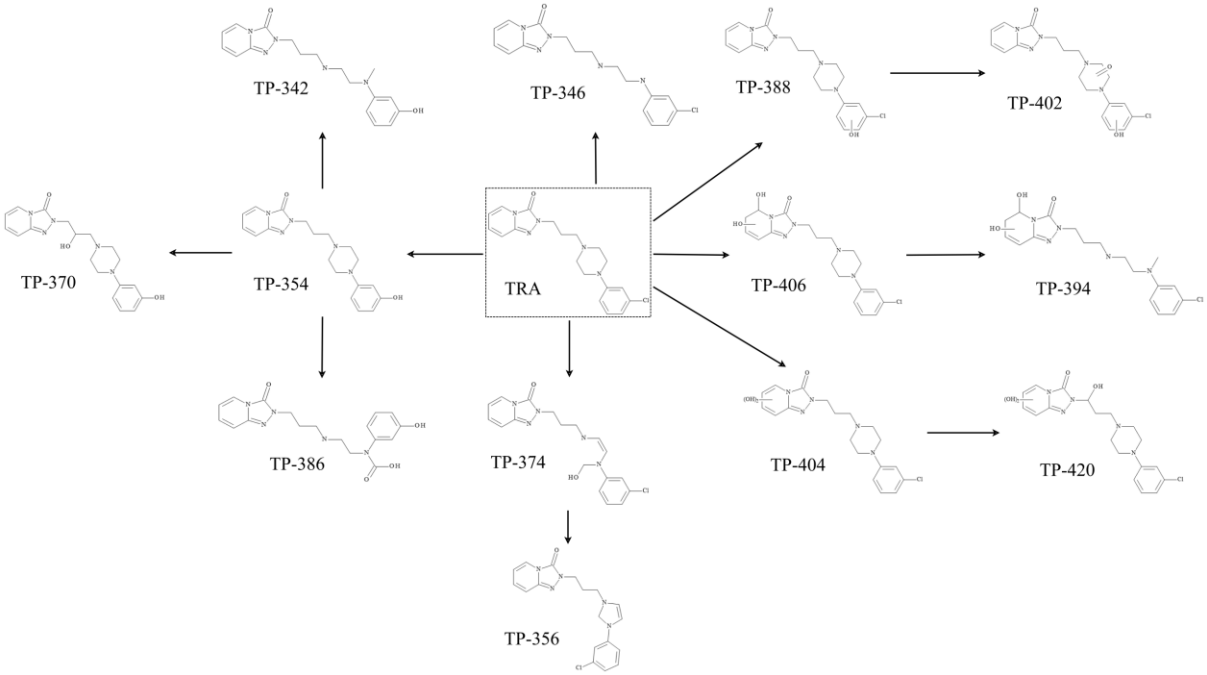

Fig. 3. Scheme of the proposed degradation pathway of TRA

3.3. *In silico* predictions

In silico predictions are based on the molecular structure of the compound and the tools use the simplified molecular-input line-entry system (SMILES) to calculate the toxicity values. For TPs such TP-404 where it was not possible to identify the exact chemical structure, the structures with the lowest toxicity values were chosen, corresponding to the highest toxic potential. Ecotoxicity predictions were performed using the endpoints from ECOSAR: fish 96-h LC_{50}, daphnid 48-h LC_{50} and green algae 96-h EC_{50}. The TRA presented high toxic potential for the three endpoints and unfortunately there are no studies with aquatic organisms to confirm these results. The TPs were classified as toxic (1−10 mg L^{-1}) for all endpoints, according to United Nations, 2011. For the mutagenicity prediction results, it was observed that the TRA

showed no mutagenic potential, contradicting the studies reporting mutagenic and cytotoxic effects on human lymphocytes by in vitro studies (Yilmaz et al. 2016). However, in our predictions, mostly of TPs showed to be positive to mutagenicity endpoint with exceptions of TP-346, TP-374, TP-386 and TP-394 (**Table 3**).

The *in silico* biodegradability prediction resulted in all products beiing not readily biodegradable in both models: Biowin 5 and Biowin 6. Studies compared the predictions of the EPI suite with the biodegradation assays according to the OECD test guideline and concluded that the predictions were in agreement with the results of these tests when studying the TPs of organic pollutants formed by the photodegradation (Gutowski et al. 2015; Mahmoud et al., 2013). These results aim to estimate the toxic potential of the formed TPs, since *in vitro*, *in vivo* or biodegradation tests were not performed, but showed that the TPs are relevant when studying the degradation of pollutants since they may present toxicity to the ecosystem and human health.

Table 3. Predicted toxicity of TRA and its TPs were calculated from ECOSAR (fish 96-h $LC_{50,}$ daphnid 48-h $LC_{50,}$ green algae 96-h EC_{50}), T.E.S.T (mutagenicity) and Biowin (Biowin 5 and Biowin 6).

	Fish 96-h LC_{50}	Daphnid 48-h LC_{50}	Green algae 96-h EC_{50}	Mutagenicity[a]	Biowin 5[b]	Biowin 6[b]
TRA	0.374	1.47	0.621	−	−0.2729	0.0007
TP-342	1.55	3.4	1.34	+	0.0142	0.0055
TP-346	0.646	2	0.821	−	−0.1302	0.0016
TP-354	1.46	3.32	1.32	+	−0.16	0.0024
TP-356	0.703	2.13	0.873	+	−0.272	0.0006
TP-370	6.65	8.58	3.18	+	−0.1465	0.0024
TP-374	2.06	4.2	1.64	−	−0.0166	0.002
TP-386	5.51	7.65	2.86	−	0.0094	0.0052
TP-388	0.618	2.03	0.841	+	−0.2645	0.0006
TP-394	2.44	4.75	1.85	−	0.136	0.0045
TP-402	1.15	3.02	1.22	+	−0.1143	0.0019
TP-404	1.5	3.56	1.42	+	−0.0582	0.0019
TP-406	2.29	4.62	1.81	+	−0.0382	0.002
TP-420	6.8	9.13	3.4	+	−0.0447	0.0019

[a] (+) indicates mutagenic potential and (−) indicates non-mutagenic potential.

[b] values below 0.5 represent non-readily degradable compounds.

4. Conclusions

The study showed that all the catalysts tested presented photocatalytic activity for the TRA degradation, in particular Fe-TNW was the most efficient in the removal of the TRA, since it has a smaller surface area among the catalysts. It was observed that Ru-TNW presented the best adsorption capacity of the pollutant, with 14% of the initial concentration during 1h. The adsorption process is also an important factor for the elimination of the pollutant.

Thirteen TPs were identified by HRMS; they were formed by processes such as dehalogenation, hydroxylation, oxidation and hydration. However, TPs exhibited different formation profiles, which shows that the catalysts have photocatalytic activity for these TPs removal. TP-354 and TP-402 highlighted for having high peak area, the first one revealed that the catalysts degraded it after 1 h of radiation. Undoped-TNW, Fe-TNW and Co-TNW were able to completely eliminate it after 8h, whereas in photolysis there was no degradation of this TP. On the other hand, the TP-402 had a high formation rate during photocatalysis, regardless the type of catalyst used. It was noted that while undoped-TNW had the highest removal rate of TRA and TP-354, it also had the highest rate of formation of TP-402.

In silico assessment showed that all TPs were toxic to aquatic organisms and were not readily biodegradable while many showed mutagenicity. However, in order to confirm the toxic potential of these TPs it is essential to perform assays in living organisms. In brief, this work demonstrated the importance of identifying the TPs in photocatalytic processes since they can be persistent and toxic.

Acknowledgments

Rodrigo A. Osawa acknowledges Brazilian Federal Agency Coordenação de Aperfeiçoamento de Pessoal de Nível Superior (CAPES) for your PhD Grant (99999.000845/2014-00). Beatriz T. Barrocas acknowledges Fundação para a Ciência e Tecnologia (FCT) for her PhD Grant (SFRH/BD/101220/2014). The authors also thank FCT for Projects UID/MULTI/00612/2019, PEstOE/QUI/UI0612/2013, IF/01210/2014, and LISBOA-01-0145-FEDER-022125.

References

Ali, L.I., El-Molla, S.A., Ibrahim, M.M., Mahmoud, H.R., Naghmash, M.A., 2016. Effect of preparation methods and optical band gap of ZnO nanomaterials on photodegradation studies. Opt. Mater. (Amst). 58, 484–490. https://doi.org/10.1016/j.optmat.2016.05.034

Baena-Nogueras, R.M., González-Mazo, E., Lara-Martín, P.A., 2017. Photolysis of Antibiotics under Simulated Sunlight Irradiation: Identification of Photoproducts by High-Resolution Mass Spectrometry. Environ. Sci. Technol. 51, 3148–3156. https://doi.org/10.1021/acs.est.6b03038

Bakhtyari, N.G., Raitano, G., Benfenati, E., Martin, T., Young, D., 2013. Comparison of In Silico Models for Prediction of Mutagenicity. J. Environ. Sci. Heal. Part C 31, 45–66. https://doi.org/10.1080/10590501.2013.763576

Barrocas, B., Silvestre, A.J., Rolo, A.G., Monteiro, O.C., 2016. The effect of ionic Co presence on the structural, optical and photocatalytic properties of modified cobalt–titanate nanotubes. Phys. Chem. Chem. Phys. 18, 18081–18093. https://doi.org/10.1039/C6CP01889K

Barrocas, B.T., Oliveira, M.C., Nogueira, H.I.S., Fateixa, S., Monteiro, O.C., 2019. Ruthenium-Modified Titanate Nanowires for the Photocatalytic Oxidative Removal of Organic Pollutants from Water. ACS Appl. Nano Mater. 2–3, 1341–1349. https://doi.org/10.1021/acsanm.8b02215

Blum, K.M., Andersson, P.L., Ahrens, L., Wiberg, K., Haglund, P., 2018. Persistence, mobility and bioavailability of emerging organic contaminants discharged from sewage treatment plants. Sci. Total Environ. 612, 1532–1542. https://doi.org/10.1016/j.scitotenv.2017.09.006

Collado, N., Rodriguez-Mozaz, S., Gros, M., Rubirola, A., Barceló, D., Comas, J., Rodriguez-Roda, I., Buttiglieri, G., 2014. Pharmaceuticals occurrence in a WWTP with significant industrial contribution and its input into the river system. Environ. Pollut. 185, 202–212. https://doi.org/10.1016/j.envpol.2013.10.040

DellaGreca, M., Iesce, M.R., Previtera, L., Rubino, M., Barone, V., Crescenzi, O., 2008. Phototransformation of the drug trazodone in aqueous solution. J. Photochem. Photobiol. A Chem. 199, 353–357. https://doi.org/10.1016/j.jphotochem.2008.06.018

Devillers, J., Pandard, P., Richard, B., 2013. External validation of structure-biodegradation relationship (SBR) models for predicting the biodegradability of xenobiotics. SAR QSAR Environ. Res. 24, 979–993. https://doi.org/10.1080/1062936X.2013.848632

Eichhorn, P., Pérez, S., Aceña, J., Gardinali, P., Abad, J.L., Barceló, D., 2012. Identification of phototransformation products of sildenafil (Viagra) and its N-demethylated human metabolite under simulated sunlight. J. Mass Spectrom. 47, 701–711. https://doi.org/10.1002/jms.2998

Geiger, E., Hornek-Gausterer, R., Saçan, M.T., 2016. Single and mixture toxicity of pharmaceuticals and chlorophenols to freshwater algae Chlorella vulgaris. Ecotoxicol. Environ. Saf. 129, 189–198. https://doi.org/10.1016/j.ecoenv.2016.03.032

Giebułtowicz, J., Nałecz-Jawecki, G., 2014. Occurrence of antidepressant residues in the sewage-impacted Vistula and Utrata rivers and in tap water in Warsaw (Poland). Ecotoxicol. Environ. Saf. 104, 103–109. https://doi.org/10.1016/j.ecoenv.2014.02.020

Golbamaki, A., Cassano, A., Lombardo, A., Moggio, Y., Colafranceschi, M., Benfenati, E., 2014. Comparison of in silico models for prediction of Daphnia magna acute toxicity. SAR QSAR Environ. Res. 25, 673–694. https://doi.org/10.1080/1062936X.2014.923041

Gutowski, L., Olsson, O., Leder, C., Kümmerer, K., 2015. A comparative assessment of the transformation products of S-metolachlor and its commercial product Mercantor Gold® and their fate in the aquatic environment by employing a combination of experimental and in silico methods. Sci. Total Environ. 506–507, 369–379. https://doi.org/10.1016/j.scitotenv.2014.11.025

Han, Y., Ma, M., Oda, Y., Rao, K., Wang, Z., Yang, R., Liu, Y., 2019. Insight into the generation of toxic products during chloramination of carbamazepine: Kinetics, transformation pathway and toxicity. Sci. Total Environ. 679, 221–228. https://doi.org/10.1016/j.scitotenv.2019.04.423

Kapelewska, J., Kotowska, U., Karpińska, J., Kowalczuk, D., Arciszewska, A., Świrydo, A., 2018. Occurrence, removal, mass loading and environmental risk assessment of emerging organic contaminants in leachates, groundwaters and wastewaters. Microchem. J. 137, 292–301. https://doi.org/10.1016/j.microc.2017.11.008

Li, A.J., Schmitz, O.J., Stephan, S., Lenzen, C., Yue, P.Y.-K., Li, K., Li, H., Leung, K.S.-Y., 2016. Photocatalytic transformation of acesulfame: Transformation products identification and embryotoxicity study. Water Res. 89, 68–75. https://doi.org/10.1016/j.watres.2015.11.035

Liu, S., Li, M., Li, S., Li, H., Yan, L., 2013. Synthesis and adsorption/photocatalysis performance of pyrite FeS2. Appl. Surf. Sci. 268, 213–217. https://doi.org/10.1016/j.apsusc.2012.12.061

Ma, L., Li, J., Xu, L., 2017. Aqueous chlorination of fenamic acids: Kinetic study, transformation products identification and toxicity prediction. Chemosphere 175, 114–122. https://doi.org/10.1016/j.chemosphere.2017.02.045

Mahmoud, W.M.M., Trautwein, C., Leder, C., Kümmerer, K., 2013. Aquatic photochemistry, abiotic and aerobic biodegradability of thalidomide: Identification of stable transformation products by LC–UV–MSn. Sci. Total Environ. 463–464, 140–150. https://doi.org/10.1016/j.scitotenv.2013.05.082

Melnikov, F., Kostal, J., Voutchkova-Kostal, A., Zimmerman, J.B., T. Anastas, P., 2016. Assessment of predictive models for estimating the acute aquatic toxicity of organic chemicals. Green Chem. 18, 4432–4445. https://doi.org/10.1039/C6GC00720A

Mohapatra, D.P., Brar, S.K., Daghrir, R., Tyagi, R.D., Picard, P., Surampalli, R.Y., Drogui, P., 2014. Photocatalytic degradation of carbamazepine in wastewater by using a new class of whey-stabilized nanocrystalline TiO 2 and ZnO. Sci. Total Environ. 485–486, 263–269. https://doi.org/10.1016/j.scitotenv.2014.03.089

Nguyen, C.H., Juang, R.-S., 2019. Efficient removal of cationic dyes from water by a combined adsorption-photocatalysis process using platinum-doped titanate nanomaterials. J. Taiwan Inst. Chem. Eng. 99, 166–179. https://doi.org/10.1016/j.jtice.2019.03.017

Oliveira, T.S., Murphy, M., Mendola, N., Wong, V., Carlson, D., Waring, L., 2015. Characterization of Pharmaceuticals and Personal Care products in hospital effluent and wastewater influent/effluent by direct-injection LC-MS-MS. Sci. Total Environ. 518–519, 459–478. https://doi.org/10.1016/j.scitotenv.2015.02.104

Önlü, S., Saçan, M.T., 2018. Toxicity of contaminants of emerging concern to Dugesia japonica: QSTR modeling and toxicity relationship with Daphnia magna. J. Hazard. Mater. 351, 20–28. https://doi.org/10.1016/j.jhazmat.2018.02.046

Osawa, R.A., Barrocas, B.T., Monteiro, O.C., Conceição Oliveira, M., Florêncio, M.H., 2019. Photocatalytic degradation of amitriptyline, trazodone and venlafaxine using modified cobalt-titanate nanowires under UV–Vis radiation: Transformation products and in silico toxicity. Chem. Eng. J. 373, 1338–1347. https://doi.org/10.1016/j.cej.2019.05.137

Osawa, R.A., Carvalho, A.P., Monteiro, O.C., Oliveira, M.C., Florêncio, M.H., 2019. Transformation products of citalopram: Identification, wastewater analysis and in silico toxicological assess. Chemosphere 217, 858–868. https://doi.org/10.1016/j.chemosphere.2018.11.027

Paíga, P., Correia, M., Fernandes, M.J., Silva, A., Carvalho, M., Vieira, J., Jorge, S., Silva, J.G., Freire, C., Delerue-Matos, C., 2019. Assessment of 83 pharmaceuticals in WWTP influent and effluent samples by UHPLC-MS/MS: Hourly variation. Sci. Total Environ. 648, 582–600. https://doi.org/10.1016/j.scitotenv.2018.08.129

Pizzo, F., Lombardo, A., Manganaro, A., Benfenati, E., 2013. In silico models for predicting ready biodegradability under REACH: A comparative study. Sci. Total Environ. 463–464, 161–168. https://doi.org/10.1016/j.scitotenv.2013.05.060

Pugazhenthiran, N., Murugesan, S., Sathishkumar, P., Anandan, S., 2014. Photocatalytic degradation of ceftiofur sodium in the presence of gold nanoparticles loaded TiO2 under UV–visible light. Chem. Eng. J. 241, 401–409. https://doi.org/10.1016/j.cej.2013.10.069

Raies, A.B., Bajic, V.B., 2016. In silico toxicology: computational methods for the prediction of chemical toxicity. Wiley Interdiscip. Rev. Comput. Mol. Sci. 6, 147–172. https://doi.org/10.1002/wcms.1240

Riva, F., Zuccato, E., Davoli, E., Fattore, E., Castiglioni, S., 2019. Risk assessment of a mixture of emerging contaminants in surface water in a highly urbanized area in Italy. J. Hazard. Mater. 361, 103–110. https://doi.org/10.1016/j.jhazmat.2018.07.099

Sharma, G., García-Peñas, A., Kumar, A., Naushad, M., Mola, G.T., Alshehri, S.M., Ahmed, J., Alhokbany, N., Stadler, F.J., 2019. Fe/La/Zn nanocomposite with graphene oxide for photodegradation of phenylhydrazine. J. Mol. Liq. 285, 362–374. https://doi.org/10.1016/j.molliq.2019.04.036

Starling, M.C.V.M., Amorim, C.C., Leão, M.M.D., 2019. Occurrence, control and fate of contaminants of emerging concern in environmental compartments in Brazil. J. Hazard. Mater. 372, 17–36. https://doi.org/10.1016/j.jhazmat.2018.04.043

Trawiński, J., Skibiński, R., 2017. Photolytic and photocatalytic degradation of tandospirone: Determination of kinetics, identification of transformation products and in silico estimation of toxicity. Sci. Total Environ. 590–591, 775–798. https://doi.org/10.1016/j.scitotenv.2017.03.050

Vulava, V.M., Cory, W.C., Murphey, V.L., Ulmer, C.Z., 2016. Sorption, photodegradation, and chemical transformation of naproxen and ibuprofen in soils and water. Sci. Total Environ. 565, 1063–1070. https://doi.org/10.1016/j.scitotenv.2016.05.132

Yilmaz, A.E., Unal, F., Yuzbasioglu, D., 2017. Evaluation of cytogenetic and DNA damage induced by the antidepressant drug-active ingredients, trazodone and milnacipran, in vitro. Drug Chem. Toxicol. 40, 57–66. https://doi.org/10.1080/01480545.2016.1174870

7.2. Conclusões

Em geral, todos os catalisadores apresentaram atividade fotocatalítica sob radiação visível, porém, o Fe-TNW foi o que apresentou melhor eficiência na degradação do TRA, se considerarmos a área superficial do catalisador pela capacidade de remoção do poluente. Adicionalmente, o Ru-TNW foi o que resultou na melhor capacidade de adsorção, com 18% do TRA removido da solução por esse processo.

Foram identificados treze TPs pela análise dos espectros obtidos por espectrometria de massa de alta resolução. Estes TPs apresentaram perfis de formação e degradação distintos para cada catalisador com destaque para os TP-354 e TP-402 pois ambos apresentaram elevadas áreas de picos nos cromatogramas. O TP-354 foi gerado e degradado em todas as experiências fotocatalíticas porém, durante a fotólise só houve a formação do mesmo, por outras palavras, este TP pode ser persistente no meio ambiente. O TP-402 apresentou o comportamento oposto do TP-354, já que teve uma taxa de geração mais alta na fotocatálise em comparação com a fotólise.

Infelizmente há poucos estudos de toxicidade do TRA em organismos aquáticos, pelo que, a analise *in silico* foi usada com o objetivo de estimar o potencial tóxico destes compostos. Todos os TPs apresentaram uma determinada toxicidade e não foram biodegradáveis, tendo alguns apresentado mutagenicidade. Porém, é essencial analisar em organismos vivos para confirmar estes resultados.

7.3. Referências

1. Osawa, R.A., Barrocas, B.T., Monteiro, O.C., Conceição Oliveira, M., Florêncio, M.H., 2019. Photocatalytic degradation of amitriptyline, trazodone and venlafaxine using modified cobalt-titanate nanowires under UV–Vis radiation: Transformation products and in silico toxicity. *Chem. Eng. J*. 373, 1338–1347. doi:10.1016/j.cej.2019.05.137

2. Barrocas, B., Silvestre, A.J., Rolo, A.G., Monteiro, O.C., 2016. The effect of ionic Co presence on the structural, optical and photocatalytic properties of modified cobalt–titanate nanotubes. *Phys. Chem. Chem. Phys*. 18, 18081–18093. doi:10.1039/C6CP01889K

3. Barrocas, B.T., Oliveira, M.C., Nogueira, H.I.S., Fateixa, S., Monteiro, O.C., 2019. Ruthenium-modified titanate nanowires for the photocatalytic oxidative removal of

organic pollutants from water. *ACS Appl. Nano Mater*. 2, 1341–1349. doi:10.1021/acsanm.8b02215

Capítulo 8

Conclusões e perspetivas futuras

8.1. Conclusões gerais

Este trabalho abordou a degradação de poluentes emergentes abrangendo diferentes áreas de conhecimento incluindo a química analítica, técnicas de separação, espectrometria de massa e métodos de degradação como a cloração, fotólise e fotocatálise com diferentes tipos de radiação.

O primeiro objetivo, descrito no capítulo 2, foi avaliar a remoção de fármacos na ETAR de Alcântara, localizada em Lisboa, Portugal. Para cumprir este objetivo foi realizada uma validação do método da extração em fase sólida usando um HPLC-TQMS no qual foram obtidos bons resultados de recuperação, entre 80,2% e 116,5%, baixos limites de quantificação, entre 2 e 4 ng L^{-1} com o efeito matriz entre 61,4% a 104,8%. Adicionalmente, foi concluído que o material da membrana de filtração pode alterar significativamente os resultados, tendo o melhor resultado sido obtido com a membrana de nylon. Foram quantificados sete fármacos no efluente, em concentrações na ordem de ng L^{-1} (AMI, CIT, CP, DUL, IF, TRA e VEN), o que significa que estes fármacos não foram removidos pelo tratamento convencional da ETAR.

Com base na investigação anteriormente realizada, foram selecionados dois fármacos: CIT e DUL para realizar estudos de degradação por processos abióticos que podem ocorrer no meio ambiente e em ETAR, para elucidar a formação dos TPs já que podem ter sido formados nessas matrizes, com base nos processos de hidrólise, fotodegradação por UV−Vis e cloração. Os processos de fotodegradação por radiação UV e cloração estão presentes no tratamento da ETAR de Alcântara, logo, foram realizadas experiências em laboratório com água superficial para simular estes processos.

Conforme especificado no capítulo 3, o CIT permaneceu estável durante a hidrólise porém, na fotólise e na cloração, foi praticamente degradado em 240 min e 60 min, respetivamente. Nos processos de degradação do CIT, foram identificados dezassete TPs produzidos por diferentes processos de hidroxilação, oxidação e demetilação da molécula de origem, sendo que alguns destes TPs permaneceram estáveis durante a experiência. Foi notado também que três TPs são considerados metabolitos humanos do CIT, por outras palavras, estes metabolitos também podem ser formados por processos físicos. Análises de toxicidade por modelos computacionais foram aplicadas para estimar a ecotoxicidade, mutagenicidade e

carcinogenicidade. Os resultados obtidos mostraram que a maior parte dos TPs apresentavam valores abaixo de 10 mg L^{-1} para a ecotoxicidade, somente dois apresentando potencial mutagénico e, pelo menos, dez mostraram resultados positivos para a carcinogenicidade. Também foram realizadas análises com o efluente para identificar estes TPs, no qual o método de extração já foi devidamente validado. O CIT foi quantificado na concentração de 137 ng L^{-1} no efluente e de 227 ng L^{-1} no influente, ou seja, a ETAR removeu aproximadamente 40% e dois TPs foram identificados no efluente.

Na degradação do DUL, pormenorizado no capítulo 4, foi observada uma completa eliminação durante a fotólise em 30 min de experiência enquanto que na cloração o fármaco foi degradado após 24 hr e apresentou estabilidade durante 4 dias na hidrólise. Em resumo, sete TPs foram identificados na fotólise e dois TPs no processo de cloração e, tanto quanto sabemos, este é o primeiro trabalho sobre a degradação do DUL focado em analises ambientais. Nas predições *in silico* a maioria dos TPs apresenta baixo potencial tóxico em comparação com o DUL e seis apresentaram potencial mutagénico. Nas análises da ETAR, o DUL foi quantificado em concentrações de 95,5 ng L^{-1} no influente e de 79,6 ng L^{-1} no efluente, por outras palavras, somente 17% do poluente foi removido. Também foi observado um TP no efluente, que acreditamos ter sido formado pelo processo de cloração durante o tratamento terciário da ETAR.

Estes resultados mostraram que é essencial analisar os TPs formados a partir dos poluentes pois muitos deles podem ser persistentes ou apresentar maior toxicidade que o composto que lhes deu origem. Além de que podem “mascarar” a degradação do poluente, uma vez que mesmo com o poluente já degradado, os TPs podem estar presentes na matriz. Devido ao avanço de técnicas como a espectrometria de massa de alta resolução, estes TPs podem ser identificados, já que para muitos deles não há padrões comerciais disponíveis e as interações no ambiente são muitas vezes complexas e desconhecidas.

Em seguida, foi avaliada a eficiência da degradação fotocatalítica usando nanomateriais, encontrando-se estes estudos detalhados nos capítulos 5, 6 e 7. O segundo objetivo destes estudos foi para verificar o comportamento dos poluentes na formação dos TPs durante a fotocatálise e fotólise.

A degradação fotocatalítica usando Co-TNW nos fármacos AMI, TRA e VEN foi realizada em água obtida da rede pública de abastecimento sob radiação UV−Vis,

conforme indicado no capítulo 5. Os resultados mostraram que houve um aumento nas taxas de degradação do AMI e VEN durante a fotocatálise em comparação com a fotólise enquanto que na degradação do TRA não houve diferenças significativas entre a fotólise e a fotocatálise, mesmo em soluções com a mistura dos três poluentes. Houve também uma pequena adsorção do AMI e TRA no catalisador, dado que o processo de adsorção também pode contribuir para a eliminação do poluente no ambiente. Foram detetados oito TPs do AMI, sendo que a maior parte se degradou ao fim de 2 hr de experiência. Foi constatado que houve um maior número de TPs formados na fotocatálise, apresentando a maioria destes TPs elevado potencial tóxico, de acordo com a predição in silico para o parâmetro 96-h f. minnow LC_{50} contudo, estes TPs não apresentaram mutagenicidade positiva. Na degradação do TRA foram gerados sete TPs tanto na fotólise quanto na fotocatálise e assim como o TRA, houve baixa atividade fotocatalítica, sendo quatro deles não totalmente eliminados após 2 hr em ambos os processos. A avaliação *in silico* mostrou potencial mutagénico para todos os TPs em pelo menos um modelo computacional. Durante a degradação do VEN foram produzidos cinco TPs na presença do Co-TNW em comparação com somente dois TPs durante a fotólise, porém, todos os TPs foram degradados em ambas as experiências e apresentaram baixo potencial tóxico segundo a avaliação dos modelos computacionais. Esse resultado mostrou que o uso do Co-TNW como catalisador, dependendo do poluente, pode apresentar baixa atividade fotocatalítica, além de que pode formar um maior número de TPs que podem apresentar persistência na fotodegradação e/ou toxicidade em organismos aquáticos.

Para complementar este estudo, foi avaliada a atividade fotocatalítica do Co-TNW na degradação do AMI em radiação visível, com o objetivo de simular a radiação solar. Foi notado que o AMI apresentou uma taxa de degradação de aproximadamente duas vezes maior pela fotocatálise em comparação com a fotólise, ao fim de 8 hr, cerca de 40% do poluente foi eliminado com o catalisador. Foi constatada também a formação de nove TPs, tendo quatro deles estruturas diferentes em referência aos TPs gerados sob radiação UV−Vis.

A atividade fotocatalítica do Ru-TNW foi avaliada para a remoção do CP e do IF, tendo sido neste trabalho utilizado efluente do tratamento secundário da ETAR de Alcântara como matriz, conforme especificado no capítulo 6. Foram demonstradas maiores taxas de degradação utilizando este catalisador no efluente, mesmo em misturas dos dois poluentes. O efluente, sendo uma solução complexa pode, quer

aumentar as taxas de remoção devido à formação dos radicais hidroxilos quer diminuir devido a matéria orgânica que impede a penetração da radiação. Foi observada também a formação de quatro TPs do CP e seis TPs do IF nos processos de degradação e a matriz teve influência nos perfis de tempo e na quantidade de TPs. Alguns destes TPs são considerados metabolitos e a maior parte deles foram degradados após 2 hr de radiação. As predições de toxicidade mostraram que os TPs podem ser tóxicos e apresentar mutagenicidade positiva.

Após os resultados de degradação dos fármacos com os catalisadores Co-TNW e Ru-TNW sob radiação UV−Vis, foi estudada a degradação do TRA sob radiação visível com estes mesmos catalisadores a que foram adicionados Fe-TNW e TNW, tal como descrito no capítulo 7. A seleção resultou do facto do TRA não apresentar diferenças significativas entre a fotólise e a fotocatálise com o Co-TNW sob radiação UV−Vis, conforme detalhado no capítulo 5. Foi constatada a formação de treze TPs, sendo nove deles inéditos, ou seja, diferentes tipos de radiação podem gerar diferentes TPs.

8.2. Perspetivas futuras

Em termos de perspetivas futuras e com o objetivo de complementar este trabalho, há alguns aspetos a serem considerados:

- Coletar amostras de efluentes em diferentes etapas do tratamento ao longo de um determinado período para quantificar e determinar as taxas de remoção dos poluentes emergentes e os respetivos TPs;
- Realizar ensaios de toxicidade *in vitro* ou *in vivo* para confirmar o potencial tóxico dos TPs no meio ambiente;
- Executar experiências de fotocatálise sob luz solar natural com o objetivo de otimizar o processo de degradação com um menor gasto energético;
- Trabalhar com concentrações reais de poluentes em efluentes para determinar as taxas de degradação (cloração ou fotodegradação), recorrendo por exemplo a SPE;
- Realizar ensaios de fotocatálise com diferentes classes de contaminantes emergentes e determinar as vias de degradação na formação dos TPs.